Morphology and Evolution of the Ceratopsian Skull

Andrew Knapp

Submitted in partial fulfilment of the requirements of the Degree of Doctor of Philosophy

School of Biological and Chemical Sciences

Queen Mary University of London

September 2019

Appendix A: Required statement of originality for inclusion in research degree theses

I, Andrew Knapp, confirm that the research included within this thesis is my own work or that where it has been carried out in collaboration with, or supported by others, that this is duly acknowledged below and my contribution indicated. Previously published material is also acknowledged below.

I attest that I have exercised reasonable care to ensure that the work is original, and does not to the best of my knowledge break any UK law, infringe any third party's copyright or other Intellectual Property Right, or contain any confidential material.

I accept that the College has the right to use plagiarism detection software to check the electronic version of the thesis.

I confirm that this thesis has not been previously submitted for the award of a degree by this or any other university.

The copyright of this thesis rests with the author and no quotation from it or information derived from it may be published without the prior written consent of the author.

Signature: Andrew Knapp

Date: 24th September 2019

Details of collaboration and publications:

Publications arising from this thesis:

Knapp A, Knell RJ, Farke AA, Loewen MA and Hone DWE (2018). Patterns of divergence in the morphology of ceratopsian dinosaurs: sympatry is not a driver of divergence. *Proc. R. Soc. B.* **285:** 20180312. http://dx.doi.org/10.1098/rspb.2018.0312

Knapp A, Knell RJ and Hone DWE (2019). Modularity in the skull of the ceratopsian dinosaur *Protoceratops* and morphometric evidence of a socio-sexually selected origin for the frill. (prepared for submission)

Collaborations:

Andy Farke and Mark Loewen provided the taxonomic character matrix used in Chapter 2.

Sandra Álvarez-Carretero performed the branch length estimations used to construct the time-scaled phylogeny in Chapter 4.

Additional publications:

O'Brien DM, Allen CE, Van Kleeck MJ, Hone DWE, Knell RJ, Knapp A, Christiansen S and Emlen DJ (2018). On the evolution of extreme structures: static scaling and the function of sexually selected signals. *Animal Behaviour.* **144;** 95 – 108.

Abstract

Socio-sexual selection has long been recognised as an important driver of evolution and is known to be an important influence on the morphology and behaviour of extant organisms. The long term macroevolutionary effects of socio-sexual selection are difficult to observe because they operate over long timescales. Theoretical work has suggested that socio-sexual selection can possibly influence speciation, adaptation and extinction rates, but these predictions remain largely untested.

The fossil record provides a potential solution for testing macroevolutionary hypotheses regarding socio-sexual selection over millions of years. Recent studies have suggested that the growth patterns of cranial ornamentation in Ceratopsian dinosaurs resemble the growth patterns predicted for a trait under socio-sexual selection. Identifying the presence of socio-sexual selection in extinct organisms is problematic, but evidence from extant taxa provide important evidence in detecting its effects on morphology.

In this project, I use a combination of traditionally defined character states and three-dimensional geometric morphometrics, on a large scale for the first time in a dinosaur clade, to test competing macroevolutionary hypotheses of socio-sexual selection. I first test the hypothesis that morphological diversity in ceratopsian dinosaurs is driven by species recognition by comparing differences in character states between ceratopsian clades. I evaluate morphological evidence for socio-sexual selection in fossil specimens, employing novel techniques to assess growth and morphological variation in the skull of the ceratopsian that is best-represented by fossil specimens, *Protoceratops andrewsi*. Lastly, I extend the morphological dataset to encompass other ceratopsian taxa and examine modularity, morphological disparity and evolutionary rates across the clade. My results refute the hypothesis that exaggerated ceratopsian traits evolved for species recognition and provide support for predictions that ceratopsian traits associated with socio-sexual selection, namely the frill and horns, formed distinct units that both developed and evolved at comparatively rapid rates.

Contents

List of tables

List of figures

List of institutional abbreviations

AMNH	American Museum of Natural History, New York, USA
BMNH	Beijing Museum of Natural History, China
BTT	Birmingham Think Tank, Birmingham, UK
CMN	Canadian Museum of Nature, Ottawa, Canada
CMNH	Carnegie Museum of Natural History, Pittsburgh, Pennsylvania, USA
MAS	Mongolian Academy of Sciences, Ulaanbaatar, Mongolia
MOR	Museum of the Rockies, Bozeman, Montana, USA
NHMUK	The Natural History Museum, London, UK
NMNH	National Museum of Natural History, Washington DC, USA
QMBC	Department of Organismal Biology, Queen Mary University of London, UK
RBINS	Royal Belgian Institute of Natural Sciences, Brussels, Belgium
ROM	Royal Ontario Museum, Toronto, Canada
RTMP	Royal Tyrrell Museum of Palaeontology, Drumheller, Alberta, Canada
UALVP	University of Alberta Laboratory of Vertebrate Palaeontology, Edmonton, Alberta, Canada
UCL	University College London, UK
UMNH	Utah Museum of Natural History, Salt Lake City, Utah, USA
YPM	Yale Peabody Museum, New Haven, Connecticut, USA
ZPAL	Institute of Paleobiology, Polish Academy of Sciences, Warsaw, Poland

Summary

Chapter 1: Introduction to sexual selection and macroevolution

- History of sexual selection theory
- Predicted effects of sexual selection on macroevolution
- Sexual selection in extant organisms
- Socio-sexual selection in the fossil record
- Empirical and theoretical hypothesis testing

Chapter 2: Species recognition in ceratopsian dinosaurs

- Testing the hypothesis of sympatry-driven divergence of ceratopsian display traits

Chapter 3: Ontogenetic variation in the ceratopsian dinosaur *Protoceratops andrewsi*

- Geometric morphometric analysis of growth of the skull of *P. andrewsi*

Chapter 4: Modularity, morphological disparity and evolutionary rates in the ceratopsian skull

- Ceratopsian modularity, morphological disparity and evolutionary rates

Chapter 5: Discussion and conclusions

- Summary of findings
- Suggestions for future research

Chapter 1: Introduction.

This chapter will consist of an overview of socio-sexual selection, discussing hypotheses, predictions and empirical evidence with a comprehensive literature review.

Chapter 2: Species recognition in ceratopsian dinosaurs

The purpose of 'exaggerated' traits in extinct taxa has long been a source of debate. One prominent hypothesis, species recognition, states that these exaggerated traits evolved to enable species to distinguish one another. Using a taxonomic character matrix, I test this hypothesis by comparing the disparity of ornamental vs. non-ornamental traits in 46 ceratopsian taxa, using the prediction that sympatric taxa should show a significantly higher disparity in ornamental traits than non-sympatric taxa.

Chapter 3: Intraspecific variation in the ceratopsian dinosaur *Protoceratops andrewsi*

Sexual selection is difficult to identify in extinct taxa, but certain patterns of growth and diversity are expected to be seen in traits that have evolved under sexual selection. Using a dataset of three-dimensional digital models of the skull of *P. andrewsi,* I analyse patterns of growth using geometric morphometric (GM) techniques, testing modularity, ontogenetic allometry and variation.

Chapter 4: Modularity, morphological disparity and evolutionary rates in the ceratopsian skull

Ceratopsians are a diverse and speciose group of dinosaurs which show elaborate cranial structures believed to have evolved under sexual selection. By conducting GM analyses of several ceratopsian species, I determine patterns of modularity in the ceratopsian skull and examine how these modules vary in both morphological disparity and evolutionary rates within and between species over time.

Chapter 5: Discussion and conclusions

Here I will summarise and discuss the findings of the previous chapters and suggest possible future investigations.

Chapter 1

Introduction

1.1 Background

1.1.1 Sexual selection

Sexual selection was first recognised as an important evolutionary concept by Darwin (1859; 1871), who proposed it as the mechanism by which extravagant and often seemingly disadvantageous morphological and behavioural traits, known as 'secondary sexual traits', arise and propagate within a population despite having no obvious adaptive role. Secondary sexual traits could, Darwin suggested, arise from intrasexual competition between males for access to females, leading to the evolution of weapons or aggressive behaviour in males, or through female choice for the most attractive male, leading to the evolution of ornamental traits and courtship behaviour in males. Sexual selection thus describes the selection of traits associated with competition for mating opportunities (Kokko et al., 2006; Shuker, 2009). Secondary sexual traits have been recognised in a range of diverse animal groups including insects, mammals, birds, teleost fish and amphibians (Darwin, 1871; Gould, 1974; Owens and Hartley, 1998; Watkins, 1998; Amundsen, 2000; Al-Khairulla et al., 2003; Emlen et al., 2005; Bro-Jørgensen, 2007; Bellamy et al., 2013).

Sexes arise from the fundamental difference between the gametes produced by males and females (Dunn et al., 2001). Females must invest more resources in producing larger, more costly gametes, leading to subsequent divergence in reproductive strategies between the sexes. This difference between the sexes leads to the typical 'competitive male/choosy female' concepts of sexual selection, but many factors may influence the degree to which this operates in any population. Many strategies have arisen for securing mates across the animal kingdom including combat between males, lekking, forced copulation, and female mimicry (Darwin, 1871; Futuyma, 2005; Clutton-Brock, 2007).

Fisher (1930) recognised that females selecting mates for attractive traits will, providing those traits are heritable, ensure that their progeny inherit those characters. Their offspring will thus have greater success in procreating further generations, as long as females continue to select for those specific traits. This concept is popularly known as the 'sexy son' hypothesis (Futuyma, 2005, pp333 - 335), and may explain rapid divergence of sexually selected features (Lande, 1981). Secondary sexual traits will almost always exert a cost on the bearer and will be selected against where the benefit they provide in securing a mate does not exceed the cost it places on survival (West-Eberhard, 1979). Our knowledge of the costs placed on the bearer by sexually selected traits is based almost exclusively on indirect evidence, making quantitative assessments difficult (Kotiaho, 2001). In 1975 Zahavi published his 'Handicap Principle' hypothesis as an alternative to the sexy son hypothesis, noting that elaborate structures of behaviour linked with attracting the opposite sex often act to handicap the bearer, either by exposing it to greater risk from predators or by imposing a cost on resources. Furthermore, he recognised Maynard-Smith's (1958) observation that sexual selection will only have evolutionary consequences if successful individuals were also fitter than the average as parents, therefore secondary sexual traits must serve as a reliable test of individual quality. Zahavi suggested that the advertisement of an individual's fitness in this instance is in the individual's ability to prosper despite such a handicap. Although Zahavi considered the handicap principle and the sexy son hypothesis to be distinct processes, the two can be reconciled to produce a long-term evolutionary model of sexual selection (Eshel et al., 2000). In this model female preference and male display coevolve, influenced by the fact that females mating with preferred males produce sexy sons (Kokko et al., 2006).

An additional role for condition-dependence in sexually selected traits stems from the prediction that a reduction in genetic diversity will result from sexual selection because relatively few males produce offspring within a population. To explain this, the 'genic capture' hypothesis was suggested to explain how condition-dependent sexually selected features would be negatively affected by deleterious mutations (Rowe and Houle, 1996). This hypothesis suggests that because secondary sexual traits are affected by many loci, they evolve condition dependence by capturing genetic variance in condition.

Secondary sexual traits therefore become an advertisement of quality and, being highly sensitive to environmental conditions and individual genetic quality, tend to show high variation within a population.

The possible reproductive strategies of a taxon are determined by its evolutionary history, and consequently the form of sexual selection that can develop within a clade is influenced by this (Knell, 2009). For example, many birds invest heavily in parental care because their young require incubation and feeding until they fledge. Parental cooperation is an advantage in this situation, and the majority of extant birds are socially monogamous (Lack, 1968; Macedo et al., 2008). Zahavi (1975) noted that sexually monomorphic kittiwakes form pairs which compete for the best position in the colonies in which they nest. Better-quality pairs tend to nest near the centre of the colony, offering protection from predators, but handicap themselves by competing for these locations by risking physical confrontation with other pairs. He hypothesised that a form of mutual selection exists within kittiwake colonies, since cooperation in nesting and foraging is clearly an important selective factor in this situation and both sexes would benefit reproductively from choosing the best-quality mate. In a cooperative situation mutual mate choice would be expected to play some role because both partners rely on one another to produce offspring (Kokko and Johnstone, 2002). Mutual sexual selection, arising from competition in such situations, has been identified in several bird taxa (Huxley, 1914; Jones and Hunter, 1993; Kraaijeveld et al., 2004).

1.1.2 Social selection

Exaggerated traits can evolve in response to competition in dominance hierarchies within a population in a similar way to their evolution under sexual selection (West-Eberhard, 1983). Animals evolve to live in social groups for various reasons such as defence or resource location and high population densities create strong selective pressure for limited resources, resulting in selection for traits that confer advantages in these situations. This is termed social selection (West-Eberhard, 1979). Because sexual selection is concerned with competition for mating opportunities within a population, it can be

considered a subset of social selection (West-Eberhard, 1983; Tobias et al., 2012). Specifically, sexual selection can be described as the relationship between a trait and its effect on fitness through sexual competition (Shuker, 2009). Individuals that can dominate social groups are often more likely to succeed in reproducing, and dominance-linked features will be expected to arise as an advertisement of quality in individuals (West-Eberhard, 1979). The risks associated with direct physical competition may in turn lead to the evolution of 'abstract' visual, olfactory or auditory signals as indicators of fitness, and the avoidance of physical confrontation (Geist, 1971; Maynard-Smith, 1974; Knell, 2009; Sheehan and Bergman, 2015). In populations in which social selection is strong, selecting the best possible mate may be an important factor in successfully producing offspring (West-Eberhard, 1983). Social selection and sexual selection are therefore inextricably linked concepts, and differentiating them may be difficult or impossible because traits may evolve due to one or both concepts (West-Eberhard, 1983). For this reason, the term 'sexual selection' hereafter refers to examples of selection for traits known to arise exclusively from competition for mating opportunities, and 'socio-sexual selection' is hereafter used to describe examples of selection for traits arising from intraspecific competition where sexual selection is not known to be the sole or principal evolutionary driver (Tobias et al., 2012).

1.1.3 Predicted effects of socio-sexual selection on macroevolution

The highly diverse nature of secondary sexual features has led to the hypothesis that sexual selection is an important driver of speciation (Kraaijeveld, 2011). Fisher (1930) recognised that runaway sexual selection could lead to rapid divergence of isolated populations, and predicted that this would lead to the eventual separation of these populations into distinct species. Within a mixed population, variation in sexual preference may allow for sympatric speciation because sensory bias and subsequent character evolution can diverge rapidly under a behaviour-segregated community (Lande, 1981; Futuyma, 2005; M'Gonigle et al., 2012). Studies of natural avian hybrid zones have indicated that strict genetic isolation is not guaranteed between closely related breeding groups that are under

sexual selection (McDonald et al., 2001; Stein and Uy, 2006), but highly selective female choice can act as an effective barrier. Interactions between sexual and natural selection are also predicted to drive speciation (Lorch et al., 2003), though it is presently unclear how these interactions contribute in nature (Maan and Seehausen, 2011; Long et al., 2012).

In addition to influencing speciation and adaptation, socio-sexual selection has been suggested as an important factor in determining a population's ability to resist extinction (Doherty et al., 2003; Lorch et al., 2003; Bellamy et al., 2013; Martinez-Ruiz and Knell, 2016). Populations under strong sexual selection are predicted to be more at risk from extinction under environmental stress due to increased susceptibility to inbreeding depression (van Oosterhout et al., 2003). This arises from smaller effective population sizes due to a skewed operational sex ratio (Kokko et al., 2006)). Conversely, the genic capture hypothesis predicts that sexual selection should lead to faster adaptation to changing environments, and a lower subsequent risk of extinction because the fittest males are best-adapted to the environment (Martinez-Ruiz and Knell, 2016). These two seemingly contrary predictions may be reconciled when population size is taken into account, with smaller populations more at risk of extinction under strong sexual selection due to the potential genetic bottleneck effect, or higher risk of demographic stochasticity due to skewed sex ratios (Jarzebowska and Radwan, 2009; Martinez-Ruiz and Knell, 2016). An improved assessment of a population's extinction risk may therefore be achieved from knowledge of its sexual selection pressures (Sorchi et al., 1998; Bellamy et al., 2013; Parrett and Knell, 2018), which may have important consequences for conservation.

1.2 Theoretical and empirical evidence for sexual selection

1.2.1 Sexual selection in extant organisms

Sexual selection operates wherever competition for mating opportunities exists, and mating is non-random with respect to individual phenotypes (Shuker, 2009). The intensity of sexual selection in a

given population can fluctuate, and results from a combination of factors such as life history, population density and operational sex ratio (Kokko and Johnstone, 2002), and strong sexual selection will tend to lead to the evolution of exaggerated secondary sexual traits, and often sexual dimorphism. As the original basis for Darwin's explanation of sexual selection (1871), examples of sexual dimorphism are found across a wide variety of groups in the animal kingdom and include some of the most extreme examples of variation within species. These include patterning of butterfly wings (Nijhout, 1991), horns and exaggerated mandibles in beetles (Emlen et al., 2005; Knell, 2011; McCullough et al., 2015), antlers and horns in mammals (Caro et al, 2003; Mateos et al., 2008) and the elaborate plumage of male birds in many species (Møller and Pomiankowski, 1993; Dale et al., 2015). Because sexually selected features are linked to reproduction their expression may be synchronised with breeding seasons (Darwin, 1871; Clutton-Brock, 2007). This is apparent in many birds which moult and regrow elaborate plumage with the seasonal breeding periods, and in cervids which moult and regrow their antlers each year. Such synchronicity is a reasonable indicator that a feature is under sexual selection, as the costs of maintaining elaborate structures may make them disproportionately disadvantageous outside the mating season (Emlen, 2001; Balmer et al., 2018). Intense sexual selection within a population may also lead to the evolution of multiple sexual signals as a more expensive advertisement of quality, as seen in many species of bird (Møller and Pomiankowski, 1993).

Beetles were first identified by Darwin (1871) as providing a good example of sexual selection in invertebrates. Many species of beetle exhibit a high degree of sexual dimorphism, and males of these species are known to compete aggressively for females (Emlen et al., 2005; Knell, 2011; Lavine et al., 2015; McCullough et al., 2015). The Scarabaeidae may be one of the best-known examples of the observation that secondary sexual features show apparently random patterns of diversification in closely related species (Knell and Sampson, 2011). The evolution of socio-sexual traits are not expected to follow a predictable path or reach an optimum state because they are under different selective pressures to naturally selected traits (West-Eberhard, 1983). It has been suggested that divergence in the forms of beetle horns may be a result of intense sexual selection for horns combined

with chance events, which are further affected by ecological factors (Emlen et al., 2005). Field studies involving scarab beetles in Borneo have provided some of the strongest evidence yet that sexual selection can determine extinction resistance in the face of environmental change (Parrett et al., 2019).

Birds provide some of the strongest evidence for the rapid evolution of secondary sexual features in extant taxa. Dale et al. (2015) examined plumage colouration and found that conspecific colouration is largely correlated in passerine birds, with increased ornamentation in larger and tropical species, and that female ornamentation increased in cooperative breeders. Strong sexual selection in males, measured by relative sexual dimorphism, appears to have antagonistic effects on female colouration, but this may be a circular effect of the definition of sexual selection strength in this study; females in strongly sexually selected taxa are more different to males because that is how strength of sexual selection is defined. Cooney et al. (2019) found that differences in the rate and direction of plumage colour evolution are predicted by dichromatism, again a proxy for sexual selection intensity, and that sexual selection has a strong positive effect on male, but not female, interspecific divergence rates.

Many mammals show clear sexual dimorphism in body size, and physical confrontation between larger males to secure females is well known in many species (Searcy, 1982; Wade and Shuster, 2005; Futuyma, 2005). In extreme examples only alpha males can exert their dominance and safeguard their breeding privilege against competitors, and sub-alpha males are often unable to mate and pass on their genes. The opportunity for males to mate in these species can be brief, and so opportunities for reproduction, when they arise, must be maximised (West-Eberhard, 1979). Social monogamy, where males and females form pair bonds, occurs in fewer than 5% of mammals (Kleiman, 1977; Komers, 1997) compared with around 90% of birds (Lack, 1968). The differences in reproductive biology between these two groups may explain this disparity, since birds are oviparous and many species remain in the nest with their young until they are fledged and mobile.

A less obvious example of sexual selection concerns mutual sexual selection, where both sexes compete for mating opportunities but there is no clear sexual dimorphism (Jones and Hunter, 1993; Hone et al., 2016a). This concept was first hinted at by Darwin in *The Descent of Man* (1871; see also Borkovic and Russell, 2014), and later expanded upon by Huxley (1914) in his study of the great crested grebe (*Podiceps cristatus*). Studies of the crested auklet, *Aethia cristatella,* have shown that males and females of this monomorphic species both exhibit a stronger reaction when faced with a potential mate with a larger head crest, suggesting that both sexes engage in opposite-sex choosiness in this species (Jones and Hunter, 1993). Mutual mate choice has been observed in a wide range of taxa as diverse as the stalk-eyed fly *Teleopsis dalmanni* (Cotton et al., 2014), the giant panda, *Ailuropoda melanoleuca* (Martin-Wintle et al., 2015), the black swan, *Cygnus atratus* (Kraaijeveld et al., 2004), the two-spotted goby, *Gobisculus flavescens* (Amundsen and Forsgren, 2001; 2003), and there is extensive evidence of it operating in a wide range of vertebrate and invertebrate taxa (Jennions and Petrie, 1997; Bonduriansky, 2001; Kraaijeveld et al., 2007). Despite being present in a wide range of disparate taxa, the study of mutual sexual selection is often limited to a few well-known examples and it may be far more widespread than currently realised (Kokko and Johnstone, 2002).

Computer simulations of the interactions between individuals in a population have frequently been used to investigate evolutionarily interactions under different scenarios, including sexual selection (Maynard Smith, 1974; Lande, 1981; Lorch et al., 2003; Kokko and Johnstone, 2002; Kokko et al., 2006; Fromhage and Kokko, 2014; Henshaw et al., 2016). Modelling communities in this way can allow for the testing of predictions of the effects of interactions on macroevolution with relative ease (Andersson, 1987). Theoretical models can lend support to predictions of sexual selection that are otherwise difficult to explore, including sexual selection-mediated adaptation (Lorch et al., 2003), sympatric speciation (Kirkpatrick, 2000), and extinction vulnerability (Knell and Mártinez-Ruiz, 2017). Experimentally determining how modes of sexual selection can arise and be maintained within a population is not possible in the macroevolutionary sense due to the timescales and population numbers required. It is apparent that sexual selection is influenced by a host of variables but the

interplay of these is little understood (Maan and Seehausen, 2011), and controlling these variables in a physical experiment may prove difficult and costly, if not impossible. By simulating various parameters the effects of ecology, community and evolutionary history can be investigated and their effect on theoretical populations can be determined (DeAngelis and Mooij, 2005). Theoretical models can also form the basis of future experiments by helping to determine important variables for investigation.

Some modelling work has been done to understand the possible underlying drivers of mutual mate choice (Kokko and Johnstone, 2002), but mutual sexual selection itself remains relatively unexplored in extant taxa. Kokko and Johnstone (2002) used a game theory model to investigate the interplay of choosiness, signalling and parental care and found that mutual mate choice should arise regularly when parental investment is high and more similar in both sexes. They questioned why, given this finding, mutual mate choice was not more commonly observed in living taxa. Using a model that simulated condition-dependent investment in a trait under conditions of perfect monogamy, and with inherited genetic quality, Hooper and Miller (2008) found that mutual mate choice could drive costly signalling as long as the phenotypic condition is sufficiently heritable and the monomorphic signalling trait is an honest reflection of condition. A product of this and other mutual choice models (e.g. Kirkpatrick et al., 1990; Johnstone et al., 1996; Johnstone, 1997) is that mutual mate choice resulted in positive-assortative mating based on the sexual trait value. This pattern has been identified in a number of extant taxa (e.g., Foote and Larkin, 1988; MacDonald and Montgomerie, 2003; Pryke and Griffith, 2007; Bitton et al., 2008; Acord et al., 2013; Jiang et al., 2013; Rueger et al., 2016; Rull et al., 2016) and this has been suggested as a test for mutual sexual selection (Trivers, 1972). Caution in this interpretation has been stressed by Kraaijeveld et al. (2007) due to other possible causes. Assortative mating may arise because of other aspects of a population's mating system, for example age correlation or spatial segregation (Jiang et al., 2013). Elsewhere in their review, Kraaijeveld et al. (2007) present evidence that mutual ornamentation is a result of mutual selection, and that it also plays a role in post-copulatory roles in some taxa. Furthermore, evidence from modelling suggests

that assortative mating is a mechanism by which sympatric speciation can occur because it can increase reproductive isolation (Kirkpatrick, 2000).

1.2.2 Socio-sexual selection in the fossil record

Attempting to infer the effects of socio-sexual selection on speciation, adaptation and extinction in extant animals can be problematic because the extinction of past lineages will remove some of this diversity and somewhat mask past speciation rates (Kraaijeveld et al., 2011; Fig. 1.1). The best approach may be to look for these patterns in the fossil record, where effects occurring over millions of years may be seen (Knell et al., 2012). Several examples of extinct animals exist in which various elaborate or exaggerated features have been interpreted as secondary sexual characters. These include feathers and streamers in fossil birds (Zhang et al., 2008), antlers in the giant elk (Gould, 1974), unusual structures in trilobites (Knell and Fortey, 2005), and cranial ornamentation in various dinosaur and pterosaur clades (Farlow and Dodson, 1975; Dodson, 1998; Tomkins et al., 2010; Hone et al., 2012; Knell et al., 2012).

Difficulties arise when attempting to test hypotheses of socio-sexual selection in fossil organisms due to the absence of behavioural and genetic evidence. Recently, several studies examining evolution and cranial morphology in the ornithischian dinosaur clades Ceratopsia and Hadrosauria have suggested that their uniquely ornamented skull morphology is a result of socio-sexual selection (Hone et al., 2016; Stubbs et al., 2019). The good fossil records of these clades, their excellent preservation, and their near-universal ornamentation suggests that they may be an ideal candidate for studying socio-sexual selection in extinct vertebrates.

The interpretation of unusual or exaggerated features in extinct animals has traditionally depended on comparison with analogous living organisms (Knell et al., 2012), and interpretation of past sexual selection patterns and mating systems likewise depend on those defined in living animals (Henshaw et al., 2016). There is controversy over how sexually selected traits should be recognised and

interpreted alongside other possible explanations for exaggerated morphological features (Knell and Sampson, 2011; Padian and Horner, 2011b; Knell et al., 2012; Mendelson and Shaw, 2012).

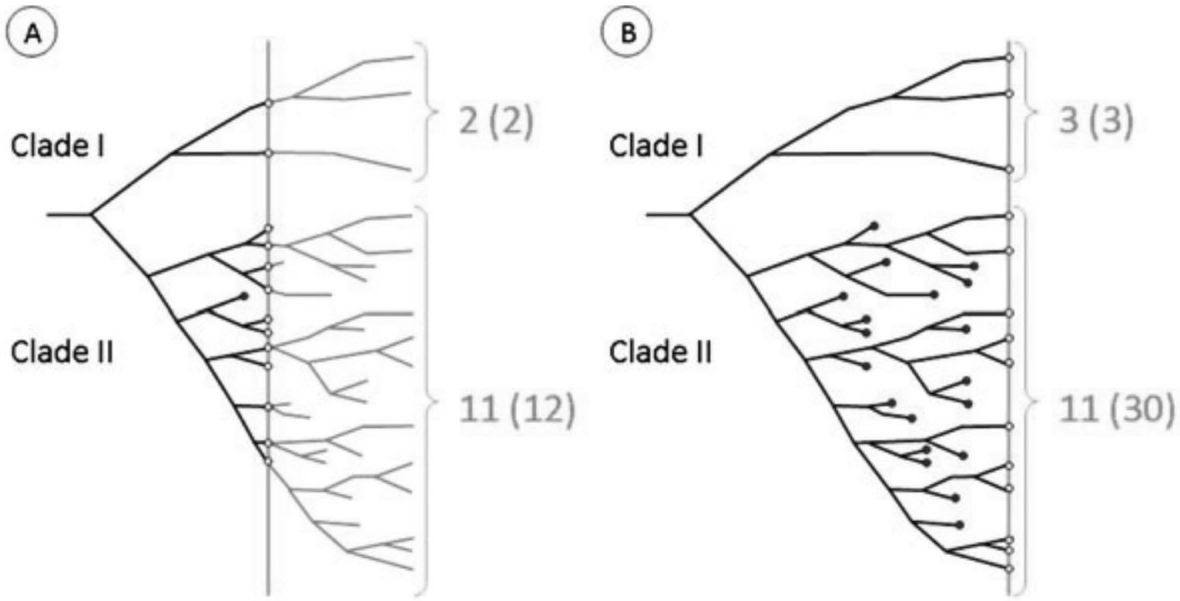

Figure 1.1: The effect of differing species turnover on apparent species richness. (A) When the two clades are compared at a point where they have recently diverged, the number of extant species (white dots) of each clade (first number) is close to the total number of speciations (number in parentheses). (B) The same comparison made at a later point in time is biased by extinctions in clade II (black dots) masking the true number of generated species, resulting in a large discrepancy between extant and total species (From Kraaijeveld et al., 2011).

Sexual dimorphism has long been cited as an example of the effects of sexual selection, and much of Darwin's (1971) original work on sexual selection deals with examples of it. Identifying the presence and influence of sexual selection in extinct taxa without the benefit of obvious morphological or behavioural sexual dimorphism is problematic (Padian and Horner, 2011a). In addition, the fossil records of many species are often too sparse to offer realistic opportunities to distinguish sexual dimorphism (Benton, 2015; Mallon, 2017, Hone and Mallon, 2017). Sexual dimorphism is sometimes accepted as a *prima facie* result of sexual selection, with some authors maintaining that Darwin's definition of sexual selection demanded it (Padian and Horner, 2011b). This interpretation has been

rejected by a number of authors who argue that while most of his examples deal with cases of sexual dimorphism, Darwin himself gives several examples of mutual sexual selection in *The Descent of Man* (Darwin, 1871; Knell and Sampson, 2011; Knell et al., 2012; Hone et al., 2012; Borkovic and Russell, 2014). In some cases it is possible to identify sexual dimorphism in fossil vertebrates, one example being the Middle Jurassic pterosaur *Darwinopterus.* A fossil female *Darwinopterus* with egg *in situ* has been found, and the lack of cranial crest in it and other 'female' specimens, along with other anatomical evidence, distinguishes them from the crested specimen that are inferred to be males found in the same strata (Lü et al., 2011). Often, however, sexual dimorphism is either not apparent in fossil organisms, or intraspecific variation is interpreted as two or more different taxa (Maiorino et al., 2015).

Determining whether a specific trait is sexually selected should be more straightforward when it has evolved to play a role in intraspecific combat, because such traits are common in living vertebrates (Darwin, 1871). The horns of the ceratopsian dinosaurs are believed to have played such a role, and damage to the regions of the skull of *Triceratops* that are predicted from intraspecific combat has been reported in several specimens (Farke et al., 2009). This hypothesis was further examined by Kraus et al. (2010), who noted that frills evolved in ceratopsians before horns and suggested that both evolved under sexual selection. They noted, however, that there is little evidence for damage caused by horns in other ceratopsian taxa, following an extensive review of ceratopsian skull elements by Tanke and Farke (2007). Hieronymous et al. (2009) conducted a review of centrosaurine cranial bone morphology and histology, and found correlates with horns and cornified pads in extant taxa that are associated with intraspecific combat. In particular, they noted the similarity between the flat, rugose nasal and postorbital bosses, which replace horns in *Pachyrhinosaurus* and *Achelousaurus,* with horny bosses of extant muskoxen (*Ovibos*), helmeted hornbills (*Buceros vigil*) and African buffalo (*Syncerus*), and suggested that such morphology is consistent with high-energy headbutting. As with all ceratopsian taxa, *Triceratops* does not display any obvious sexual dimorphism and so hypotheses of intrasexual combat are difficult to demonstrate. Lack of facial damage in a fossil specimen does not in

itself indicate that the individual was not involved in combat. Studies of extant mammals have revealed that traits that appear to function as weapons may often evolve to play a role as visual dominance signals and so intraspecific combat, and the injuries expected from it, may subsequently become relatively rare (Geist, 1971; Gould, 1974). Furthermore, intrasexual resource competition has been associated with the evolution of female weaponry in living beetles (Watson and Simmons, 2010), and horns are found in both sexes of many species of extant bovids (Caro et al., 2003). The long neck of male giraffes is an example of an ecologically functional structure that is also used in intrasexual combat. Despite the implications for this sex-limited behaviour on sexual selection for larger necks, no studies have found any clear correlation between sex and neck size in either living giraffes, or in extinct long-necked sauropods, that are not explained by overall size differences between sexes (Senter 2006; Mitchell et al., 2009; Taylor et al., 2011; Wilkinson and Ruxton, 2012).

Socio-sexual traits that act as signals of quality must be sensitive to individual condition if they are honest signals and should therefore show increased variance. Finding heightened variance may provide a further clue to the function of a trait (Rowe and Houle, 1996; O'Brien et al., 2018). Traits with mechanical functions are more limited in their variance due to functional constraints acting to optimise performance.

The identification of sexually selected traits is further compounded by the possibility of multifunctionality of these traits (Tomkins et al., 2010; Hone and Faulkes, 2013; Hone and Naish, 2013). Features with no real analogies in extant taxa, such as the frills of ceratopsians, have been variously interpreted as being used for socio-sexual signalling, species recognition, defence, jaw musculature attachment, or temperature regulation, among others (Tomkins et al., 2010; Padian and Horner, 2011a; Maiorino et al., 2017). The species recognition hypothesis in particular has emerged as an alternative explanation for 'bizarre' structures in extinct organisms (Padian and Horner, 2011a). This hypothesis suggests that exaggerated traits evolved to aid in the identification of conspecifics for various reasons, and offers predictions that should be straightforward to test with fossil specimens

(Knell and Sampson, 2012). There are, however, several arguments against this hypothesis (West-Eberhard, 1983; Zahavi and Zahavi, 1997; Maynard Smith and Harper, 2003)

Detailed examinations of the growth patterns of secondary sexual traits in living birds, mammals, insects, crustaceans and lizards have found positive allometric growth to be common in sexually selected traits (Petrie, 1992; Kodric-Brown et al., 2006; Tomkins et al., 2010; O'Brien et al., 2018), though not all positively allometric traits are sexually selected (Green, 1992). Positive allometry arises when a trait scales at a higher rate than body size (Hone et al., 2016a). There has been some debate over the pattern of allometric growth that would be expected in sexually selected traits, with isometry (Bonduriansky and Day, 2003), positive (Fromhage and Kokko, 2014) and sexually-differentiated (Bonduriansky, 2007) allometries all proposed as being possible. These differing results can be explained by the function of the trait itself (Eberhard et al., 2018; O'Brien et al., 2018). Secondary sexual traits connected with aggressive competition, where body size is emphasised, are predicted to show strong positive allometry because they act as honest signals, whereas pure courtship signals and weapons may show a more isometric or even negatively allometric relationship with body size (Eberhard et al., 2018; Rodríguez and Eberhard, 2019). Detection of a significantly positive allometric signal may therefore indicate a trait that has a role in intraspecific aggression, or that the trait is an honest signal of individual quality. O'Brien et al. (2018) suggested that a more reliable method for identifying a secondary sexual trait is to compare its allometric slope to that of a non-sexually selected 'reference' trait, rather than with isometry (i.e. a regression slope of 1). Using this method secondary sexual traits can be more reliably distinguished from non-sexually selected traits that show positive allometry themselves. Analysis of allometry has been applied to the cranial frill of an extinct species of ceratopsian dinosaur, *Protoceratops andrewsi.* Using a sample of over 30 specimens ranging from hatchling-sized to large adult individuals (Fig. 1.2) Hone et al. (2016) found that the length of the parietal-squamosal frill showed significant positive allometry. This pattern of growth fits that expected of a trait with a socio-sexual signalling function, suggesting that the frill had a socio-sexual role. Changes in allometry during ontogeny, as observed in *Protoceratops*, are expected from traits which

are important in mature individuals but not juveniles, particularly secondary sexual traits (Knell et al., 2012).

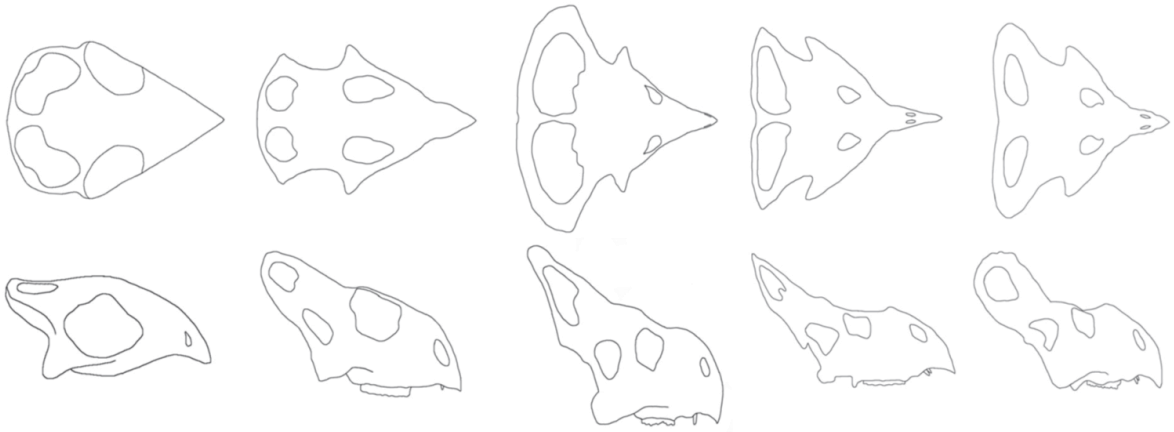

Figure 1.2: **Changes in skull shape with ontogeny of Protoceratops andrewsi, illustrating growth of frill**. Skulls represent dorsal (upper row) and lateral (lower row) views. Sizes range, from left to right, small juvenile (1st) through to juvenile (2nd), subadult (3rd) and adult 'female' (4th) and adult 'male' (5th). From Hone et al., 2016a.

1.2.3 Ceratopsian dinosaurs

The Ceratopsia is an extinct clade of herbivorous ornithischian dinosaurs, commonly known as the 'horned dinosaurs', which first appears in the fossil record in the Late Jurassic period of Asia (Ca. 158 million years ago; Dodson, 1996; Xu et al., 2006). Early ceratopsians were small (~1 metre in length) and bipedal, and lacked the enlarged parietal-squamosal frill and facial horns that typify the more derived ceratopsids of the Late Cretaceous (Sereno, 1986; Hailu and Dodson, 2004). Basal ceratopsians are known from many localities in China and Mongolia, the most well-studied belonging to the genus *Psittacosaurus* (Sereno, 2010). The earliest known North American ceratopsian, *Aquilops americanus*, was found in Lower Cretaceous formations of Montana of between 104 and 109 million years ago (Farke et al., 2014). Although remains of early ceratopsians from North America are rare, the Late Cretaceous saw an extraordinary radiation of ceratopsian taxa in the clade Ceratopsidae, culminating in large, quadrupedal taxa such as *Triceratops,* which persisted to the end-Cretaceous extinction event

(Dodson et al., 2004; Sampson and Loewen, 2010). Late Cretaceous ceratopsids are well-known for the morphological diversity of their crania, including enlarged parietal-squamosal frills projecting from the rear of their skulls, and nasal and postorbital horns and bosses in many taxa (Fig. 1.3; Dodson et al., 2004). Complex patterns of epiossifications projecting from the rear margin of the frill are known from many taxa, and are often the most important diagnostic character (Kirkland and DeBlieux, 2010; Ryan et al., 2010). The fossil record of these Late Cretaceous North American taxa is particularly good, and many well-preserved specimens have been discovered in the past century (Sampson and Loewen, 2010).

Figure 1.3: Examples of ceratopsian cranial diversity. L-R (Top row): *Psittacosaurus sinensis, Protoceratops andrewsi, Centrosaurus apertus;* (Bottom row): *Diabloceratops eatoni, Chasmosaurus belli, Triceratops horridus.*

The function of the frills and horns of ceratopsian dinosaurs has been a source of debate since the discovery of *Triceratops* in the late 19th Century (Hatcher, 1907; Dodson, 1996; Dodson et al., 2004). Horns are obvious examples of weapons, and have been suggested to have evolved for intraspecific

combat and/or predator defence in ceratopsians (Hone et al., 2011). Evidence of combat has been found in one taxon, *Triceratops*, but there is little evidence for intraspecific horn use in any other taxa (Farke et al., 2009). Similarly, a defensive role is unlikely because these traits are limited to the skull (Hone et al., 2011). The frill, sometimes referred to as a 'neck shield', has been suggested as having evolved for protection in intraspecific combat and thus should show patterns of coevolution with horns, but similarly shows no significant evidence of damage from intraspecific combat in any taxa (Krauss et al., 2010). Furthermore, the frills of most ceratopsians have large weight-saving fenestrae, which would negate any protective benefits. A notable exception is *Triceratops*, which had a solid, unfenestrated frill which has been shown to have strong structural properties (Farke et al., 2010). Thermoregulation has also been suggested as a functional explanation for the frill and horns of ceratopsians, with some evidence to support this claim (Barrick et al., 1998). Hone et al. (2012) discussed the various additional possible functions of ceratopsian frills in some detail. It is possible to rule out more directly physical functions by biomechanical analysis (Rayfield, 2005; Tomkins et al., 2010) and identifying associated microstructures such as blood vessels and muscle attachments (Benton, 2015, pp159-160). Species recognition is another widespread explanation for the elaborate ornamentation of ceratopsians (Padian and Horner, 2011a), though this hypothesis has little support in any extant taxa and has not been tested in ceratopsians (Zahavi and Zahavi, 1997; Knell and Sampson, 2011). Furthermore, the sheer size of ceratopsian skulls (Maidment at al., 2014) suggest that species recognition is an unlikely driver of their evolution because it should not be expected to exact a high cost (Maynard Smith and Harper, 2003). Some researchers have noted that exaggerated, costly morphology in extant taxa is often sexually selected, and this is therefore the most plausible explanation for the evolution and persistence of the diverse traits seen in ceratopsians (Tomkins et al., 2010). Numerous exaggerated traits are known in extant taxa which are not sexually selected, so this interpretation should be treated with caution (Knell et al., 2012). It is possible that exaggerated ceratopsian traits could have had multiple additional functions, including some combination of predator defence and thermoregulation, as horns in extant bovids may do (Stankowich and Caro,

2009), but it is unlikely from the evidence that any of these processes is the primary driver of their evolution and diversification (Hone et al., 2011).

The good fossil record of ceratopsians informs us of many important aspects of their biology, from growth and development (Sampson et al., 1997; Erickson and Tumanova, 2000; Ryan et al., 2001; Tanke and Farke, 2007; Lee and Werning, 2008; Handa et al., 2012; Hone et al., 2016; Erickson et al., 2017), to evolution (Sampson and Loewen, 2010; Sereno, 2010; Brown and Henderson, 2015; Ryan et al., 2016), and possible social aspects of many taxa. Social aspects include monospecific aggregations of mixed age groups in *Centrosaurus, Agujaceratops* and *Pachyrhinosaurus* (Ryan et al., 2001; Lehman, 2007; Currie, Langston and Tanke, 2008; Farke et al., 2011; Fanti et al., 2015), age-segregated groups in *Psittacosaurus, Protoceratops* and *Triceratops* (Zhao et al, 2007; Mathews et al., 2009; Fastovsky et al., 2011; Hone et al., 2014), and intraspecific combat in *Triceratops*. Our knowledge of many aspects of ceratopsian biology and evolution, combined with the large number of well-preserved specimens, make them an ideal subject for macroevolutionary morphometric studies and may be our best opportunity to investigate the connection between exaggerated traits and socio-sexual selection in a fossil clade (Hone and Faulkes, 2013).

1.3 Methodology

1.3.1 Geometric morphometrics

Techniques for describing and analysing fossil specimens have traditionally focussed on the presence or absence of discrete morphological characters and the covariation of point-to-point distance measurements from two-dimensional (2D) images. These techniques provide useful information of overall dimensions, but fail to consider even basic aspects of morphology (MacLeod, 1999). With the advent of affordable computing, an early solution to this problem was landmark analysis. An equal number of ‘landmark’ points based on homologous structures (e.g. suture junctions) are designated

and the distance variation of these points between specimens quantified (Bookstein, 1986; Frost et al., 2003). Landmarks of this type are known as Bookstein Type 1 or anatomical landmarks (Bookstein, 1991; Goswami et al., 2019). Although anatomical landmarks are an excellent means of directly analysing shape variation, they rely on easily identifiable homologous points which cannot easily be designated on smooth or featureless surfaces (Bookstein, 1996; MacLeod, 1999). Semilandmarks offer an opportunity to overcome the latter limitation. Instead of designated fixed points on homologous structures, semilandmarks allow a fixed number of landmarks to be positioned along a curve, allowing analysis of two-dimensional shape (Bookstein, 1996; MacLeod and Rose, 1993; Goswami et al., 2019). Developments in computing power have since led to the development of several methods for analysing morphology in three dimensions. Eigensurface analysis extends the semilandmark principal to create a three-dimensional sampling grid from a digital mesh (Sievwright and MacLeod, 2012), and automated processes have been developed to allow the placement of surface semilandmarks on a large number of specimens from a single template (Felice and Goswami, 2018; Bardua et al., 2019). Specimens can be compared by superimposition of their landmark sets using a generalised Procrustes analysis (GPA), which minimises the effects of position, orientation and scale between specimens and provides a set of eigenvectors describing differences in landmark position (Rohlf and Slice, 1990).

The aim of geometric morphometric techniques is to allow for a much more detailed examination and interpretation of biological morphology, and to remove elements of subjectivity in making direct comparisons. Detailed study of variation in gross morphology can reveal overlooked or difficult to identify differences between and within taxonomic groups, and enable statistical analyses of such variations in a way not possible using traditional morphometric techniques (Sievwright and MacLeod, 2012; Goswami et al., 2019).

1.3.2 Modularity and evolutionary rates

Integration and modularity are related concepts that refer to the tendency of sets of traits to covary to differing degrees (Klingenberg, 2008). Integration and modularity apply to many biological

concepts, from molecules to genes to anatomy. While integration results from sets of traits becoming more closely-linked, modularity relaxes linkages between these sets of traits and allows them to vary independently of one another. Understanding the degree to which an organism's morphology is partitioned into modules provides the basis for understanding the interplay between development and evolution (Klingenberg and Marugán-Lobón, 2013; Klingenberg, 2014). The developmental and evolutionary independence of phenotypic modules enables them to respond to selection in different ways (Goswami et al., 2014). Determining modularity in analyses of shape variation can therefore provide important information about different selective regimes acting upon a set of traits (Goswami and Polly, 2010b; Felice et al., 2018; Felice et al., 2019; Bardua et al., 2019a). Identifying modularity has the added benefit of allowing specimens to be partitioned in a way that removes a degree of subjectivity in their interpretation, and allows for direct comparisons of morphological disparity and evolutionary rates of modules (Felice et al., 2018). Treating a highly modular structure as a single biological unit, for example measuring the total length of a highly modular skull, may be a poor reflection of reality (Watanabe et al., 2019).

Methods for assessing modularity generally take one of two approaches, exploratory or confirmatory (Goswami and Polly, 2010b). Exploratory analyses (e.g., cluster analyses) make fewer *a priori* assumptions but are typically less informative and less consistent than confirmatory analyses (e.g., RV coefficient, covariance ratio). The recent development of a maximum likelihood approach to assessing modularity, EMMLi (Goswami and Finarelli, 2016), advances the concept of exploratory analyses by allowing the simultaneous assessment of competing modularity hypotheses. The most likely modularity hypothesis returned by EMMLi can then be statistically tested with a confirmatory analysis such as covariance ratio (CR; Adams, 2016).

Evolutionary rates are regularly estimated in extant taxa using molecular sequences, which can provide an accurate basis for estimating relative divergence times (Futuyma, 2005). This method is, of course, impossible with older fossil taxa because DNA sequences are not preserved over long

timescales. One approach in estimating divergence times of fossil taxa is to model character evolution under the Mk model (Lewis, 2001). A development of this method employs continuous quantitative characters derived from 3D landmark data for Bayesian inference of species divergence times (Álvarez-Carretero et al., 2019). This method can be employed in the estimation of branch lengths for separate phenotypic modules, providing a relative measure of evolutionary rate using the σ^2_{mult} statistic for multivariate data (Adams, 2014). Rates can be estimated for both entire modules and for individual landmarks with this method, and can inform us of differential levels of selection across an organism (Felice et al., 2018). This can include identifying sexually selected traits, which are expected to undergo rapid evolution (Knell et al., 2012; Cooney et al., 2019; Stubbs et al., 2019)

1.3.3 Data collection

Many techniques exist for capturing three-dimensional shape data from specimens. Computed tomography (CT) uses x-rays to build a 3D volumetric model, and can distinguish between materials of different densities to visualise internal structure. The proliferation of micro-CT (µCT) scanners in many museums and universities has enabled data collection on a large scale. A major limitation of CT scanners is their size; most scanners available to researchers in biological and Earth sciences cannot handle samples as large as a typical ceratopsian skull. Larger CT scanners are produced for engineering and are used extensively in automotive and aerospace industries, but costs of use combined with specimen transportation can be prohibitive.

Surface data from large specimens can now be cheaply and easily collected using structured light scanners, surface laser scanners and photogrammetry (Marcey et al., 2018). Photogrammetry allows the construction of accurate three-dimensional models of specimens using an ordinary camera and specialist software, providing a cheap and flexible method for data collection (Falkingham, 2011; Bennett, 2015). Photogrammetry has been used extensively in forensics (Urbanova et al., 2015), archaeology (Van Damme, 2015) and geography (Tonkin et al., 2016) in recent years. Photogrammetry has additional benefits not available to other forms of surface scanning; models can be constructed

using any set of photographs covering a specimen in sufficient detail, and can be used to construct models of specimens in museum galleries that are inaccessible (behind glass, for example). Not only can three-dimensional models of specimens be constructed, but the accurate measurement of point-to-point distances can be made from the resulting scans using imaging software. Although it is becoming more common in museum digitisation programmes, the use of photogrammetry in data collection for biological applications so far remains limited (Waite et al., 2011; Freiss, 2012; Knauss and Yacobucci, 2014; Meise et al., 2014), and there is much scope for its use in providing digital models for use in geometric morphometric analyses.

1.3.4 Limitations of fossil specimens

Using fossil specimens in any analysis of shape presents a number of potential problems. Firstly, fossil vertebrate specimens are rare and sample sizes are usually limited. Although a few dinosaur taxa are known from a large number of specimens, this is the exception rather than the rule (Benton, 2015). Secondly, palaeontological specimens have often been subjected to the effects of taphonomic deformation during fossilisation including breakage, warping and shear (Lawing and Polly, 2010). This has obvious consequences for morphometric analyses because it is an inaccurate representation of natural biological form, and this taphonomic deformation must be taken into account (Angielczyk and Sheets, 2007). Methods have been developed to allow for the retrodeformation of structures distorted in this way, which can allow for the inclusion of specimens which would previously have been omitted due to their condition (Tallman et al., 2014; Lautenschlager, 2016). Correction is important in datasets which are often limited by number of viable specimens.

1.4 Aims and objectives

This aims of this project are to use three-dimensional geometric morphometrics to investigate patterns of morphological variation in ceratopsian dinosaurs and establish whether they fit predictions of traits under socio-sexual selection, using modularity, allometric and evolutionary rates analysis. These will be achieved with the following aims:

1. Assess patterns of intraspecific variation in ceratopsians with a discrete character matrix to test predictions of the species recognition hypothesis
2. Assemble the most comprehensive data set of accurate, three-dimensional digital scans of ceratopsian crania to date for the purpose of geometric morphometrics analysis.
3. Using 3D geometric morphometrics, investigate patterns of modularity, growth, variation and possible sexual dimorphism in the skull of the ceratopsian dinosaur *Protoceratops andrewsi.*
4. Using 3D geometric morphometrics, investigate interspecific variation and modularity in a number of ceratopsian taxa, putting morphological evolution in a phylogenetic context.
5. Estimate divergence times and evolutionary rates of ceratopsian taxa using whole skulls and separate cranial modules, employing a recently developed Bayesian method optimised for continuous characters.

1.5 Hypotheses

1. Exaggerated traits in ceratopsian skulls, typically associated with display, will not show greater divergence in sympatric taxa than in non-sympatric taxa.
2. The ceratopsian cranium will show a significant modular structure, with putative ornamental/signalling traits forming distinct modules.
3. Intraspecific patterns of growth, in the form of changes in shape and size of modules containing exaggerated traits, and morphological variation of exaggerated structures will resemble those seen in sexually selected traits of extant organisms.
4. Modules associated with display with show greater interspecific morphological disparity than other modules.
5. Modules associated with display will show higher estimates for evolutionary rates than other modules.

Chapter 2

Patterns of divergence in the morphology of ceratopsian dinosaurs: sympatry is not a driver of ornament evolution.

(This chapter was published as: Knapp A, Knell RJ, Farke AA, Loewen MA and Hone DWE (2018). Patterns of divergence in the morphology of ceratopsian dinosaurs: sympatry is not a driver of divergence. *Proc. R. Soc. B.* **285;** DOI: 10.1098/rspb.2018.0312)

2.1 Abstract

Establishing the origin and function of unusual traits in fossil taxa provides a crucial tool in understanding macroevolutionary patterns over long periods of time. Ceratopsian dinosaurs are known for their exaggerated and often elaborate horns and frills, which vary considerably between species. Many explanations have been proposed for the origin and evolution of these 'ornamental' traits, from predator defence to socio-sexual dominance signalling and, more recently, species recognition. A key prediction of the species recognition hypothesis is that two or more species possessing divergent ornamental traits should have been at least partially sympatric. For the first time I test this hypothesis in ceratopsians by conducting a comparison of the morphological characters of 46 species. A total of 350 ceratopsian cladistic characters were categorised as either 'internal', 'display' (i.e. ornamental) or 'non display'. Patterns of diversity of these characters were evaluated across 1035 unique species pairs. Display characters were found to diverge rapidly overall, but sympatric species were not found to differ significantly in their ornamental disparity from non-sympatric species, regardless of phylogenetic distance. The prediction of the species recognition hypothesis, and thus the idea that ornamentation evolved as a species recognition mechanism, has no statistical support among known ceratopsians.

2.2 Introduction

Exaggerated and elaborate anatomical features are well-known among many fossil taxa, including trilobites, amphibians, non-avian dinosaurs and artiodactyls (Knell et al., 2012). These features can take the form of bony processes, spines, horns, crests, and frills, often with no obvious functional explanation. Several hypotheses have been suggested for the presence and evolution of such ornaments, including predator defence, mechanical support, thermoregulation, social or sexual signalling, and species recognition (Knell and Fortey, 2005; Farke et al., 2009; Padian and Horner, 2011a; Hone et al., 2012). The first three of these proposed explanations have been considered and ruled out in many analyses of specific systems, leaving species recognition and sexual selection as the two main competing hypotheses that could offer a more general explanation for the evolution of ornaments. There is now growing evidence that sexual selection can influence macroevolutionary processes such as speciation, extinction and adaptation. The fossil record offers the opportunity to test these ideas over considerably longer timescales than possible in extant organisms.

The Ceratopsia was a major clade of non-avialan dinosaurs (hereafter 'dinosaurs') of over 70 known species, all of which possessed large, ornamented, morphologically diverse skulls (Dodson, 1998; Sampson and Loewen, 2010; n.b., 'Ornament' refers here to any exaggerated morphological feature that was externally visible in life and has no obvious utilitarian function, presumably functioning in part as a visual signal. We do not distinguish between ornaments and weapons to avoid presupposing function; McCullough et al., 2016). Ceratopsians are well-represented in the fossil record and, coupled with their diverse skull morphology and rapid species turnover, are well-suited for the study of macroevolutionary patterns. Cranial ornamentation in ceratopsians variously takes the form of frills (composed of enlarged parietal and squamosal bones), nasal and postorbital horns, prominent jugal ('cheek') spikes, and epiossifications around the posterior margin of the frill (Fig. 2.1; Sereno, 2010). Sexual dimorphism is not known from any ceratopsian species (Maiorino et al., 2015), and no similar ornamentation is found in extant taxa. Early ceratopsians, such as *Psittacosaurus* and *Liaoceratops*

(Fig. 2.1A), had combinations of enlarged jugal spikes, and small, incipient frills (Dodson, 1998). Enlarged frills and horns appeared first in the basal neoceratopsian *Zuniceratops* (Wolfe et al., 2010), and appear to have reached their peak diversity and complexity in the Centrosaurinae between 80 and 70 MA (Fig. 2.1) (Sampson and Loewen, 2010; Weishampel; et al., 2010). Despite the great diversity in ornament morphology, at no point were horns or frills completely lost in any ceratopsian lineage once established (Dodson et al., 2004).

Sexual selection is difficult to determine in extinct taxa because of the lack of behavioural or genetic data, and there is no single, reliable means of recognising it from morphology alone (Knell et al., 2012). The absence of any obvious sexual dimorphism has led some to conclude that sexual selection cannot provide an explanation for ornamentation in ceratopsians, and that the best explanation is therefore species recognition (Padian and Horner, 2011a). Species recognition has been proposed as an alternative hypothesis for the divergence of ornaments in extant species as a means of avoiding hybridisation; closely-related sympatric species should, it is argued, develop contrasting morphological characters to differentiate themselves, a process known as reproductive character displacement (Brown and Wilson, 1956; Grant 1972; Sætre et al., 1997; Pfennig and Pfennig, 2009; Okamoto and Grether 2013). Such characters are not expected to have an obvious mechanical function, and the process is distinct from ecological character displacement (Futuyma, 2005). Morphological characters involved in species recognition are expected to function early on in social interactions between individuals (Hieronymous et al., 2009) and should be highly visible, an obvious characteristic of highly ornamented ceratopsian skulls.

Padian and Horner (2011a) suggested two tests for identifying species recognition traits in extinct animals. These are;

1) Patterns of diversification of ornaments should be relatively random
2) There should be evidence that at some point, several closely related species with divergent ornaments lived at the same time in environments that at least partially overlap

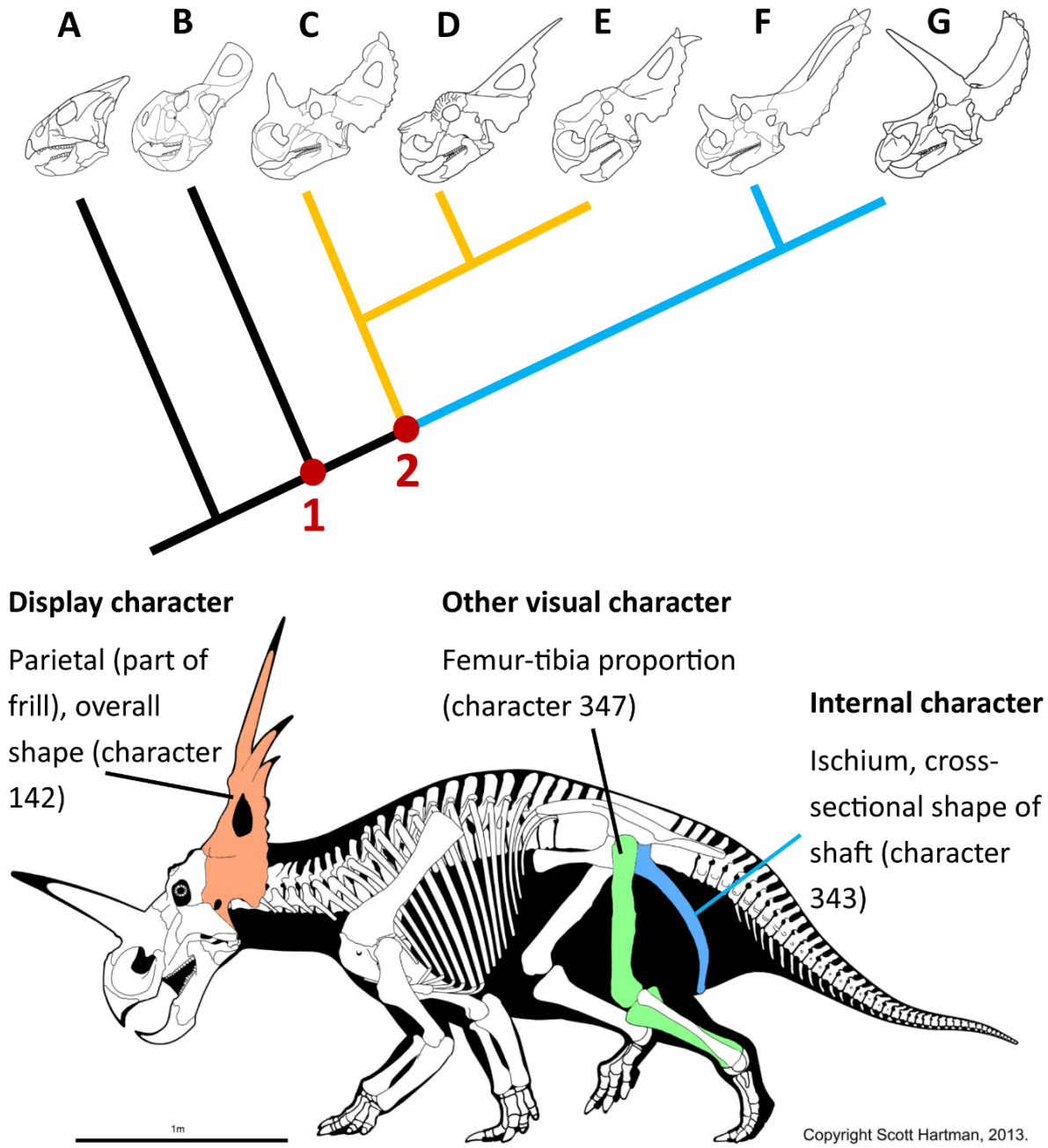

Figure 2.1: Line drawings of ceratopsian skulls in simplified phylogeny, illustrating morphological diversity of cranial ornaments within the clade. **A**: *Liaoceratops yangzigouensis*; **B**: *Protoceratops andrewsi*; **C**: *Centrosaurus apertus*; **D**: *Achelousaurus horneri*; **E**: *Pachyrhinosaurus canadensis*; **F**: *Chasmosaurus belli*; **G**: *Triceratops horridus*. Node 1 represents the clade Coronosauria, containing all taxa with enlarged frills. Node 2 represents the clade Ceratopsoidea, encompassing Centrosaurinae (orange branch) and Chasmosaurinae (blue branch), within which the majority of cranial ornamental diversity, and all horned taxa, are found. Lower image: full-body illustration of *Styracosaurus albertensis* (Centrosaurinae) with highlighted examples of the three different character classes used in this study (refer to Appendix table A1 for full list of characters). Line drawings courtesy of Scott Hartman.

The first hypothesis is not useful in distinguishing species recognition traits since sexually selected features also sometimes show apparently 'random' patterns of divergence (Prum, 1997; Emlen et al., 2005; Knell and Sampson, 2011; Qvarnstrom et al., 2012). Given the reasonably dense fossil record of the Ceratopsia, however, it should be possible to test a modified version of the second hypothesis using species that are known to have been sympatric. If species recognition is a driver of trait evolution, then morphological disparity in ornamentation should be significantly higher between sympatric species because species that are not sympatric have minimal selective pressure to evolve obvious visual differences (Grant, 1972). Species recognition should therefore promote the divergence of these traits to a greater degree between sympatric species than between species which did not coexist. The species recognition hypothesis can be easily tested with knowledge of morphology and species distributions, both of which are well-known in ceratopsians.

Here, I perform the first evaluation of species recognition in a fossil vertebrate clade with an assessment of ceratopsian dinosaur data. I combine information on ornamental and other traits with information on sympatry to test the hypothesis that sympatric ceratopsian taxa evolved features that visually distinguish them from one another.

2.3 Methods

All known valid ceratopsian species were listed using existing sources (Weishampel et al., 2004; Ryan et al., 2010). Known geographical occurrences for each species were determined from the primary literature (Table 2.1). Temporal ranges follow published dates of their host formations, using more precise dates for occurrences within the formation where possible.

Phylogenetic information was compiled from a number of sources, and a composite tree constructed (Fig. 2.2; Xu et al., 2006; Makovicky 2010; Xu et al., 2010; Sereno, 2010; Sampson et al., 2010; Sampson and Loewen, 2010; Longrich,2011; Mallon et al., 2013; Sampson et al., 2013; Farke et al., 2014; Brown

and Henderson, 2015; Zheng et al., 2015; Lund et al., 2016; Mallon et al., 2016). The phylogenetic distance between each species pair was calculated using a method (Grafen, 1989) adapted for extinct taxa; the number of speciation events since the last common ancestor was counted for each possible species pair, omitting species radiations that occurred after the more recent occurrence of the two species. This avoids overweighting of clades that subsequently underwent large species radiations.

Trait comparisons were performed using a total of 350 defined and scored cladistic characters (Appendix A1). Each character was classed as either *external* or *internal,* based on whether it was likely to influence the exterior appearance of the animal in life. External characters were further subdivided into *display* and *non-display*, defined as whether or not the character in question was deemed whole or part of an ornament (i.e. in ceratopsians, the frill, horns and bosses of the skull). The classification of characters in this way resulted in three character classes:

Internal characters (196 characters)

Display characters (86 characters)

Non-display (other) characters (68 characters)

Each species pair was compared using the formula:

$$\boldsymbol{Difference\ index} = \frac{|\boldsymbol{n_{tot}} - \boldsymbol{n_{same}}|}{\boldsymbol{n_{tot}}}$$

where $\boldsymbol{n_{tot}}$ is the total number of characters present in both taxa and $\boldsymbol{n_{same}}$ is the number of characters with matching states in both taxa. This resulted in a 'difference index' value of between 0 and 1, where species pairs possessing all identical characters are scored 0 and absolutely different pairs are scored 1.

Table 2.1: Temporal calibrations and geographical locations of ceratopsian species. Taxa that are included in the morphological character state analysis are indicated in bold type. Region abbreviations: Asia: **A**; North America: **NA**; Europe: **E**.

Taxon	Region	Lower Bound	Upper Bound	Source
Yinlong downsi	A	161.2	155.7	Xu et al., 2006
Chaoyangsaurus youngi	A	168.3	166.1	Zhao et al., 1999
Hualianceratops wucaiwnensis	A	162.2	159.7	Han et al., 2015
Xuanhuaceratops niei	A	152.6	145	Zhao et al., 2006
Psittacosaurus lujiatunensis	A	132	127	Swisher et al., 1999; Changfu et al., 2006
Psittacosaurus mongoliensis	A	124	108	Sereno, 2010
Psittacosaurus neimongoliensis	A	113.5	112.5	Sereno, 2010
Psittacosaurus meileyingensis	A	121	119.6	Sereno, 2010
Psittacosaurus sibiricus	A	129.4	113	Sereno, 2010
Psittacosaurus sinensis	A	121	119	Gao and Cheng, 1999; Sereno, 2010
Mosaiceratops azumai	A	93	77	Zheng, Jin and Xu, 2015
Liaoceratops yangzigouensis	A	125	121	Xu et al., 2002
Yamaceratops dorngobiensis	A	71.5	70.5	Shuvalov, 2000
Auroraceratops rugosus	A	121	119.6	You et al., 2005
Archaeoceratops yujingziensis	A	125	121	You, Tanoue and Dodson, 2010
Archaeoceratops oshimai	A	121	119.6	You and Dong, 2003
Aquilops americanus	NA	109	104	Farke et al., 2014
Unescoceratops koppeihusi	NA	76.5	75.8	Ryan et al., 2012
Grypoceratops morrisoni	NA	84.6	83.6	Ryan et al., 2012
Zhuchengceratops inexpectus	A	76	73.5	Xu et al., 2010a
Helioceratops brachygnathus	A	100	72	Liyong et al., 2009
Koreaceratops hwaseongensis	A	113	103	Lee et al., 2010
Asiaceratops salsopaludalis	A	99.5	98.5	Ryan et al., 2012
Cerasinops hodgkissi	NA	78	76.5	Ryan et al., 2012
Montanoceratops cerorhynchus	NA	74	66	Chinnery and Weishampel, 1998
Prenoceratops pieganensis	NA	80	76.5	Ryan et al., 2012
Leptoceratops gracilis	NA	66.8	66	Ott, 2007
Udanoceratops tschizhovi	A	72	71	Dodson, 1996
Graciliceratops mongoliensis	A	100.5	83.6	Maryańska and Osmólska, 1975; Hicks et al, 1999
Protoceratops andrewsi	A	76.38	72.05	Shuvalov, 2000; Dashzeveg et al., 2005
Protoceratops hellenikorhinus	A	76.38	72.05	Shuvalov, 2000; Lambert, 2001; Dashzeveg et al., 2005
Ajkaceratops kozmai	E	86	84	Osi et al., 2010
Bagaceratops rozhdestvenskyi	A	81	79	Maryańska and Osmólska, 1975
Turanoceratops tardabilis	A	91	90	Sues and Averianov, 2009
Zuniceratops christopheri	A	91	90	Wolfe et al., 2010
Diabloceratops eatoni	NA	79.5	79.1	Kirkland and Deblieux, 2010; Roberts et al., 2013
Machairoceratops cronusi	NA	80.1	77	Lund et al., 2016
Albertaceratops nesmoi	NA	78.2	76.4	Ryan, 2002
Medusaceratops lokii	NA	78	77	Ryan, Russell and Hartman, 2010
Xenoceratops formostensis	NA	79.5	79	Ryan, Evans and Shepherd, 2012
Wendiceratops pinhornensis	NA	79	78.7	Evans and Ryan, 2015
Sinoceratops zhuchengensis	A	79	73.5	Xu et al., 2010
Nasutoceratops titusi	NA	76	75.5	Lund, 2010
Avaceratops lammersi	NA	79	78	Dodson, 1986
Spinops sternbergorum	NA	78	77	Farke et al., 2011
Coronosaurus brinkmani	NA	78	77	Ryan and Russell, 2005

Centrosaurus apertus	NA	77	75.5	Arbour, Burns and Sissons, 2009
Styracosaurus albertensis	NA	75	74.5	Sampson and Loewen, 2010
Rubeosaurus ovatus	NA	75	74	McDonald and Horner, 2010
Einiosaurus procurvicornis	NA	75	74	Sampson, 1995
Achelousaurus horneri	NA	75.8	74	Sampson, 1995
Pachyrhinosaurus canadensis	NA	72	68.3	Ryan et al., 2010
Pachyrhinosaurus lakustai	NA	73.5	72.5	Currie, Langston and Tanke, 2008
Pachyrhinosaurus perotorum	NA	70	69	Fiorillo and Tykoski, 2011
Kosmoceratops richardsoni	NA	76.5	76	Sampson et al., 2010
Spiclypeus shipporum	NA	76.2	75.2	Mallon et al., 2016
Vagaceratops irvinensis	NA	75	74.5	Sampson and Loewen, 2010
Agujaceratops mariscalensis	NA	77.5	77	Sampson et al., 2010
Mercuriceratops gemini	NA	79	77	Ryan et al., 2014
Mojoceratops perifania	NA	76.5	75	Longrich, 2010
Chasmosaurus belli	NA	77	76	Sampson et al., 2010
Chasmosaurus russelli	NA	76	75	Sampson et al., 2010; Longrich, 2010
Utahceratops gettyi	NA	76.5	75.5	Sampson et al., 2010
Pentaceratops sternbergi	NA	74.5	73.5	Sampson et al., 2010
Coahuilaceratops magnacuerna	NA	71	70.5	Sampson et al., 2010
Anchiceratops ornatus	NA	72	71.5	Sampson et al., 2010
Bravoceratops polyphemus	NA	70	69	Wick and Lehman, 2013
Regaliceratops peterhewsi	NA	68.5	67.5	Brown and Henderson, 2015
Arrhinoceratops brachyops	NA	71.5	70.6	Sampson and Loewen, 2010
Ojoceratops fowleri	NA	68	67.5	Sampson et al., 2010
Titanoceratops ouranos	NA	74.7	73.6	Longrich, 2011
Torosaurus latus	NA	66.8	66	Farke, 2007
Torosaurus utahensis	NA	69.5	68.5	Sullivan, Boere and Lucas, 2005
Eotriceratops xerinsularis	NA	68.5	68	Sampson et al., 2010
Nedoceratops hatcheri	NA	67	66	Farke, 2011
Triceratops horridus	NA	66.8	66.4	Sampson et al., 2010 ; Scanella et al., 2014
Triceratops prorsus	NA	66.4	66	Renne et al., 2013 ; Scanella et al., 2014

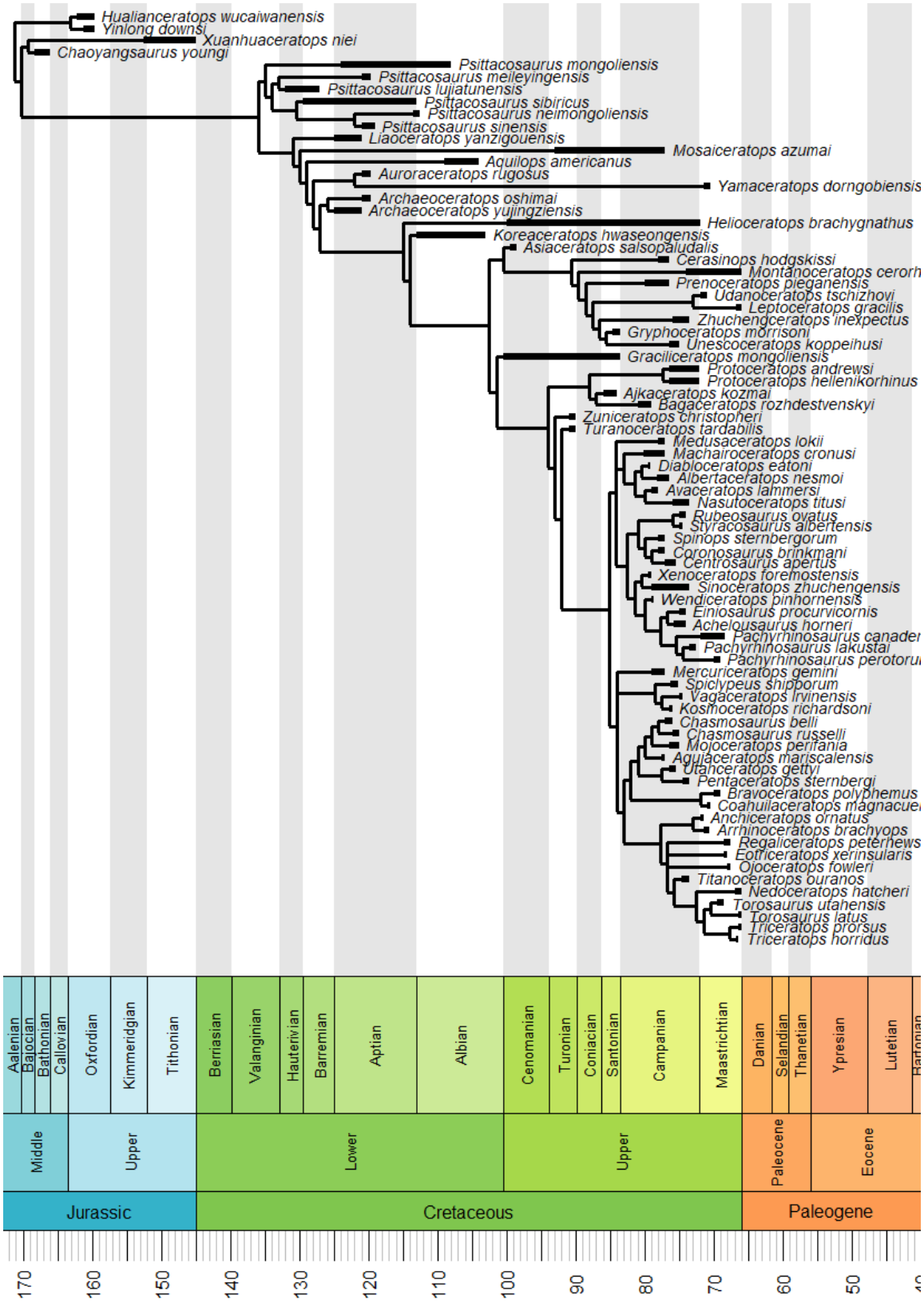

Figure 2.2: Phylogeny of all known ceratopsian species, used to calculate relative phylogenetic distances. Estimated species ranges are indicated by thick bars at branch tips. Created using *strap* package for R (Bell and Lloyd, 2014).

Because of the low confidence arising from comparisons of poorly known species with many unknown characters, a minimum cut-off value of 40% possession of characters was used. This retained a high number of species in the analysis while simultaneously excluding those known from limited remains. This latter group consisted of mainly the earlier, more basal members of the clade, and was deemed an acceptable omission since this study is concerned with the exaggerated structures associated primarily with Neoceratopsia. After these criteria were applied, a total of 46 ceratopsian species were retained from the initial total of 77. Phylogenetic distance values were not altered.

Comparisons of species pairs were determined by a pairwise comparison grid of $\frac{n^2-n}{2}$ possible combinations, where *n* is the number of taxa. If sympatry is defined as the as the situation where species pairs are known to be found in the same place and at the same time, we classify only 38 species pairs of a total of 1035 used in this study as sympatric. Given the incomplete nature of the fossil record and the possibility of dating errors, however, this is likely to be an underestimate and so a series of criteria were used to describe how likely each species pair was to have been present in the same place at the same time, as follows:

- **Sympatric**: species pairs are found in the same location with overlap in their temporal range (38 pairs)
- **Allopatric**: species pairs overlap in their temporal range and are found on the same continent, but are not known from the same locality (63 pairs)
- **Pseudo-sympatric**: species pairs are found in the same region and do not overlap temporally, but are dated within 1 million years of one another (119 pairs)
- **Contemporary**: species pairs overlap in their temporal range (a combination of sympatric and allopatric criteria; 101 pairs)
- **Not sympatric**: species pair not known to overlap geographically within 1 million years temporally (815 pairs)

Padian and Horner (2011a) suggested the 'ghost of species recognition' concept to test the species recognition hypothesis; divergent clades with 'exaggerated features' need only to have been known to have coexisted. This hypothesis is untestable as presented because it does not require physical evidence of contemporary forms, and we cannot know if contemporary lineages were morphologically distinct without fossil evidence. Furthermore, all divergent lineages would at some time have been contemporary by definition. In an attempt to address this concept, the 'contemporary' category was created by merging the sympatric and allopatric categories. Categorising species in this way ensures that fossil evidence is available for comparison of the morphology of contemporary species, and avoids speculating that morphological divergence had occurred at a specific point.

To ensure that the relatively smaller samples of the sympatry categories were not affecting comparison, species pairs were randomly sampled from the complete dataset to simulate populations of the same size as each sympatry category. This process was repeated 10000 times for each category to provide a distribution of regression parameters, and the equivalent values for each sympatry category were compared with these distributions.

Finally, each character was individually assessed to test if sympatry was driving the divergence of individual traits. This was done by individually comparing the mean difference values of each character in the three main sympatry classes with the equivalent means in the remaining, non-sympatric species pairs.

2.4 Results

All unique pairwise comparisons, excluding same-species comparisons ($\frac{n^2-n}{2} = 1035$), were plotted against relative phylogenetic distance (Fig. 2.3, row A). Trend lines in all cases are fitted with a second-order polynomial regression. This method captured the distribution of data while keeping the number of parameters low (Montgomery and Peck, 1992). Morphological disparity increases with increasing relative phylogenetic distance, but the form of this relationship varies with the different classes of

trait. The relatively low intercept values of internal (-0.028) and non-display characters (0.033), and shallower slope at low phylogenetic distances suggests comparatively high levels of conservation of these characters between closely related species. In contrast, display characters show a higher intercept (0.100) across all species pairs (Fig. 2.3, cell A2), and these characters are notably more divergent in closely related species pairs than are the internal or non-display characters.

Rows B-E of Figure 2.3 show the divergence values for each character class when the species pairs are divided into the four sympatry categories. In the plots for the display characters, the allopatric and contemporary sympatry categories appear to depart slightly from the trend seen for all species pairs, but only at high relative phylogenetic distances. The trend lines for sympatric (B1) and pseudo-sympatric (D1) species pairs in the non-visual character class show a small deviation from the all-species trend at intermediate and high values of relative phylogenetic distance respectively. This is not seen in the plots of this character class for other sympatry categories.

The three second-order polynomial regression parameter values obtained for each of the observed character classes were plotted with the values obtained from random sampling for all species pairs (Fig. 2.4). All sympatry category parameters appear to fall well within the distribution of parameters from the randomly sampled datasets.

Z-scores were calculated for all the regression parameters, and all fell well within ±1.96 standard deviations (95% confidence interval) from the mean of the distribution of parameter values of the randomly sampled datasets (Table 2.2). This analysis, coupled with visual inspection of the plots in Figure 2.3, suggests that sympatry does not have a significant effect on divergence of morphology in these groups.

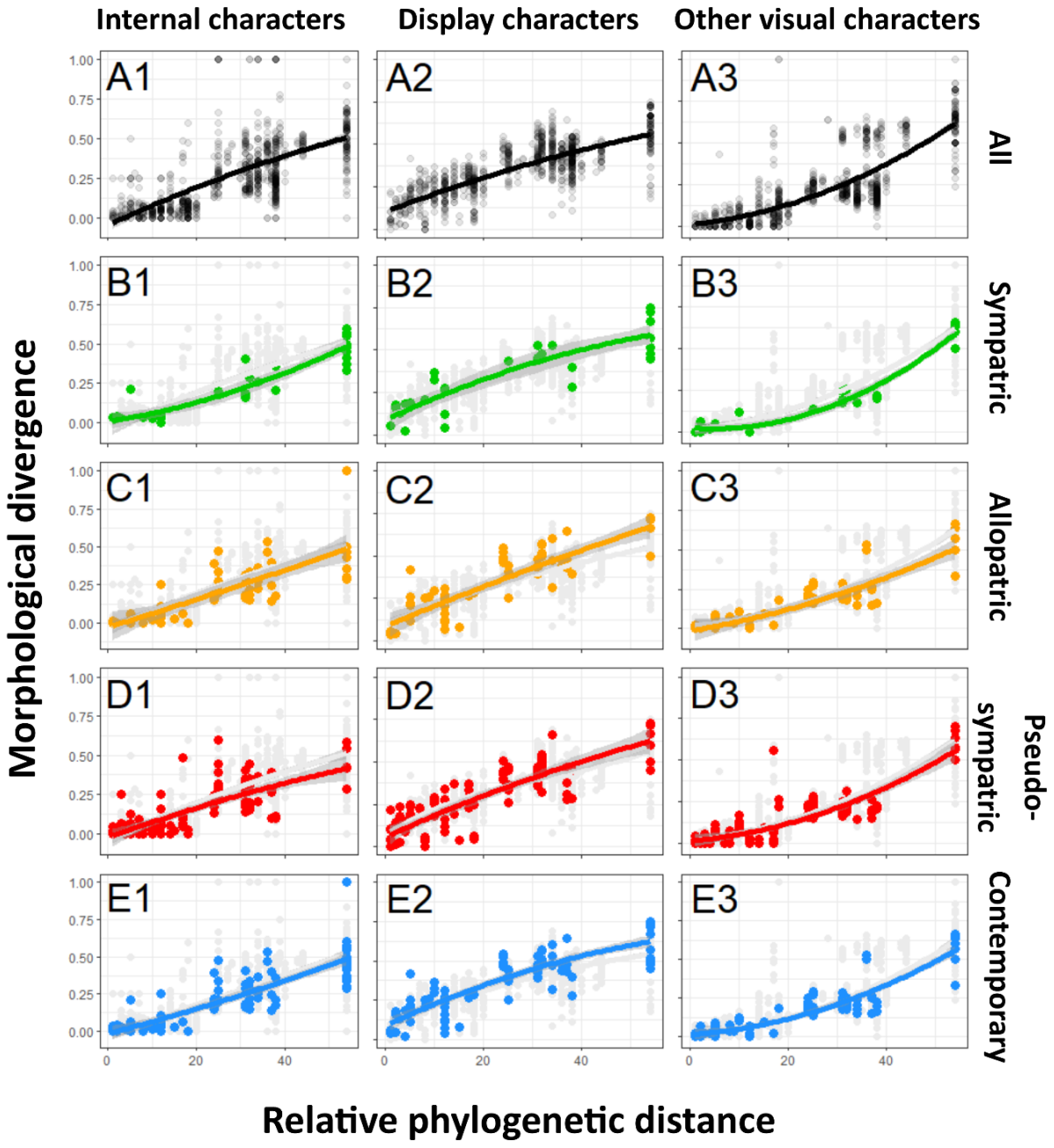

Figure 2.3: Pairwise comparison plots for sympatry categories (rows **A - E**) and character classes (columns 1 - 3). Species pairs that do not fall into sympatry categories are shown in light grey in rows **B** to **E** for reference. Second order polynomial regressions are fitted with confidence intervals are set at 95%.

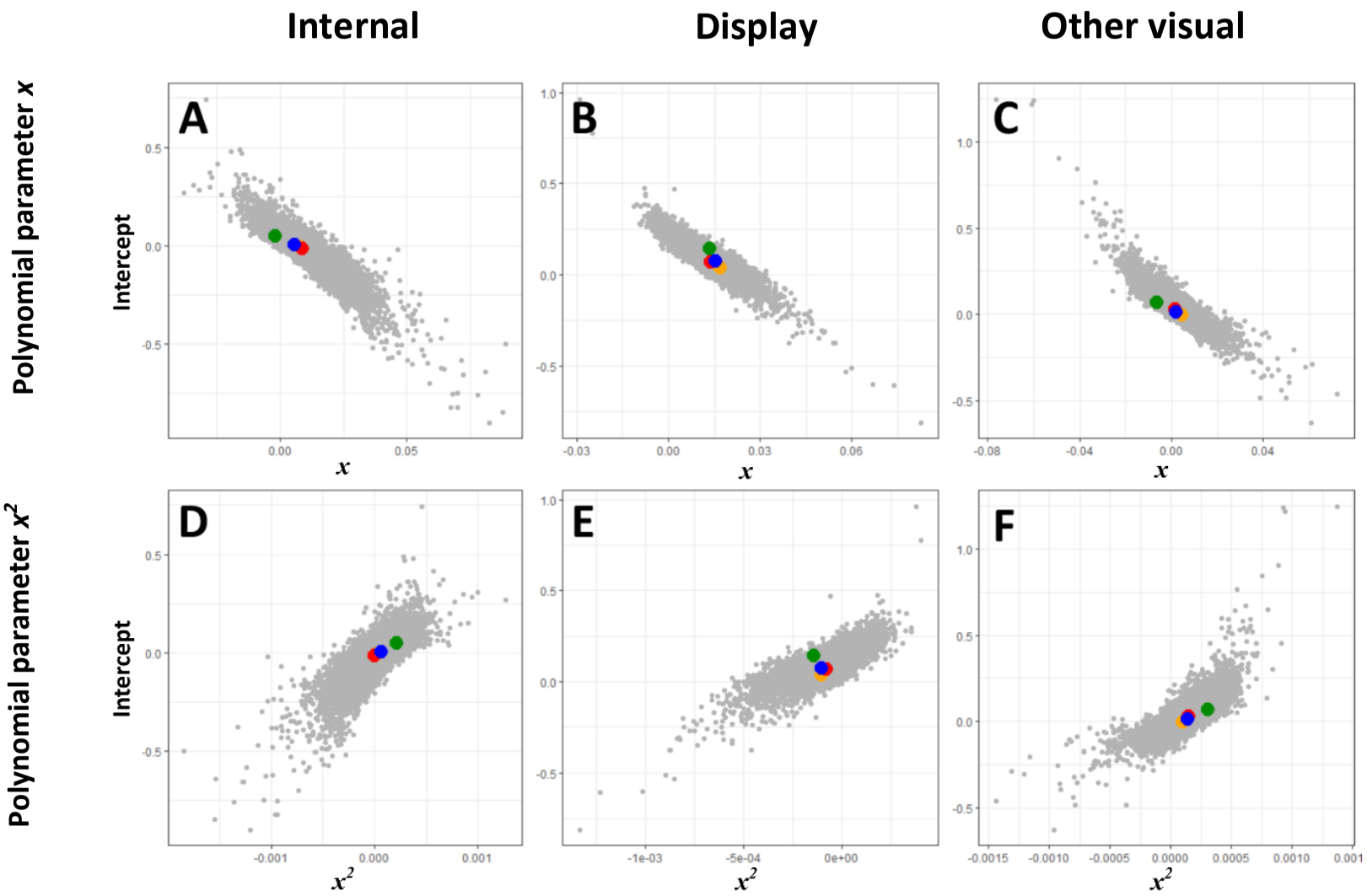

Figure 2.4: Distributions of second-order polynomial model output parameters for 10000 randomly sampled n species pairs of internal (**A** and **D**), display (**B** and **E**), and other visual (**C** and **F**) character classes. Randomly sampled values are shown in grey. Values calculated for sympatry categories are overlaid in coloured points for each character class (green: sympatric; orange: allopatric; red: pseudo-sympatric; blue: contemporary).

Figure 2.5: Mean difference values of each individual character for each main sympatry category for internal (**A**), display (**B**), and other visual (**C**) character classes (n.b. here, characters are numbered according to order rather than their corresponding numbers from the character list). Means are shown for sympatric (green), allopatric (orange), pseudosympatric (red) and all other (black) species pairs. Characters range along the y-axis from 0 (all identical) to 1 (all different).

Table 2.2: z-scores of three second-order polynomial regression parameters which describe the fit of the regression curve to the data. Polynomial regressions were carried out on observed species pairs vs. 10000 randomly sampled species pairs of number *n* for each sympatry category, and the values listed here thus describe the difference in regression curve between observed and randomly-sampled data for each sympatry category (as outlined in the chapter introduction). All parameters fall within ±1.96 standard deviations, representing a 95% confidence interval.

	Internal						
		intercept		***x***		***x²***	
	n	*z*	*p*	*z*	*p*	*z*	*p*
Sympatric	38	0.65	0.516	-0.99	0.322	0.80	0.424
Allopatric	63	-0.14	0.889	-0.16	0.873	0.08	0.936
Pseudosympatric	119	-1.41	0.159	-0.51	0.610	0.00	1.00
Contemporary	101	0.39	0.697	-0.73	0.465	0.53	0.596
	Display						
		intercept		***x***		***x²***	
	n	*z*	*p*	*z*	*p*	*z*	*p*
Sympatric	38	-0.07	0.944	0.24	0.810	-0.06	0.952
Allopatric	63	-0.30	0.764	0.73	0.465	-0.02	0.984
Pseudosympatric	119	-1.36	0.174	0.88	0.379	-0.21	0.834
Contemporary	101	-0.45	0.653	1.16	0.246	-0.52	0.603
	Other visual						
		intercept		***x***		***x²***	
	n	*z*	*p*	*z*	*p*	*z*	*p*
Sympatric	38	-0.01	0.992	-0.79	0.430	0.70	0.484
Allopatric	63	-0.96	0.337	0.98	0.327	-1.24	0.215
Pseudosympatric	119	-0.76	0.447	0.20	0.841	-0.49	0.624
Contemporary	101	-0.36	0.719	0.39	0.697	-0.58	0.562

Mean difference values for individual characters only show noticeably greater values in sympatric species pairs than other sympatry categories for two display characters (157 and 182; Fig. 2.5). In only 6 out of a total of 86 display characters (Fig. 2.5B) do sympatric species pairs show the highest average, and only two of these have a mean value of 1, indicating consistent difference. These two characters are represented by only one and three sympatric species pairs, and so are likely to be anomalous due to small sample size. The lack of any clear pattern in the display characters plot (Fig. 2.5B) does not suggest that individual characters are used as distinguishing traits in sympatric species. Internal characters (Fig. 2.5A) also show universal differences (mean value = 1.00) in three instances. As with display characters, these are associated with small numbers of species pairs sharing known states in

each character (Characters 252, 262, and 296, representing two, two and one species pairs for each character respectively).

2.5 Discussion

The results of this study show no support for the hypothesis that sympatry correlates with higher ornament divergence in ceratopsian dinosaurs, nor for the wider species recognition explanation (Padian and Horner, 2011a) for the evolution of horns, frills and other display traits in the Ceratopsia. Firstly, the divergence between ornaments of contemporary species is not significantly different from randomly sampled species, either individually or when considered as a suite of complimentary ornamental traits. This is true regardless of the level of sympatry, offering little support to the idea that the driver of ornament diversity was the need to differentiate between contemporary species. Secondly, although ornaments appear to show more rapid initial divergence than other structures, this pattern is not expected to be exclusive to species recognition-specific features; those involved in sexual selection or resource acquisition are known to undergo rapid morphological evolution and divergence (Boag, 1981; Prum, 1997; Knell et al., 2012).

Several criticisms have been made of the species recognition hypothesis, chiefly that the drive to differentiate closely related species should evolve towards minimal cost (Knell and Sampson, 2011). Under the circumstances where two parties benefit from differentiating one another, low-cost signals are evolutionarily stable since neither party would benefit from either a dishonest or costly signal (Maynard Smith and Harper, 2003). Although attempting to explain the divergence of ornamentation among ceratopsians, species recognition does not explain why all neoceratopsians evolved and maintained broadly similar structures in order to differentiate themselves from other species. The skulls of some neoceratopsians such as *Chasmosaurus* (Fig. 2.1F) have been shown to be such a large component of overall body mass that the centre of mass of the animal is shifted forwards to a degree

that renders them obligately quadrupedal (Maidment et al., 2014). The amount of resources and energy required to grow and maintain such a structure is not consistent with a low-cost modification.

The few examples of species recognition-driven character divergence (as opposed to ecological character displacement) in extant species suggest low-cost modifications to pre-existing features that are common to both taxa in the non-overlapping portions of their ranges. Examples include facial markings in the rock nuthatches, *Sitta tephronata* and *S. neumayer* (Grant, 1972), plumage colouration in trogons (Bitton and Doucet, 2009) and the flycatcher *Ficedula* (Sætre et al., 1997), and dewlap colouration in the lizard genus *Anolis* (Van Hooydonck et al., 2009). No example is known of a large, costly structure evolving to serve primarily as a recognition signal in extant taxa (Hone and Naish, 2013). Unique phenotypes may, of course, enable a member of a species to easily identify conspecifics, but for the examples known in extant taxa a different explanation of their origin exists (Zahavi and Zahavi, 1997). An example is known of a so-called 'social mimic' in extant bird taxa, where two visually identical species overlap substantially in their ranges and are known to flock and forage together, but are nevertheless genetically distinct (Lopes et al., 2017). There is seemingly no impediment to their stable coexistence that warrants divergence of visual characters, as would be expected if species recognition were important.

An additional result of this study is in the comparison of curves for each character class across all species (Fig 2.3, row A). The intercepts of the curves in both the *internal* (Fig 2.3, A1) and *other visual* (Fig 2.3, A3) categories show a lower, near-zero initial value than that seen in the *display* (Fig 2.3, A2) category. This difference suggests that traits associated with display in ceratopsians diverge at a quicker rate than do other features. This raises two possibilities: display features, implicated in visual communication, generally underwent rapid evolution during divergence of ceratopsian taxa, or that traits with a specific mechanical function (i.e. non-display characters; teeth, limbs, etc.) were under stronger stabilising selection than display characters. The species recognition hypothesis does not appear to adequately account for this phenomenon because the pattern is a general trend observed

across all included taxa, not simply those that are known or are implied to be sympatric. Visual signals are predicted to diverge rapidly under both sexual selection (Knell et al., 2012) and species recognition (Padian and Horner, 2011a), but the effects of species recognition would only be seen in sympatric taxa where failure to distinguish conspecifics is costly.

The largest and most elaborate ceratopsian ornaments are found within the clade Ceratopsoidea, including such well-known taxa as *Centrosaurus, Triceratops* and *Styracosaurus* (Fig. 2.1C, G and main image, respectively; Sampson and Loewen, 2010). The seemingly rapid and random diversification of skull ornamentation within this clade may point to one or several situations acting across it (Maiorino et al., 2017). Firstly, interspecific selection acting in different directions would promote divergence between species. This may occur as a result of sympatric ecological niche partitioning, allopatric ecological selection, or as a result of the need for signalling diversity, as in species recognition (Futuyma, 2005; Padian and Horner, 2011a). Secondly, intraspecific mutually antagonistic coevolution where novelty is favoured creates conditions where arms races within species drive morphological evolution. An example of this is the evolution of weapons for use in intrasexual combat (Emlen, 2008). Thirdly, very flat selective landscapes create conditions where morphology is not constrained to evolve in a particular direction and so is free to evolve randomly from ancestral states. This last explanation seems unlikely given the high cost of ceratopsian ornaments, which were retained in almost all the species within the clade (Sampson and Loewen, 2010). Niche partitioning and species recognition require some degree of interspecific interaction and, thus, sympatry. I have demonstrated here that sympatry has no significant effect on morphological disparity in ceratopsians. In the absence of any functional ecological role for ornamentation in ceratopsians (Hone and Naish, 2013), only intraspecific mutually antagonistic coevolution favouring novelty seem to apply to this clade, given the available evidence.

Sexual selection or social-sexual signalling has previously been proposed as a driver of ornament evolution and diversity in ceratopsians (Dodson, 1976; Horner et al., 1992; Knell and Sampson, 2011;

Knell et al., 2012; Hone et al., 2012; Hone and Naish, 2013). Most studies of sexually selected ornaments and weapons in extant taxa focus on sexually dimorphic examples (Andersson, 1994; Emlen et al., 2005), and there is no clear evidence of sexual dimorphism in Ceratopsia or any other dinosaur clade (Maiorino et al., 2015; Mallon, 2017). Except in extreme examples, large sample sizes are needed to distinguish sexes based on morphology alone (Hone and Mallon, 2017). Furthermore, mutual mate choice is also known to lead to the evolution of similar ornaments in both sexes in extant taxa (Jones and Hunter, 1993; Hone et al., 2012). If sexual selection is indeed the process behind the unique ornamentation of ceratopsians, it points to a set of conditions acting upon ceratopsians without obvious parallel in extant taxa. Nevertheless, sexually selected ornaments are expected to show characteristic patterns of growth, diversity and rapid evolution regardless of the taxa or characters in question (Knell et al., 2012). Some support has been found for this in the positively allometric growth patterns of the ceratopsian *Protoceratops* (Hone et al., 2016), and the patterns of ornament divergence seen in Ceratopsia (Sampson and Loewen, 2010) are similar to those seen in the sexually selected horns of the scarab beetle genus *Onthophagus* (Emlen et al., 2005). Identifying these patterns is a challenge in fossil taxa, but an important step in the study of evolutionary palaeobiology, and evolutionary theory in general.

Chapter 3

Ontogeny and intraspecific variation of the ceratopsian dinosaur *Protoceratops andrewsi*

3.1 Abstract

The purpose of the unique parietal-squamosal frill of ceratopsian dinosaurs has long been a source of debate. Recent studies have supported the hypothesis that the frill is a socio-sexually selected trait, but these findings have been based on limited linear measurements. Here I use three-dimensional geometric morphometrics to examine an ontogenetic series of 31 specimens of *Protoceratops andrewsi*, using a maximum likelihood approach to evaluate phenotypic modularity of the skull and to enable the assessment of relative growth patterns of different skull regions. I find that the frill formed a distinct phenotypic module, suggesting its growth and evolution were somewhat independent from the rest of the skull. The frill was found to have a significantly higher rate of both size and shape change than any other module, and had highest variance. Together, these findings provide the strongest support yet for a socio-sexual role for the frill of *Protoceratops*.

3.2 Introduction

Sexual selection arises from competition for mating opportunities and is predicted to be a powerful driver of evolution (Darwin 1871; Fisher 1930). Experimental data can inform us of its short-term processes in extant taxa but identifying sexual selection in the fossil record is a crucial step in both understanding how it can shape the evolution of clades, and in testing predictions of speciation and extinction (Knell et al., 2012). The large, highly ornamented skulls of ceratopsian dinosaurs have no obvious analogue in living taxa, and the function of the diverse horns and frills borne on them is still a cause for debate (Padian and Horner, 2010; Knell and Sampson, 2011; Hone et al., 2016). Sexual selection has been proposed as a driver of ornament evolution in ceratopsians and has gained support in recent years, but has been rejected by some researchers due to the apparent lack of sexual dimorphism in any ceratopsian taxa (Padian and Horner, 2010). As an explanation, sexual selection is further complicated by the possibility of social selection (West-Eberhard, 1979), which deals with more general intrasexual dominance hierarchies and of which sexual selection can be considered a subset (Kraaijeveld et al., 2007; Tobias et al., 2012).

In common with many other ceratopsian taxa *Protoceratops andrewsi* possesses a large frill projecting caudally from the skull, formed from expansion of the parietal and squamosal bones (Fig. 3.1), and these have been suggested to have evolved under sexual selection (Dodson, 1976; Hone et al., 2016). A relatively large number of complete specimens of *P. andrewsi* are known from a broad ontogenetic range, making it an ideal subject for investigations of ontogenetic trends and intraspecific. Previous studies have used this taxon to address questions of morphological variation, including sexual dimorphism (Dodson 1976; Maiorino et al. 2015) and ontogenetic allometry (Hone et al., 2016; O'Brien et al, 2018).

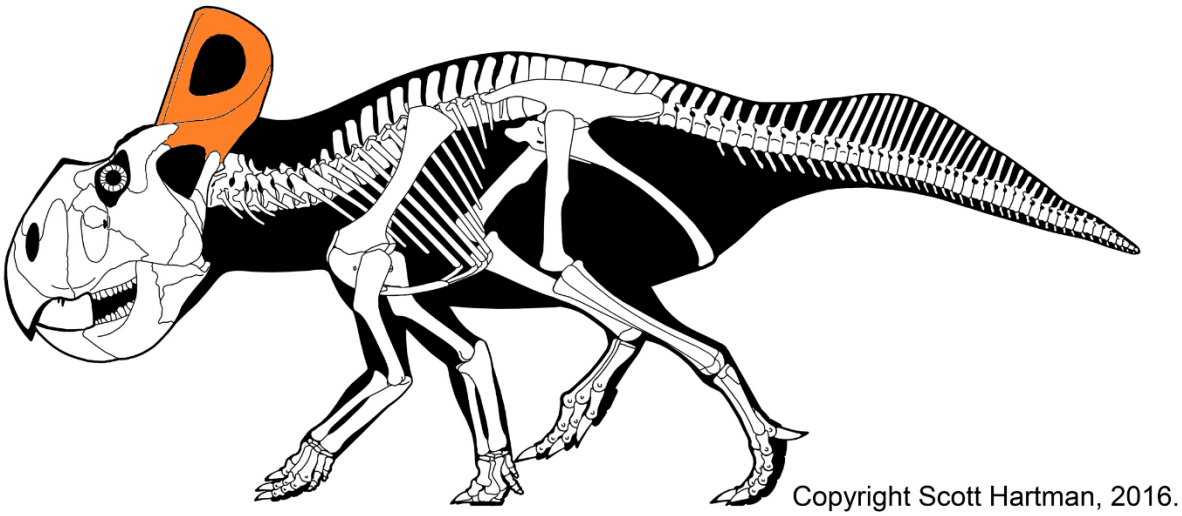

Figure 3.1: Illustration of adult *Protoceratops andrewsi* skeleton, showing prominent parietal-squamosal frill highlighted in orange (Image courtesy of Scott Hartman).

Identifying sexually selected traits in the fossil record is difficult but some patterns can be indicative of sexual selection even if none are completely diagnostic (Knell et al., 2012). As indicators of quality, socio-sexual signals cannot persist in a population without some degree of condition-dependence, and corresponding sensitivity to fluctuating environmental conditions results in heightened trait variability (Eshel et al., 2000; O'Brien et al., 2018). Sexual signalling structures are also expected to scale more steeply with body size than other non-signal traits because they are maximally expressed at sexual maturity and hence growth is accelerated. The frill of *Protoceratops* has been shown to be positively allometric, reflecting this pattern (Tomkins et al., 2010; Hone et al., 2016; O'Brien et al., 2018). To strengthen support when assessing possible socio-sexual selection in the morphology of extinct taxa it is therefore important to combine several lines of evidence such as allometry and variance, putting the putative sexually selected traits in context with other structures.

Ongoing improvements in three-dimensional (3D) shape capture and of 3D geometric morphometric (GM) techniques together enable more comprehensive analyses of shape and allow a wider range of

questions to be addressed using a single dataset (Adams, Rohlf and Slice, 2013; Felice and Goswami, 2017; Felice et al., 2018). Regions of relatively high morphological integration, phenotypic modules, can be identified by comparing patterns of morphological covariance (Klingenberg, 2008; Goswami and Polly, 2010b; Klingenberg, 2014; Goswami and Finarelli, 2016). By partitioning biological structures into discrete units that can be analysed simultaneously, phenotypic modules can serve as the basis of the analysis of growth and variation (Felice, Randau and Goswami, 2018; Bardua et al., 2019; Felice et al., 2019). Recent studies have used the 'common allometric component' (CAC), the component of shape change most closely aligned with size, to show allometric growth trajectories between different species (Mitteroecker et al., 2004) and in the ontogeny of sexually dimorphic species (Evans et al., 2018). This concept can be applied to individual phenotypic modules to assess relative rates of shape change. Removal of the CAC also allows genuine intraspecific variation to be more accurately quantified and separated from ontogenetic variation (Mitteroecker et al., 2004). Here I use 3D GM techniques to evaluate modularity, allometry and variance in the skull of *P. andrewsi,* testing the hypothesis that the parietal-squamosal frill is a socio-sexually selected structure.

If, as predicted, the frill of *P. andrewsi* is under socio-sexual selection, we would expect it to form a distinct phenotypic module, because modularity allows the developmental and evolutionary independence of distinct regions upon which selection can act (Klingenberg, 2014). As well as greater ontogenetic change in both size and shape, modules under socio-sexual selection should display higher morphological variation independent of size than those that are not because of condition-dependence and selection for greater trait expression combined with relaxation of functional constraints (Eshel et al., 2000; O'Brien et al., 2018; Evans et al., 2018). Using *P. andrewsi* as a model species will enable us to understand the selective forces that shaped the evolution of the distinctive ceratopsian skull and will provide a basis for further analyses across evolutionary time. *P. andrewsi* is one of the few examples of fossil terrestrial vertebrates with a large enough sample size to test patterns of ontogenetic growth, giving us one of the best opportunities to explore these questions.

3.3 Methods

3.3.1 Experimental design

To gain an accurate representation of skull morphology in *P. andrewsi*, three-dimensional digital mesh models of all specimens were created with photogrammetry (Agisoft Photoscan Professional v. 1.4.3 build 6529). Specimens with small amounts of asymmetric taphonomic deformation were retrodeformed using Landmark v. 3.0 (Wiley et al., 2005), using protocols outlined in Lautenschlager (2016). Specimens that were severely taphonomically deformed were omitted from the dataset, giving a total of 31 complete and 20 partial skulls (see Appendix for specimen details).

Landmarks were placed on digital models using Landmark v. 3.0 (Wiley et al., 2005; Fig. 3.2). Only the right half of each skull was landmarked to increase processing speed and reduce redundancy from incorporating symmetrical elements in the analysis (Cardini, 2016). This method also increases sample size by allowing the incorporation of bilaterally incomplete specimens, and by allowing the digital mirroring of the left half when the right is incomplete. A total of 33 landmarks (Bookstein type I and II landmarks; Zelditch et al., 2004) were used per specimen. Semilandmark curves of 10 semilandmark points each were used to describe the shape of sutures and edges of skull elements. A total of 56 semilandmark curves were used (Fig. 3.2), totalling 522 semilandmarks on each specimen with duplicates omitted. Landmarks were only placed on the upper surface of the skull due to the focus of this study being the external morphology of the skull, and because the underside of several specimens was inaccessible.

To describe surface morphology, additional surface semilandmarks were added using a semi-automated process in the *Morpho* package for R (R Core Team, 2013; Schlager, 2017; Felice and Goswami, 2017; Bardua et al., 2019b), bringing the total number of landmarks to 862 (Fig. 3.2).

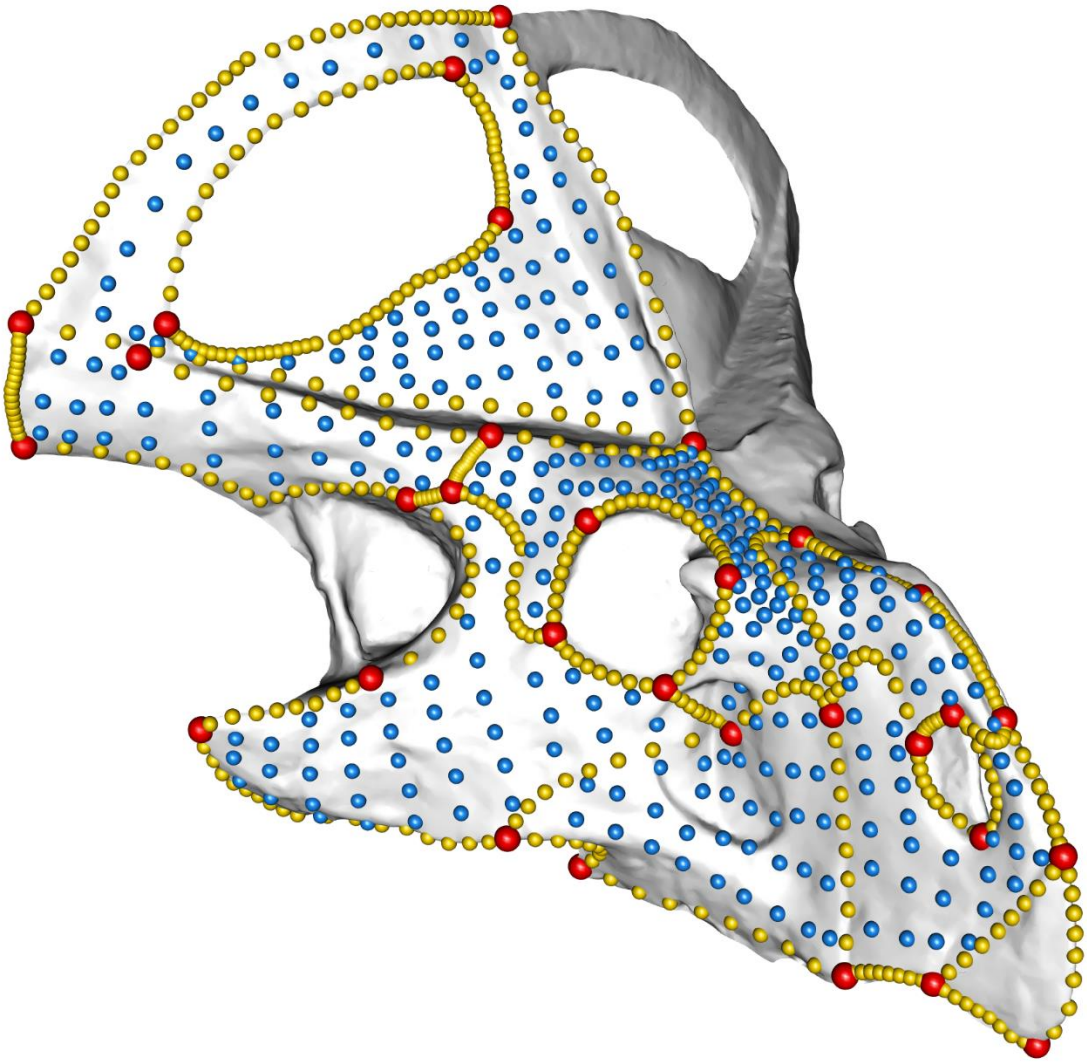

Figure 3.2: Layout of landmarks on *P. andrewsi* skull (specimen AMNH 6439)**.** Anatomical landmarks are shown as red points, points on semilandmark curves are coloured yellow, and surface patch semilandmarks are shown in blue.

All landmarks were first reflected across the midline of the skull to improve accuracy of the alignment, the midline of the bilaterally symmetrical skull acting as a baseline for alignment (Cardini, 2016). A generalised Procrustes alignment was then performed with the *geomorph* v.3.5.2 package for R (Adams and Otárola-Castillo, 2013). Procrustes alignment removes effects of scale, position and rotation between specimen landmark coordinate data (Rohlf and Slice, 1990). After alignment,

reflected landmarks were removed and all analyses were performed on the remaining pre-aligned right-side landmarks. A principal components analysis (PCA) was used to visualise shape variation using projected shapes. The dilation component of taphonomic deformation, a potential source of non-biological variation, was identified and quantified by examining PCA outputs (Angielczyk and Sheets, 2007).

3.3.2 Statistical analysis

Modules were estimated using the maximum likelihood (ML) method, implemented with the R package *EMMLi* (Goswami and Finarelli, 2016). A total of 20 module hypotheses were tested (Appendix), from a two-module to an 8-module hypothesis. Because this study is explicitly concerned with growth-related changes in *P. andrewsi*, modularity was tested initially with data uncorrected for allometry (Goswami and Polly, 2010b). In addition to EMMLi, modularity was also assessed with the covariance ratio (CR; Adams, 2016) of both the raw and allometry-corrected datasets, applied in *geomorph* v.3.5.2 (Adams and Otárola-Castillo, 2013). The covariance ratio returns a *p*-value which allows us accept or reject modularity for the entire skull.

Allometry was explored with the 'procD.lm' function in the *geomorph* package for R (Adams and Otárola-Castillo, 2013). Both whole-skull centroid size (the square root of the sum of squared distances of all landmarks of an object from their centroid; Zelditch et al., 2004) and the straight-line basal length of the maxilla (landmark points 16 to 17, Appendix) were used as size components in this analysis to account for possible interdependence of skull centroid size and that of highly size-variable modules (i.e., frill). Global Procrustes alignment was performed on all modules in order to preserve information about relative orientation and scaling between modules (Baab, 2013). The CAC was then removed from the Procrustes-aligned data and analyses repeated on the size-corrected dataset. Sexual dimorphism was assessed with Hartigan's dip test for unimodality (Hartigan and Hartigan, 1985), using the 'dip.test' function in the R package *diptest* v.0.75-7 (Maechler, 2016). Dip tests were performed on the first 8 principal components (i.e., residual shape components; RSC) of allometry-corrected

datasets for whole-skull Procrustes-aligned data, plus separate tests for all modules both globally and individually aligned.

To visualise variation across the skull, individual landmark disparity was calculated by summing the variance of the three-dimensional Procrustes-aligned values for each landmark (Felice, Randau and Goswami, 2018). This calculation was performed both on the initial Procrustes-aligned data, and the allometry-corrected data to remove ontogenetic variance.

Ontogenetic variation was assessed in two ways:

1) Individual module centroid sizes were regressed against whole-skull centroid size for each specimen to give a measure of relative size change with ontogeny for each module. Regression slopes were compared between different modules using an ANCOVA (O'Brien et al., 2018).

2) Separate modules were extracted from the globally-aligned whole-skull data, and the CAC of each module was regressed against centroid size of the whole skull (Evans et al., 2018). This method gives a relative measure of rate of shape change. Separate module slopes were compared using an ANCOVA.

The output of the allometry model was used to calculate Procrustes variance for all defined modules and for the entire skull using the 'morphol.disparity' function in the R package *geomorph* (999 iterations). Variance of each module was divided by number of landmarks for that module to provide comparable results (Bardua et al., 2019a).

3.4 Results

3.4.1 Morphological trends in the skull of *Protoceratops andrewsi*

Overall shape variation of 31 complete *P. andrewsi* skulls is visualised in a PCA (Fig. 3.3). The shape changes accounted for by the first two principal components (PCs) are shown as maximum and minimum value shape projections along the relevant PC axes. PC1 accounts for 61.8% of total shape variation and shows a transition from a shape typical of small individuals (with short, flattened frill) at positive values to a shape typical of the largest individuals (large, upright frill) at negative values. PC2 accounts for 10.4% of total shape variation and shows a change from a narrow, flattened, backwards-extending frill to a more upright and wider frill. Examination of the projected maximum and minimum shapes of the first 8 PCs suggest that PC4, accounting for 4.8% of total shape variation, represents the effects of taphonomic deformation (Angielczyk and Sheets, 2007). This low contribution to total shape variation suggests that taphonomic deformation is unlikely to contribute a great deal to morphological variation in this dataset.

3.4.2 Variance and whole-skull allometry

The allometric analysis of *P. andrewsi* shows a significant correlation between size and shape (p = <0.01, R^2 = 0.56; Fig. 3.4A), indicating that around 56% of total shape variation in this dataset can be accounted for by differences in skull size. Distribution of specimens in the CAC-RSC1 morphospace (Fig. 3.4B) resemble those seen in the PC1-PC2 morphospace in Fig. 3.3, suggesting that the majority of total shape variation in this dataset is strongly correlated with size.

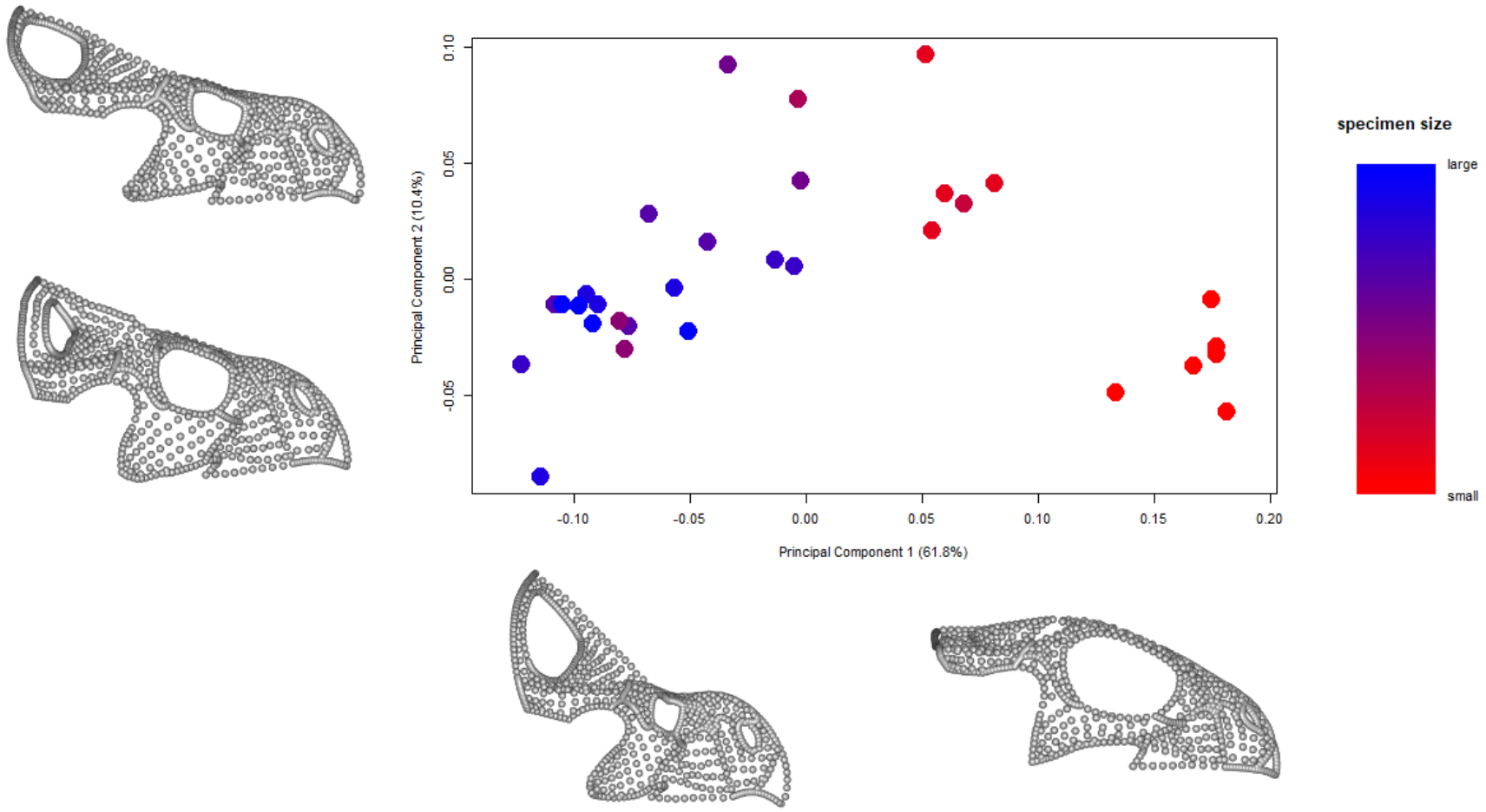

Figure 3.3: Principal component analysis of 31 complete *P. andrewsi* skulls, landmarked with 862 points and including surface semilandmarks. The first two principal components account for 61.2% and 10.6% of total shape variation respectively. The first 12 and 23 principal components account for 95% and 99% of total shape variation respectively. Along PC1 projected shapes resemble the smallest (right) and largest (left) individuals in the dataset.

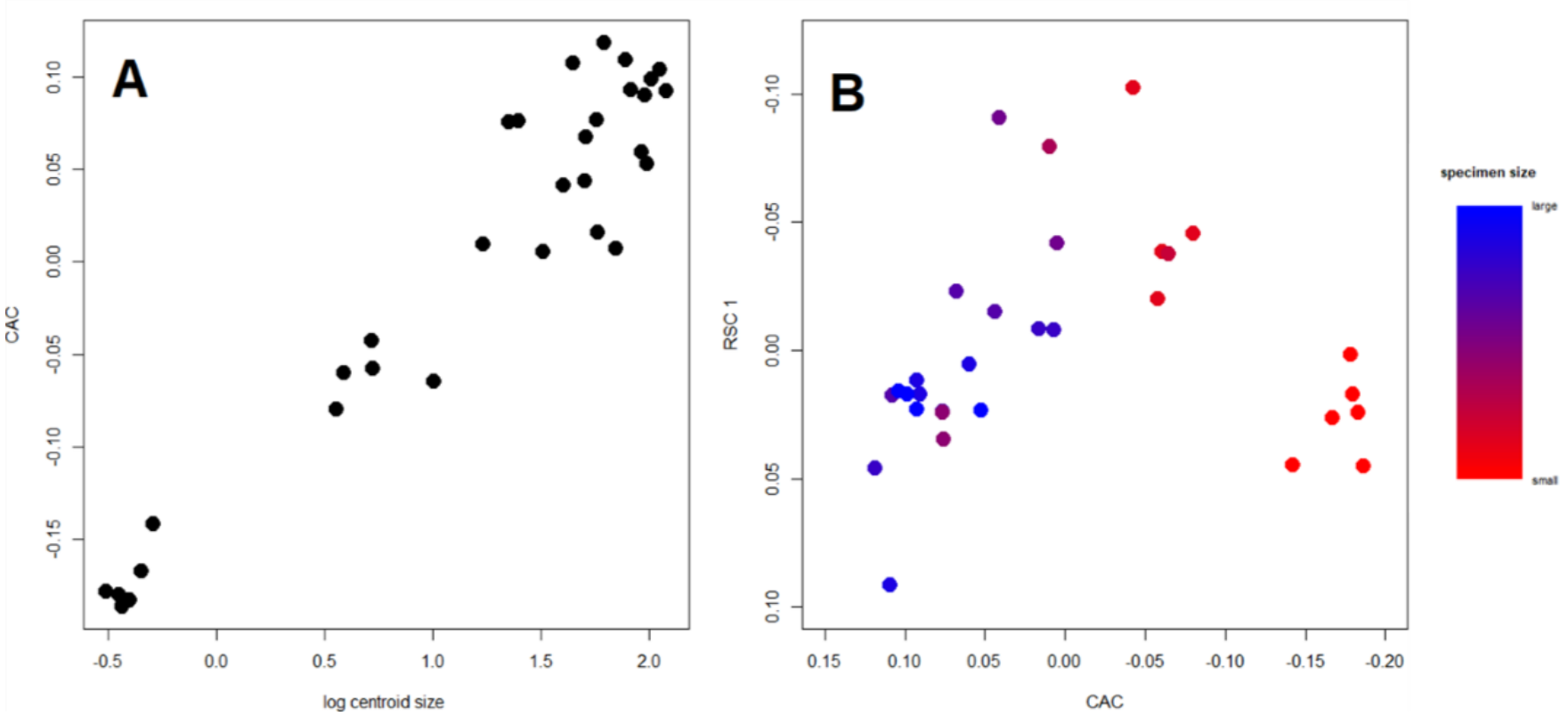

Figure 3.4: Results of allometry analysis for whole-skull data**.** Shown are regression of common allometric component (CAC) against centroid size (**A**), and CAC against residual shape component (RSC) 1 (**B**). Colours in **B** represent relative specimen centroid size, add range from smallest (red) to largest (blue).

Per-landmark variation across 31 specimens in the ontogenetic series is displayed in Fig. 3.5. In the uncorrected dataset (Fig. 3.5A) the greatest variance (red) occurs in the outermost portion of the frill reflecting the drastic shape change in the frill during ontogeny. The side of the facial region, around the maxilla and premaxilla, and the dorsal region of the postorbital shows the lowest variance. When corrected for allometry (Fig. 3.5B) absolute variance levels are lower for the entire skull. The greatest variance in the allometry-corrected dataset occurs again in the lateral extremities of the frill, but relatively higher variance is also seen in the jugal. This suggests that intraspecific variance in the jugals is moderate, but this variance is not ontogenetic in nature. The lowest variance is again concentrated around the maxilla/premaxilla boundary, but here extends upwards to the rostral portion of the postorbital.

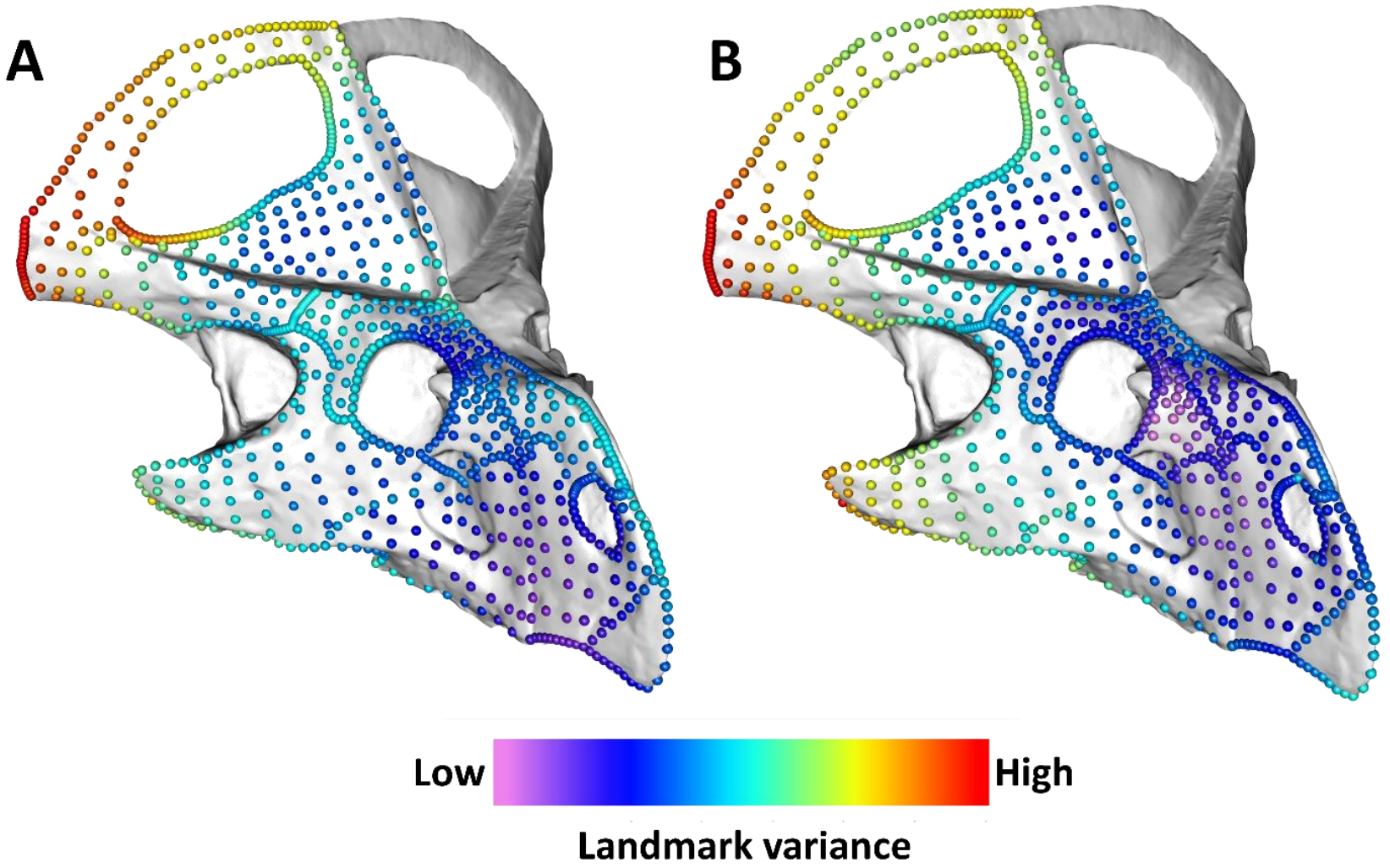

Figure 3.5: Per-landmark variance in the skull of *P. andrewsi*, showing raw variance (**A**) and variance adjusted for allometry (**B**). Landmarks are log-transformed and are colour-coded from least variable (purple) to most variable (red).

3.4.3 Modularity

Assessing modularity using the maximum likelihood method (Goswami and Finarelli, 2016) resulted in strongest support for the 8-module hypothesis. High-density landmark coverage, as used in this study, tend to support higher numbers of modules (Bardua et al., 2019a). To compensate for this, we examined correlation coefficients within and between modules and created integration thresholds where the between-region correlation value was within 0.1 of the lowest within-region correlation value (Felice and Goswami, 2016; Bardua et al., 2019a). If the between-module correlation value fell within this threshold, these modules were merged into a single module. Five separate modules were retrieved from this method: frill, postorbital, nasal-premaxilla-rostral complex (hereafter 'snout'), maxilla and jugal (Fig. 3.6). The relatively weak correlations between the frill and other parts of the skull further justify its designation as a separate module (Table 3.1). Applying this method to the allometry-corrected dataset decreased the between-module correlation values a small amount, but because our objective was quantifying relative changes in the skull through ontogeny in *P. andrewsi* we retained the module hypothesis obtained from our initial, uncorrected dataset. Analysis of covariance ratio (CR) returned support for a significantly modular structure of the skull (CR = 0.85 for raw data; CR = 0.67 for allometry-corrected data, $p < 0.01$).

Shape changes of individual modules between minimum and maximum skull centroid sizes are shown in Fig. 3.7 and are ranked in descending order of relative CAC change from greatest to least. The greatest total shape change is seen in the frill (Fig. 3.7A), which undergoes a relatively rapid change in shape from a short, flat, narrow projection at minimum size, extending first caudally at intermediate sizes and then expanding to a broad, upward-curved shape at maximum size. The maxilla (Fig. 3.7E) shows the smallest amount of relative shape change through ontogeny.

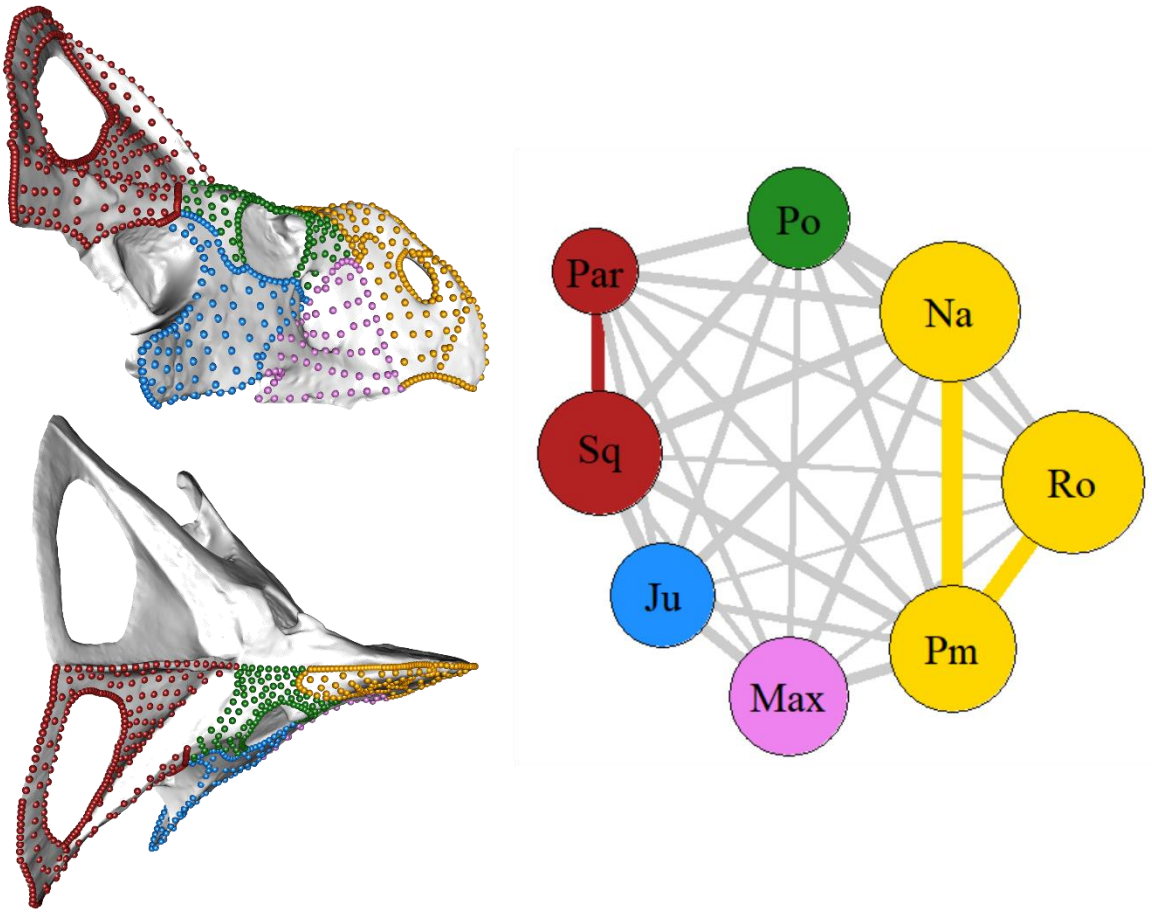

Figure 3.6: Modules identified in the skull of *P. andrewsi* from *EMMLi* analysis. Meshes on the left show right lateral (left upper image) and top (left lower image) views of specimen AMNH 6439, with landmarks colour-coded according to module. The network graph (right) shows all analysed skull elements, arranged to roughly correspond to their position in the skull and coloured according to module. Node size is scaled according to within-module correlation value. Between-module correlations are represented by connecting lines. Line thickness represents correlation value, and where this value exceeds the predetermined integration threshold the lines are coloured appropriately. Elements are **Par:** parietal; **Sq:** squamosal; **Ju:** jugal; **Po**: postorbital; **Na:** nasal; **Max:** maxilla; **Pm:** premaxilla; **Ro:** rostral. Module colours are **frill**: red; **jugal**: blue; **postorbital**: green; **maxilla:** pink; **snout:** yellow.

Table 3.1: Results of maximum likelihood (*EMMLi*; blue cells) and covariance ratio (CR; orange cells) analyses.

Raw data

	Parietal	Squamosal	Jugal	Postorbital	Nasal	Premaxilla	Maxilla	Rostral
Parietal	0.52	0.85	0.76	0.78	0.71	0.72	0.75	0.81
Squamosal	0.42	0.76	0.98	0.94	0.94	0.82	0.84	0.87
Jugal	0.29	0.42	0.63	0.94	0.93	0.84	0.86	0.87
Postorbital	0.36	0.37	0.31	0.6	0.95	0.85	0.86	0.92
Nasal	0.34	0.4	0.35	0.46	0.85	0.81	0.83	0.84
Premaxilla	0.32	0.37	0.28	0.36	0.67	0.78	0.92	0.86
Maxilla	0.24	0.24	0.38	0.24	0.34	0.38	0.72	0.83
Rostral	0.25	0.18	0.16	0.34	0.32	0.62	0.2	0.87

Allometry-corrected data

Parietal	0.47	0.78	0.43	0.61	0.51	0.38	0.54	0.47
Squamosal	0.29	0.75	0.83	0.73	0.75	0.62	0.63	0.54
Jugal	0.14	0.41	0.73	0.66	0.7	0.67	0.6	0.63
Postorbital	0.16	0.28	0.27	0.63	0.86	0.63	0.59	0.65
Nasal	0.11	0.18	0.22	0.32	0.72	0.61	0.52	0.6
Premaxilla	0.11	0.16	0.13	0.15	0.47	0.67	0.77	0.71
Maxilla	0.09	0.1	0.38	0.18	0.18	0.27	0.68	0.67
Rostral	0.11	0.12	0.07	0.22	0.22	0.56	0.21	0.87

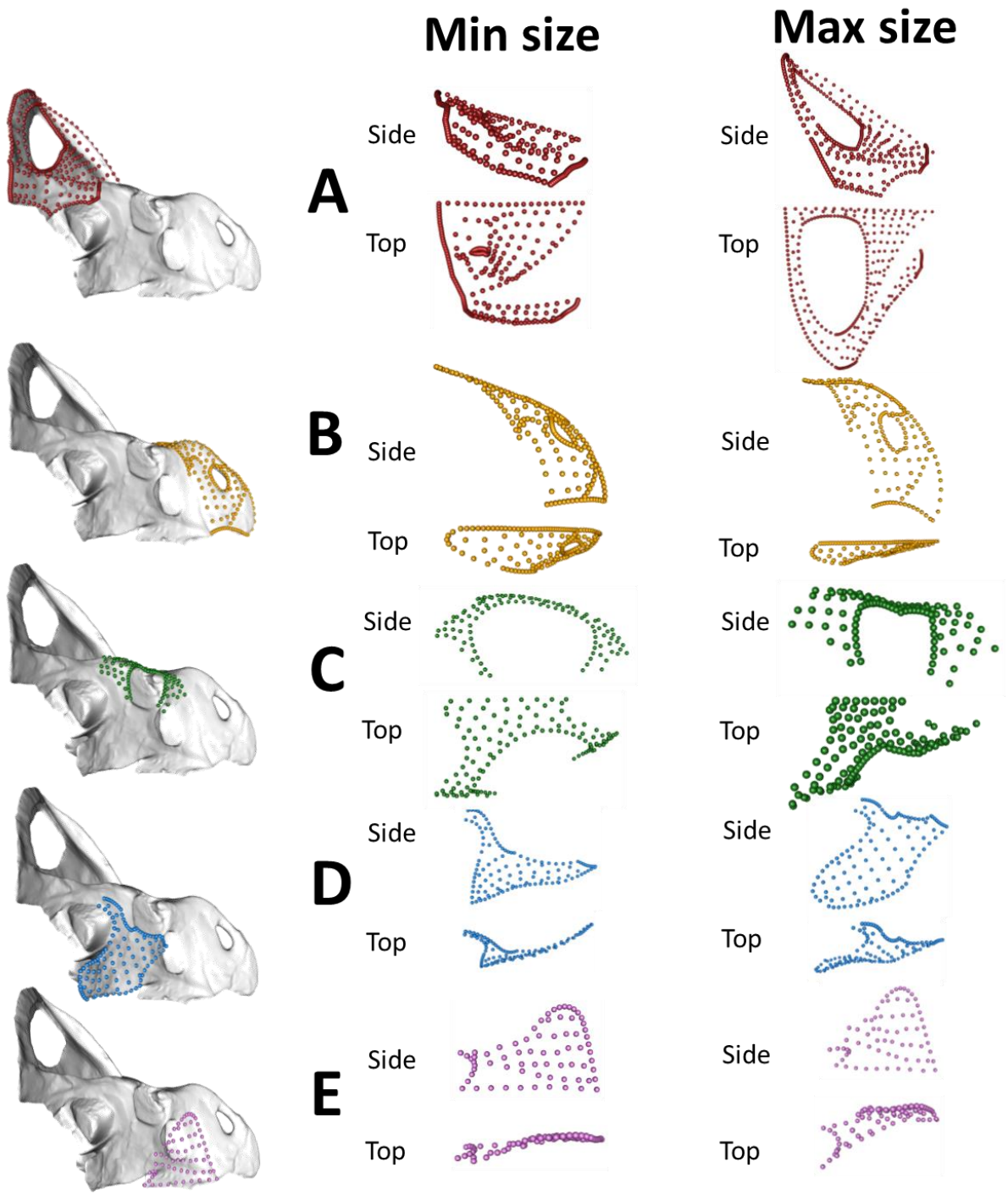

Figure 3.7: Projected shapes at minimum (Min) size and maximum (Max) size of the five modules identified in *EMMLi.* The left column shows mesh models of *P. andrewsi* (AMNH 6439), with landmarks of each corresponding module superimposed. Right: shape of individual modules at maximum and minimum projected specimen size (not to scale). Modules are ranked **A** (highest relative shape change) to **E** (lowest total shape change). **A:** parietal-squamosal frill; **B:** snout; **C:** postorbital; **D:** jugal; **E**: maxilla. All individual modules are shown in right-lateral and dorsal views for both sizes.

3.4.4 Sexual dimorphism

In assessing possible dimorphism, no dip test was below the 5% significance level for any PC for either whole-skull data, or for any individual module (Table 3.2). This was true for the whole-skull dataset and for the dataset with juveniles removed. Only PC6 of the whole-skull data analysis for all specimens showed a *p*-value approaching 0.05 ($p = 0.09$; $R^2 = 0.04$). Because this principal component contributes only 2.5% of total skull shape variation it is unlikely to represent true population-level dimorphism.

Table 3.2: Results of Hartigan's dip test. Shown are *p*-values for dip test performed on the first 8 principal components for whole-skull and individual modules, for all specimens (**A**) and with juveniles excluded (**B**).

A: All specimens

Module	***n***	**PC1**	**PC2**	**PC3**	**PC4**	**PC5**	**PC6**	**PC7**	**PC8**
Skull	31	0.99	0.85	0.66	0.79	0.94	0.09	0.59	0.4
Frill	39	0.51	0.81	0.92	0.99	0.36	0.43	0.84	0.7
Jugal	43	0.52	0.99	0.97	0.71	0.3	0.82	0.83	0.81
Snout	33	0.2	0.8	0.6	0.67	0.2	0.7	0.65	0.82
Maxilla	41	0.71	0.95	0.69	0.98	0.98	0.32	0.87	0.92
Postorbital	39	0.99	0.60	0.6	0.87	0.62	0.22	0.89	0.8

B: Juveniles excluded

Module	***n***	**PC1**	**PC2**	**PC3**	**PC4**	**PC5**	**PC6**	**PC7**	**PC8**
Skull	20	0.5	0.64	0.91	0.58	0.63	0.83	0.81	0.59
Frill	27	0.9	0.95	0.48	0.4	0.49	0.99	0.89	0.37
Jugal	30	0.77	0.8	0.6	0.68	0.75	0.83	0.99	0.95
Snout	22	0.18	0.38	0.15	0.42	0.94	0.63	0.99	0.69
Maxilla	28	0.93	0.58	0.99	0.77	0.35	0.93	0.81	0.71
Postorbital	25	0.96	0.97	0.61	0.88	0.33	0.47	0.98	0.99

3.4.5 Module allometry

Changes in individual module centroid size against skull centroid size (Fig. 3.8A) show that the frill undergoes the highest rate of size change during ontogeny. The allometric slope of the frill is significantly greater than that of the next-steepest module, the snout (p = <0.0001; Table 3.3). The difference between the rate of growth of the snout and the next fastest-growing module, the maxilla, was not significant (p = 0.32). Similarly, the frill displays the greatest change in shape with size of all modules (Fig. 3.8B), significantly steeper than that of the next fastest-growing module, the snout (p = <0.0001). The difference in relative rates of shape change between the snout and next fastest-changing module, the postorbital, was also non-significant (p = 0.49).

Table 3.3: Results of ANCOVA for comparison of regression slopes of module centroid size against skull centroid size, and CAC against skull centroid size. Results for the three steepest-scaling modules in each analysis are shown.

	Centroid size		**Common allometric component**	
	F	***p***	***F***	***p***
Frill/snout	52.175	<0.0001*	36.802	<0.0001*
Frill/maxilla	63.789	<0.0001*	NA	NA
Maxilla/snout	0.9934	0.3231	NA	NA
Postorbital/snout	NA	NA	0.4741	0.494
Frill/postorbital	NA	NA	48.123	<0.0001*

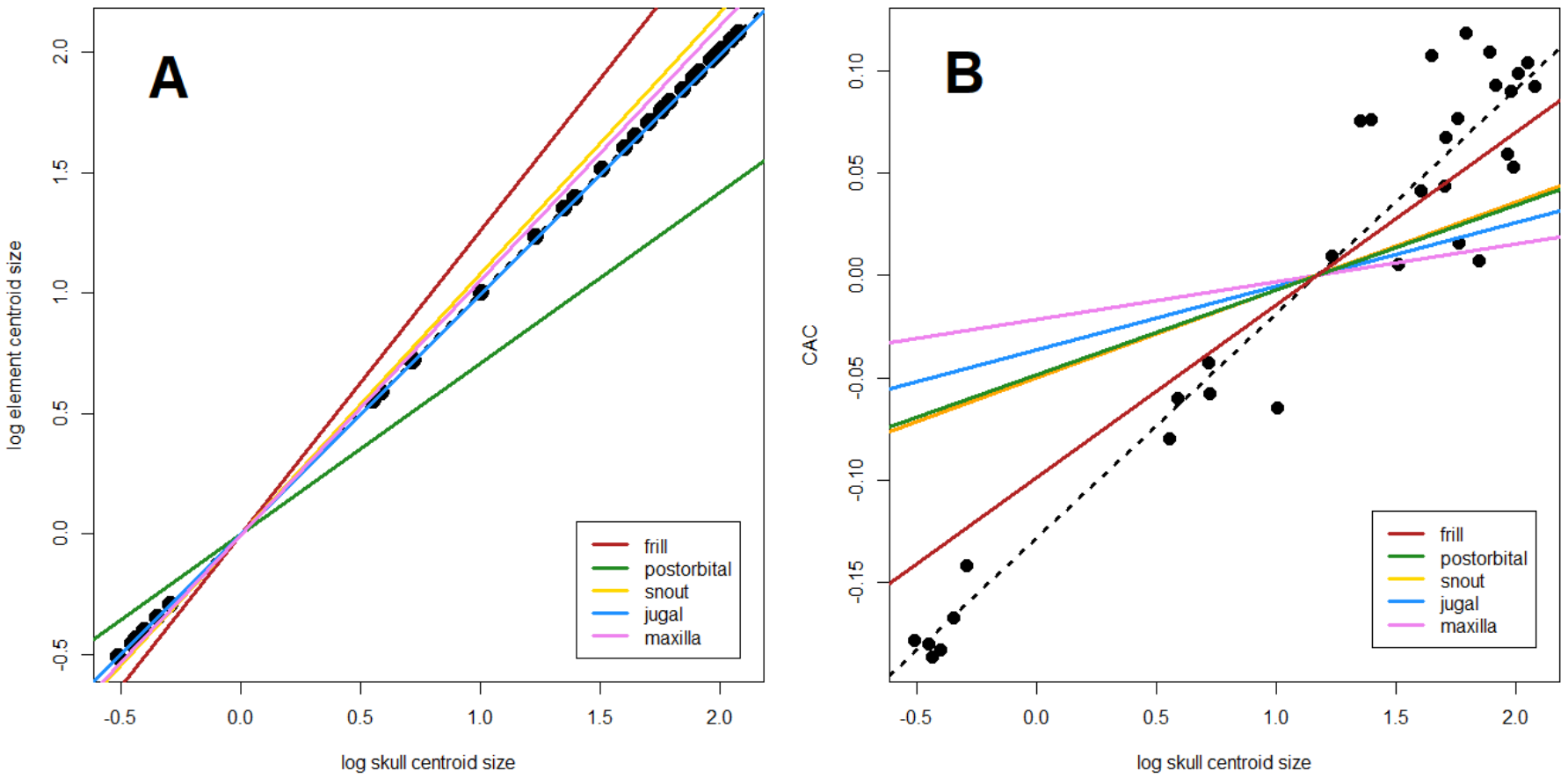

Figure 3.8: Log centroid size values of individual modules regressed against log skull centroid size (**A**) and common allometric component regressed against log skull centroid size (**B**). Black points in both plots represent whole-skull values, with best-fit line for whole-skull represented by black dashed line. Individual module regression lines are coloured according to module. Intercepts for module centroid sizes (**A**) are set to zero to standardise comparisons.

3.4.6 Module disparity

When corrected for allometry, disparity was found to be highest in the frill (1.27×10^{-5}) and jugal (1.05×10^{-5}), and lowest in the postorbital module (4.12×10^{-6}; Fig. 3.9). No significant relationship was found between Procrustes variance (disparity) and either growth rate (represented by slope of module centroid size regressed against whole-skull centroid size; Fig 3.9A) or within-module correlation (derived from *EMMLi* analysis; Fig. 3.9B). The lack of correlation between disparity and within-module correlation reflects the findings of previous studies in other taxa (Goswami and Polly, 2010a; Bardua et al., 2019a).

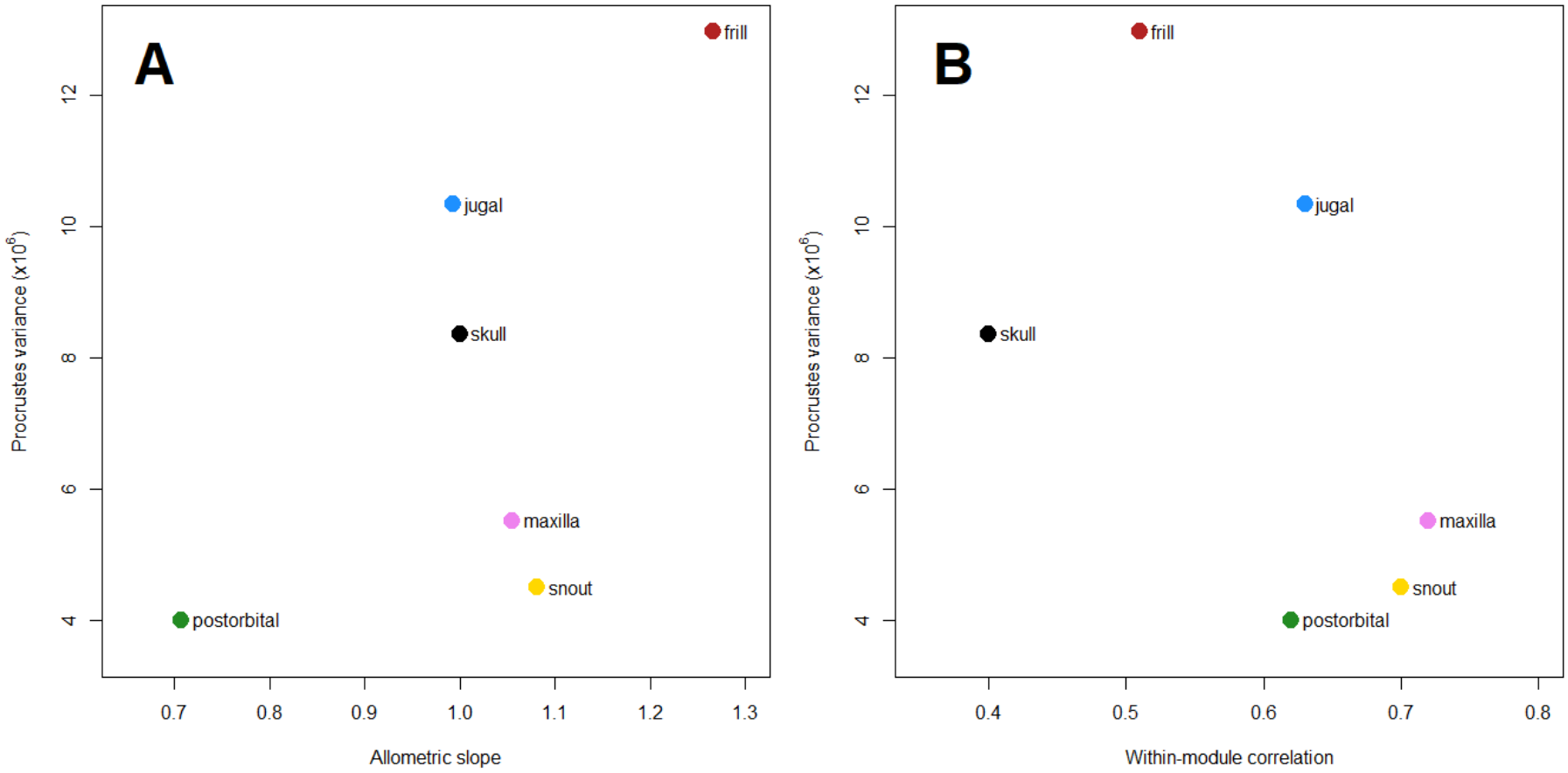

Figure 3.9: Relationship between Procrustes variance and growth rate (Allometric slope; **A**) and Procrustes variance and within-module correlation (**B**). Neither relationship is significant. Procrustes variance in both plots is allometry-corrected and divided by number of landmarks in each module.

3.5 Discussion

This study is the first large-scale geometric morphometric study of a single dinosaur taxon to investigate modularity and quantify ontogenetic growth with dense 3D geometric morphometric data. My findings show that the cranium of *Protoceratops andrewsi* is divided into at least five distinct phenotypic modules that independently vary in their rate of growth, ontogenetic shape change, and morphological variance. The identification of discrete phenotypic modules in *Protoceratops* is an important finding because it provides a developmental framework by which skull elements can differentiate and become co-opted for a variety of different purposes (Klingenberg, 2008, 2014). Identifying modularity also allows partitioning of the skull for comparative analyses in a less subjective way than previous studies, being less reliant on the limited number of measurements that can be captured by separate linear values.

The highly significant allometric signal in the skull of *P. andrewsi* accounts for around 56% of total shape variation in this dataset, suggesting drastic changes in skull shape during ontogeny (Evans et al., 2018). In all analyses of individual modules, the parietal-squamosal frill consistently displayed the highest rates of size and shape change through ontogeny, and the highest morphological variance independent of size, expanding significantly during ontogeny to form a very large, conspicuous structure (Fig. 3.10). This supports the hypothesis that the frill is distinct from the remainder of the skull and most likely functioned as a socio-sexually selected signal trait, displaying the accelerated rates of both shape and size change and relatively high levels of morphological disparity that are predicted for such signals. An alternative signalling role, namely species recognition, can be ruled out as the primary function of the frill because growing and carrying such a structure will have imposed significant resource and energy costs (Hone and Naish, 2013). Species identification signals, when they can be identified, tend to be largely cost-free because these operate in a context where both signaller and receiver benefit from the signal being transmitted correctly: thus, there is no requirement for species recognition signals to be costly to maintain honesty (Knell and Sampson, 2011). By contrast,

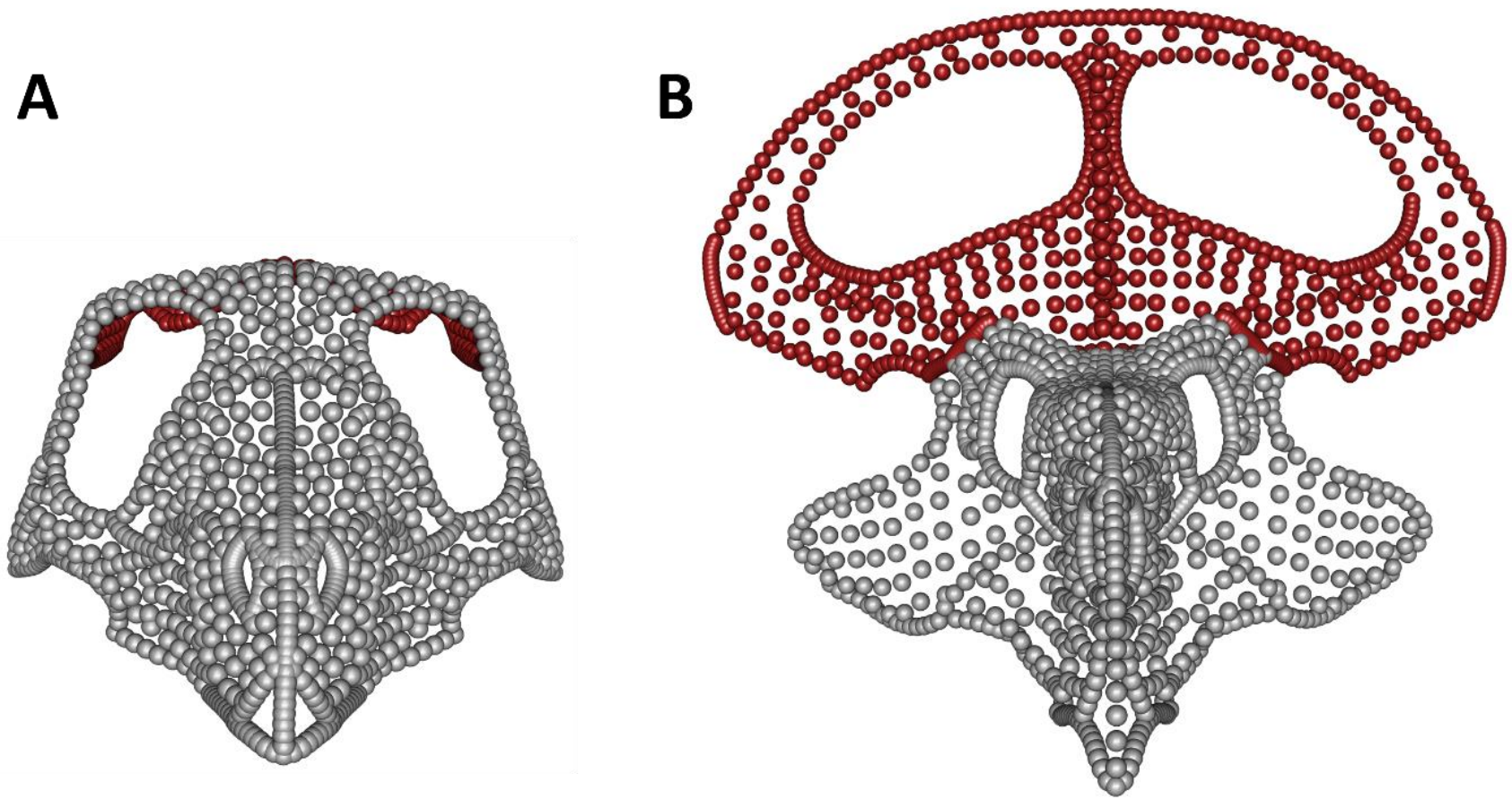

Figure 3.10: Front view of projected shape at minimum (**A**) and maximum (**B**) size of the skull of *Protoceratops andrewsi* (not to scale). The frill is coloured in red landmarks to illustrate the difference in both size and shape from these two extremes of size. Skulls are orientated approximately the same for comparison, and landmarks are reflected across the midline to better represent the natural biological shape.

traits that act as adverts of their bearers' quality should be honest signals in order to be maintained within a population and are therefore expected to impose a cost on the bearer to maintain the honesty of the signal (Eshel et al., 2000). Similarly, other functional explanations for the frill, such as a defensive or thermoregulatory structure, have little support (Padian and Horner, 2010; Dodson et al., 2004; Johnstone et al., 2009). Without the explicit structural and functional constraints of mechanical traits sexually selected traits are free to vary much more readily within a population but will be opposed by natural selection if they are not selected for (Kraaijeveld et al., 2007). These findings are consistent with a role as a display structure for which increased size brought increased benefits, a hallmark of a socio-sexual trait.

Moving onto the other skull modules, the dorsal surface of the nasals shows bulging and a moderate lateral bifurcation in the largest specimens but not to the extent of forming a distinct, fused nasal horn as in closely-related taxa (Ryan et al., 2001; Sampson and Loewen, 2010; Czepiński, 2019). It is possible that this thickened region functioned in intraspecific combat, as some authors have suggested (Dodson, 1976), but testing this hypothesis would require structural analysis of the nasals to determine if they have the structural strength necessary to function as weapons (Rayfield 2005). The jugals have also been suggested as secondary sexual traits in *Protoceratops* (Hone et al., 2016). The data presented here are ambiguous on this issue: although the jugals do show the second highest allometry-adjusted Procrustes variance, they do not fit the patterns of either heightened growth rate or shape change seen in the frill. Prominent jugals are a characteristic feature of a wide range of ceratopsian taxa (Dodson et al., 2004) and are particularly pronounced in basal genera such as *Psittacosaurus* (Sereno, 2010). Multiple sexually selected signals are common in extant taxa, but their relative expression may be influenced by different factors (Johnstone et al., 2009; Cooney et al., 2018). Quantifying evolutionary rates across a range of ceratopsian taxa will enable patterns of evolution of different cranial modules to be explored and may provide a clearer picture of the role of jugals in ceratopsians (Felice, Randau and Goswami, 2018).

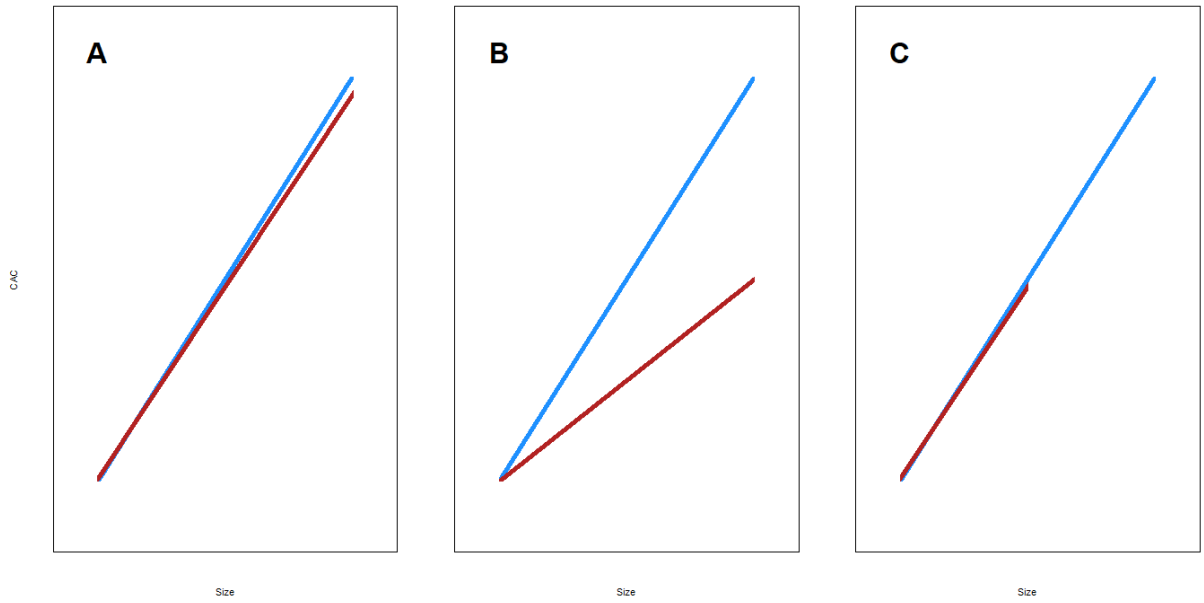

Figure 3.11: Hypothetical examples of allometric trajectories under different forms of sexual dimorphism. Coloured lines represent growth trajectories (CAC against size; Cf. Fig. 3.6B) of two sexes. **A**: Sexually monomorphic; No difference in size or shape between sexes. **B**: Sexual dimorphism in shape; sexes grow to same size but one sex undergoes greater change in shape, represented by differing slope of lines. **C**: Sexual size dimorphism; sexes follow same growth trajectory but one sex grows to larger overall size and shows greater shape change at larger sizes as a result.

No support was found for sexual dimorphism of *Protoceratops andrewsi* in this study, either in individual modules or in whole-skull data. Previous attempts to determine sexual dimorphism in *P. andrewsi* using linear measurements, descriptive observations and two-dimensional morphometrics have met with mixed results (Dodson, 1976; Handa et al., 2012; Maiorino et al., 2015). Without pronounced differences creating distinct allometric trajectories between sexes (e.g. Fig. 3.11B), sexual size dimorphism can be difficult to detect in a sample without prior knowledge of sex, even with a very large sample size (Mallon 2017; Hone & Mallon 2017). These findings suggest that *Protoceratops* is either not skeletally sexually dimorphic (Fig. 3.11A), or that males and females share a similar growth trajectory but are separated by overall size (Fig. 3.11C). Sexual dimorphism of soft tissues cannot be confirmed or ruled out because of the limits of detecting soft tissue variation with only skeletal remains (Felice and O'Connor, 2016).

Using a geometric morphometric approach, I have shown that the frill of *P. andrewsi* shows several characteristics consistent with a socio-sexually selected trait. Socio-sexual selection is predicted to be a powerful driver of evolution, resulting in both sexually mutual ornamentation and runaway selection under certain circumstances (Fisher, 1930; West-Eberhard, 1979; Jones and Hunter, 1993; Eshel et al., 2000; Kokko and Johnstone, 2002; Kraaijeveld et al., 2007; Hooper and Miller, 2008; Shuker, 2009; Hone et al., 2012; Clutton-Brock and Huchard, 2013). Identifying socio-sexual signal traits in an extinct taxon has implications for not only better understanding the palaeobiology of that taxon (Funghi et al., 2018), but also in unravelling the evolutionary implications of socio-sexual selection. If the frill of *Protoceratops* functioned as a socio-sexual signal of dominance and/or individual genetic quality, as we suggest, it implies that intraspecific social interaction of some kind was important in this species (West-Eberhard, 1979; Tobias et al., 2012). Some evidence for social behaviour has been suggested for a number of ceratopsian taxa, including *Protoceratops* (Ryan et al., 2001; Lehman, 2007; Zhao et al., 2007; Currie, Langston and Tanke, 2008; Mathews et al., 2009; Farke et al., 2011; Fastovsky et al., 2011; Hone et al., 2014; Fanti et al., 2015). Confirming sexual selection would ultimately rely on establishing a connection between trait expression and reproductive success (Shuker, 2009), an impossibility in any fossil taxon. Ultimately, the distinction between sexual and social selection may not be important because both sexual and social selection result from intraspecific competition for resources and are thus intimately connected (Kraaijeveld et al., 2007; Tobias et al., 2012). Extending similar morphometric analyses to other ceratopsian taxa will allow us to explore evolutionary rates and morphological diversification of this clade, with the potential to both expand upon more general studies of modularity and trait evolution, and address socio-sexual hypotheses within an evolutionary framework.

Chapter 4

Modularity, morphological disparity and evolutionary rates in the ceratopsian skull

4.1 Abstract

It has been suggested by a number of researchers that the exaggerated and diverse cranial ornamentation (i.e. parietal-squamosal frill and postorbital and nasal horns) that characterise the Late Cretaceous ceratopsian clade Ceratopsidae display characteristics that are typical of socio-sexually selected traits, namely elevated evolutionary rates and high morphological disparity. Assessing interspecific patterns of evolution in the skulls of extant tetrapod clades has generally relied on identifying phenotypic modules, regions of highly integrated traits which are able to develop and evolve semi-independently, but this approach has not yet been attempted with the ceratopsian skull. Here, for the first time, I apply three-dimensional geometric morphometric techniques using a dataset of 74 specimens, representing 27 ceratopsian taxa, to assess phenotypic modularity in the ceratopsian skull. Strongest support was found for a six-module model of the skull with the parietal-squamosal frill forming a distinct module. Evolutionary rates and morphological disparity were assessed using the morphometric data and were found to be strongly correlated, with highest net rates in the frill, and regions of high disparity and rates also found in both the postorbital and nasal horns. Allometry was found to have a significant effect on shape, and accounted for around 44% of total shape variation, adding support to the hypothesis that the ceratopsian skull displays heterochrony. Together, the modularity, rapid evolution and high morphological disparity of the exaggerated traits in the ceratopsian skull provide strong support to the hypothesis that evolution of these traits was driven by socio-sexual selection.

4.2 Introduction

The cranial morphology of ceratopsian dinosaurs is notable for its diversity, and the function of the prominent horns and frills they possessed has long been a source of debate (Hatcher, 1907; Dodson, 1976; Dodson et al., 2004; Knell and Sampson, 2011). During the course of the Cretaceous Period, ceratopsians underwent a seemingly rapid evolution from small, bipedal taxa (e.g. *Psittacosaurus*) to large, quadrupedal forms with enlarged cranial frills and horns, exemplified by *Triceratops* which survived to the very end of the Cretaceous (Dodson et al., 2004). The distinctive ornamented skulls of ceratopsians, coupled with their high taxonomic diversity in the Late Cretaceous have led some researchers to suggest that these 'ornaments' evolved at a rapid rate, and that a relationship might exist between rapid evolution and the diverse skull morphology seen in ceratopsians (Hone et al., 2012; Knell et al., 2012). Although ceratopsians are generally well-studied, few attempts have been made to quantify morphological diversity and evolutionary rates in this clade. Studies assessing morphological diversity have tended to focus on a limited number of taxa and have dealt either with questions of sexual dimorphism (Dodson, 1976; Maiorino et al., 2015) or taxonomy (Maiorino et al., 2013). Maiorino et al. (2017) attempted to estimate evolutionary rates in ceratopsian skulls using two-dimensional (2D) landmark-based geometric morphometrics. In their study, they focussed on coarse-scale patterns across the skull and jaw and did not specifically examine the mosaic evolution expected to result from traits under different forms of selection, and hence evolving at different rates (Felice and Goswami, 2018).

A leading explanation for the combination of rapid growth and high morphological diversity in ceratopsian cranial ornaments is that these traits evolved through socio-sexual selection (Farlow and Dodson, 1975; Farke et al., 2009; Knell and Sampson, 2011; Hone et al., 2012; Hone et al., 2016). Determining whether socio-sexual selection was indeed the evolutionary driver of exaggerated traits in ceratopsians is important because it would allow us to examine its effects over long periods of time (Knell et al., 2012). Rapid evolution of secondary sexual traits was predicted by Fisher (1930), and

sexual selection-mediated adaptation to changing environments has found support from theoretical models in recent studies (e.g. Lorch et al., 2003; Martínez-Ruiz and Knell, 2016). Longer-term effects of sexual selection are difficult to experimentally test in extant taxa, although several recent studies have found evidence for rapid evolution of sexually selected *Onthophagus* beetle horns (Emlen et al., 2005), bird plumage (Dale et al., 2015; Cooney et al., 2019) and squamate cranial ornamentation (Watanabe et al., 2019). In addition, strong sexual selection has been found to increase survival probability of beetle populations during environmental disturbance (Parrett et al., 2019). Natural selection is also known to drive rapid morphological evolution through ecological adaptation (Futuyma, 2005; Watanabe et al., 2019), so care must be taken in interpreting such findings. Differentiating between ecologically adaptive traits and those under socio-sexual selection may prove challenging, but ecological traits are more likely to evolve towards optimal shapes and show some kind of ecologically adaptive function. An example of an ecologically adaptive trait in the ceratopsian cranium would be those associated with the feeding apparatus, e.g. the premaxilla and maxilla.

The ornamental traits (i.e. horns and frill) present in ceratopsians vary between clades, and these traits appear to evolve at different stages through their evolutionary history (Hailu and Dodson, 2004; Dodson et al., 2004; Brown and Henderson, 2015). Enlarged parietal-squamosal frills appear in the Coronosauria (Fig. 4.1, point 2), and are present in all known taxa in this clade. Morphologically diverse forms of the nasal and postorbital horns are present in Ceratopsidae (Brown and Henderson, 2015; Fig. 4.1, point 3). Within Ceratopsidae, Chasmosaurinae show a general pattern of long postorbital/short nasal, and Centrosaurinae exhibit long nasal/short postorbital horns. A great deal of both inter- and intraspecific variation exists in both traits (Dodson, 1996). This general pattern of diverse ornamentation is further complicated by bony outgrowths, termed epiossifications, which occur around the posterior margin of the frill in many taxa within Ceratopsidae (Fig. 4.1, point 3). These epiossifications form distinctive shapes that are often highly distinctive (e.g. *Styracosaurus*), but also show high levels of intraspecific variation (Tanke and Rothschild, 2010). It is uncertain how epiossifications are related in chasmosaurines and centrosaurines due to the different arrangement

and forms of growth between these two taxa (Sampson, 1997; Brown and Henderson, 2015). In some chasmosaurines, such as *Triceratops*, epiossifications appear to form separately from the frill in young individuals and fuse to it through ontogeny, often being resorbed into the frill in the largest individuals (Tanke and Farke, 2007) This contrasts with centrosaurines, where epiossifications appear to grow directly from the frill margin (Kirkland and DeBlieux, 2010).

Assessing patterns of morphological variation and evolution within a morphological framework requires a clear understanding of the relationship between traits (Klingenberg and Marugán-Lobón, 2013). The partitioning of correlated traits into evolutionary and developmentally independent regions, phenotypic modules, is a consequence of differential selection on these traits leading to divergent development (Goswami and Polly, 2010b; Felice and Goswami, 2017). Modularity has been assessed in tetrapod skulls from several clades including mammals (Goswami and Polly, 2010a), birds (Felice and Goswami, 2017), caecilians (Bardua et al., 2019a), squamates (Watanabe et al., 2019), and archosaurs (Felice et al., 2019b). Mosaic evolution, the differential evolution of traits, may follow modularity (Felice and Goswami, 2017). The highly varied morphology of the ceratopsian skull suggests that it may have had a modular structure, with differing levels of selection resulting in mosaic evolution (Dodson et al., 2004; Mallon et al., 2015). Failure to account for modularity, and consequently treating a modular structure as a single, integrated character, can give a poor understanding of true biological form (Watanabi et al., 2019). Identifying modules is an important first step in partitioning traits, and subsequently quantifying evolutionary rates and morphological diversity between them (Klingenberg, 2014; Goswami and Finarelli, 2016).

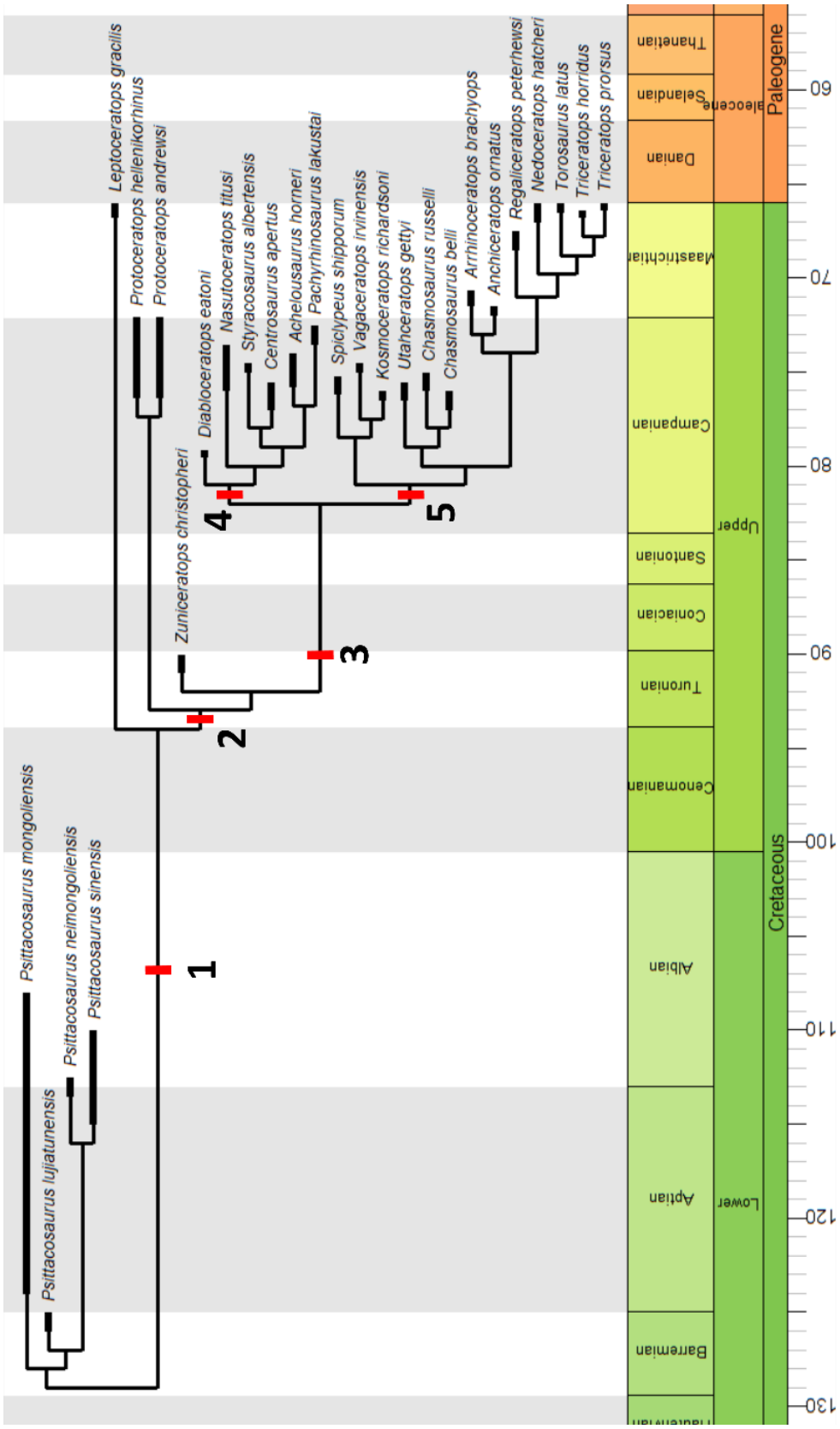

Figure 4.1: Time-scaled phylogeny of 27 ceratopsian taxa used in this study. Black horizontal bars at branch tips represent estimated temporal range of each species. Major clades are designated by red bars, and represent **1:** Neoceratopsia; **2:** Coronosauria; **3:** Ceratopsidae; **4:** Centrosaurinae; **5:** Chasmosaurinae (Adapted from Sereno, 2010; Brown and Henderson, 2015; Ryan et al., 2016).

Traits under strong selection of any kind should form distinct phenotypic modules because they face different selection pressures, and modularity allows traits to respond to selection with a degree of independence (Klingenberg, 2008; Goswami et al., 2014). Modules that function as socio-sexual traits are expected to show heightened rates of evolution compared to other traits (West-Eberhard, 1983), and comparing evolutionary rates between traits may help to resolve the claim that the unique frill and horns of ceratopsians followed this pattern. The application of three-dimensional (3D) morphometrics to shape data allows for a much more detailed assessment of both shape variation and modularity than is possible with either two-dimensional (2D) anatomical landmarks or linear measurements, particularly when dealing with complex 3D structures such as tetrapod skulls (Adams et al., 2013; Goswami et al., 2019). No study has yet employed these methods to evaluate the 3D morphology of the ceratopsian skull across a range of ceratopsian taxa (Mallon et al., 2015; Felice et al., 2019b).

The relationship between evolutionary rate and morphological disparity can provide information about how developmental and functional interactions, defined by integration and modularity, determine diversification and constraint in biological traits (Felice et al., 2018). While methods to estimate divergence times, as well as evolutionary rates, using molecular data and/or discrete morphological data are relatively well-established and widely used (e.g. Yang, 2007; Ronquist et al., 2012), models integrating quantitative data have not been widely explored, resulting in a lack of methods that can deal with continuous morphological characters. Recently, Álvarez-Carretero et al. (2019) implemented a Bayesian approach in the dating software *MCMCtree* (Yang, 2007), which enables the use of morphological continuous data (either alone or combined with molecular data) for divergence times estimation under quantitative character evolution following a Brownian motion model (Felsenstein, 1973). An important feature of this method is the possibility of using different partitions in the Bayesian analysis, which can be molecular, morphological, or a combination of both. MCMCtree can also estimate the mean evolutionary rates per partition in a dataset partitioned by phenotypic modules.

Integrated phenotypic traits (i.e. modules) are generally predicted to follow a Brownian motion model, where the relationship between evolutionary rates and morphological disparity is proportional (Felice et al., 2018). Deviation from this null model can provide information about the evolutionary history of these modules. Secondary sexual traits, which are generally not expected to show strong functional constraints and are more free to vary and evolve than ecological traits, may fall within the constraints of the null model, albeit with higher rates of evolutionary rate and morphological disparity than other traits (Felice et al., 2018). Under ecological or developmental constraint, traits will show lower disparity than expected for a given evolutionary rate.

Allometry, the variation of shape with size, is known to be an important factor of variation in many extant taxa (von Bertalanffy and Pirozynski, 1952; Mitteroecker et al., 2004; McNamara, 2012; Evans et al., 2018). Ceratopsian evolution is typified by a transition from small-bodied taxa with unadorned crania in the Late Jurassic and Early Cretaceous to large, quadrupedal taxa with large ornamented skulls in the Late Cretaceous (You and Dodson, 2004), hinting at a relationship between shape and size, and it has been observed that juveniles of different ceratopsian taxa resemble one another more than do the adults (McNamara, 2012). Heterochrony refers to changes in the timing and rate of developmental events and has been suggested to have played a role in the evolution of the ceratopsian skull, but these effects have not yet been quantified (McNamara and Long, 2012; Mallon et al., 2015). Analysis of allometry, and correcting for its effects where necessary, is an important consideration when assessing morphology.

In this study, I conduct the most comprehensive geometric morphometric study of ceratopsian skulls to date. I assess modularity, morphological disparity and evolutionary rates in the ceratopsian skull to test whether evolutionary patterns of exaggerated ornamental traits fit the patterns of rapid evolution and disparity predicted under socio-sexual selection.

4.3 Methods

4.3.1 Data collection

A total of 74 complete skulls from 27 ceratopsian species were digitised using photogrammetry (Agisoft Photoscan Professional 64 bit, V. 1.4.3, Build 6529). The specimens used represent the two major radiations of horned ceratopsians (Centrosaurinae and Chasmosaurinae) along with members of earlier-branching lineages; two species of *Protoceratops*, *Leptoceratops gracilis*, and four species of *Psittacosaurus* (Fig. 4.1; see Appendix for specimen details). Missing portions of specimens were reconstructed by digitally mirroring symmetrical elements where possible (Lautenschlager, 2016). Asymmetry resulting from taphonomic deformation (Angielczyk and Sheets, 2007) was corrected with the 'retrodeform' tool in *IDAV Landmark* (v. 3.0, Wiley et al., 2005) where appropriate, using the protocol outlined in Lautenschlager (2016). Rare examples of fluctuating asymmetry are known from ceratopsian epiossifications (Tanke and Rothschild, 2010), but this method assumes basic symmetry of the natural biological shape of the skull.

Thirty-three anatomical landmarks were first placed on the digital models, defining anatomically homologous points that could be identified on all specimens (Bardua et al., 2019b). Landmarks were placed on the right side of each skull to reduce redundancy by duplication (Cardini, 2016). Specimens that were more complete on the left side were digitally mirrored before landmarking. Eight separate skull elements (rostral, premaxilla, nasal, maxilla, postorbital, jugal, squamosal and parietal) were defined with a total of 67 semilandmark curves of 10 semilandmarks each (Fig. 4.2). With duplicate landmarks excluded, each skull was landmarked with 591 total landmarks and semilandmarks (Appendix). The 'postorbital' designation incorporated the postorbital, frontal, prefrontal and lachrymal of all specimens due to suture obliteration during ontogeny making these elements difficult to distinguish in many taxa (Ryan et al., 2007).

To describe the surface morphology of the skull in detail, a semi-automated process was used to place a further 208 surface semilandmarks on all specimens with the function 'placePatch' in the R package *morpho* (version 2.5.1; Schlager, 2017), following procedures outlined in Bardua et al. (2019b). With the addition of these surface semilandmarks the total number of landmarks and semilandmarks per specimen was brought to 799 (Fig. 4.2).

The frill of many ceratopsid ceratopsians (clade **3** in Fig. 4.1) is adorned with epiossifications, which are present on both the parietal and squamosal. These are considered an important component of ornamentation in ceratopsids, but are not known from other clades (Sampson, 1997; Kirkland and Deblieux, 2010). Because of their importance in ceratopsian taxonomy, epiossifications were landmarked and analysed separately for taxa in which they are present. The arrangement and number of epiossifications varies according to species and instances of intraspecific variation are known from the squamosal (Maidment and Barrett, 2011; Brown and Henderson, 2015), making landmarking them difficult. The first five epiossifications radiating outwards from the midline of the frill seem to be the most consistent within and between clades, and capture the majority of distinct patterns of variation. These were landmarked following the designation proposed by Sampson et al. (1997) for the taxa in which they are present, using five type 1 landmarks to designate the tips and ten semilandmark curves to describe the perimeter of these structures. This resulted in an additional 5 anatomical landmarks and 85 semilandmarks for this analysis.

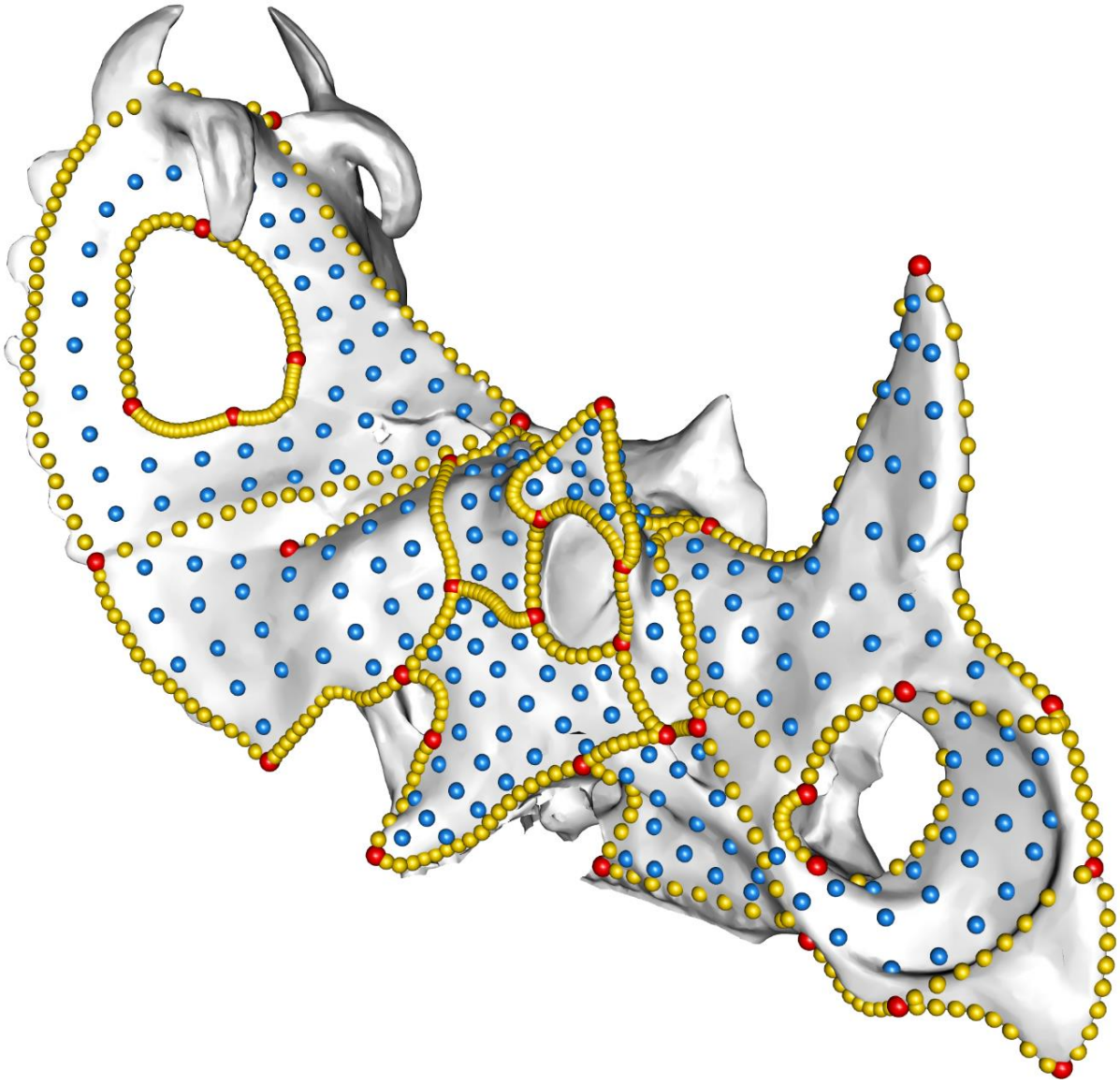

Figure 4.2: Landmark guide. Landmarks are shown on mesh model of *Centrosaurus apertus* (ROM 767) and are **Red:** Type I and II landmarks; **Yellow:** sliding semilandmark curves; **Blue:** sliding surface semilandmarks. See Appendix for landmark descriptions.

After the landmarking process, all analyses and data manipulation were performed in RStudio v. 1.1.383 (R Core Team 2013) unless otherwise stated. Because of issues arising from aligning one half of a bilaterally symmetrical structure, all landmarks were reflected across the skull midline to produce a bilaterally symmetrical set of landmarks before the Procrustes alignment (Cardini, 2016). A generalised Procrustes alignment (GPA) was performed on this manipulated dataset and the reflected landmarks were then removed, leaving the original set of right-side landmarks. All analyses were performed both on the complete dataset (n = 74), and a subset of the dataset consisting of one specimen per taxon (n = 27). This was done because current phylogenetic analyses of morphometric data cannot accommodate multiple specimens per taxon, and so the dataset was divided in this way for consistency between different analyses where multiple specimens per taxon could not be accommodated (Ives et al., 2007; Garamszegi and Møller, 2010; Adams and Otárola-Castilo, 2013). Representative specimens were chosen based on closeness to mean shape for taxa with multiple specimens. This method was chosen to avoid morphological disparity biases caused by extreme morphologies, a problem that may affect highly diverse socio-sexual traits (Cardini et al., 2015; Felice and Goswami, 2017).

A principal component analysis (PCA) was used to identify and visualise major trends of shape variation across ceratopsians. Morphological disparity (i.e. Procrustes variance) was assessed using the 'morphol.disparity' function in the R package *geomorph* (Adams and Otárola-Castilo, 2013), both for the entire cranium and for individual modules. The disparity value for each module was divided by the number of landmarks in that module to allow direct comparison of morphological disparity between modules. Per-landmark disparity was also calculated to visualise regional variation in disparity across the skull (Felice et al., 2018). When taphonomic deformation affects specimens in a dataset the dilation component of taphonomic deformation (i.e. that accounting for symmetrical deformation) is represented by a principal component of the Procrustes-aligned data and can be identified by examining the projected maximum and minimum shapes for each principal component. This method was used to estimate the effect size of taphonomic deformation on the dataset by noting

the contribution to total shape variation of the relevant principal component (Angielczyk and Sheets, 2007).

4.3.2 Effects of size on shape

Allometry, the relationship of shape and size, can have a significant effect on morphological analysis. The effects of static allometry (i.e. allometry between traits of individuals here assumed to represent adults) were quantified with the function 'procD.lm' in the R package *geomorph* (Adams and Otárola-Castilo, 2013), using skull centroid size as the size variable. The 'Common Allometric Component' (CAC), the component of shape variation most closely aligned with size, was identified and removed from the raw shape data with this method, creating an allometry-corrected dataset (Mitteroecker et al., 2004).

4.3.3 Modularity testing

Phenotypic module hypotheses were assessed using a maximum likelihood (ML) approach, implemented in the R package *EMMLi* (Goswami and Finarelli, 2016). A total of 24 module hypotheses were tested (Appendix), ranging from two (frill and rest of skull as two separate modules) to ten modules (treating eight landmarked skull bones and both the nasal and postorbital horn cores as separate modules; see Appendix for details). In addition to this ML approach, modularity was also tested with the covariance ratio (CR) method implemented with the 'modularity.test' function in the R package *geomorph* v.3.5.2 (Adams and Otárola-Castillo, 2013; Adams, 2016). The CR method returns a significance value which allows us to reject the null hypothesis of no modularity in the skull. Modularity tests were performed on all specimens (n = 74), and on the subset of specimens (n = 27). In addition, modularity tests were performed on the allometry-corrected datasets of these two specimen groups to test if allometric effects influenced modularity assessment.

4.3.4 Divergence times estimation

Bayesian inference of divergence times was carried out with MCMCtree v4.9 (Yang, 2007) on a fixed topology for the taxa used in this study (Fig. 4.1). This Bayesian approach using continuous morphological data (Álvarez-Carretero et al., 2019) is based on a model of quantitative character evolution under Brownian motion (Felsenstein, 1973).

There are several factors that might affect the data set (e.g., allometry, population variance, etc.). The combination of these factors (inclusion/exclusion) resulted in several models under which the data set could be analysed. In order to decide which of these models best fits the ceratopsian dataset, a Bayesian model selection analysis was carried out. This approach consists of using the marginal likelihood values estimated under each model to compute the Bayes factors, which ultimately are informative about the best-fitting model. The software MCMCtree was used to sample from *n* power posteriors (i.e. the number of models analysed, here *n* = 16) the likelihood values for each model. Subsequently, the R package *mcmc3r* (dos Reis et al., 2018) uses the collected likelihood values for each model and estimates the corresponding marginal likelihood using the stepping-stones approach (Xie et al., 2011). It then computes the Bayes factors and posterior probabilities, which help to select the model that best explains the data. Once this step is completed, Bayesian inference of divergence times can proceed with the best-fitting model.

The models under which the morphological dataset was analysed took into account (i) the process followed by the evolutionary rate (i.e., either under an independent log-normal distribution, ILN; Rannala and Yang, 2007; Lemey et al., 2010; or a geometric Brownian motion, GBM; Thorne et al., 1998; Yang and Rannala, 2006), (ii) accounting or not for allometry, and (iii) the morphological shape (using a representative specimen per taxon or the mean species shape to build the morphological data set). The mean shape was calculated for each taxon where more than one adult specimen was present in the dataset. Of the taxa included in the dataset, *Regaliceratops peterhewsi* is known from only one specimen which has been complexly deformed by taphonomic processes and contrasts with simpler

compaction seen in the majority of taphonomically deformed specimens in the dataset (Brown and Henderson, 2015). This type of deformation is unique to this specimen in the dataset and cannot be simply estimated or corrected for (for discussion, see Angielczyk and Sheets, 2007). For this reason, this specimen was removed from the dataset. The morphological alignments for these dataset combinations were generated with the 'mcmc3r' R package as described in Álvarez-Carretero et al. (2019), although here they were not corrected for population noise or character correlation. This was because at present, the highly varied nature of ceratopsian skull morphology does not allow assumptions of between-taxa similarity to be made with the existing method. All divergence times were estimated under the best-fitting model according to the Bayes factors for both unpartitioned (whole-skull shape data in one partition) and dataset partitioned according to separate modules previously identified with the *EMMLi* modularity analysis.

4.3.5 Phylogenetic factors affecting shape

Evolutionary allometry, the evolutionary change in shape that is associated with evolutionary change in size, and describes the degree to which allometry is phylogenetically structured (Klingenberg and Marugán-Lobón, 2013; Voje et al., 2014). It was assessed using the 'procD.pgls' function in *geomorph* (Adams and Otárola-Castilo, 2013), a phylogenetic generalised least squares analysis for geometric morphometric data. This analysis was performed over 1000 iterations on the globally-aligned Procrustes data on whole-skull data and for each module individually.

Phylogenetic signal in the shape data was quantified with the $\boldsymbol{K_{mult}}$ statistic (Adams, 2014b), which calculates phylogenetic signal in multivariate data under a Brownian motion model of evolution using the dated phylogeny output from MCMCtree. This process was performed on the whole skull and individual module data using the 'physignal' function in the R package *geomorph* v. 3.1.2 (Adams and Otárola-Castillo, 2013). The output of this model returns significance value and an estimate of the phylogenetic signal which varies between 0 (phylogenetic independence) and 1 (species' traits covary in proportion to their evolutionary history; Tidière et al., 2017).

Net evolutionary rate (σ^2_{mult}; Adams, 2014a) for each module was calculated with the 'compare.multi.evol.rates' function in the R package geomorph (Adams and Otárola-Castillo, 2013), using the dated phylogeny. In addition, per-landmark evolutionary rates across the entire skull were calculated with the 'compare.evol.rates' function in the R package *geomorph* to visualise fine-scale regional evolutionary rates, and also to give a per-landmark basis for comparing evolutionary rates with morphological disparity (Felice et al., 2018; Bardua et al., 2019a). The relationship between per-landmark morphological disparity and evolutionary rate was investigated with a linear regression for the entire skull. These were compared against a simulated null expectation for all landmarks under a Brownian motion model of evolution for the shape data, calculated with the 'sim.char' function in the R package *geiger* over 100 simulations (Harmon et al., 2008). The null model is based on the expected morphological disparity given the observed evolutionary rates for the dataset (Felice et al., 2018). Confidence intervals of 95% were generated for this regression to determine which landmarks fell outside this expected model of evolution. All rate and disparity analyses were performed both on raw Procrustes-aligned shape data, and with data where the allometric component of shape variation had been removed.

4.4 Results

4.4.1 Modularity

The maximum likelihood analysis of modularity returned highest support for the maximum 10-module hypothesis from the raw landmark data. Because of the tendency of densely-sampled landmarks to return the maximum number of modules with the ML method, the within- and between-module correlations in the ten-module model were examined to determine whether any regions could be merged, using the process outlined in Felice and Goswami (2017). A between-module discrepancy value of 0.2 was used as a merging threshold, as discussed by Bardua et al. (2019a), and modules were

merged where the value fell within this threshold. Four element pairs were merged into single modules through this process (Fig. 4.3). These were the parietal-squamosal (hereafter 'frill'), the postorbital-postorbital horncore, the nasal-nasal horn core and the premaxilla-rostral. Running the modularity analysis after correcting for allometry resulted in small changes in correlation values but general patterns of modularity remained unchanged (Fig. 4.3C). The covariance ratio (CR) analysis confirmed that this dataset has a significantly modular structure (CR = 0.69, p = 0.001). Modularity analyses performed on both the raw and allometry-corrected subgroup of the entire dataset (i.e. single representative specimen per taxon) showed patterns of integration and modularity that were consistent with the whole dataset analysis.

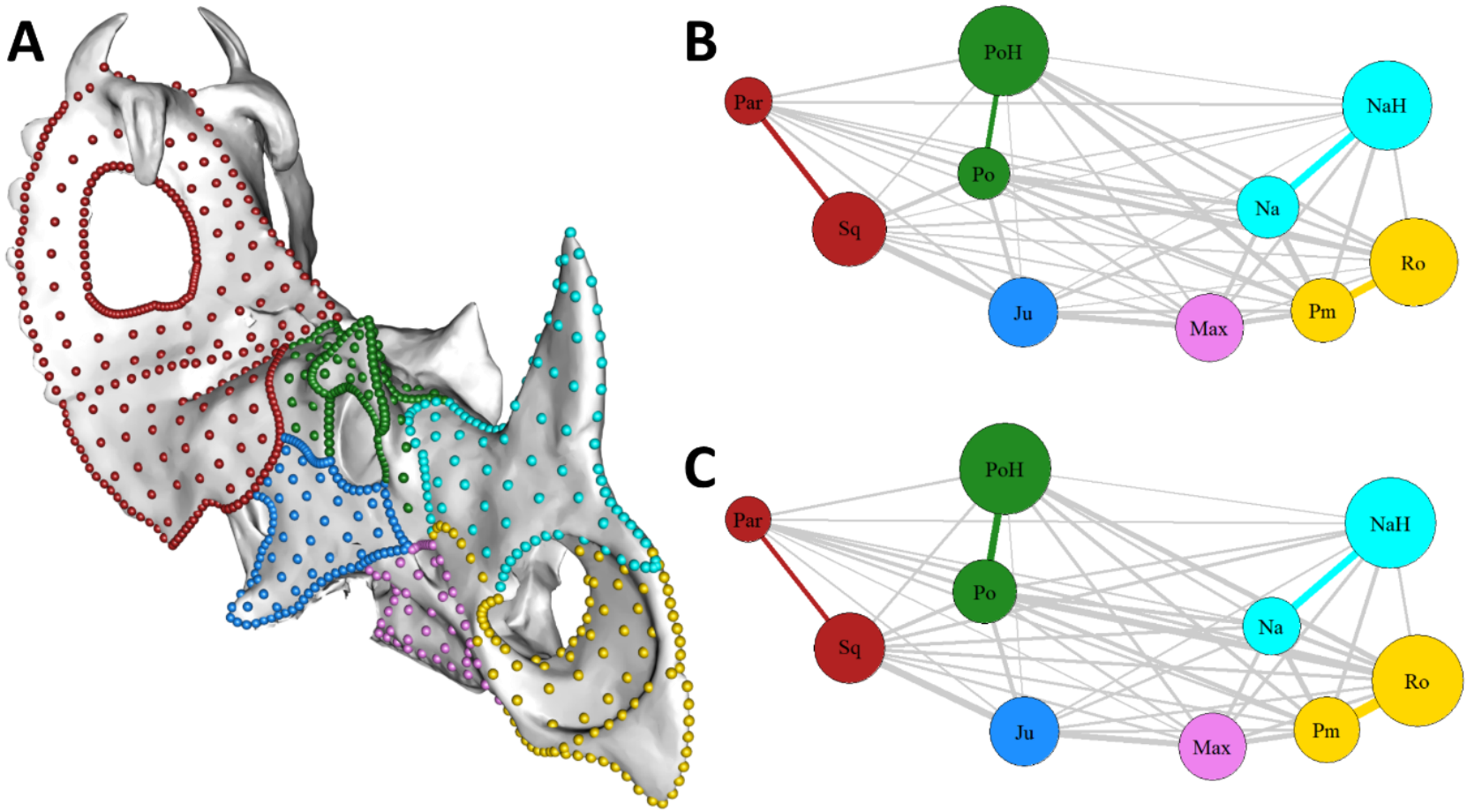

Figure 4.3: Results of EMMLi modularity test. Landmarks are coloured according to module on example mesh (*Centrosaurus apertus* ROM 767) in 4.3A. Network plots (4.3B and 4.3C) show internal correlations for each skull element (circle size) and between-element correlation values (line thickness). Skull elements are positioned to roughly correspond with their relative positions in the ceratopsian skull. Coloured lines indicate a strong between-element link (< 0.2 difference), resulting in merging of elements into single modules. Shown are EMMLi results for raw data (4.3B) and allometry-corrected data (4.3C). Element abbreviations are: **Par:** parietal; **Sq:** squamosal; **Ju:** jugal; **Po**: postorbital; **PoH:** postorbital horn core; **Na:** nasal; **NaH:** nasal horn core; **Max:** maxilla; **Pm:** premaxilla; **Ro:** rostral.

4.4.2 Morphological variation

The Bayesian factors computed during the Bayesian model selection analyses found that the best-fitting model was the one that (i) accounted for allometry, (ii) used mean-shape data to build the morphological alignment, and (iii) the morphological evolutionary rate followed an ILN distribution. The time-calibrated phylogeny inferred under this model was used to create a phylomorphospace (i.e., a principal components analysis of the Procrustes-aligned shape data combined with the tree), using one representative specimens from each group to show the relationships between taxa (Fig. 4.4). The shape variation described by a principal components can be visualised by constructing projected shapes at extreme values for each principal component, and these are shown for the first three PCs in Fig. 4.4. Closely-related species form distinct clusters with the more derived ceratopsids clustering at negative PC values. PC1 accounts for 44.4% of total shape variation and describes a transition from a *Psittacosaurus*-like shape at positive values to a *Torosaurus*-like shape at negative values (Fig. 4.4A). PC2 accounts for 13.1% of total shape variation and describes a transition from a wide-frilled and hornless shape at positive PC values, resembling *Protoceratops*, to a shape resembling *Triceratops* at negative PC values. PC3 accounts for 9.7% of total shape variation and describes the general differences between the long-frilled chasmosaurines and shorter, saddle-shaped frills of centrosaurines (Fig. 4.4B). Despite forming clusters at broader taxonomic levels, examination of the underlying phylogeny reveals that specimens that are closer in morphospace are not necessarily the most closely related. A notable observation is that *Torosaurus* does not cluster with closely-related *Triceratops,* but instead occupies a region of morphospace closer to *Chasmosaurus.* Together, the first 13 principal components account for 95% of total shape variation.

To illustrate the relative morphological disparity of individual modules, phylomorphospaces of the six modules identified by EMMLi were plotted, grouped by clade with convex hulls (Fig. 4.5). Species tend to group by clade in most cases, but some exceptions are apparent. The jugals show noticeably higher disparity in the three species of *Psittacosaurus* than does any other module for this genus, suggesting

relatively high shape variation of jugals in this clade. Centrosaurines show the largest degree of morphological disparity in the nasal module, spanning the majority of PC1. This is reflected in their distinct morphologies from the long, upright nasal horncores in *Centrosaurus* and *Styracosaurus*, to wide, flattened nasal bosses in *Pachyrhinosaurus* and *Achelousaurus.* Chasmosaurines show less relative morphological diversity in the nasal. The postorbital, including the horncore, shows relatively high disparity in Ceratopsids (chasmosaurines and centrosaurines), reflecting the high morphological variation of postorbital horns in this clade. Clades are well defined for the frill, resembling the morphospace distribution of the first two principal components illustrated in Fig. 4.4A. This suggests that frill morphology tends to be conserved within taxa, and has a strong influence on overall skull shape. The phylomorphospace for the premaxilla-rostral module shows clear clade groupings, with the exception of the centrosaurines. This is possibly a combination of the unusually narrow, deep premaxillary morphology of the basal taxa *Diabloceratops* and *Nasutoceratops* with the generally wider shape of later taxa such as *Styracosaurus* and *Achelousaurus*.

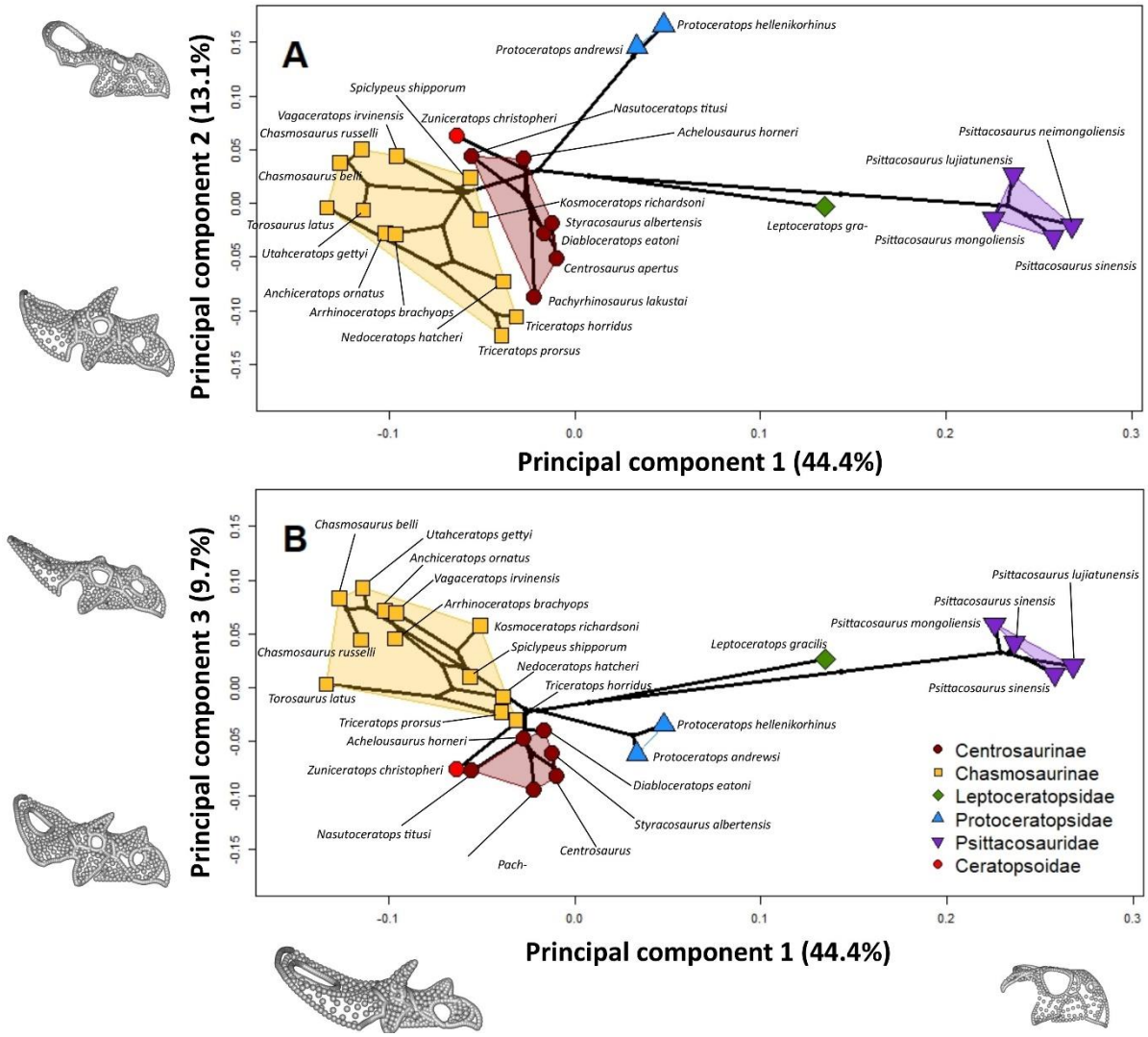

Figure 4.4: Phylomorphospace of whole-skull shape data for ceratopsian taxa included in this study. The x-axis represents PC1 for both plots, the y-axis represents PC2 (4.4A) and PC3 (4.4B). Convex hulls group taxa according to subfamily or equivalent levels. The first three PCs account for 44.4%, 13.1% and 9.7% of total shape variation respectively. Phylogeny is represented by solid black lines. Landmark configurations on axes represent shape changes along the relevant principal component.

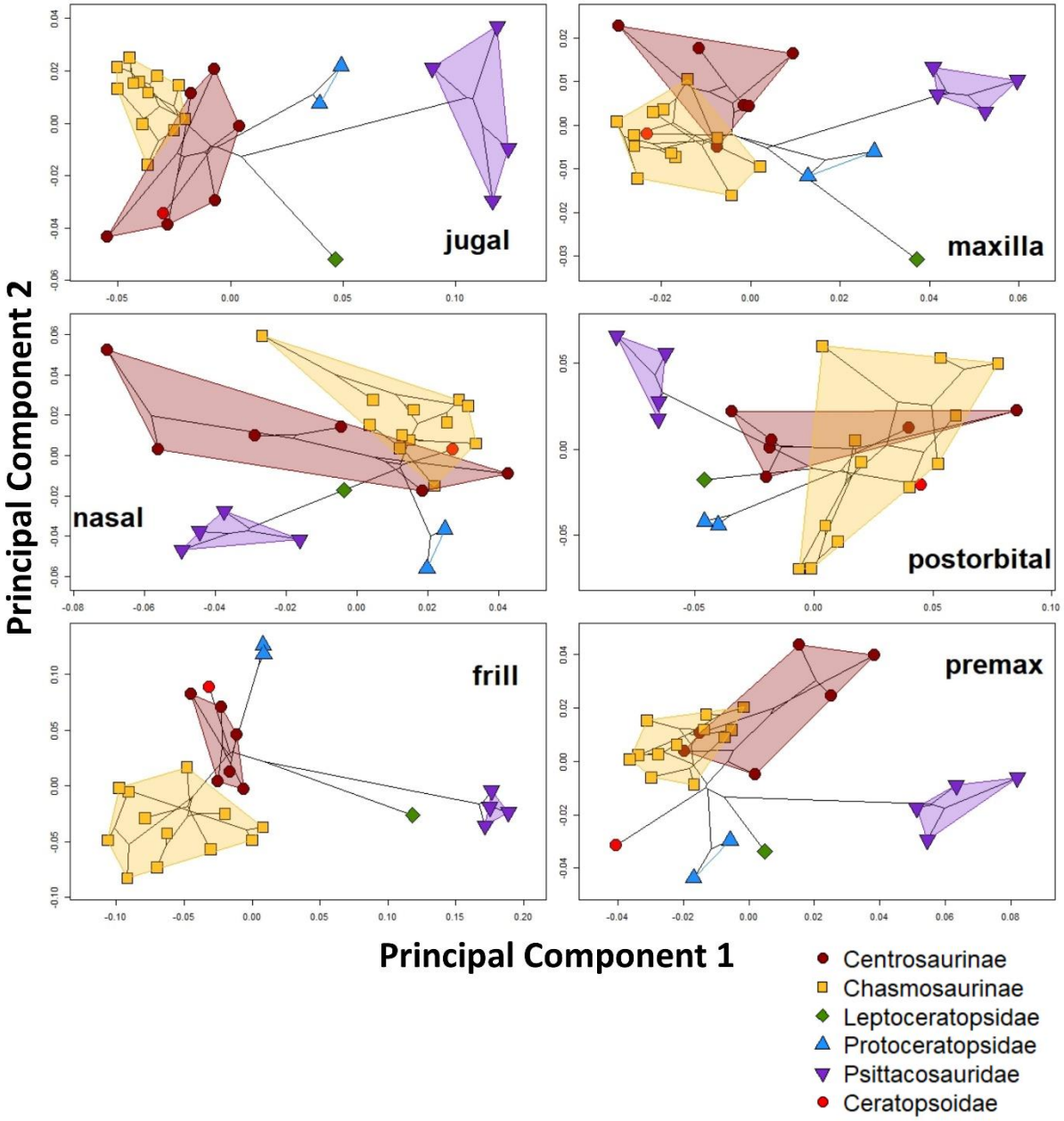

Figure 4.5: Phylomorphospaces of individual modules for all taxa, projected along PCs 1 and 2 (x and y axes, respectively). Specimens are coloured according to clades. Phylogenetic tree is represented by solid black lines in each plot.

4.4.3 Allometry

Allometry is a significant component of shape variation in both the whole dataset (R^2 = 0.26, p = <0.01), and the representative (i.e. one specimen per taxon) subsample of the dataset (R^2 = 0.4, p = <0.01; Table 4.1). The subset of the overall dataset containing only one specimen per taxon does not encompass intraspecific variation to the extent that the complete dataset does, where some species are represented by multiple specimens. The greater proportion of total shape variation accounted for by allometry in the representative dataset (~40% compared with ~26% in the full dataset) suggests that intraspecific variation is fairly high in ceratopsians. Allometry analyses were performed on individual modules, the results of which are summarised along with whole-skull allometry analyses in Table 4.1. Although both subdivisions of the dataset show significant effects of size on shape for individual modules, representative specimens (i.e. one specimen per taxon) show the highest effect size (R^2) values. The jugal and maxilla show the highest and second highest R^2 values respectively, suggesting that morphological variation in these modules is largely correlated with size. The lowest R^2 value is seen in the nasal, reflecting the highly diverse nasal horn morphology of ceratopsids. Projected shapes at maximum and minimum size for each module are shown in Fig. 4.6. The projected module shapes at maximum and minimum sizes resemble their counterparts in the projected shapes at positive and negative values for PC1 in Fig. 4.4A. Module shapes at maximum sizes resemble typical chasmosaurine morphology (e.g. *Torosaurus*) and those at minimum sizes resemble the morphology of *Psittacosaurus.* Small sizes are associated with a rudimentary parietal-squamosal frill, large orbit, deep, narrow premaxilla-rostral complex, and narrower, flared jugal. Larger sizes are associated with greatly enlarged frill, long, shallow premaxilla-rostral complex, broad and rounded jugals, and horns on the nasal and postorbital.

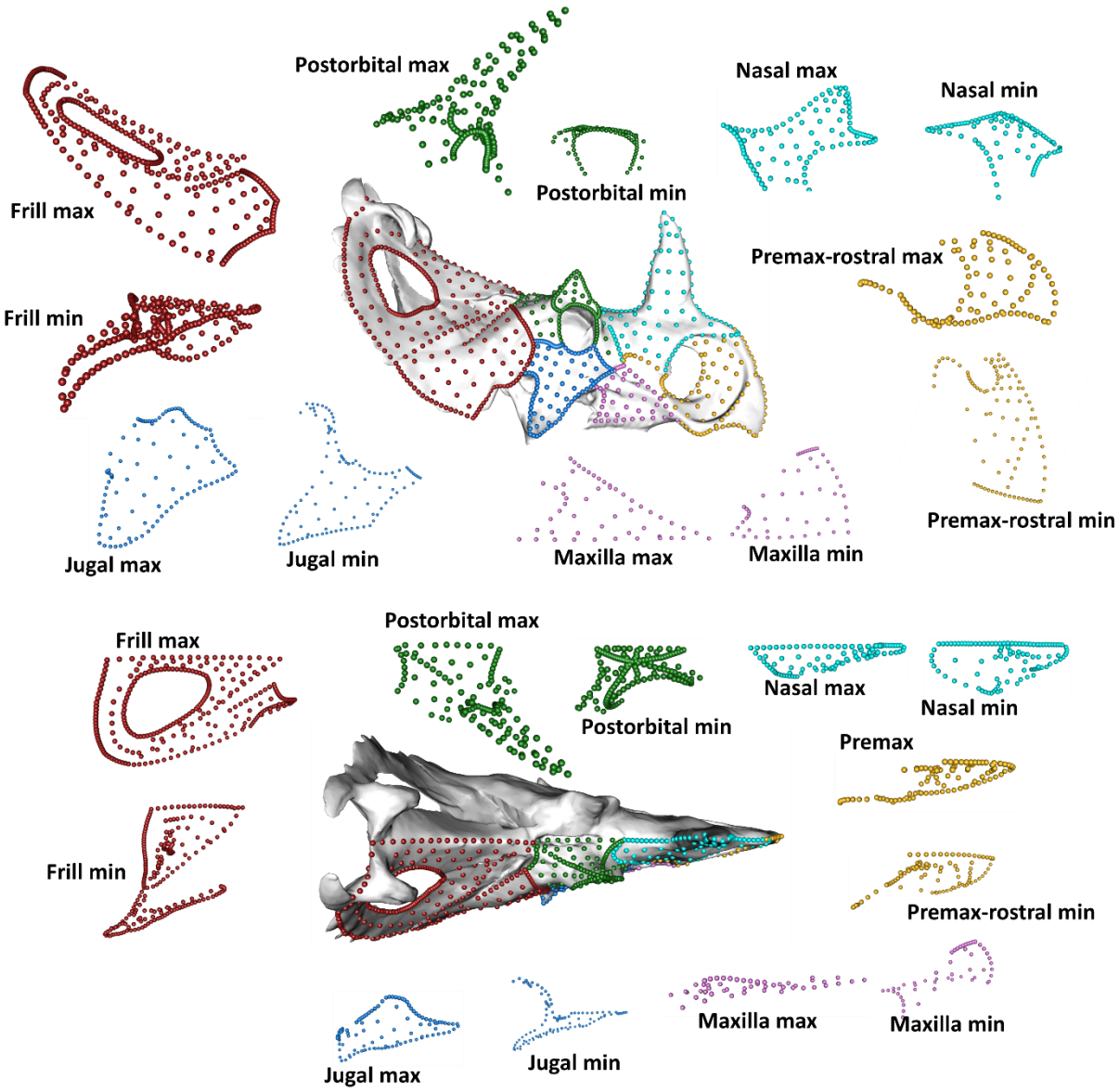

Figure 4.6: Individual module shapes shown at maximum and minimum sizes along with whole-skull representation of their relative positions (not to scale). Shown are side views (upper panel) and top views (lower panel).

Table 4.1: Results of allometry analyses for whole dataset (**A**) and representative specimens (**B**). Results show R^2 and *p* values for each analysis.

Module	A		B	
	R^2	*p*	R^2	*p*
Whole skull	0.273	<0.002	0.400	<0.002
Nasal	0.190	<0.002	0.243	<0.002
Postorbital	0.204	<0.002	0.256	<0.002
Jugal	0.530	<0.002	0.626	<0.002
Maxilla	0.371	<0.002	0.504	<0.002
Frill	0.253	<0.002	0.404	<0.002
Premax-rostral	0.201	<0.002	0.364	<0.002

Overall skull size in ceratopsians was visualised in a phylogenetic context by plotting centroid sizes onto the phylogeny (Fig. 4.7). A pattern of increasing size seems apparent, with a notable increase in size at the base of Ceratopsidae (Fig. 4.1, point 3). The smallest skulls are found in the several species of *Psittacosaurus*, and the largest occur in chasmosaurines, particularly *Torosaurus* and *Triceratops.*

Evolutionary allometry was found to be significant but with a low effect size, accounting for 9% of shape variation in the entire skull (Table 4.2). In addition, the frill, jugal, maxilla and premax-rostral showed significant phylogenetic signal but with low effect sizes, ranging from 8% in the premaxilla-rostral to 11% in the frill.

Table 4.2: Results of phylogenetic least-squares analysis of evolutionary allometry, for whole-skull data and individual modules. Statistically significant *p*-values ($p < 0.05$) are marked *.

	R^2	*P*
Skull	0.087	0.018*
Frill	0.106	0.013*
Jugal	0.104	0.030*
Nasal	0.020	0.716
Maxilla	0.093	0.043*
Postorbital	0.065	0.123
Premax-rostral	0.080	0.047*

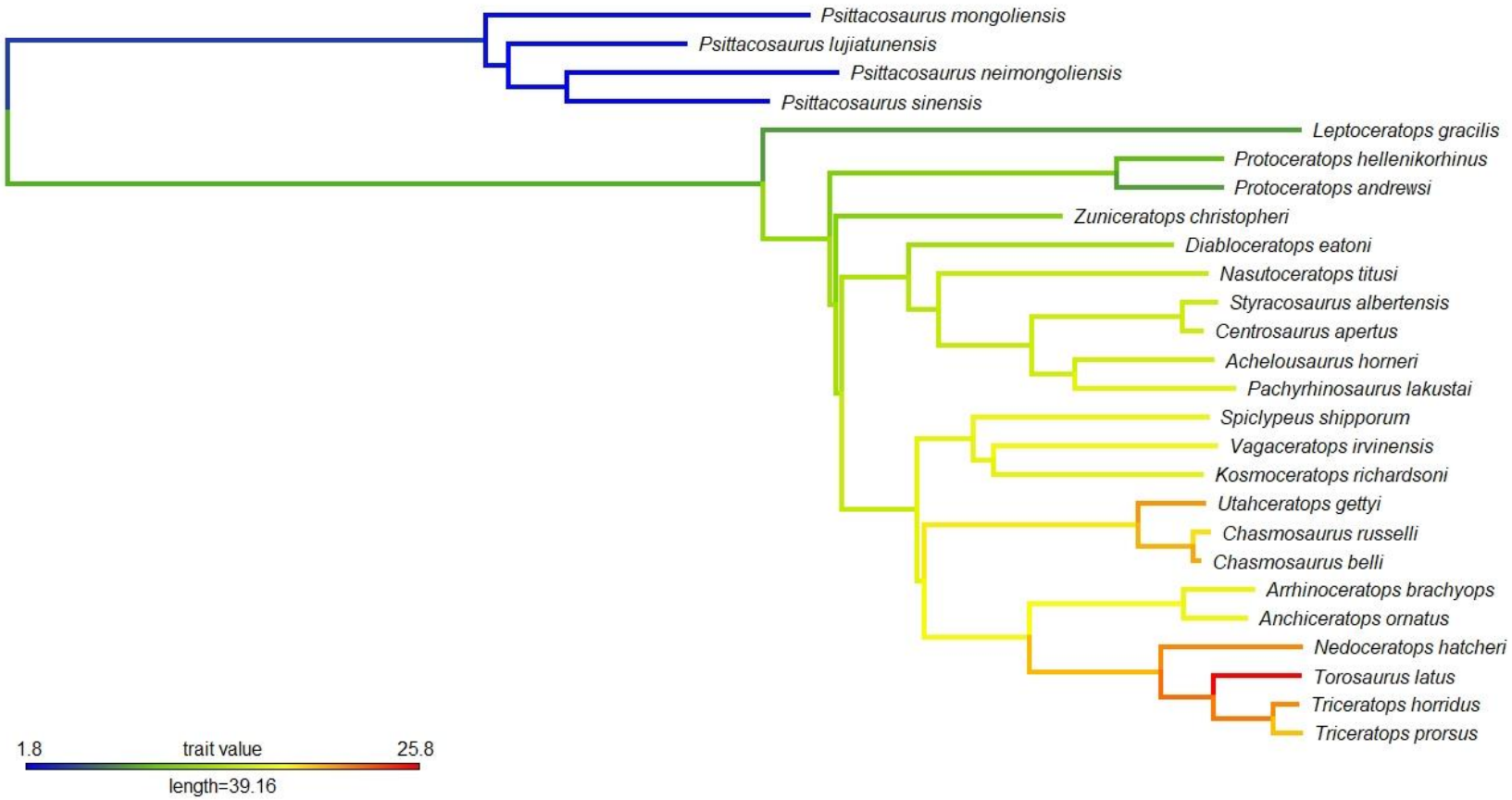

Figure 4.7: Evolution of skull size in ceratopsians on time-scaled phylogeny. Branches are coloured according to centroid size; blue represents smallest sizes and red largest sizes.

Comparing absolute module sizes across species which vary greatly in overall size is not informative of how relative module sizes evolve. A more informative illustration of relative module size was gained by calculating the ratio of module centroid size and skull centroid size for each species (ratio = $Csize_{module}/Csize_{skull}$). This value can inform of major changes in the size of modules relative to the whole skull. The results of this for each module are shown on the phylogeny in Fig. 4.8, and some clear patterns are apparent. The frill shows a large increase in relative size at the base of the Coronosauria (*Protoceratops* - *Triceratops* clade), corresponding with the enlarged frills seen in these taxa. It is highest in the chasmosaurine taxa, particularly *Chasmosaurus* and *Torosaurus.* The maxilla, premax/rostral and jugal modules show almost opposite trends to that of the frill, having the largest ratios in basal *Psittacosaurus* taxa and lowest among the chasmosaurines *Chasmosaurus* and *Torosaurus.* The modules that encompass horns in some species, i.e. the postorbital and nasal, show elevated values in which the horns are maximally expressed, as may be expected, but the postorbital also shows high ratio in the basal *Psittacosaurus* taxa, which do not possess postorbital horns. The high postorbital size ratio in these species can be explained by the relatively large size of the orbit, which is surrounded largely by the postorbital, increasing the relative size of this module in these taxa.

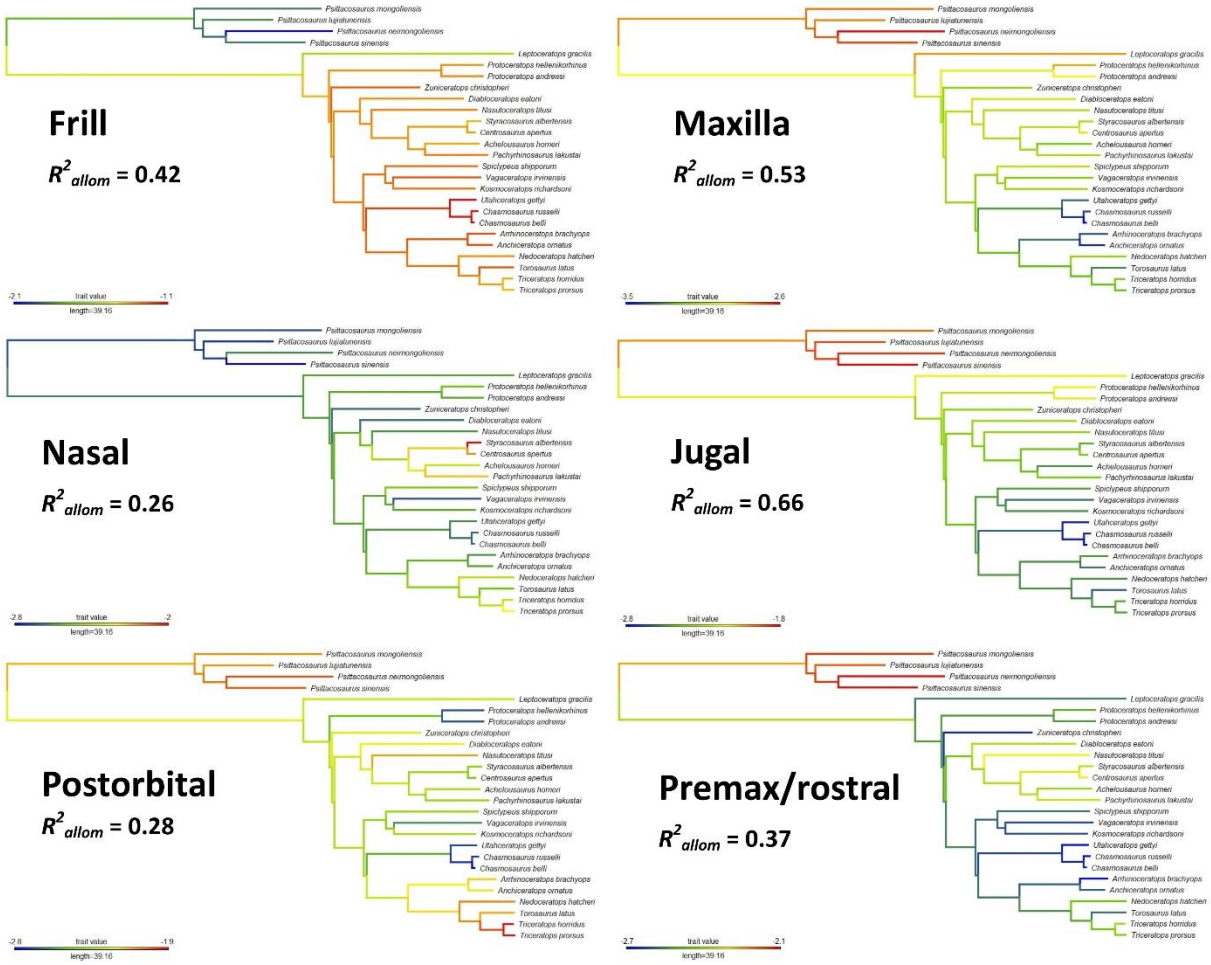

Figure 4.8: Ratio of module centroid size to skull centroid size plotted onto time-scaled phylogeny. Branch colours represent low (blue) to high (red) ratio of module size to skull size. The effect size of allometry (R^2_{allom}) for each module is displayed alongside the appropriate plot.

By removing the common allometric component, the component of shape that is most closely aligned with size, it is possible to visualise the shape variation in ceratopsians that is not correlated with size (Klingenberg and Marugán-Lobón, 2013). These size-independent shape components, or residual shape components (RSC), here act as allometry-corrected principal components. The first three allometry-corrected PCs are shown as phylomorphospaces in Fig. 4.9. As with the PCA plots in Fig. 4.4, specimens are again grouped according to clade, but separations between clades are less distinct. PC1 accounts for 23.7% of total shape variation, describing a transition from shorter-frilled forms to larger, *Protoceratops*-like forms, similar to PC2 of Fig. 4.4. Early-diverging taxa (i.e. *Psittacosaurus* and

Leptoceratops) appear to group in the centre of the morphospace, with chasmosaurine taxa (yellow convex hull) occupying a region of morphospace surrounding this. Centrosaurine taxa (red convex hull) are largely separated from chasmosaurines along PC2. The two *Protoceratops* taxa occupy a region of morphospace separated from all other taxa along PC1, suggesting their morphology diverged strongly from other taxa in the dataset during the evolution of this clade. PC3 (4.9B), accounting for 11% of allometry-corrected shape variation, describes a transition from an upright-frilled shape with prominent postorbital horns at positive values to a more flattened frill with a large, upright nasal horn at negative values. No clear separation between clades is visible along this principal component.

4.4.4 Phylogenetic signal and evolutionary rates

Multivariate phylogenetic signal (Table 4.3) was significant but had weaker phylogenetic signal than expected under a Brownian model for the whole-skull data ($\boldsymbol{K_{mult}}$ = 0.846, p = <0.001). Phylogenetic signal was relatively low for all modules except the jugal, and varied in strength from highest in the jugal ($\boldsymbol{K_{mult}}$ = 1.418, p = 0.001) to lowest in the nasal ($\boldsymbol{K_{mult}}$ = 0.548, p = 0.001; Table 4.3). Per-module evolutionary rates ($\boldsymbol{\sigma^2_{mult}}$) are also displayed in Table 4.3. Evolutionary rate is highest in the frill ($\boldsymbol{\sigma^2_{mult}}$ = 6.11 x 10^{-7}), almost three times that of the lowest rate, seen in the maxilla ($\boldsymbol{\sigma^2_{mult}}$ = 2.22 x 10^{-7}). The postorbital shows the second-highest rate, at $\boldsymbol{\sigma^2_{mult}}$ = 2.95 x 10^{-7}. Correcting for allometry by removing the CAC from the shape data results in reduced values for both phylogenetic signal and evolutionary rates, but relative rank remains similar. The phylogenetic signal of the jugal (p = 0.08) and the maxilla (p = 0.1) are non-significant when corrected for allometry, suggesting that variation in the shapes of these modules is largely due to size variation, and is otherwise similar. In addition, the phylogenetic signal for the frill in the allometry-adjusted dataset ($\boldsymbol{K_{mult}}$ = 0.239) is lower than the equivalent value for the postorbital ($\boldsymbol{K_{mult}}$ = 0.245).

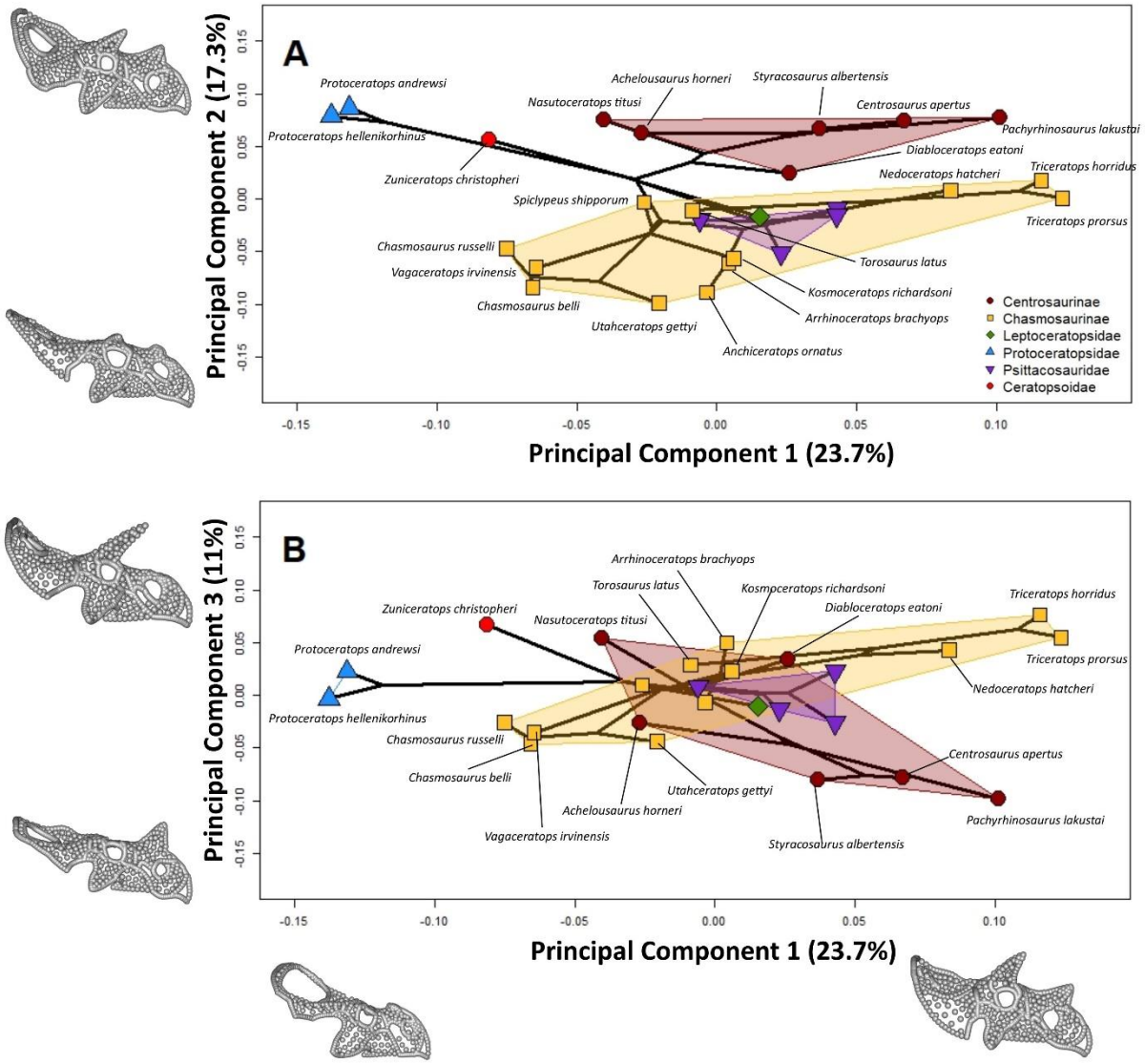

Figure 4.9: Allometry-corrected phylomorphospace of ceratopsian taxa, grouped by convex hulls according to clade. Shown are PC1 (x-axis of both plots), PC2 (y-axis of **A**) and PC3 (y-axis of **B**). Projected skull shapes at maximum and minimum PC values are show along the relevant axes.

Table 4.3: Results of phylogenetic signal analysis (K_{mult}), and module net evolutionary rate analysis (σ^2_{mult}) for ceratopsian shape data. Statistically significant values (p = <0.05) are indicated with *.

Module	K_{mult}		σ^2_{mult}	
	Raw shape	Allometry-adjusted	Raw shape	Allometry-adjusted
Whole skull	0.846*	0.322*	-	-
Frill	0.898*	0.322*	6.110×10^{-7}*	5.734×10^{-7}*
Jugal	1.418*	0.250	3.088×10^{-7}*	2.948×10^{-7}*
Premaxilla/rostral	0.715*	0.296*	2.506×10^{-7}*	2.485×10^{-7}*
Nasal	0.548*	0.297*	3.622×10^{-7}*	3.695×10^{-7}*
Postorbital	0.615*	0.322*	3.880×10^{-7}*	3.868×10^{-7}*
Maxilla	0.956*	0.247	2.221×10^{-7}*	2.159×10^{-7}*

Of all the modules identified in this study, the frill showed the highest overall whole-module morphological disparity (Fig. 4.10A). Modules that are typically associated with a feeding role (e.g. maxilla and rostral/premaxilla) show comparatively low values of morphological disparity. The postorbital and jugal modules show slightly higher levels of disparity. Per-module evolutionary rates show relatively similar patterns to values for morphological disparity, suggesting a relationship between rates and disparity. When the morphological data is corrected for allometry, relative rates and disparity remain broadly similar (Fig. 4.10B). Absolute rate values change little after correction for allometry, but disparity shows a noticeable reduction for the frill and small increase in disparity for the remaining modules. The exception is the nasal, which shows a doubling of morphological disparity after correction for allometry.

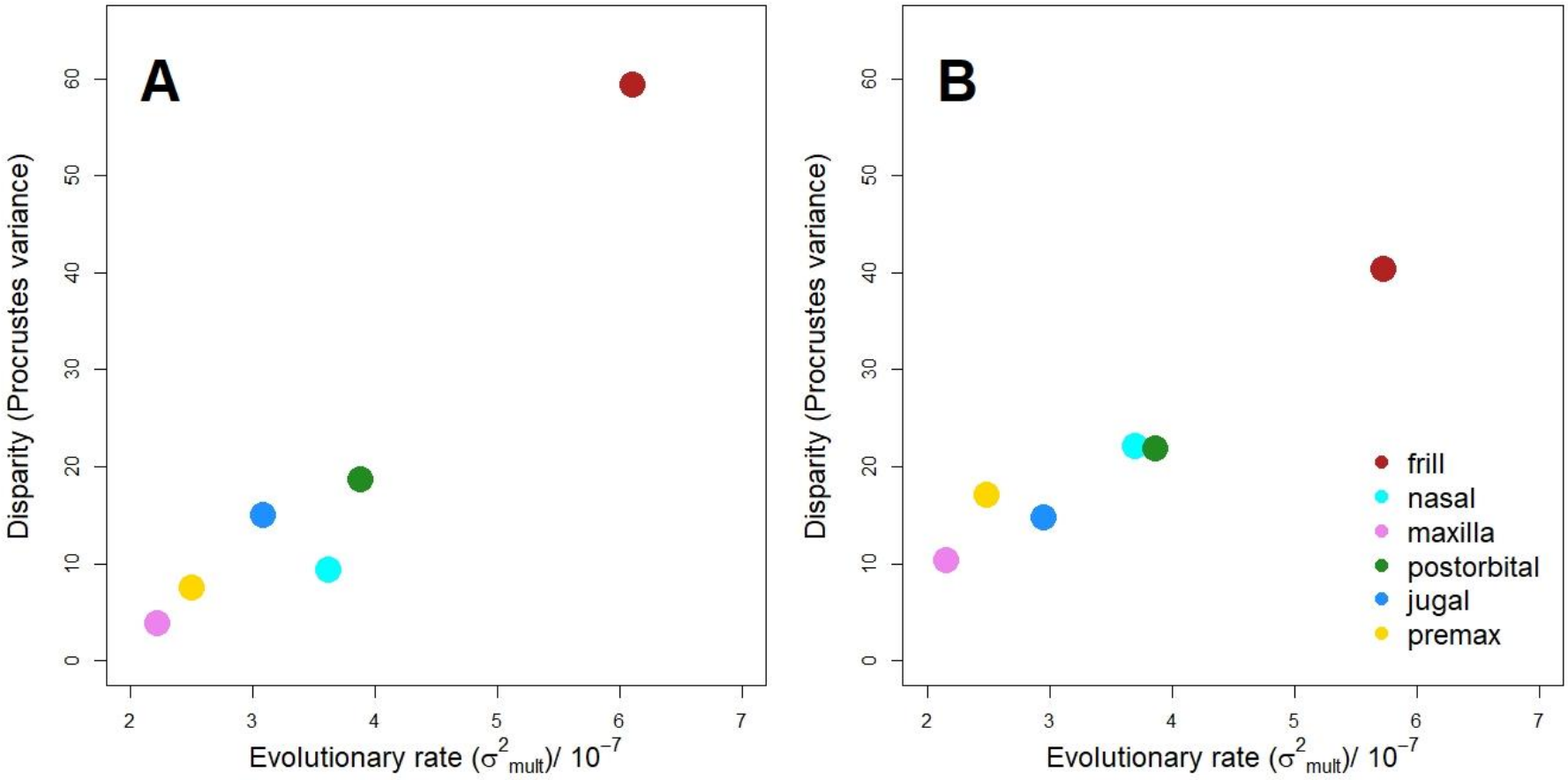

Figure 4.10: Relationship of net module disparity and evolutionary rate for raw (**A**) and allometry-corrected (**B**) shape data.

Per-landmark morphological disparity and evolutionary rate are coloured according to magnitude and shown projected onto a specimen of *Centrosaurus apertus* in Figure 4.11 (A and B, respectively). The regions of greatest morphological disparity are seen in the frill (particularly the lateral margin of the squamosal and the region of squamosal-parietal contact), and the tips of the nasal and postorbital horns (Fig. 4.11A). Lowest disparity is seen in the region of the postorbital-maxilla-nasal-jugal-premaxilla junction. Per-landmark evolutionary rate (σ^2_{mult}) is highest in the postorbital horns and at the outer edge of the squamosal, and lowest around the orbits and lateral regions of the region encompassing the maxilla, premaxilla and nasal (Fig. 4.11B). The relative similarity between these two plots suggests that morphological disparity and evolutionary rates are regionally correlated (Felice et al., 2018).

The relationship between per-landmark morphological disparity and evolutionary rate for each module in the dataset show distinct linear trends for each module, with the exception of the frill (Fig. 4.12A). The relationship between morphological disparity and evolutionary rate (σ^2_{mult}) is highly significant (p = <0.001). Modules often associated with exaggerated traits, namely the frill, nasal and jugal, show high levels of disparity and rates compared with the maxilla and premaxilla/rostral modules. The Brownian expected relationship between morphological disparity and evolutionary rates, represented by the black regression line, is noticeably lower than the regression for the whole-skull data (red line). Despite this, all landmarks fall within the 95% confidence intervals for this model, represented by the grey shaded area, with the exception of a number from the frill. The higher than expected morphological variance in these landmarks given their evolutionary rate suggests that constraint is relaxed in some regions of the frill. Correcting the landmark data for allometry greatly reduces the spread of values, particularly those for morphological disparity (Fig. 4.12B). Frill (red points) and jugal (blue points) cluster much more closely around the regression line for the landmark data (red line). The reduction in disparity values caused by correcting for allometry has the effect of reducing the slope of the regression line for the landmark data, bringing it closer to the regression for

the simulated variance – rate relationship (black line). Furthermore, all points fall well within the 95% confidence intervals (grey shaded area).

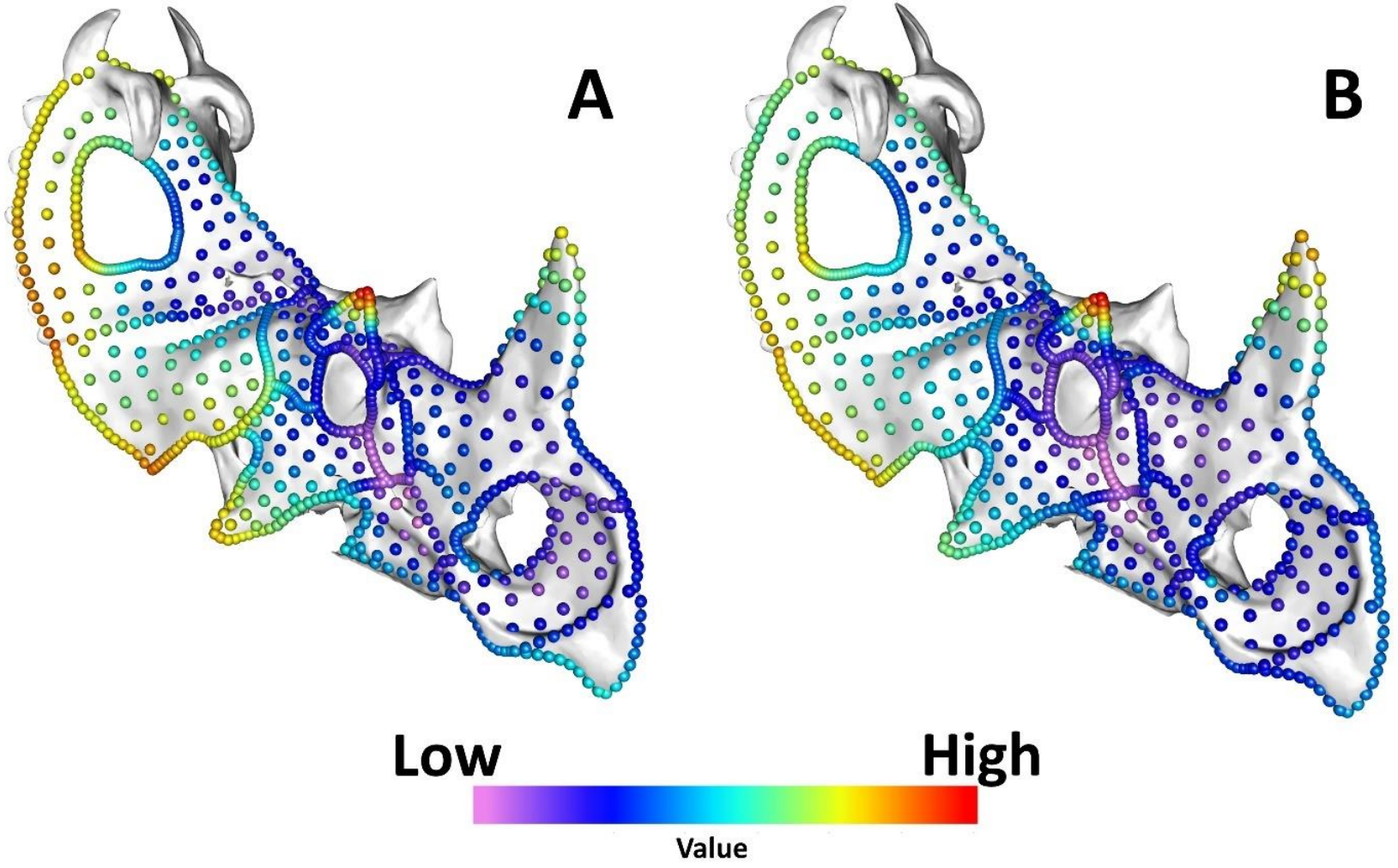

Figure 4.11: Per-landmark morphological disparity (**A**) and evolutionary rate (**B**) for all taxa shown on *Centrosaurus apertus* (specimen ROM 767). Landmarks are coloured according to relative values.

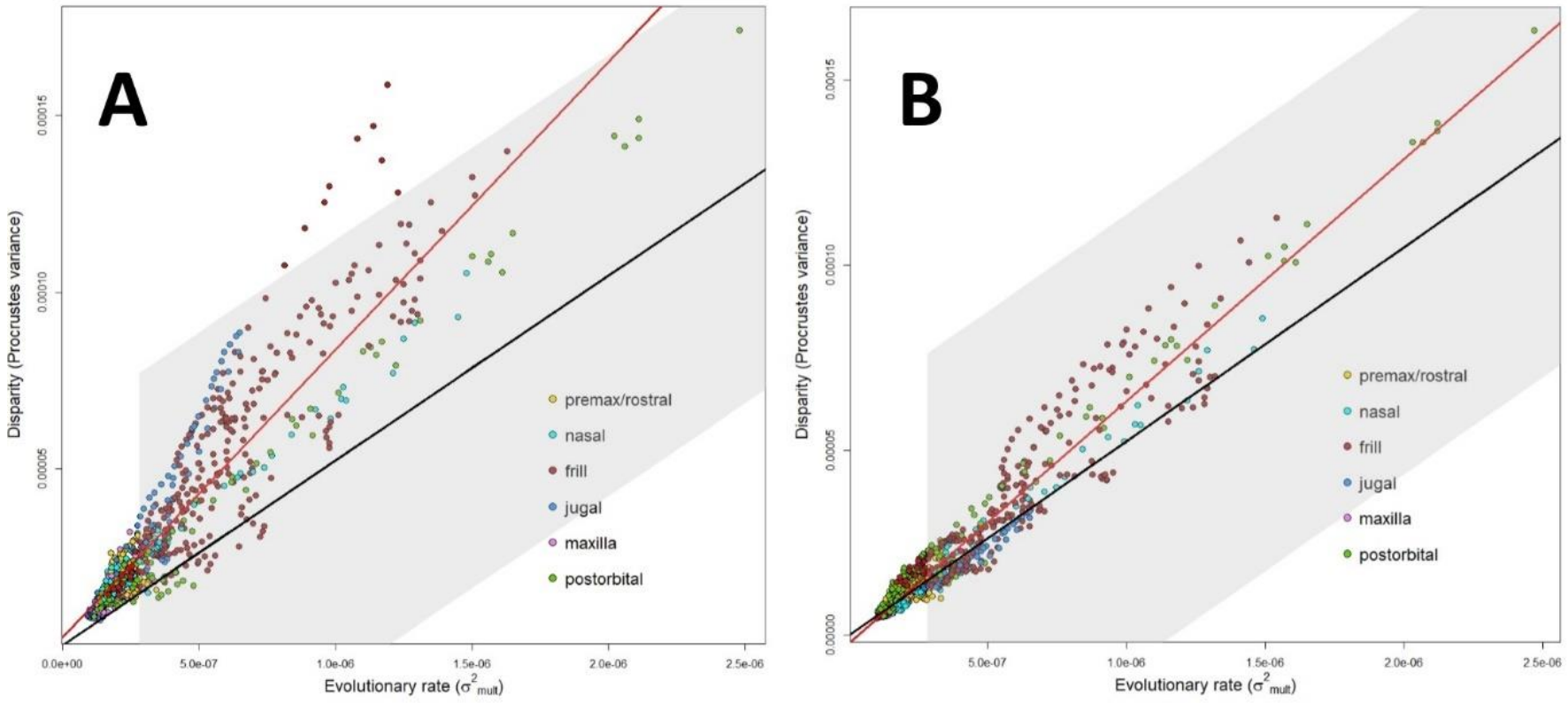

Figure 4.12: Regression of per-landmark disparity on evolutionary rate for raw morphological data (**A**) and allometry-corrected morphological data (**B**), coloured according to module. Black line represents expected relationship under a Brownian model of evolution, with 95% confidence interval represented by grey shaded region. Red line is regression for the entire skull.

4.4.5 Ceratopsid epiossifications

Taxa that possess epiossifications were aligned using a generalised Procrustes analysis (Fig. 4.13). Species were compared with all skull landmarks (Fig. 4.13A), frill and epiossification landmarks (Fig. 4.13B) and epiossifications landmarks only (Fig. 4.13C). Species are grouped with convex hulls according to clade (centrosaurine or chasmosaurine). When whole-skull and frill + epiossification data are examined, clades are clearly separated (Fig. 4.13A and B). When examining epiossifications alone, overlap between clades is apparent (Fig. 4.13C). In all cases, chasmosaurines (yellow convex hull) show noticeably higher morphological diversity than centrosaurines (red convex hull), but the distribution of chasmosaurines in morphospace appears to remain largely similar in all three PCAs. Centrosaurines remain grouped relatively closely together.

Static allometry was found to be non-significant in ceratopsids (R^2 = 0.1, p = 0.08), suggesting that the majority of shape variation in this clade is independent of size. For this reason, further analyses of epiossifications were not allometry-adjusted. Analyses of phylogenetic signal ($\boldsymbol{K_{mult}}$) and net evolutionary rates ($\boldsymbol{\sigma^2_{mult}}$) of ceratopsids modules, including epiossifications as a separate module, were performed using a modified version of the time-scaled phylogeny, and results are shown in Table 4.4. Phylogenetic signal is significant for all modules, and ranges from 0.39 in maxilla and epiossifications, and 0.61 in the postorbital. The low phylogenetic signal in both maxilla and epiossifications contrasts with their extreme relative differences in evolutionary rates and morphological disparity, suggest that low signal is due to the high lability of the epiossifications and the stable morphology of the maxilla (Symonds and Blomberg, 2014). Net evolutionary rates do not differ considerably from those found for the whole dataset (Table 4.2), but epiossifications show a rate over double that of the next highest, the frill. This suggests that epiossifications underwent rapid evolution in ceratopsids. Morphological disparity in ceratopsids was found to be highest in epiossifications (Table 4.4), and lowest in the maxilla. Excluding the epiossifications, levels of disparity

are consistent with those seen in the whole dataset (Fig. 4.10), with the frill, postorbital and nasal showing the three highest disparity values in descending order.

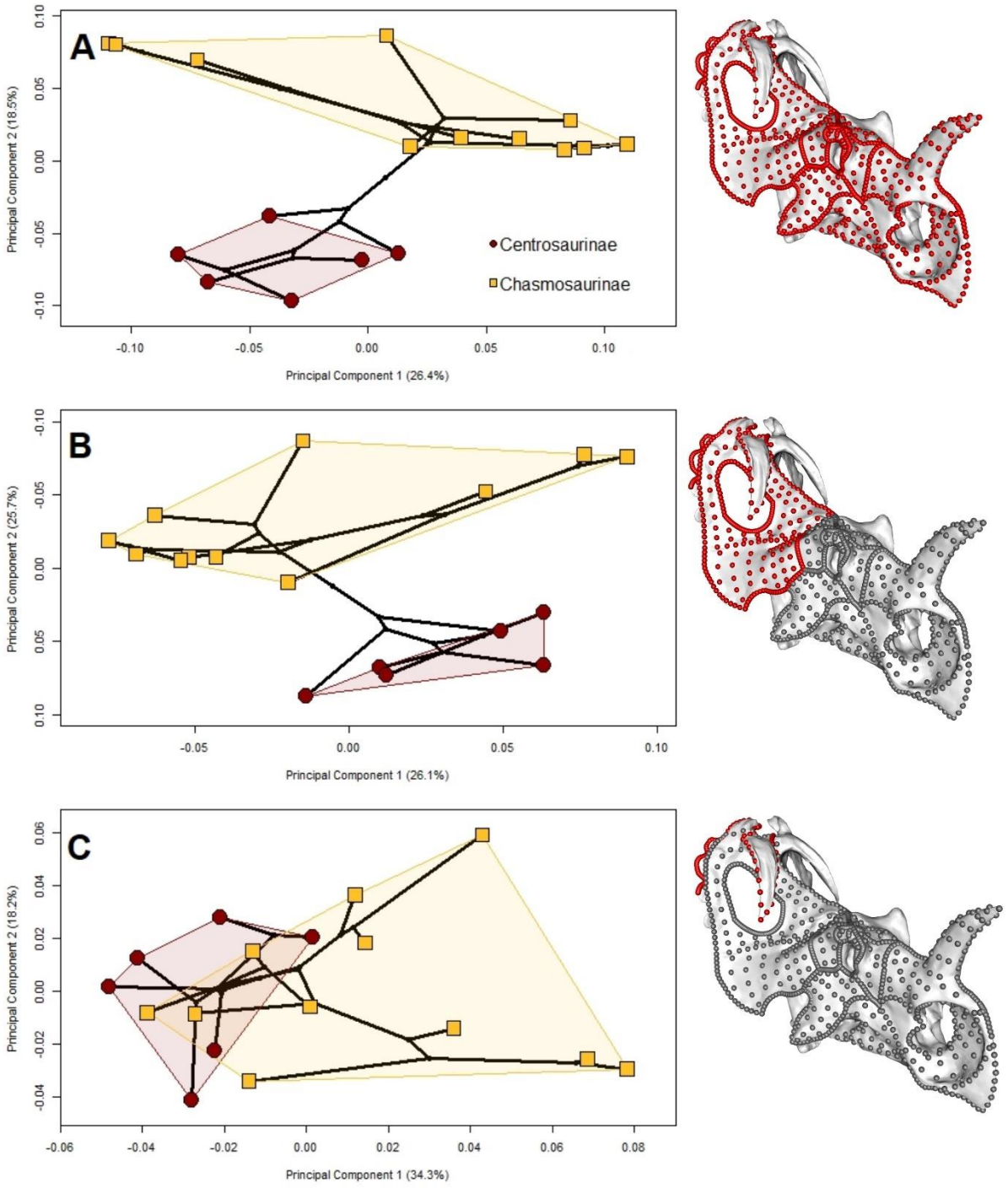

Figure 4.13: Phylomorphospaces of whole-skull (**A**), frill and epiossifications (**B**) and epiossifications only (**C**). A mesh of a single specimen (*Centrosaurus apertus* YPM 2015) with overlaid landmarks is included in relevant PCAs to highlight the landmarks analysed in each morphospace (red). Chasmosaurines are represented by square points and centrosaurines are represented by circles. Convex hulls group taxa according to clade, and phylogeny is represented by solid black lines.

Table 4.4: Results of phylogenetic signal (K_{mult}), net evolutionary rates (σ^2_{mult}) and morphological disparity in ceratopsids, including epiossifications.

	Phylogenetic signal		Evolutionary rates	Morphological disparity
	K_{mult}	p	σ^2_{mult}	
Skull	0.83	0.001	-	2.08×10^{-5}
Frill	0.89	0.001	4.93×10^{-7}	2.58×10^{-5}
Nasal	0.89	0.004	3.37×10^{-7}	1.64×10^{-5}
Jugal	0.70	0.01	2.21×10^{-7}	8.57×10^{-6}
Postorbital	0.89	0.001	3.42×10^{-7}	2.10×10^{-5}
Premaxilla-rostral	0.73	0.005	2.44×10^{-7}	9.63×10^{-6}
Maxilla	0.70	0.007	1.85×10^{-7}	7.09×10^{-6}
Epiossifications	0.70	0.007	1.16×10^{-6}	4.32×10^{-5}

Per-landmark morphological disparity and evolutionary rates of specimens with epiossifications were calculated, and the results are shown in Fig. 4.14. Landmarks associated with the postorbital (green) show higher disparity than expected given their rates compared with Fig. 4.12, falling outside the 95% confidence intervals of the null model (grey shaded area). The epiossifications (orange) show the highest maximum disparity and rates and fall within the 95% confidence intervals of the null model. At least two trajectories are apparent, suggesting that different epiossifications may form distinct modules. The frill (red points) appears to show lower disparity and rates relative to the postorbital when compared to Fig. 4.12. This may be explained by rapid evolution of postorbital horns in ceratopsids and non-ceratopsid taxa lacking postorbital horns, resulting in long periods of slower evolution of this module in the more expansive phylogeny.

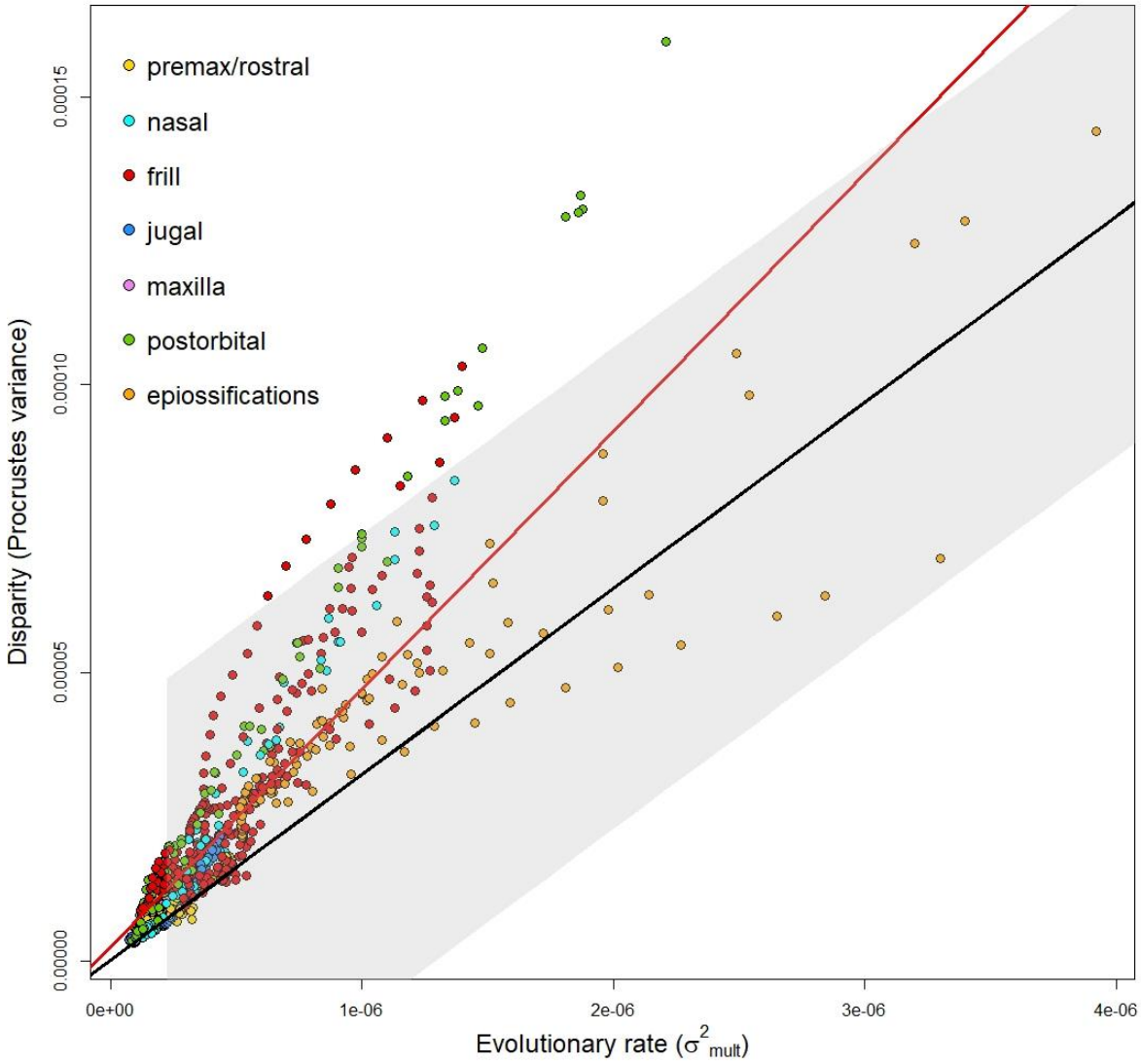

Figure 4.14: Comparison of per-landmark disparity and evolutionary rates for taxa with frill epiossifications. Points are coloured according to module. Red line represents regression of disparity against rates. Black line represents expected relationship under a Brownian model of evolution, with 95% confidence interval represented by shaded region.

4.4.6 *Triceratops, Torosaurus* and *Nedoceratops* morphology comparison

Three taxa included in this dataset, *Nedoceratops*, *Torosaurus* and *Triceratops,* are considered synonymous by some researchers (Scanella and Horner, 2010, 2011; Maiorino et al., 2013). To explore this issue using the 3D data presented here, a PCA of the Procrustes-aligned data for all specimens of these taxa in the complete dataset is shown in Figure 4.15. There is little overlap between species (shown by coloured convex hulls) in the first two principal components, which together account for 55.3% of total shape variation. Two specimens of *Torosaurus* occupy a region of morphospace far removed from the two species of *Triceratops*, but *Nedoceratops* falls within the region of morphospace occupied by *T. horridus.* Nevertheless, morphological variation in *Tr. horridus* is relatively high, and specimen number is low.

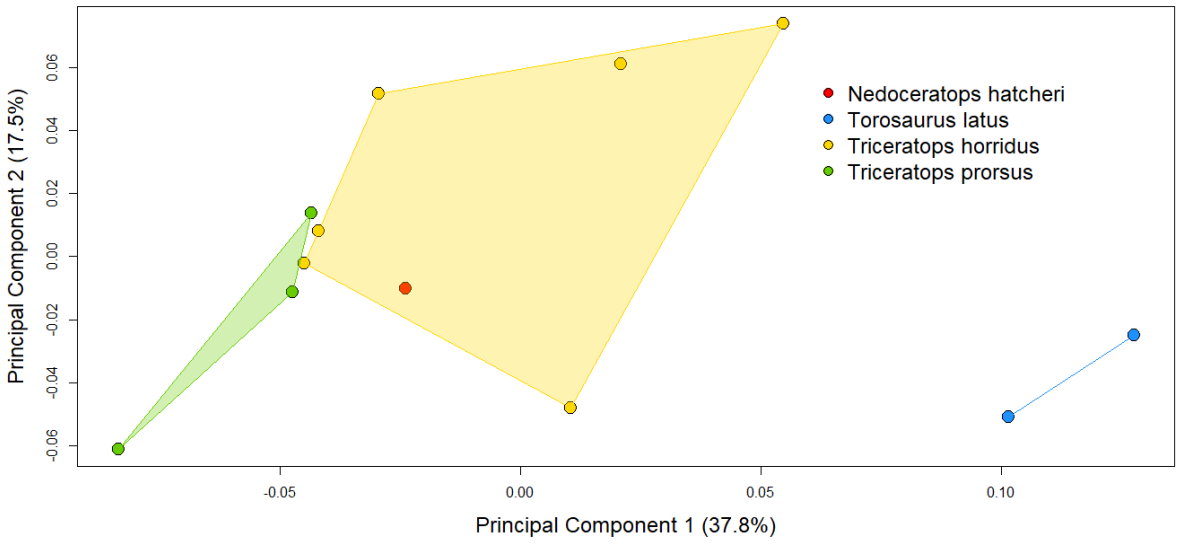

Figure 4.15: PCA of *Nedoceratops, Torosaurus* and *Triceratops* specimens included in this study. Principal components 1 and 2 are shown, accounting for 37.8% and 17.5% of total shape variation between these specimens respectively. Convex hulls are used to group specimens by species.

4.5 Discussion

4.5.1 Overview

This study has, for the first time, used densely-sampled three-dimensional morphometrics to quantify morphological disparity, modularity and evolutionary rates of the ceratopsian skull. Analyses of modularity have revealed that the ceratopsian skull had a modular structure, and this may have enabled the morphological diversification of ceratopsians via mosaic evolution (Felice and Goswami, 2017). Analysis of separate phenotypic modules supports the hypothesis that the modules associated with unique 'exaggerated' traits of ceratopsians, namely the frill, horns and epiossifications, may have functioned as socio-sexual traits due to their higher evolutionary rates and morphological disparity than other modules (West-Eberhard, 1983). Size and shape were found to be significantly correlated in the ceratopsian skull and this variation accounted for around 44% of total shape variation across all taxa. This supports previous claims that heterochrony had an important influence on skull shape evolution in ceratopsians (McNamara and Lord, 2012; Mallon et al., 2015), but the exact nature of these effects is unclear.

4.5.2 Modularity

The maximum likelihood modularity test provided strong support for the six-module hypothesis, contrasting with the five identified in *Protoceratops* ontogeny (Chapter 3). Modularity, the tendency of sets of traits to form independently covarying units, defines the ability of these traits to respond to selection (Goswami and Polly, 2010a). Ceratopsians appear to show a greater degree of integration in the skull compared to other non-avian dinosaurs. In this study, the parietal and squamosal of ceratopsians showed relatively high correlation values and so were combined into a single module. This contrasts with a recent analysis of modularity in archosaurs which found these bones to form separate modules across a broader sample of non-avian dinosaurs, including but not limited to ceratopsians (Felice et al., 2019b). Additionally, the bones surrounding the upper part of the orbit,

namely the postorbital, frontal and lachrymal, were found to form separate modules across non-avian dinosaurs (Felice et al., 2019b). In ceratopsians, these bones are often fused to the extent that the sutures are obliterated in adults and impossible to identify (Dodson et al., 2004; Mallon et al., 2015). Nevertheless, the high correlation values of the postorbital module returned from the maximum likelihood modularity test support treating this as a single module in ceratopsians (Fig. 4.3).

The identification of the nasal as a distinct module in this study reflects its highly variable morphology among ceratopsians in general, contrasting with its more constrained morphology in *Protoceratops* (Chapter 3). In ceratopsids, and centrosaurines in particular, the nasal shows high morphological diversity which is exemplified by the transition from deep, narrow, nearly hornless forms such as *Nasutoceratops* and *Diabloceratops*, through the single, upright nasal horn of *Centrosaurus* and *Styracosaurus*, to the large, flattened nasal boss of *Achelousaurus* and *Pachyrhinosaurus* (Dodson et al., 2004; Hieronymous et al., 2009). The nasal horn morphology of some centrosaurine taxa, for example *Centrosaurus* and *Pachyrhinosaurus* are known to show high intraspecific variation which may be correlated with ontogeny (Currie et al., 2008; Hieronymous et al., 2009; Frederickson and Tumarkin-Deratzian, 2014). Although these two genera have vastly different horn morphologies (single horn vs. flattened nasal boss, respectively), that may not be the case for more closely-related taxa. Analysis of horn morphology of these taxa, for which there is ample material, will help to determine the relationship between inter- and intraspecific variation of the nasal horn. The postorbital likewise forms a module, fitting a prediction made by Mallon et al. (2015). The tip of the postorbital horn encompassed the region of highest morphological disparity and evolutionary rate, but the region around the orbit shows among the lowest values for rate and disparity (Figs. 4.11 and 4.12). This high difference within a single module may explain the relatively low net morphological disparity and evolutionary rates compared to the frill (Fig. 4.10). Postorbital horns are known to show high intraspecific variation in taxa such as *Triceratops* (Scanella et al., 2014), which may affect estimations of evolutionary rates and morphological disparity.

The finding that the parietal-squamosal frill forms a phenotypic module across ceratopsians, as in *Protoceratops,* supports the treatment of this structure as a distinct trait (Klingenberg, 2014). The frill is perhaps the most recognisable feature of ceratopsians, and several arguments have been put forwards regarding its function (Hatcher, 1907; Dodson, 1996; Padian and Horner, 2010; Hone et al., 2012). Demonstrating that the frill formed a distinct phenotypic module forms the basis for further analyses of its morphological variation and evolution (Klingenberg, 2014). Analyses of relative integration and modularity in other clades have shown that these factors influence the trajectory and magnitude of the response to selection, and evolutionary rates can subsequently vary enormously across a set of traits depending on their degree of phenotypic integration (Goswami et al., 2014). The formation of phenotypic modules therefore suggests that differential development and selection pressures are acting across different regions of an organism. We do not know from this dataset if patterns of modularity and integration change through ontogeny or evolution of ceratopsian taxa. The analysis of modularity in separate taxa across the ceratopsian phylogeny would help to resolve this question, but would depend largely on sample availability.

The strongest trait correlation in this dataset occurs between the premaxilla and rostral bones (Fig. 4.3). This association is probably a result of the rostral bone, unique to ceratopsians, forming as an extension of the premaxilla to form an efficient feeding apparatus. A previous study using 2D anatomical landmark data by Maiorino et al. (2017) suggested that integration in the ceratopsian skull is strongly influenced by food processing, and that the frill drove the evolution of lower jaw shape. My study did not examine mandible morphology, and so my results are not directly comparable with those of Maiorino et al. (2017). One of the component bones of the frill, the parietal, acted as a site of jaw adductor muscle attachment in ceratopsians, but the large, expanded frill seen in ceratopsids appears to extend well beyond the muscle attachment zone (Nabavizadeh, 2018). The lack of strong correlation between the frill and modules containing feeding apparatus in the cranium (i.e. maxilla and premaxilla-rostral), combined with their different evolutionary rates, suggest that these modules underwent somewhat independent evolution. Inclusion of more basal taxa that lack an exaggerated

frill may help to determine how conserved the muscle attachment regions of the parietal are, and how well integrated it is with the feeding apparatus of the cranium. Other studies have investigated the relationship between ceratopsian skull shape and feeding and have found that ceratopsids could exert powerful bite forces, and that skull shape may have influenced bite force (e.g. Henderson, 2010; Mallon and Anderson, 2015). These other findings suggest that ceratopsian skull evolution was influenced at least in part by the development of unique aspects of their specialised feeding apparatus (Dodson, 1996; Dodson et al, 2004; Mallon and Anderson 2014a & 2014b), and the initial enlargement of the parietal in basal taxa may have been driven by selection for larger, more powerful jaw muscles. A comprehensive analysis of skull evolution with the inclusion of mandible morphology and more basal taxa will help to explore this possibility.

4.5.3 Allometry and phylogenetic signal

Size was found to have a significant and strong correlation with shape in the ceratopsian skull, accounting for around 40% of total shape variation. Skull size was also found to have a significant correlation with individual module shape, ranging from 24% of shape variation of the nasal to 63% of total shape variation of the jugal (Table 4.1). Although significant, evolutionary allometry (i.e. allometry accounting for phylogeny) did not have a strong effect size for either the entire cranium, or for individual modules (Table 4.2), and no significant effect was found in the nasal or postorbital. This may be due to the diverse morphology of horns in ceratopsids.

Changes in the timing and rate of developmental events through evolution, or heterochrony, are known to have profound effects on shape (McNamara, 2012). The results of this study support observations of heterochrony in ceratopsians because shape and size are significantly correlated and account for a large proportion (~44%) of total shape variation. This suggests that size is a strong predictor of shape and that ceratopsian taxa largely lie along a single allometric trajectory (McNamara and Long, 2012). It is not possible to confirm heterochrony in the evolution of the ceratopsian skull with this dataset, but comparing the ontogenetic trajectories of several taxa may help to resolve this

issue (Mitteroecker et al., 2004; Mallon et al., 2015). Examination of the ratios of individual module size to skull size suggests that size changes do not all follow obvious patterns (Fig. 4.8). A notable observation is that the ceratopsid subset of specimens (used in the analysis of frill epiossifications) did not show significant correlation of shape with size. This may be due to their relatively similar skull size as a group, compared with the much smaller earlier-diverging taxa such as *Psittacosaurus* and *Protoceratops*. These taxa show high morphological disparity and evolutionary rates in exaggerated traits such as horns, frill and epiossifications (Fig. 4.14).

The observation that lineages tend to show increasing trends in body size through evolutionary history is commonly known as Cope's Rule and has been used to explain the very large sizes attained by many dinosaurs, although the precise mechanism may be due to a number of different reasons, from greater digestive efficiency (Clauss et al., 2013), to predator defence and sexual selection (Hone and Benton, 2005). The strong correlation of size and shape in the ceratopsian skull raises one of two possibilities that cannot be easily tested with this dataset but are not necessarily mutually exclusive. Firstly, evolutionary increases in size were a direct result of socio-sexual selection for larger body sizes, which are better able to dominate social groups (Gould, 1974). Both males and females of a wide range of extant animal taxa are known to preferentially mate with larger individuals of the opposite sex because of the benefits large size confers on fitness (Bonduriansky, 2001; Kraaijeveld et al., 2007). This may then lead to the evolution of exaggerated traits, in this case the frill, that act as honest signals to emphasise body size (Geist, 1971; O'Brien et al., 2018). Secondly, an increase in size through natural selection, e.g. by selecting for a longer gut to improve digestive efficiency (Clauss et al., 2013), led to an increase in social interactions, which subsequently led to the evolution of exaggerated traits via another process such as socio-sexual selection. This scenario could occur where larger animals form herds for mutual protection from predators (Hamilton, 1971), because concealment is a less viable option for larger animals. It is unlikely that the exaggerated traits of the ceratopsian skull would have been exclusively a by-product of increasing body size without performing a specific function because the resources used in growing and maintaining them are considerable (Maidment et al., 2014), and

would have been better employed in increasing body size itself. Natural selection for larger body size would likely have reduced these traits if there was no selection to maintain them.

Multivariate phylogenetic signal (K_{mult}) was found to be highly significant in the entire skull and for all modules in the raw shape data, but had a lower than expected value (i.e. <1) for a number of modules, particularly the nasal and postorbital. Phylogenetic signal can be reduced by both high and low variation, where morphology is more or less correlated than expected given shared relationships (Symonds and Blomberg, 2014). The signal strength was noticeably reduced when the shape data was corrected for allometry (Table 4.3), reflecting the removal of the trends seen in Fig. 4.6. This becomes apparent when the allometric component of shape variation is removed and the shape data is plotted in a PCA (Fig. 4.9). Here, separation between clades, particularly between early-diverging *Psittacosaurus* and *Leptoceratops,* and the more derived ceratopsids largely disappears when compared with the same analysis for uncorrected data, emphasising the differences in shape between these taxa that is due to size (Fig. 4.9).

4.5.4 Evolutionary rates and morphological disparity

Consistent with the patterns of mosaic evolution in other vertebrates (Felice and Goswami, 2017), the evolutionary rate analysis of the six phenotypic modules identified in these ceratopsian taxa reveals that they evolved at different rates. Net evolutionary rates (σ^2_{mult}) across all taxa are highest in the frill, and are more than 50% higher than for the next highest rate, the postorbital (Table 4.3). Correcting the data for allometry narrows the spread of net evolutionary rates, but the frill retains the highest value (Fig. 4.10). These results lend some support to the hypothesis that the frill of ceratopsians was a socio-sexually selected trait because it exhibits the heightened evolutionary rates predicted of these traits (West-Eberhard, 1983; Cooney et al., 2019).

Per-landmark evolutionary rates and morphological disparity show similar distributions of high and low values across the skull (Fig. 4.11), and are significantly correlated (Fig. 4.12). The tip of the

postorbital horn shows the highest rates and disparity in the entire skull. Horns in extant taxa often perform an intrasexual confrontational role (Geist, 1971; Gould, 1974; Caro et al., 2003), and their presence in ceratopsians, along with their high evolutionary rates and morphological disparity, suggest that they may have performed a similar role here. Unlike the landmarks of other modules, those of the frill do not follow a clear linear relationship between disparity and rates. Disparity is higher than expected for some regions of the frill given their rates. Felice et al. (2018) suggest that this may be expected where disruptive selection is operating, or where phenotypic integration acts to facilitate phenotypic change, and this may be consistent with runaway selection on the ceratopsian frill driving morphological divergence. The regression of morphological disparity against evolutionary rate for the whole skull in Fig. 4.12A (red line) has a steeper slope than the null model of Brownian evolution (black line), although most landmarks show low disparity and rates and fall within the 95% confidence intervals. Consistent with the prediction of equivalent rate/variance, high evolutionary rates are generally correlated with high morphological disparity, particularly noticeable in the landmarks of the postorbital horn, and fall well within the predicted relationship between the two. Correcting for allometry brings the disparity/rates relationship much more in line with the Brownian null model, and all points fall within the 95% confidence intervals (Fig. 4.12B). This suggests that size variation may somehow act to relax morphological constraint in the frill of ceratopsians. In the case of the ceratopsian frill this may be a result of runaway selection driving extreme expansion and taxa evolved larger sizes, and may be consistent with the disruptive selection scenario suggested by Felice et al. (2018). The relatively low rates and disparity seen in the maxilla and premaxilla-rostral suggest that shape was largely conserved throughout ceratopsian evolution, with shifts in morphology occurring between the major clades (Fig. 4.5). This is probably a result of functional constraint on these traits, which is expected of traits under selection for mechanical efficiency.

A hallmark of socio-sexual traits is that they show high intraspecific variation (O'Brien et al., 2018), and that is likely to be the case of the frills and horns of ceratopsians, as it is of the frill of *Protoceratops* (Chapter 3). The difference between the effect size of allometry for all specimens in this study (R^2 =

0.27) with the same result for the representative specimens (R^2 = 0.4) suggest that this is also the case for ceratopsians. Although rarely considered in phylogenetic comparative analyses (Symonds and Blomberg, 2014) intraspecific variation can introduce bias into the estimates produced in these studies (Garamszegi and Møller, 2010). No phylogenetic comparative analyses used in this study can currently deal with multiple specimens per taxon using multivariate geometric morphometric data (Adams and Otárola-Castillo, 2013). Furthermore, large samples are often unavailable for the majority of taxa when using fossil specimens, and so intraspecific variation is difficult to estimate; attempting it with suboptimal numbers of specimens per taxon can increase the magnitude of estimate inaccuracies (Cardini et al., 2015). To attempt to mitigate the possible bias of including extreme morphologies into the analysis, representative specimens were chosen based on their condition and on their proximity to species mean shape in taxa where multiple specimens were available. Although not a perfect solution, this approach allows us to mitigate possible issues with extreme morphologies biasing phylogeny-based estimates. The significant phylogenetic signal (Table 4.3) suggests that intraspecific variation does not have a strong effect on this dataset. Improving methods for estimating intraspecific variance across all taxa will allow this potential source of error to be better quantified in future morphometric studies.

4.5.5 Epiossifications

Epiossifications are an important diagnostic feature of ceratopsid ceratopsians (Ryan et al, 2010). Procrustes analysis of epiossifications reveals that, although they make little contribution to gross morphology, they show a considerable amount of morphological disparity when examined independently of the rest of the skull (Fig. 4.10C), supporting claims made in previous studies (Dodson et al., 2004; Sampson and Loewen, 2010). The data presented here suggest that epiossification morphology is relatively more diverse in chasmosaurines than centrosaurines (Fig. 4.14C), despite epiossifications being considered a more important diagnostic trait in centrosaurines (Sampson et al., 1997; Ryan et al., 2010). Although centrosaurine epiossifications are often extreme in form (e.g.

Styracosaurus, which has three long spikes emerging from the frill on each side of the midline) they appear to be variations on a standard organisational pattern, whereas chasmosaurine epiossifications show diversity in both form and orientation, from simple triangular shapes in taxa such as *Triceratops*, to complex combinations of long, curved horn- and hook-like processes in taxa such as *Kosmoceratops* and *Spiclypeus* (Sampson and Lowen, 2010). The evolutionary and developmental relationship of epiossifications between centrosaurines and chasmosaurines is not fully understood at present, and homology is uncertain (Brown and Henderson, 2015), but the landmark scheme used in this study does give some measure of relative shape. The epiossifications show the highest evolutionary rates and disparity across ceratopsids, but relatively low phylogenetic signal (Table 4.4). The overlap of epiossification morphologies in morphospace seen in Fig. 4.15C suggests that some degree of morphological convergence occurred in ceratopsids, leading to a breakdown in clade distinctions. Although functional constraints can lead to convergence, it is not presently clear what functions epiossifications could have performed given their extraordinary morphological diversity, other than signalling. Convergence in morphology is consistent with a signalling function because signals often evolves to be conspicuous and evolution need not necessarily proceed in a predictable direction (Knell et al., 2012). It may be possible that overall frill morphology influences epiossification Procrustes alignment because the shape of the frill dictates the relative position of the epiossifications. Examination of the per-landmark disparity and rates comparison in Fig. 4.15 reveals at least two different trajectories for epiossification landmarks (orange points), suggesting that epiossifications form separate modules. A better understanding of the relationship between epiossifications in different clades will help to resolve this issue, but this relies on a more detailed analysis of ontogenetic stages of epiossifications in both centrosaurines and chasmosaurines.

4.5.6 Status of *Nedoceratops* and *Torosaurus*

Two taxa included in this study (*Nedoceratops hatcheri* and *Torosaurus latus*) are considered *nomen dubia* by some authors, who suggest that they represent ontogenetic stages in the growth series of

Triceratops (Scanella and Horner, 2010; Scanella and Horner, 2011). *Triceratops* would be considered the senior synonym in this instance because it is the earliest published taxon (Hatcher, 1907). Maiorino et al. (2010) tested the validity of these taxa by performing a two-dimensional geometric morphometric analysis of *Triceratops* and *Torosaurus* (with *Nedoceratops*) specimens, and found that they occupy distinct regions of morphospace. Revisiting this with high-density 3D data allows additional comments on this finding. Examining the distribution of specimens in morphospace, both for whole-skull and individual module data (Figs. 4.4 and 4.5), show that *Nedoceratops* more often clusters closer *Triceratops horridus* than to any other taxa. When multiple specimens of these taxa are included, *Nedoceratops* falls within the region of morphospace occupied by *T. horridus* (Fig. 4.16). *Nedoceratops* thus resembles a specimen of *T. horridus* from a purely geometric perspective. Similarly, *Torosaurus* clusters closer to other chasmosaurines, namely *Chasmosaurus* and *Anchiceratops,* than it does to either *Nedoceratops* or to the two *Triceratops* species in all morphospaces (Figs. 4.4 and 4.5). The growth of the skull of *Protoceratops* shown in Chapter 3, reveal the drastic shape changes that ceratopsian taxa may undergo during ontogeny. It is possible that the morphospace placement of *Torosaurus* may reflect a similarly large ontogenetic morphological disparity of *Triceratops* but is unlikely for two reasons. Firstly, the number of large *Triceratops* specimens included in the dataset do not occupy intermediate regions of morphospace closer to *Torosaurus*, even when *Nedoceratops,* a potential intermediate form suggested by Scanella and Horner (2011), is included (Figs. 4.4 and 4.16). Secondly, most of the variation in *Protoceratops* morphology is between hatchling-sized individuals and large adult sizes, whereas *Triceratops* and *Torosaurus* are exclusively represented by large individuals. If *Torosaurus* is a mature growth stage of *Triceratops,* as suggested by Scanella and Horner (2011), this implies that a second stage of drastic morphological change occurred in *Triceratops* after an initial stage of large shape and size change from juvenile forms, with a period of relative morphological consistency at the *Triceratops*-type morphology. This two-stage growth pattern is unprecedented in any other ceratopsian. *Torosaurus* resembles a distinct taxon based solely on the limited morphological data presented here, but a greater number of specimens of both *Triceratops*

and *Torosaurus*, including juveniles, would be needed to provide statistical support to this observation. Separate data from more detailed taxonomic analysis and histological assessment of the specimens in question would also help to resolve this question.

4.5.7 Conclusions

The use of digital 3D data in this study has allowed patterns of modularity, evolutionary rates and morphological disparity to be quantitatively explored in the ceratopsian skull in far greater detail than has been attempted before. The ceratopsian skull was found to have a significantly modular structure, and its division into six modules allowed different regions of the skull a degree of independence to develop and evolve at different rates. The frill and horns, unique exaggerated traits that appear highly diverse in ceratopsians, showed the highest values of morphological disparity and evolutionary rates, which are consistent with predictions of socio-sexual traits in living taxa. These findings provide support that the frill and horns evolved under socio-sexual selection. The epiossifications, too, showed extremely high rates of evolution and morphological disparity, suggesting that these traits, unique to ceratopsids, may have also acted as socio-sexual signals. An additional finding is that shape is strongly correlated with size in ceratopsians, suggesting that heterochrony may have played a role in the evolution of the ceratopsian skull. The precise nature of the interactions that drove exaggerated trait evolution and body size are presently unclear, but the findings presented here provide a basis for future investigations. Socio-sexual selection is an important driver of evolution, and identifying it in extinct taxa provides an important first step in addressing important evolutionary questions which can be explored with palaeontological data spanning millions of years, including those of adaptation, speciation, and extinction.

Chapter 5

Conclusions

5.1 Summary of findings

In Chapter 1, I summarised the concept of sexual selection, put it into the context of social selection and discussed examples of socio-sexual selection in extant taxa.

In Chapter 2, I tested the hypothesis of species recognition in ceratopsian dinosaurs, often cited as an alternative mechanism by which exaggerated traits might have evolved in this clade and other extinct taxa (Padian and Horner, 2011a). Species recognition is a commonly cited explanation of morphological evolution in both extinct and extant clades despite both a lack of solid evidence of its existence and consensus of its definition (West Eberhard, 1983). Nevertheless, the predictions that the species recognition hypothesis makes have been clearly made (Padian and Horner, 2011a), making testing it reasonably straightforward (Knell and Sampson, 2011). Species recognition should evolve to differentiate separate populations with overlapping ranges, where inability to identify conspecifics lowers fitness in some way. A prediction arising from this hypothesis is that signalling traits should diverge to a greater extent in sympatric taxa than non-sympatric taxa, and I tested this for the exaggerated frills and horns of ceratopsian dinosaurs using a ceratopsian character matrix to conduct a pair-by-pair comparison of 45 ceratopsian species. I found that there was no significant difference between sympatric and non-sympatric species pairs in either exaggerated or other traits. The implications for this finding are that sympatry had no effect on morphological diversity in ceratopsian dinosaurs, and therefore that species recognition was unlikely to have driven ornament evolution in this clade. If misidentification of species did result in a significant cost to fitness, we would expect to see the evolution of low-cost recognition traits, because neither population would benefit from investing more than the minimum necessary resources into such traits (Maynard Smith and Harper,

2003). The large, costly skull ornaments of ceratopsians are not consistent with the low-cost expectation of species recognition traits. The high intraspecific variability of ceratopsian frills and horns (Chapters 3 and 4) are also not consistent with the concept of species recognition; juveniles do not resemble adults of the same species, and adults often show variability that species recognition should select against. Species recognition may play a role in the evolution of conspicuous traits but there is little evidence for it in extant taxa, other than character displacement of pre-existing traits in closely-related species whose ranges overlap (Brown and Wilson, 1956; Grant, 1972). Zahavi and Zahavi (1997) noted that many traits could serve as species recognition aids, regardless of their primary function.

In Chapter 3, I used 3D geometric morphometrics to analyse patterns of ontogenetic morphology in *Protoceratops andrewsi.* This is one of the commonest ceratopsian dinosaurs in terms of number of specimens, making it one of the few ceratopsian taxa for which sufficient material exists to allow exploration of morphological trends through ontogeny. I found that the skull of this taxon had a modular structure, and that these modules changed shape and size at different rates through ontogeny. The frill showed the highest morphological variance of all these modules, and significantly higher rates of change in both size and shape than any other. These findings support the hypothesis that the frill of *P. andrewsi* functioned as a socio-sexual signal. Rapid growth is predicted from traits under socio-sexual selection because they are maximally expressed in mature individuals. My analysis failed to find sexual dimorphism of adult *Protoceratops*, either in whole-skull shape or individual module shape, supporting the findings of Maiorino et al. (2015) and Mallon (2017).

Chapter 4 used the 3D morphometric methods employed in Chapter 3 and expanded the dataset to include a further 26 ceratopsian species to examine patterns of evolution of the ceratopsian skull. This analysis found a similar pattern of skull modularity across all ceratopsian taxa to that found in *Protoceratops*, except that the nasal was resolved as a separate module. This is probably explained by the evolution of the prominent nasal horn in ceratopsids (Dodson et al., 2004). Size was found to have

a strong correlation with shape in the ceratopsian dataset. This finding echoes similar patterns in the antlers of cervids (Gould, 1974), but the nature of the relationship remains unclear. The frill was found to have the highest net values of morphological disparity and evolutionary rates among all modules. These findings again fit predictions of traits under socio-sexual selection, because both rapid evolution and high morphological diversity are predicted of socio-sexual traits (Fisher, 1930; West-Eberhard, 1983). Rapid evolution has been identified in the sexually-selected plumage of modern birds (Cooney et al., 2019), and high variation of sexually selected traits is known from many examples in extant taxa (O'Brien et al., 2018). The regions of highest evolutionary rate in the ceratopsian skull were found in the horn tips and around the outer margins of the frill. When the analysis was repeated on the more limited dataset of ceratopsid taxa possessing frill epiossifications, the evolutionary rate of epiossifications was found to be higher even than the frill. This suggests that epiossifications were also under strong selection. The significant and strong correlation of shape with size in the ceratopsian skull suggests that heterochrony played a role in ceratopsian evolution, but confirming this would require the comparison of ontogenetic series from several taxa. The process by which size and shape coevolved in the ceratopsian skull is presently unclear, but our understanding may be improved by including more early-diverging taxa in the analysis.

5.2 Implications of study and future research

5.2.1 Overview

This thesis has shown that patterns expected of traits under socio-sexual selection can be detected in the morphology of extinct animals, and these findings add support to the hypothesis that the large, ornamented skulls of ceratopsian dinosaurs evolved in response to socio-sexual selection. Although the results presented here are by no means conclusive, together they provide the strongest support yet for the socio-sexual selection hypothesis of evolution of exaggerated traits in ceratopsians.

Detecting socio-sexual selection in extinct taxa is an important step because it can allow us to make predictions about what we do not yet know but might expect to find from future discoveries. The complex biology of extinct organisms can be determined from several lines of evidence, from direct comparison of morphology with analogies in extant taxa, to structural and mechanical modelling, and from reconstructing their environments (Benton, 2015). Behaviour is much more difficult to infer without the benefits of direct observation, but may be inferred from indirect lines of evidence (Hone and Faulkes, 2013).

5.2.2 Modularity and evolution

In common with many other tetrapod clades (e.g. Goswami and Polly, 2010a; Felice and Goswami, 2017; Bardua et al., 2019a; Watanabe et al., 2019; Felice et al., 2019), analysis of the ceratopsian skull found that it had an evolutionary modular structure. The pattern of modularity and integration in the ceratopsian skull differs from that seen in other taxa examined to date, showing higher integration in the frill and postorbital region than other archosaurs, and this may be explained by the evolution of the ceratopsian skull being driven by selection for exaggerated traits such as the frill and horns. If socio-sexual selection is the driver of the patterns of modularity and evolution seen in the ceratopsian skull, this may be the most extreme example yet of the evolution of a tetrapod clade being driven by selection of this kind.

The use of 3D morphometrics enables the entire surface of the skull to be analysed simultaneously, removing a degree of subjectivity involved in defining and comparing linear measurements (e.g. Dodson, 1976; Hone et al., 2016). Geometric morphometric methods can provide a much more detailed analysis of form because they are able to describe changes in shape across a structure that may be too complicated or too subtle to described with more traditional linear measurements (Goswami et al., 2019). Modularity partitions the skull into semi-independent traits which can develop and evolve at different rates. By separating the skull in this way, the evolutionary history of individual modules can be traced through different lineages and changes in their evolutionary rates and disparity

can be determined. This allows us to infer changes in function and selection of individual traits, and may hint at shifts in socio-sexual selection where present. Patterns of integration and modularity can also evolve over time and may similarly hint at shifts in strength and mode of selection, including possible transitions between signals. An example is the relaxation of the correlations between the nasal and premaxilla between the *Protoceratops* dataset (Chapter 3) and the ceratopsian-wide dataset (Chapter 4), possibly resulting from the evolution of the nasal horn in ceratopsids. The inclusion of more taxa and larger sample sizes within species would allow this to be explored across the entire ceratopsian phylogeny, and might allow better exploration of the postorbital module which is largely fused in the more derived ceratopsids.

5.2.3 Evolutionary rates and disparity

Evolutionary rates varied across the ceratopsian skull, but were found to be highest in the frill and towards the tips of the nasal and postorbital horns. This is consistent with predictions of traits under socio-sexual selection (Fisher, 1930; West-Eberhard, 1983) and provides one of the strongest lines of evidence that these unique ceratopsian traits evolved to perform a socio-sexual function. Likewise, morphological disparity of regions of these modules were highest among the entire skull, confirming high variability of these traits. This effect was seen both within and between taxa, suggesting morphological disparity is both ontogenetic and evolutionary in nature. These findings are again consistent with socio-sexual signalling traits, which show rapid rates of growth through ontogeny, and high disparity between taxa (Hone and Naish, 2013; Dale et al., 2015). Perhaps the most unusual finding regarding rates and disparity lies in the regions of the ceratopsian frill which show higher disparity than expected for a given evolutionary rate under the Brownian null model (Fig. 4.12A). As discussed in Chapter 4, this may be a result of runaway selection for extreme morphologies of this trait because the unusually high disparity falls within expected ranges when corrected for allometry, suggesting that size may somehow be responsible for this pattern. Most studies using high-density 3D data have to date focussed on general patterns of evolution and have avoided including specimens

with traits that may be involved in socio-sexual competition because of their extreme morphologies (Felice et al., 2017; Bardua et al., 2019a). Conducting a similar analysis with extant taxa that specifically focusses on known socio-sexual traits may reveal whether this pattern is one that might be expected in such traits. Comparison of socio-sexual traits in these taxa with ecologically adaptive traits that are known to evolve rapidly (e.g. Watanabe et al., 2019) may provide answers to the relative rates and disparity that can be expected between ecologically adaptive and socio-sexual traits.

5.2.4 Allometry, Cope's rule and heterochrony

Size appears to be an important factor in ceratopsian skull evolution. We cannot know from this study whether large sizes evolved via natural selection and the frill and horns of the skull evolved as a by-product of changes in biology caused by this change in size, or whether increased size itself is an evolutionary consequence of socio-sexual selection that also led to exaggerated traits in the skull to emphasise body size. Natural selection may lead to increases in body size for a variety of reasons, including increasing the size of the gut to improve food processing efficiency (Clauss et al., 2017) and predator defence (Hone and Benton, 2005). Larger body sizes incur their own costs, which may further affect biology. For example, larger animals may not be able to conceal themselves as effectively from predators as smaller animals and population aggregates may subsequently form for protection, as in extant ungulates (Hamilton, 1971). There is evidence that some ceratopsian species were very common in the late Cretaceous (Chiarenza et al., 2019), and that some existed at least temporarily in large monospecific aggregations (Tanke and Farke, 2007; Lehman, 2007; Currie et al., 2008). High population densities can lead to intense competition for resources (Knell, 2009) and in some instances, intense intraspecific competition is predicted to lead to the evolution of socio-sexual traits to aid in establishing dominance hierarchies in some instances (West-Eberhard, 1983). Similar socio-sexual traits may evolve in both males and females where competition is of more equal intensity between the sexes, and may be enhanced by more equal parental investment between the sexes (Kokko and Johnstone, 2002; Hooper and Miller, 2008).

Unlike the closely-related hadrosaurs, there is presently little evidence of nesting behaviour in ceratopsians, and only one example is known of embryonic specimens (in *Protoceratops;* Erickson et al., 2017). Examination of growth lines in the teeth of these embryos reveal a minimum incubation time of 83 days, a slow development rate that is more reptile- than bird-like. Erickson et al. (2017) suggest that large clutches of relatively small eggs were laid to offset the higher risks associated with longer incubation periods. We do not know if ceratopsians attended their nests during the incubation period, or if hatchlings were cared for by adults, but there is ample evidence for this behaviour in extant archosaurs (i.e. birds and crocodilians) suggesting that it is plausible in ceratopsians (Tullberg et al., 2002). Fossil evidence for nest attendance or parental care would provide support for the presence of socio-sexual traits as a consequence of selection for parental investment (Kokko and Johnstone, 2002). Longer incubation periods also restrict the feasible environmental ranges within which nesting can occur, which may also restrict the ranges of the adults (Erickson et al., 2017). There is some evidence that some ceratopsids taxa were regionally endemic in the Late Cretaceous continent of Laramidia (Horner et al., 1992), but this is not true for all taxa, *Triceratops* being a notable exception (Weishampel et al., 2004). The impression of regional endemism may be an effect of poor preservation and/or sampling bias, and so care must be taken in this interpretation.

5.2.5 Species recognition

There are many reasons why species recognition is not a plausible explanation for the evolution of exaggerated traits in extant or extinct taxa (see Hone and Naish, 2013 for comprehensive discussion, also West-Eberhard, 1983; Zahavi and Zahavi, 1997; Maynard Smith and Harper, 2003; Knell and Sampson, 2011). My analysis found no support for the prediction that sympatric taxa should show more divergent putative signalling traits than non-sympatric taxa. This analysis was performed on more traditional discrete taxonomic characters which allow for a larger number of taxa to be included but are limited in their flexibility and sometimes accuracy. A construction of a larger database of

accurate 3D digital data would allow a direct comparison to this study to be made using geometric morphometrics.

5.2.6 A hypothesis for the role of the frill in ceratopsian evolution

Ceratopsians evolved several unique mechanisms for processing tough vegetation, and selection on feeding apparatus was likely strong (Mallon and Anderson, 2014a; 2014b, 2015). In extant taxa, phenotypic modules associated with feeding, particularly the articular surface of the jaw joint, often show the highest evolutionary rates of the entire skull (Bardua et al., 2019b; Watanabe et al., 2019). The morphometric analyses carried out in this thesis could not take into account the equivalent structure in ceratopsians, i.e. the jaw articulation of the quadrate and quadratojugal (Dodson et al., 2004). Although not assessed in my analyses, these regions of the skull may be included in future studies, along with the mandible (Maiorino et al., 2017), to investigate the role of feeding in ceratopsian evolution.

It is notable that the most conspicuous and fastest-evolving module in the ceratopsian skull, the frill, encompasses the parietal, which serves as an attachment site for the jaw adductor muscles (Nabavizadeh, 2018). It was previously suggested by some researchers that the entire frill functioned as an anchor point for jaw muscles (e.g. Ostrom, 1966), but this hypothesis has been rejected due to the fragile nature of the frill in many taxa, and because of the inefficiency of longer muscles in generating bite force (Dodson et al., 2004). Moderate enlargement of the parietal early in ceratopsian evolutionary history which resulted from more powerful jaw muscles may have acted as a signal of social dominance within a population, because larger individuals had a more powerful bite which could have served not only in food processing but also in intraspecific competition. A similar example is known in extant collared lizards (*Crotaphytus*) in which territorial males engage in gaping displays to expose UV-reflective patches on their jaw adductor muscles (Lappin et al., 2006). The size of these patches is a strong predictor of bite force, and the authors of the study suggest that similar mechanisms are widespread in the animal kingdom. Expansion of the frill in ceratopsians may have

consequently resulted from runaway socio-sexual selection for large parietals without affecting the attachment site for the jaw adductor muscles, which are attached at the rostral region of the parietal (Nabavizadeh, 2018). The squamosals may have evolved in concert to (i) provide support for the parietal and (ii) increase the surface area of the frill. The frill therefore evolves as a social dominance signalling trait, and epiossifications may subsequently have evolved as accessory ornaments to the frill.

Recently, Maiorino et al. (2017) reported a correlation between the frill and lower jaw in an analysis of ceratopsian skull morphology. Their analysis used fixed 2D anatomical landmarks and so did not encompass the range of morphology possible with the 3D surface landmarks used in my study, but, given the association of the parietal with jaw musculature, a 3D surface morphology study encompassing the quadrate-quadratojugal jaw joint and lower jaw, combined with an analysis of jaw mechanics may provide a clearer answer. Examination of these structures in basal taxa might provide support for this hypothesis. The shape of muscle attachment sites on the parietal are likely to correlate with size because they perform a mechanical function where efficiency is selected for, which may affect the form of the attachment site. The shape of the parietal should therefore be functionally constrained in non-coronosaurian taxa (i.e., those without an enlarged frill). Outside of this region, the parietal is free to vary considerably because functional constraint is relaxed. This pattern should be consistent across ceratopsian taxa, but the correlation of the regions of the parietal associated with muscle attachment and the regions outside of this are likely to become weaker as the frill expands in size, and as clades diverge.

5.2.7 Limitations of fossil data and possible solutions

As with all sources of data reliant on fossil specimens, the biggest limitations in this study have been availability and completeness of specimens. For the analyses in this thesis I have constructed the largest 3D datasets available of a single ceratopsian species (*Protoceratops*), and of multiple ceratopsian taxa. Despite this, roughly two thirds of known ceratopsian taxa could not be included in

this study. Naturally, our knowledge of past biodiversity depends on discoveries of better-quality specimens and of new taxa, and so any study using fossil specimens is likely to be improved with future developments. Three-dimensional morphometric techniques consist of a range of powerful analytical tools, but require good quality data. The use of 3D data is becoming more prevalent in advanced morphometric studies of extant taxa (Adams et al., 2013), and fossil specimens are increasingly being used both alongside modern specimens (Watanabe et al., 2019), and as standalone datasets (Felice et al., 2019). The ease at which digital morphological data can be stored and shared make it an ideal source of information for researchers worldwide (Adams et al., 2013).

Taphonomy can severely affect specimens, and its effects on the true biological shape of specimens is well-known (Angielczyk and Sheets, 2007). Developing new techniques to correct taphonomic deformation are important not only in increasing the number of specimens available to us, but in improving the accuracy of morphometric studies (Lautenschlager, 2016). For example, deformation may increase integration values across a structure, or may lead to overestimates of morphological disparity in a dataset. Although estimated to contribute only 5% of total shape variation in the analyses performed with these datasets, correcting for taphonomic deformation will help us be more confident in our conclusions, and will allow us to include more specimens from rare taxa.

Large-scale evolutionary morphometric studies typically use one specimen per taxon (Symonds and Blomberg, 2014; Garamszegi and Møller, 2010), and phylogenetic analyses of shape are optimised to analyse data in this way. This approach cannot, however, account for intraspecific variation and assuming that one specimen can encompass the range of morphological variance in a taxon may lead to errors in interpretation (Ives et al., 2007; Garamszegi and Møller, 2010). Furthermore, attempting to assess intraspecific variation with a suboptimal number of specimens may introduce large errors in variance estimates which may overwhelm the true signal (Cardini et al., 2015). Some effects can be mitigated to an extent by including multiple specimens per taxon for a number of analyses (e.g. modularity analyses), or by selecting specimens based on their representation of the taxon as a whole.

To improve our estimates of phylogenetic signal and evolutionary rates, future developments must be able to account for intraspecific variation in a phylogenetic context. This is particularly true for the highly-variable morphology expected of socio-sexual traits, which often exhibit heightened phenotypic plasticity.

Acknowledgements

For the past four years of my life, everyone I know has helped me in some way or other on this epic journey that I've embarked on. I cannot possibly mention every single one of them, but I will attempt to do as many justice as possible. My PhD was funded by a NERC DTP studentship (NE/L002485/1).

Undoubtedly, this PhD would not have been possible without the help and support of a great many museum staff from institutions from all around the globe, who without exception accommodated me and my various requests with good patience and humour. At the NHM, Susie Maidment, Sandra Chapman, Paul Barrett, Roberto Portelo-Miguez, Natalie Cooper, Richard Sabin, Anjali Goswami and Robin Hansen. At the Royal Tyrrell Museum of Palaeontology, Caleb Brown, Don Brinkman, Don Henderson, Rhian Russel, Tom Courteney, Becky Sanchez and Brandon Strilisky. At the AMNH, Carl Mehling, Mark Norell and Ruth O'Leary. At the Yale Peabody Museum, Dan Brinkman and Jamie Henderson. At the Smithsonian National Museum of Natural History, Mike Brett-Surman, Holly Little and Jennifer Strotman. At the Carnegie Museum of Natural History, Amy Henrici and Matt Lamana. At the Royal Ontario Museum, Brian Iwama, Kevin Seymour and Dave Evans. At the Canadian Museum of Nature, Kieren Shepherd, Margaret Currie, Jordan Mallon and Nick Campione. At the University of Alberta, Phil Currie, Katherine Bramble, Howard Gibbons and Scott Persons. At the Warsaw Instytut Paleobiologii, Jolanta Koblylinska, Justyna Słowiak and Łukasz Czepínski. At Birmingham Think Tank, Lukas Large. At the Mongolian Academy of Sciences, Khishigav Tsogtbaatar, Purevdorj Khataanbaatar and Nyamkhishig Tsogjargal. At The Museum of the Rockies, John Scanella, Scott Williams and Amy Atwater. At the Royal Belgian Institute of Natural Sciences, Annelise Folie. Finally, Joao Vasco-Leite helped me expand my dataset by sending me scans from Utah, a place I wasn't able to visit. Extra special thanks go to Darren Tanke and Patty Ralrick of the RTMP, who twice accommodated me on visits to Drumheller, and to Jessica Burylo, who kindly chauffeured me the three hours from Edmonton to Drumheller after I falsely assumed that public transport was a thing in rural Alberta.

Collaboration is a vital part of scientific research, and I am indebted to the many people I have collaborated with. Andy Farke and Mark Loewen provided me with the data I needed for my first published paper, and they did so without hesitation. Their comments and advice on this paper were invaluable, and I was delighted to include them as co-authors. Doug Emlen, Devin O'Brien and their colleagues at the University of Montana asked us to collaborate on a paper back in 2017. Despite my modest contribution to the data they were gracious enough to include me on the author list. I look forward to working with them in the future. Tom Raven of the NHM was my research partner and travel buddy in Mongolia in the summer of 2018. He made what could have been a daunting trip a

breeze. Finally, Scott Hartman was kind enough to let me use his excellent skeletal drawings in my 2018 publication.

Knowing which of my dear friends and family to thank is easy; they all are. They have picked me up when I've been down without even knowing it. They have been there for me. They make my life what it is. I love them.

My office mates in Fogg 5.18, and fellow students in QMUL SBCS Organismal Biology, have kept me sane over the years. Many have come and gone, but all feel like family. My four Queen Mary DTP compatriots, Emeline, Carlos, Emma and Niall, have been with me the whole way. I know they will all succeed in whatever they do next, and I will miss seeing and talking to them every day.

Academic staff of QMUL, who always have an open door and who are always happy to help, are among the best I have encountered anywhere and are due extra thanks. This was especially true of Steve Le Comber, who sadly died the week before I was due to submit. Steve was an excellent academic and an incredible human being, and many people I know, including me, would not be where they are today without his unwavering support. He will be missed by all who knew him.

Sandra Álvarez-Carretero deserves special mention for her ability to adapt my incoherent and shambolic R skills into something almost worthy of art. I owe her a huge debt of gratitude not only for this, but for helping me with a very important aspect of my thesis. I have no doubt that she has made me a better R coder, and for that she has my gratitude.

Likewise, my geometric morphometric skills would have undoubtedly fallen short without the help and guidance of Ryan Felice at UCL and the NHM, who gave me an invaluable crash-course in surface semilandmarking and provided essential advice and feedback with my analyses.

I can be absolutely certain that the past four years of my life wouldn't have been the same without the love, support and friendship of my fellow London NERC DTP students, a truly incredible bunch of people and the real crème-de-la-crème. A PhD is a journey into the unknown and it is a journey we have made together, despite taking different routes. I owe them more than they can know.

No acknowledgements would be complete without mentioning my supervisors, Dave and Rob. They have been through much in the past few years, not least Dave, but I am eternally grateful for their support, and for taking me on as their student at the very beginning.

References

Adams DC and Otárola-Castillo E (2013). Geomorph: An R package for the collection and analysis of geometric morphometric shape data. *Meth. in Ecol. and Evol.* **4;** 393 – 399. DOI: 10.1111/2041-210X.12035.

Adams DC, Rohlf FJ and Slice DE (2013). A field comes of age: geometric morphometrics in the 21st Century. *Hystrix, It. J. Mamm.* **24;** 7 – 14. DOI: 10.4404/hystrix-24.1-6283.

Adams DC (2014a). Quantifying and comparing phylogenetic evolutionary rates for shape and other high-dimensional phenotypic data. *Syst. Biol.* **63;** 166 – 177. DOI: 10.1093/sysbio/syt105.

Adams DC (2014b). A generalized *K* statistic for estimating phylogenetic signal from shape and other high-dimensional multivariate data. *Syst. Biol.* **63;** 685 – 697. DOI: 10.1093/sysbio/syu030.

Adams DC (2016). Evaluating modularity in morphometric data: challenges with the RV coefficient and a new test measure. *Meth. in Ecol. and Evol..* **7;** 565 – 572. DOI: 10.1111/2041-210X.12511.

AgiSoft PhotoScan Professional (Version 1.4.3) (Software). (2019). Retrieved from http://www.agisoft.com/downloads/installer/.

Al-Khairulla H, Warburton D, and Knell RJ (2003). Do the eyestalks of female diopsid flies have a function in intrasexual aggressive encounters? *Journ. Ins. Behav*. **16;** 679 – 686. DOI: 10.1023/B:JOIR.0000007703.84691.ad.

Álvarez-Carretero S, Goswami A, Yang Z and Dos Reis M (2019). Bayesian estimation of species divergence times using correlated quantitative characters. *Syst. Biol.* DOI: 10.1093/sysbio/syz015.

Amundsen T (2000). Why are female birds ornamented? *Trends Ecol. Evol*. **15;** 149 – 155. DOI: 10.1016/S0169-5347(99)01800-5.

Andersson MB (1987). Genetic models of sexual selection: some aims, assumptions and tests. In Bradbury JW and Andersson MB (eds). *Sexual Selection: Testing the Alternatives*. John Wiley & Sons Limited.

Andersson M (1994). *Sexual Selection.* Princeton, NJ: Princeton University Press.

Andersson M and Iwasa Y (1996). Sexual selection. *Trends Ecol. Evol*. **11;** 53 – 58. DOI: 10.1016/0169-5347(96)81042-1.

Angielczyk KD and Sheets HD (2007). Investigation of simulated tectonic deformation in fossils using geometric morphometrics. *Paleobiology*. **33;** 125 – 148. DOI: 10.1666/06007.1

Arbour VM, Burns ME and Sissons RL (2009). A redescription of the ankylosaurid dinosaur *Dyoplosaurus acutosquameus* Parks, 1924 (Ornithischia: Ankylosauria) and a revision of the genus. *J. Vertebr. Paleo.* **29;** 1117 – 1135. DOI: 10.1671/039.029.0405.

Baab KL (2013). The impact of superimposition choice in geometric morphometric approaches to morphological integration. *J. Hum. Evol*. **65;** 689 – 692. DOI: 10.1016/j.jhevol.2013.07.004.

Bahr DB, Hutton EWH, James PM, Syvitski PM and Pratson LF (2001). Exponential approximations to compacted sediment porosity profiles. *Computers and Geosciences.* **27;** 691 – 700. DOI: 10.1016/S0098-3004(00)00140-0.

Balmer AJ, Brakefield PM, Brattström O and van Bergen E (2018). Developmental plasticity for secondary sexual traits in a group of polyphonic tropical butterflies. *Oikos.* **127;** 1812 – 1821. DOI: 10.1111/oik.05291.

Bardua C, Wilkinson M, Gower DJ, Sherratt E and Goswami A (2019a). Morphological evolution and modularity of the caecilian skull. *BMC Evolutionary Biology.* DOI: 10.1186/s12862-018-1342-7.

Bardua C, Felice RN, Watanabe A, Fabre AC and Goswami A (2019b). A practical guide to sliding and surface semilandmarks in morphometric analyses. *Integr. Org. Biol.* DOI: 10.1093/iob/obz016.

Barrick RE, Stoskopf MK, Marcot JD, Russell DA and Showers WJ (1998). The thermoregulatory functions of the *Triceratops* frill and horns: heat flow measured with oxygen isotopes. *J. Vertebr. Paleontol.* **18;** 746 – 750. DOI: 10.1080/02724634.1998.10011103.

Bebbington K and Hatchwell BJ (2015). Coordinated parental provisioning is related to feeding rate and reproductive success in a songbird. *Behav. Ecol*. **27;** 652 – 659. DOI: 10.1093/beheco/arv198.

Bell MA and Lloyd GT (2014). *strap*: Stratigraphic Tree Analysis for Palaeontology. R package version 1.4. https://CRAN.R-project.org/package=strap.

Bellamy L, Chapman N, Fowler K, and Pomiankowski A (2013). Sexual traits are sensitive to genetic stress and predict extinction risk in the stalk-eyed fly, *Diasemopsis meigenii*. *Evolution*. **67;** 2662 – 2673. DOI: 10.5061/dryad.sc6k5.

Bennett MJ (2015). Evaluating the Creation and Preservation Challenges of Photogrammetry-based 3D Models. *UConn Libraries Published Works.* Paper 52.

Benton MJ (2015). *Vertebrate Palaeontology*. Wiley Blackwell.

Bitton PP and Doucet SM (2016). Sympatric black-headed and elegant trogons focus on different plumage characteristics for species recognition. *Anim. Behav.* **116;** 213 – 221. DOI: 10.1016/j.anbehav.2016.03.035.

Blanckenhorn WU, Stillwell RC, Young KA, Fox CW, and Ashton KG (2006). When Rensch meets Bergmann: Does sexual size dimorphism change systematically with latitude? *Evolution*. **60;** 2004 – 2011. DOI: 10.1554/06-110.1.

Boag PT and Grant PR (1981). Intense natural selection in a population of Darwin's finches (Geospizinae) in the Galapagos. *Science*. **214;** 82 – 85. DOI: 10.1126/science.214.4516.82.

Bonduriansky R (2001). The evolution of male mate choice in insects: a synthesis of ideas and evidence. *Biol. Rev.* **76;** 305 – 339. DOI: 10.1017/S1464793101005693.

Bonduriansky R and Day T (2003). The evolution of static allometry in sexually selected traits. *Evolution*. **57;** 2450 – 2458. DOI: 10.1554/03-213.

Bonduriansky R (2007). Sexual selection and allometry: A critical reappraisal of the evidence and ideas. *Evolution.* **61;** 838 – 849. DOI: 10.1111/j.1558-5646.2007.00081.x.

Bonduriansky R (2011). Sexual selection and conflict as engines of ecological diversification. *Am. Nat.* **178;** 729 – 745. DOI: 10.1086/662665.

Bookstein FL (1986). Size and shape spaces for landmark data in two dimensions. *Stat. Sci*. **1;** 181 – 242. DOI: 10.1214/ss/1177013696.

Bookstein FL (1996). Landmark methods for forms without landmarks: localizing group differences in outline shape. *Medi. Image Anal*. **1;** 225 – 243. DOI: 10.1016/S1361-8415(97)85012-8.

Borkovic B and Russell A (2014). Sexual selection according to Darwin: A response to Padian and Horner's interpretation. *C. R. Palevol.* **13;** 701 – 707. DOI: 10.1016/j.crpv.2014.06.006.

Boyd CA (2015). The systematic relationships and biogeographic history of ornithischian dinosaurs. *PeerJ*. **3;** DOI: 10.7717/peerj.1523.

Bro-Jørgensen J (2007). The intensity of sexual selection predicts weapon size in male bovids. *Evolution*. **61;** 1316 – 1326. DOI: 10.1111/j.1558-5646.2007.00111.x.

Brown W and Wilson EO (1956). Character displacement. *System. Zool*. **5;** 49 – 64. DOI: 10.2307/2411924.

Brown CM and Henderson DM (2015). A new horned dinosaur reveals convergent evolution in cranial ornamentation in Ceratopsidae. *Current Biology.* **25;** 1641 – 1648. DOI: 10.1016/j.cub.2015.04.041.

Cardini A, Seetah K and Barker G (2015). How many specimens do I need? Sampling error in geometric morphometrics: testing the sensitivity of means and variances in simple randomized selection experiments. *Zoomorphology.* **134;** 149 – 163. DOI: 10.1007/s00435-015-0253-z.

Cardini A (2016). Left, right or both? Estimating and improving accuracy of one-side-only geometric morphometric analyses of cranial variation. *J. Zool. Syst. Evol. Res.* **55;** DOI: 10.1111/jzs.12144.

Caro TM, Graham CM, Stoner CJ and Flores MM (2003). Correlates of horn and antler shape in bovids and cervids. *Behav. Ecol. Sociobiol*. **55;** 32 – 41. DOI: 10.1007/s00265-003-0672-6.

Changfu Z, Keqin G, Fox RC and Shuihua C (2006). A new species of Psittacosaurus (Dinosauria: Ceratopsia) from the Early Cretaceous Yixian Formation, Liaoning, China. *Palaeoworld* **15;** 100 – 114. DOI: 10.1016/j.palwor.2005.11.001.

Chiarenza AA, Mannion PD, Lunt DJ, Farnsworth A, Jones LA, Kelland SJ and Allison PA (2019). Ecological niche modelling does not support climatically-driven dinosaur diversity decline before the Cretaceous/Paleogene mass extinction. *Nature Comm.* DOI: 10.1038/s41467-019-08997-2.

Chinnery BJ and Weishampel DB (1998). *Montanoceratops cerorhynchus* (Dinosauria: Ceratopsia) and relationships among basal neoceratopsians. *J. Vertebr. Paleo.* **18**; 569 – 585. DOI: 10.1080/02724634.1998.10011085.

Clauss M, Steuer P, Müller DWH, Codron D and Hummel J (2013). Herbivory and body size: allometries of diet quality and gastrointestinal physiology, and implications for herbivore ecology and dinosaur gigantism. *PLoS ONE.* **8;** DOI: 10.1371/journal.pone.0068714.

Clune J, Mouret JB, and Lipson H (2013). The evolutionary origins of modularity. *Proc. R. Soc. B.* **280;** DOI: 10.1098/rspb.2012.2863.

Clutton-Brock T (2007). Sexual selection in males and females. *Science*. **318;** 1882 – 1885. DOI: 10.1126/science.1133311.

Clutton-Brock T and Huchard E (2013). Social competition and its consequences in female mammals. *Journ. Zool.* **289;** 151 – 171. DOI: 10.1111/jzo.12023

Cooney CR, MacGregor HEA, Seddon N and Tobias JA (2018). Multi-modal signal evolution in birds: re-examining a standard proxy for sexual selection. *Proc. R. Soc. B.* **285;** DOI: 10.1098/rspb.2018.1557.

Cooney CR, Varley ZK, Nouri LO, Moody, CJA, Jardine MD and Thomas GH (2019). Sexual selection predicts the rate and direction of colour divergence in a large avian radiation. *Nature Comm.* **10;** DOI: 10.1038/s41467-019-098597-7.

Creelman E and Storey AE (1991). Sex differences in reproductive behaviour of Atlantic puffins. *The Condor*. **93;** 390 – 398. DOI: 10.2307/1368955.

Currie PJ, Langston W, and Tanke DH (2008). A new species of Pachyrhinosaurus (Dinosauria, Ceratopsidae) from the Upper Cretaceous of Alberta, Canada. pp. 1-108. In: Currie PJ, Langston W and Tanke DH 2008. *A New Horned Dinosaur from an Upper Cretaceous Bone Bed in Alberta*. NRC Research Press, Ottawa, Ontario, Canada.

Czepiński Ł (2019). Ontogeny and variation of a protoceratopsid dinosaur *Bagaceratops rozhdestvenskyi* from the Late Cretaceous of the Gobi Desert. *Histor. Biol.* DOI: 10.1080/08912963.2019.1593404.

Dale J, Dey CJ, Delhey K, Kempenaers B and Valcu M (2015). The effects of life history and sexual selection on male and female plumage colouration. *Nature.* **527;** 367 – 370. DOI: 10.1038/nature15509

Darwin C (1859). *The Origin of Species*. London, John Murray.

Darwin C (1871). *The Descent of Man and Selection in Relation to Sex*. London, John Murray.

Dashzeveg D, Dingus L, Loope DB, Swisher CC, Dulam T and Sweeney MR (2005). New stratigraphic subdivision, depositional environment, and age estimate for the Upper Cretaceous Djadokhta Formation, Southern Ulan Nur Basin, Mongolia. *Am. Museum Nov.* **3498;** 1–31.

DeAngelis DL, and Mooij WM (2005). Individual-based modelling of ecological and evolutionary processes. *Annu. Rev. Evol. Syst.* **36;** 147 – 168. DOI: 10.1146/annurev.ecolsys.36.102003.152644.

Denton JSS and Adams DC (2015). A new phylogenetic test for comparing multiple high-dimensional evolutionary rates suggests interplay of evolutionary rates and modularity in lanternfishes (Myctophiformes; Myctophidae). *Evolution.* **69;** 2425 – 2440. DOI: 10.1111/evo.12743.

Dodson P (1976). Quantitative aspects of relative growth and sexual dimorphism in *Protoceratops*. *J. Paleo.* **50;** 929 – 940. www.jstor.org/stable/1303590.

Dodson P (1986). *Avaceratops lammersi*: a new ceratopsid from the Judith River Formation of Montana. *Proc. Acad. Nat. Sci. Phil.* **138;** 305 – 317. DOI: https://www.jstor.org/stable/4064910.

Dodson P (1998). *The Horned Dinosaurs.* Princeton University Press.

Dodson P, Forster CA and Sampson SD (2004). Ceratopsidae. In Weishampel DB, Dodson P and Osmólska H (Eds). *The Dinosauria.* University of California Press, Berkeley.

Doherty PF et al. (2003). Sexual selection affects local extinction and turnover in bird communities. *PNAS.* **100;** 5858 – 5862. DOI: 10.1073/pnas.0836953100.

dos Reis M, Gunnell GF, Barba-Montoya J, Wilkins A, Yang Z and Yoder AD (2018). Using phylogenomics data to explore the effects of relaxed clocks and calibration strategies on divergence time estimation: primates as a test case. *Syst. Biol.* **67;** 594 – 615. DOI: 10.1093/sysbio/syy001.

Dunn PO, Whittingham LA, and Pitcher TE (2001). Mating systems, sperm competition, and the evolution of sexual dimorphism in birds. *Evolution.* **55;** 161 – 175. 10.1111/j.0014-3820.2001.tb01281.x.

Eastick DL, Tattersall GJ, Watson SJ, Lesku JA and Robert KA (2019). Cassowary casques act as thermal windows. *Sci. Rep.* **9;** DOI: 10.1038/s41598-019-38780-8.

Eberhard WG (2002). Natural history and behavior of *Chymomyza mycopelates* and *C. exophthalma* (Diptera: Drosophilidae), and allometry of structures used as signals, weapons, and spore collectors. *Can. Entomol*. **134;** 667 – 687. DOI: 10.4039/Ent134667-5.

Emlen DJ (2001). Costs and the diversification of exaggerated animal structures. *Science.* **291;** 1534 – 1536. DOI: 10.1126/science.1056607.

Emlen DJ, Marangelo J, Ball B and Cunningham CW (2005). Diversity in the weapons of sexual selection: horn evolution in the beetle genus *Onthophagus* (Coleoptera: Scarabidae). *Evolution*. **59;** 1060 – 1084. DOI: 10.1111/j.0014-3820.2005.tb01044.x.

Emlen DJ (2008). The evolution of animal weapons. *Annu. Rev. Ecol. Syst.* **39;** 387 – 413. DOI: 10.1146/annurev.ecolsys.39.110707.173502.

Emlen ST and Oring LW (1977). Ecology, sexual selection, and the evolution of mating systems. *Science*. **197;** 215 – 233. DOI: 10.1126/science.327542.

Erickson GM and Tumanova TA (2000). Growth curve of *Psittacosaurus mongoliensis* Osborn (Ceratopsia: Psittacosauridae) inferred from long bone histology. *Zool. Jour. Linn. Soc.* **130;** 551 – 566. DOI: 10.1006/zjls.2000.0243.

Erickson GM, Zelenitsky DK, Kay DI and Norell MA (2017). Dinosaur incubation periods directly determined from growth-line counts in embryonic teeth show reptilian-grade development. *PNAS.* **114;** 540 – 545. DOI: 10.1073/pnas.1613716114.

Eshel I, Volovik I and Sansone E (2000). On Fisher-Zahavi's handicapped sexy son. *Evol. Eco. Res.* **2;** 509 – 523.

Evans KM, Bernt MJ, Kolmann MA, Ford KL and Albert JS (2018). Why the long face? Static allometry in the sexually dimorphic phenotypes of Neotropical electric fishes. *Zool. Jour. Linn. Soc.* DOI: 10.1093/zoolinnean/zly076.

Falkingham PL (2011). Acquisition of high-resolution three-dimensional models using free, open-source, photogrammetric software. *Palaeo. Electr*. **15;** 1T – 15p. DOI: 10.26879/264.

Fanti F, Currie PJ and Burns ME (2015). Taphonomy, age and paleoecological implication of a new *Pachyrhinosaurus* (Dinosauria: Ceratopsidae) bonebed from the Upper Cretaceous (Campanian) Wapiti Formation of Alberta, Canada. *Can. J. Earth Sci.* **52**; 250 – 260. DOI: 10.1139/cjes-2014-0197.

Farke AA (2007). Cranial osteology and phylogenetic relationships of the chasmosaurine ceratopsid *Torosaurus latus.* In Carpenter K (ed.). *Horns and Beaks.* Indiana University Press, Bloomington and Indiana.

Farke AA, Wolff EDS and Tanke DH (2009). Evidence of combat in *Triceratops*. *PLos ONE*. **4;** DOI: 10.1371/journal.pone.0004252.

Farke AA, Chapman RE and Andersen A (2010). Modeling structural properties of the frill of *Triceratops.* In Ryan MJ, Chinnery-Allgeier BJ and Eberth DA, editors. *New Perspectives on Horned Dinosaurs: The Royal Tyrrell Museum Ceratopsian Symposium.* Bloomington and Indianapolis: Indiana University Press.

Farke AA (2011). Anatomy and Taxonomic Status of the Chasmosaurine Ceratopsid *Nedoceratops hatcheri* from the Upper Cretaceous Lance Formation of Wyoming, USA. *PLoS ONE* **6;** DOI: 10.1371/journal.pone.0016196.

Farke AA, Ryan MJ, Barrett PM, Tanke DH, Braman DM, Loewen MA and Graham MR (2011). A new centrosaurine from the Late Cretaceous of Alberta, Canada, and the evolution of parietal ornamentation in horned dinosaurs. *Acta Palaeo. Polon*. **56;** 691 – 702. DOI: 10.4202/app.2010.0121.

Farke AA, Maxwell WD, Cifelli RL and Wedel MJ (2014). A ceratopsian dinosaur from the Lower Cretaceous of Western North America, and the biogeography of Neoceratopsia. *PLoS ONE*. **9;** DOI: 10.1371/journal.pone.0112055.

Farlow JO and Dodson P (1975). The behavioral significance of frill and horn morphology in ceratopsian dinosaurs. *Evolution*. **29;** 353–361. DOI: 10.1111/j.1558-5646.1975.tb00214.x.

Fastovsky DE, Weishampel DB, Watabe M, Barsbold R, Tsogtbaatar KH and Narmandakh P (2011). A nest of *Protoceratops andrewsi* (Dinosauria, Ornithischia). *J. Paleo.* **85;** 1035 – 1041. DOI: 10.1666/11-008.1.

Felice RN and O-Connor PM (2016). The evolution of sexually dimorphic tail feathers is not associated with tail skeleton dimorphism. *J. Avian Biol.* **47;** 371 – 377. DOI: 10.1111/jav.00801.

Felice RN and Goswami A (2017). Developmental origins of mosaic evolution in the avian cranium. *PNAS.* **115;** 555 – 560. DOI: 10.1073/pnas.1716437115.

Felice RN, Randau M and Goswami A (2018). A fly in a tube: macroevolutionary expectations for integrated phenotypes. *Evolution.* **72;** 2580 – 2594. DOI: 10.1111/evo.13608.

Felice RN, Tobias JA, Pigot AL and Goswami A (2019a). Dietary niche and the evolution of cranial morphology in birds. *Proc. R. Soc. B.* **286;** DOI: 10.1098/rspb.2018.2677.

Felice RN, Watanabe A, Cuff AR, Noirault E, Pol D, Witmer LM, Norell MA, O'Connor PM and Goswami A (2019b). Evolutionary integration and modularity in the archosaur cranium. *Integr. Compar. Biol.* **59;** 371 – 382. DOI:10.1093/icb/icz052.

Felsenstein J (1973). Maximum-likelihood estimation of evolutionary trees from continuous characters. *Am. J. Hum. Genet.* **25;** 471 – 492.

Fiorello AR and Tykoski RS (2011). A new Maastrichtian species of the Centrosaurine ceratopsid *Pachyrhinosaurus* from the north slope of Alaska. *Acta Palaeo. Polon.* **57;** 561 – 573. DOI: 10.4202/app.2011.0033.

Fisher RA (1930). The Genetical Theory of Natural Selection. *Oxford Clarendon Press.*

Friederickson JA and Tumarkin-Deratzin AR (2014). Craniofacial ontogeny in *Centrosaurus apertus. PeerJ*. 2:e252; DOI 10.7717/peerj.252.

Friess M (2012). Scratching the surface? The use of surface scanning in physical and paleoanthropology. *J. Anthro. Sci*. **90;** 7 – 31. DOI: 10.4436/jass.90004.

Fromhage L and Kokko H (2014). Sexually selected traits evolve positive allometry when some matings occur regardless of the trait. *Evolution*. **68;** 1332 – 1338. DOI: 10.1111/evo.12349.

Frost SR, Marcus LF, Bookstein FL, Reddy DP and Delson E (2003). Cranial allometry, phylogeography, and systematics of large-bodied Papionins (Primates: Cercopithecinae) inferred from geometric morphometric analysis of landmark data. *Anatom. Rec. A*. **275**; 1048 – 1072. DOI: 10.1002/ar.a.10112.

Funghi C, Trigo S, Gomes ACR, Soares MC and Cardoso GC (2018). Release from ecological constraint erases sex differences in social ornamentation. *Behav. Ecol. and Socio.* **72;** DOI: 10.1007/s00265-018-2486-6.

Futuyma D (2005). *Evolution*. Sunderland, MA: Sinauer Associates.

Gao K and Cheng Z (1999). A new lizard from the Lower Cretaceous of Shandong, China. *J. Vert. Paleo.* **19**; 456 – 465. DOI: 10.1080/02724634.1999.10011158.

Garamszegi LZ and Møller AP (2010). Effects of samples size and intraspecific variation in phylogenetic comparative studies: a meta-analytical review. *Biol. Rev.* **85;** 797 – 805. DOI: 10.1111/j.1469-185X.2010.00126.x.

Geist V (1971). *Mountain sheep. A study in behaviour and evolution*. Univ. of Chicago Press.

Goswami A and Polly PD (2010a). The influence of modularity on cranial morphological disparity in carnivora and primates (Mammalia). *PLoS One.* **5;** DOI: 10.1371/journal.pone.0009517.

Goswami A and Polly PD (2010b). Methods for studying morphological integration and modularity. In Alroy J and Hunt G (eds), *Quantitative Methods in Paleobiology.* Pp. 213 – 243. The Paleontological Society.

Goswami A, Smaers JB, Soligo C and Polly PD (2014). The macroevolutionary consequences of phenotypic integration: from development to deep time. *Phil. Trans. R. Soc. B.* **369;** DOI: 10.1098/rstb.2013.0254.

Goswami A and Finarelli JA (2016). EMMLi: A maximum likelihood approach to the analysis of modularity. *Evolution*. **70;** 1622 – 1637. DOI: 10.1111/evo.12956.

Goswami A, Watanabe A, Felice RN, Bardua C, Fabre AC and Polly PD (2019). High-density morphometric analysis of shape and integration: the good, the bad, and the not-really-a-problem. *Integr. and Comp. Biol*. **59;** 669 – 683. DOI: 10.1093/icb/icz120.

Gould SJ (1974). The origin and evolution of 'bizarre' structures: Antler size and skull size in the 'Irish elk,' *Megaloceros giganteus*. *Evolution*. **2;** 191 – 220. DOI: 10.1111/j.1558-5646.1974.tb00740.x.

Grafen A (1989). The Phylogenetic Regression. *Phil. Trans. R. Soc. Lon.* **336;** 119 – 157. DOI: 10.1098/rstb.1989.0106.

Grant P (1972). Convergent and divergent character displacement. *Bio. Jour. Linn. Soc*. **4;** 39 – 68. DOI : 10.1111/j.1095-8312.1972.tb00690.x.

Green AJ (1992). Positive allometry is likely with mate choice, competitive display and other functions. *Anim. Behav.* **43;** 170-172. DOI: 10.1016/S0003-3472(05)80086-7.

Hamilton WD (1971). Geometry for the selfish herd. *J. Theor. Biol.* **31;** 395 – 311. DOI: 10.1016/0022-5193(71)90189-5

Han F, Forster CA, Clark JM and Xu X (2015). A new taxon of basal ceratopsian from China and the early evolution of ceratopsian. *PLoSone.* DOI: 10.1371/journal.pone.0143369.

Handa N, Watabe M and Tsogtbaatar K (2012). New specimens of *Protoceratops* (Dinosauria: Neoceratopsia) from the Upper Cretaceous in Udyn Sayr, southern Gobi area, Mongolia. *Paleo. Res.* **16;** 179 – 198. DOI: 10.2517/1342-8144-16.3.179.

Harmon LJ, Weir JT, Brock CD, Glor RE and Challenger W (2008). GEIGER: investigating evolutionary radiations. *Bioinformatics*. **24;** 129 – 131. DOI: 10.1093/bioinformatics/btm538.

Hartigan JA and Hartigan PM (1985). The dip test of unimodality. *Annals Stat.* **13;** 70 – 84**.** https://www.jstor.org/stable/2241144.

Hatcher JB (1907). *The Ceratopsia*. United States Geological Survey, Washington D.C.

Henshaw JM, Kahn AT, and Fritzsche K (2016). A rigorous comparison of sexual selection indexes via simulations of diverse mating systems. *PNAS*. E300 – E308. DOI: 10.1073/pnas.1518067113.

Henderson DM (2010). Skull shapes as indicators of niche partitioning by sympatric chasmosaurine and centrosaurine dinosaurs. In Ryan MJ, Chinnery-Allgeier BJ and Eberth DA, editors. *New Perspectives on Horned Dinosaurs: The Royal Tyrrell Museum Ceratopsian Symposium.* Bloomington and Indianapolis: Indiana University Press.

Hicks JF, Brinkman DL, Nichols DJ and Watabe M (1999). Paleomagnetic and palynologic analyses of Albian to Santonian strata at Bayn Shireh, Burkhant, and Khuren Dukh, eastern Gobi Desert, Mongolia. *Cret. Res.* **20;** 829 – 850. DOI: 10.1006/cres.1999.0188.

Hieronymous TL, Wittmer LM, Tanke DH and Currie PJ (2009). The facial integument of centrosaurine ceratopsids: morphological and histological correlates of novel skin structures. *Anat. Rec.* **292;** 1370 – 1396. DOI: 10.1002/ar.20985.

Hoefs M (2000). The thermoregulatory potential of *Ovis* horn cores. *Can. J. Zool.* **78;** 1419 – 1426. DOI: 10.1139/z00-075.

Hone DWE and Benton MJ (2005). The evolution of large size: how does Cope's Rule work? *TREE.* **20;** 4 – 6. DOI: 10.1016/j.tree.2004.10.012.

Hone DWE, Naish D, and Cuthill IC (2012). Does mutual sexual selection explain the evolution of head crests in pterosaurs and dinosaurs? *Lethaia*. **45;** 139 – 156. DOI: 10.1111/j.1502-3931.2011.00300.x.

Hone DWE and Naish D (2013). The 'species recognition hypothesis' does not explain the presence and evolution of exaggerated structures in non-avialan dinosaurs. *J. Zool.* **290;** 172 – 180. DOI: 10.1111/jzo.12035.

Hone DWE and Faulkes CG (2013). A proposed framework for establishing and evaluating hypotheses about the behaviour of extinct organisms. *J. Zool*. **292;** 260 – 267. DOI: 10.1111/jzo.12114.

Hone DWE, Farke AA, Watabe M, Shigeru S and Tsogbaatar K (2014). A new mass mortality of juvenile *Protoceratops* and size-segregated aggregation behaviour in juvenile non-avian dinosaurs. *PLoS ONE.* DOI: 10.1371/journal.pone.0113306.

Hone DWE, Wood D, and Knell RJ (2016). Positive allometry for exaggerated structures in the ceratopsian dinosaur *Protoceratops andrewsi* supports socio-sexual signalling. *Palaeo. Electro.* **19.1.5A;** 1 – 13. DOI: 10.26879/591.

Hone DWE, Farke AA, and Wedel MJ (2016). Ontogeny and the fossil record: what if anything is an adult dinosaur? *Biol. Lett*. **12;** DOI: 10.1098/rsbl.2015.0947.

Hone DWE and Mallon JC. (2017). Protracted growth impedes the detection of sexual dimorphism in non-avian dinosaurs. *Palaeontology.* **60;** 1 -11. DOI: 10.1111/pala.12298.

Hooper PL and Miller G (2008). Mutual mate choice can drive costly signalling even under perfect monogamy. *Adap. Behav*. **16;** 53 – 69. DOI: 10.1177/1059712307087283.

Horner JR, Varricchio DJ and Goodwin MB (1992). Marine transgressions and the evolution of Cretaceous dinosaurs. *Nature.* **358;** 59 – 61. DOI: 10.1038/358059a0.

Horner JR and Goodwin MB (2006). Major cranial changes during *Triceratops* ontogeny. *Proc. R. Soc. Lond. B: Biol. Sci.* **273;** 2757 – 2761. DOI: 10.1098/rspb.2006.3643.

Huxley JS (1914). The court-ship habits of the Great Crested Grebe, *Podiceps cristatus*; With an addition to the theory of sexual selection. *Proc. Zool. Soc. Lond.* **35;** 491 – 562. 10.1111/j.1469-7998.1914.tb07052.x.

Ives AR, Midford PE and Garland T (2007). Within-species variation and measurement error in phylogenetic comparative methods. *Syst. Biol.* **56;** 252 – 270. DOI: 10.1080/10635150701313830.

Jarzebowska M and Radwan J (2010). Sexual selection counteracts extinction of small populations of the bulb mites. *Evolution*. **64** 1283– 1289. Doi: 10.1111/j.1558-5646.2009.00905.x.

Jiang Y, Bolnick DI and Kirkpatrick M (2013). Assortative mating in animals. *Am. Nat.* **181;** E125 – E138. DOI: 10.5061/dryad.r706v

Johnstone RA, Rands SA and Evans MR (2009). Sexual selection and condition-dependence. *J. Evol. Biol.* **22;** 2387 – 2394. DOI: 10.1111/j.1420-9101.2009.01822.x.

Jones IL and Hunter FM (1993). Mutual sexual selection in a monogamous seabird. *Nature.* **362**; 238 – 239. DOI: 10.1038/362238a0.

Kirkland JI and DeBlieux DD (2010). New basal centrosaurine ceratopsian skulls from the Wahweap Formation (Middle Campanian), Grand Staircase–Escalante National Monument, southern Utah, In: Ryan MJ, Chinnery-Allgeier BJ and Eberth DA (eds.) *New Perspectives on Horned Dinosaurs: The Royal Tyrrell Museum Ceratopsian Symposium*. Bloomington, Indiana University Press. Pp. 117 – 140.

Kirkpatrick M (2000). Reinforcement and divergence under assortative mating. *Proc. R. Soc. Lond. B.* **267;** 1649 – 1655. DOI: 10.1098/rspb.2000.1191.

Kleiman DG (1977). Monogamy in mammals. *Q. Rev. Biol*. **52;** 39 – 69. DOI: 10.1086/409721.

Klingenberg CP (2008). Morphological integration and developmental modularity. *Annu. Rev. Ecol. Syst.* **39;** 115 – 132. 10.1146/annurev.ecolsys.37.091305.110054.

Klingenberg CP and Marugán-Lobón J (2013). Evolutionary covariation in geometric morphometric data: analysing integration, modularity and allometry in a phylogenetic context. *Syst. Biol.* **62;** 591 – 610. DOI: 10.1093/sysbio/syt025.

Klingenberg CP (2014). Studying morphological integration and modularity at multiple levels: concepts and analysis. *Phil. Trans. R. Soc. B.* **369;** DOI: 10.1098/rstb.2013.0249.

Knauss MJ and Yacobucci MM (2014). Geographic Information Systems technology as a morphometric tool for quantifying morphological variation in an ammonoid clade. *Palaeo. Electr.* **17;** 19 – 27. DOI: 10.26879/418.

Knell RJ, Pomfret JC, and Tompkins JL (2004). The limits of elaboration: curved allometries reveal the constraints on mandible size in stag beetles. *Proc. R. Soc. Lond. B.* **271;** 523–528. DOI: 10.1098/rspb.2003.2641

Knell RJ and Fortey RA (2005). Trilobite spines and beetle horns: sexual selection in the Palaeozoic? *Biol. Lett*. **1;** 196 – 199. DOI:10.1098/rsbl.2005.0304.

Knell RJ (2009). Population density and the evolution of male aggression. *J. Zool*. **278;** 83 – 90. DOI: 10.1111/j.1469-7998.2009.00566.x.

Knell RJ (2011). Male contest competition and the evolution of weapons. In Simmons LW and Ridsdill-Smith TJ (eds). *Ecology and Evolution of Dung Beetles*. Blackwell Publishing Ltd.

Knell RJ and Sampson S (2011). Bizarre structures in dinosaurs: species recognition or sexual selection? A response to Padian and Horner. *J. Zool*. **283;** 18 – 22. DOI: 10.1111/j.1469-7998.2010.00758.x.

Knell RJ, Naish D, Tompkins JL, and Hone DWE (2012). Sexual selection in prehistoric animals: detection and implications. *TREE.* **28;** 38 – 47. DOI: 10.1016/j.tree.2012.07.015.

Knell RJ and Martínez-Ruiz C (2017). Selective harvest focused on sexual signal traits can lead to extinction under directional environmental change. *Proc. R. Soc. B.* **284;** DOI:10.1098/rspb.2017.1788.

Kodric-Brown A, Sibly RM, and Brown JH (2006). The allometry of ornaments and weapons. *PNAS*. **103;** 8733 – 8738. DOI: 10.1073/pnas.0602994103.

Koehl P and Hass J (2015). Landmark-free geometric methods in biological shape analysis. *J. R. Soc. Int*. **12;** DOI: 10.1098/rsif.2015.0795.

Kokko H and Johnstone R (2002). Why is mutual mate choice not the norm? Operational sex ratios, sex roles and the evolution of sexually dimorphic and monomorphic signalling. *Philos. Trans. R. Soc. Lond. B: Biol. Sci*. **357;** 319 – 330. DOI: 10.1098/rstb.2001.0926.

Kokko H, Jennions MD and Brooks R (2006). Unifying and testing models of sexual selection. *Ann. Rev. Ecol. Evol. Syst.* **37;** 43 – 66. DOI: 10.1146/annurev.ecolsys.37.091305.110259.

Kotiaho JS (2001). Costs of sexual traits: a mismatch between theoretical considerations and empirical evidence. *Biol. Rev*. **76;** 365 – 376. DOI: 10.1017/S1464793101005711.

Kraaijeveld K, Gregurke J, Hall C, Komdeur J and Mulder RA (2003). Mutual ornamentation, sexual selection, and social dominance in the black swan. *Behav. Eco.* **15;** 380 – 389. DOI: 10.1093/beheco/arh023.

Kraaijeveld K, Kraaijeveld-Smit FJ, Komdeur J (2007). The evolution of mutual ornamentation. *Anim. Behav*. **74;** 657 – 677. DOI: 10.1016/j.anbehav.2006.12.027.

Kraaijeveld K, Kraaijeveld-Smit FJL and Maan ME (2011). Sexual selection and speciation: the comparative evidence revisited. *Biol. Rev*. **86**; 367 – 377. DOI: 10.1111/j.1469-185X.2010.00150.x.

Krauss DA, Pezon A, Nguyen P, Salame I and Rywkin SB (2010). Evolutionary interactions between horn and frill morphology in chasmosaurine ceratopsians. In Ryan MJ, Chinnery-Allgeier BJ and Eberth DA, editors. *New Perspectives on Horned Dinosaurs: The Royal Tyrrell Museum Ceratopsian Symposium.* Bloomington and Indianapolis: Indiana University Press. Pp. 282 – 292.

Lack D (1968). *Ecological adaptations for breeding in birds.* Methuen, London.

Lambert O, Godefroit P, Li H, Shang CY and Dong ZM (2001). A new species of *Protoceratops* (Dinosauria, Neoceratopsia) from the Late Cretaceous of Inner Mongolia (P. R. China). *Bull. l'Inst. R. Sci. Nat. Belg., Sci. Terre*: 5 – 28. https://www.researchgate.net/publication/288618447

Lande R (1981). Models of speciation by sexual selection on polygenic traits. *PNAS*. **78;** 3721 – 3725. DOI: 10.1073/pnas.78.6.3721.

Lappin AK, Brandt Y, Husak JF, Macedonia JM and Kemp DJ (2006). Gaping displays reveal and amplify a mechanically based index of weapon performance. *Am. Nat.* **168;** 100 – 113. DOI: 10.1086/505161.

Lautenschlager S (2016). Reconstructing the past: methods and techniques for the digital restoration of fossils. *R. Soc. Open Sci.* **3;** DOI: 10.1098/rsos.160342.

Lavine L et al. (2015). Exaggerated trait growth in insects. *Annu. Rev. Entomol*. **60;** 453 – 472. DOI: 10.1146/annurev-ento-010814-021045.

Lawing AM and Polly PD (2009). Geometric morphometrics: recent applications to the study of evolution and development. *J. Zool*. **280;** 1 – 7. DOI: 10.1111/j.1469-7998.2009.00620.x.

Lee AH and Werning S (2008). Sexual maturity in growing dinosaurs does not fit reptilian growth models. *PNAS*. **105;** 582–587. DOI: 10.1073/pnas.0708903105.

Lee YN, Ryan MJ and Kobayashi Y (2011). The first ceratopsian dinosaur from South Korea. *Naturwissenschaften* **98;** 39–49. DOI: 10.1007/s00114-010-0739-y.

Lehman TM (2007). Growth and population age structure in the horned dinosaur *Chasmosaurus.* In Carpenter K (Ed). *Horns and Beaks: Ceratopsian and Ornithopod Dinosaurs.* Indiana University Press, Bloomington and Indianapolis.

Lemey P, Rambaut A, Welch JJ and Suchard MA (2010). Phylogeography takes a relaxed random walk in continuous space and time. *Mol. Biol. Evol*. **27;** 1877-1885. DOI: 10.1093/molbev/msq067.

Liyong J, Jun C, Shuqin Z and Godefroit P (2009). A new basal neoceratopsian dinosaur from the Middle Cretaceous of Jilin Province, China. *Act. Geol. Sin.* **83;** 200 – 206. DOI: 10.1111/j.1755-6724.2009.00023.x.

Long TF et al. (2012). The effect of sexual selection on offspring fitness depends on the nature of genetic variation*. Curr. Biol*. **22;** 204–208. DOI: 10.1016/j.cub.2011.12.020.

Longrich NR (2010). *Mojoceratops perifania,* a new chasmosaurine ceratopsid from the late Campanian of Western Canada. *J. Paleo.* **84;** 681 – 694. DOI: 10.1017/S002233600005839X

Longrich N (2011). *Titanoceratops ouranos*, a giant horned dinosaur from the late Campanian of New Mexico. *Cret. Res*. **32;** 264 - 276. DOI : 10.1016/j.cretres.2010.12.007.

Lopes LE, Chaves AV, de Aquino MM, Silveira LF and dos Santos FR (2017). The striking polyphyly of *Suiriri:* Convergent evolution and social mimicry in two cryptic Neotropical birds. **56;** 270 – 279. *J. Zool. Syst. Evol. Res.* DOI: 10.1111/jzs.12200.

Lorch PD, Proulx S, Rowe L and Day T (2003). Condition-dependent sexual selection can accelerate adaptation. *Evol. Ecol. Res*. **5;** 867 – 881.

Lü J et al. (2011). An egg–adult association, gender, and reproduction in pterosaurs. *Science*. **331;** 321 – 324. DOI: 10.1126/science.1197323.

Lund EK, O'Connor PM, Loewen MA and Jinnah ZA (2016). A new centrosaurine ceratopsid, *Machairoceratops cronusi* gen et sp. nov., from the Upper Sand Member of the Wahweap Formation (middle Campanian), southern Utah. *PLoS ONE*. **11;** DOI: 10.1371/journal.pone.0154403.

Maan ME and Seehausen O (2011). Ecology, sexual selection and speciation. *Ecol. Lett*. **14**; 591–602. DOI: 10.1111/j.1461-0248.2011.01606.x.

Macedo RH, Karubian J, and Webster MS (2008). Extrapair paternity and sexual selection in socially monogamous birds: are tropical birds different? *The Auk*. **125;** 769 – 777. DOI: doi.org/10.1525/auk.2008.11008.

MacLeod N and Rose KD (1993). Inferring locomotor behavior in paleogene mammals via eigenshape analysis. *Am. J. Sci*. **293;** 300 – 355. DOI: 10.2475/ajs.293.A.300.

MacLeod N (1999). Generalizing and extending the eigenshape method of shape visualization and analysis. *Paleobiol.* **25;** 107–138. DOI: 10.1666/0094-8373.

Maechler M (2016). diptest: Hartigan's Dip Test Statistic for Unimodality - Corrected. R package version 0.75-7. https://CRAN.R-project.org/package=diptest.

Maidment SCR and Barrett PM (2011). A new specimen of *Chasmosaurus belli* (Ornithischia: Ceratopsidae), a revision of the genus, and the utility of postcrania in the taxonomy and systematics of ceratopsid dinosaurs. *Zootaxa.* **2963;** 1 – 47. DOI: 10.11646/zootaxa.2963.1.1.

Maidment SCR, Henderson DM and Barrett PM (2014). What drove reversions to quadrupedality in ornithischian dinosaurs? Testing hypotheses using centres of mass modelling. *Naturwissenschaften*. **101;** 989 - 1001. DOI: 10.1007/s00114-014-1239-2.

Maiorino L, Farke AA, Kotsakis T, and Piras P (2013). Is *Torosaurus Triceratops*? Geometric morphometric evidence of late Maastrichtian ceratopsid dinosaurs. *PLoS ONE*. **8;** DOI: 10.1371/journal.pone.0081608.

Maiorino L, Farke AA, Kotsakis T, and Piras P (2015). Males Resemble Females: Re-Evaluating Sexual Dimorphism in *Protoceratops andrewsi* (Neoceratopsia, Protoceratopsidae). *PLoS ONE* **10;** DOI: 10.1371/journal.pone.0126464.

Maiorino L, Farke AA, Kotsakis T and Piras P (2017). Macroevolutionary patterns in cranial and lower jaw shape of ceratopsian dinosaurs (Dinosauria: Ornithischia): phylogeny, morphological integration and evolutionary rates. *Evo. Ecol. Res*. **18;** 123 - 167.

Makovicky P (2010). A rediscription of the *Montanoceratops cerorhynchus* holotype with a review of referred material. In Ryan MJ, Chinnery-Allgeier BJ and Eberth DA, editors. *New Perspectives on*

Horned Dinosaurs: The Royal Tyrrell Museum Ceratopsian Symposium. Bloomington and Indianapolis: Indiana University Press. 68 - 82.

Mallon JC, Evans DC, Ryan MJ and Anderson JS (2013). Feeding height stratification among the herbivorous dinosaurs from the Dinosaur Park Formation (upper Campanian) of Alberta, Canada. *BMC Ecol*. **13;** http://www.biomedcentral.com/1472-6785/13/14.

Mallon JC and Anderson JS (2014a). Implications of beak morphology for the evolutionary palaeoecology of the megaherbivorous dinosaurs from the Dinosaur Park Formation(upper Campanian) of Alberta Canada. *Palaeogeo., Palaeoclim., Palaeoeco.* **394;** 29–41. DOI: 10.1016/j.palaeo.2013.11.014.

Mallon JC, and Anderson JS (2014b). The Functional and palaeoecological implications of tooth morphology and wear for the megaherbivorous dinosaurs from the Dinosaur Park Formation (upper Campanian) of Alberta, Canada. *PLoS ONE* **9;** DOI: 10.1371/journal.pone.0098605.

Mallon JC and Anderson JS (2015). Jaw mechanics and evolutionary paleoecology of the megaherbivorous dinosaurs from the Dinosaur Park Formation (upper Campanian) of Alberta, Canada. *J. Vert. Paleo.* **35;** DOI: 10.1080/02724634.2014.904323.

Mallon JC, Ryan MJ and Campbell JA (2015). Skull ontogeny in *Arrhinoceratops brachyops* (Ornithischia: Ceratopsidae) and other horned dinosaurs. *Zool. J. Linn. Soc.* **175;** 910 – 929. DOI: 10.1111/zoj.12294.

Mallon JC, Ott CJ, Larson PL, Iuliano E and Evans DC (2016). *Spiclypeus shipporum* gen. st sp. nov., a boldy audacious new chasmosaurine ceratopsid (Dinosauria: Ornithischia) from the Judith River Formation (Upper Cretaceous: Campanian) of Montana, USA. *PLoS ONE*. **11;** DOI: 10.1371/journal.pone.0154218.

Mallon JC. (2017). Recognizing sexual dimorphism in the fossil record: lessons from nonavian dinosaurs. *Paleobiol.* **43;** 495 – 507. DOI: 10.1017/pab.2016.51.

Martin TE (1996). Life history evolution in tropical and south temperate birds: what do we really know? *J. Avian Biology*. **27;** 263 – 272. DOI: 10.2307/3677257.

Martínez-Ruiz C and Knell RJ (2016). Sexual selection can both increase and decrease extinction probability: reconciling demographic and evolutionary factors. **86;** 177 – 127. *J. Anim. Ecol.* DOI: 10.1111/1365-2656.12601.

Maryańska T and Osmólska H (1975). Protoceratopsidae (Dinosauria) of Asia. *Palaeo. Polon.* **33;** 133-181.

Mateos C, Alarcos S, Carranza J, Sanchez-Prieto CB and Valencia J (2008). Fluctuating asymmetry of red deer antlers negatively relates to individual condition and proximity to prime age. *Anim. Behav.* **75;** 1629 – 1640. 10.1016/j.anbehav.2007.10.016.

Mathews JC, Brusatte SL, Williams SA and Henderson MD (2009). The first *Triceratops* bonebed and its implications for gregarious behavior. *J. Vert. Paleo.* **29;** 286 – 290. DOI: 10.1080/02724634.2009.10010382.

Maynard-Smith J (1958). In *A Century of Darwin* (S. A. Barnett, ed.). Cambridge: Harvard Univ. Press.

Maynard-Smith J (1974). The theory of games and the evolution of animal conflicts. *J. Theor. Biol.* **47;** 209 – 221. DOI: 10.1016/0022-5193(74)90110-6.

Maynard Smith J and Harper D (2003). *Animal Signals.* Oxford, UK: Oxford University Press.

McCullough EL, Ledger KJ, O'Brien DM, and Emlen DJ (2015). Variation in the allometry of exaggerated rhinoceros beetle horns. *J. Animal Behaviour*. **109;** 133 – 140. DOI: 10.1016/j.anbehav.2015.08.013.

McCullough EL, Miller CW and Emlen DJ (2016). Why sexually selected weapons are not ornaments. *TREE*. **31;** 742 - 751. 10.1016/j.tree.2016.07.004.

McDonald AT and Horner JR (2010). New material of *"Styracosaurus" ovatus* from the Two Medicine Formation of Montana. In: Ryan, M.J., Chinnery-Allgeier, B.J., and Eberth, D.A. (eds.) *New Perspectives on Horned Dinosaurs: The Royal Tyrrell Museum Ceratopsian Symposium*. Bloomington, Indiana University Press. Pp. 156 – 168.

McDonald DB, Clay RP, Brumfield RT, and Braun MJ (2001). Sexual selection on plumage and behaviour in an avian hybrid zone: experimental tests of male-male interactions. *Evolution*. **55;** 1443 – 1451. DOI: 10.1111/j.0014-3820.2001.tb00664.x.

McNamara KJ (2012). Heterochrony: the evolution of development. *Evo. Edu. Outreach.* **5;** 203 – 218. DOI: 10.1007/s12052-012-0420-3.

McNamara KJ and Long JA (2012). The role of heterochrony in dinosaur evolution. In: Brett-Surman M, Holtz TR, Farlow JO (eds). *The Complete Dinosaur.* Bloomington: Indiana University Press. Pp. 779 – 802.

Meise K, Mueller B, Zein B and Trillmich F (2014). Applicability of single-camera photogrammetry to determine body dimensions of pinnipeds: Galapagos sea lions as an example. *PLoS ONE*. **9;** DOI: 10.1371/journal.pone.0101197.

Mendelson TC and Shaw KL (2012). The (mis)concept of species recognition. *TREE*. **27;** 421–427. DOI: 10.1016/j.tree.2012.04.001.

M'Gonigle LK et al. (2012). Sexual selection enables long-term coexistence despite ecological equivalence. *Nature*. **484;** 506–509. DOI: 10.1038/nature10971

Mitchell G, van Sittert SJ and Skinner JD (2009). Sexual selection is not the origin of long necks in giraffes. *J. Zool.* **278;** 281 – 286. DOI: 10.1111/j.1469-7998.2009.00573.x.

Mitteroecker P, Gunz P, Bernhard M, Schaefer K and Bookstein FL (2004). Comparison of cranial ontogenetic trajectories among great apes and humans. *J. Hum. Evol.* **46;** 679 – 698 DOI: 10.1016/j.jhevol.2004.03.006.

Møller AP and Pomiankowski A (1993). Why have birds got multiple sexual ornaments? *Behav. Ecol. Sociobiol.* **32;** 167 – 176. DOI: 10.1007/BF00173774.

Montgomery DC and Peck EA (1992). *Introduction to Linear Regression Analysis*. 2nd ed. New York: Wiley-Interscience, John Wiley and Sons, Inc.

Nabavizadeh A (2018). New reconstruction of cranial musculature in ornithischian dinosaurs: implications for feeding mechanisms and buccal anatomy. *Anat. Rec.* DOI: 10.1002/ar.23988.

Nijhout HF (1991). *The development and evolution of butterfly wing patterns.* Smithsonian Institution Press, Washington, DC.

O'Brien DM, Allen CE, Van Kleeck MJ, Hone DWE, Knell RJ, Knapp A, Christiansen S and Emlen DJ (2018). On the evolution of extreme structures: static scaling and the function of sexually selected signals. *Anim. Behav.* **144;** 95 – 108. DOI: 10.1016/j.anbehav.2018.08.005.

Okamoto KW and Grether GF (2013). The evolution of species recognition in competitive and mating contexts: the relative efficacy of alternative methods of character displacement. *Ecol. Lett*. **16;** 670 - 678. DOI: 10.1111/ele.12100.

Osi A, Butler RJ, and Weishampel DB (2010). A Late Cretaceous ceratopsian dinosaur from Europe with Asian affinities. *Nature.* **465;** 466 – 468. DOI: 10.1038/nature09019.

Ostrom JH (1966). Functional morphology and evolution of the ceratopsian dinosaurs. *Evolution.* **20;** 290 – 308. DOI: 10.1111/j.1558-5646.1966.tb03367.x.

Ott CJ (2007). Cranial anatomy and biogeography of the first *Leptoceratops gracilis* (Dinosauria: Ornithischia) specimens from the Hell Creek Formation, southeast Montana. In Carpenter, K. (ed.). *Horns and Beaks.* Indiana University Press, Bloomington and Indiana.

Owens IPF and Hartley IR (1998). Sexual dimorphism in birds: why are there so many different forms of dimorphism? *Proc. R. Soc. Lond. B*. **265;** 397 – 407. DOI: 10.1098/rspb.1998.0308.

Padian K and Horner JR (2011a). The evolution of 'bizarre structures' in dinosaurs: biomechanics, sexual selection, social selection or species recognition? *J. Zool.* **283;** 3 – 17. DOI: 10.1111/j.1469-7998.2010.00719.x.

Padian K and Horner JR (2011b). The definition of sexual selection and its implications for dinosaurian biology. *J. Zool.* **283;** p. 23 – 27. DOI: 10.1111/j.1469-7998.2010.00761.x.

Park RG (1983). *Foundations of Structural Geology.* Blackie, Glasgow and London.

Parker WG (2016). Revised phylogenetic analysis of Aetosauria (Archosauria: Pseudosuchia); assessing the effects of incongruent morphological character sets. *PeerJ*. **4;** DOI: 10.7717/peerj.1583.

Parrett JM and Knell RJ (2018). The effect of sexual selection on adaptation and extinction under increasing temperatures. *Proc. R. Soc. B.* **285;** DOI: 10.1098/rspb.2018.0303.

Parrett JM, Mann DJ, Chung AYC, Slade EM and Knell RJ (2019). Sexual selection predicts the persistence of populations within altered environments. 1629–1637. **22;** *Ecol. Lett.* DOI:10.1111/ele.13358.

Petrie M, Halliday T and Sanders C (1991). Peahens prefer peacocks with elaborate trains. *Anim. Behav*. **41;** 323–331. DOI: 10.1016/S0003-3472(05)80484-1.

Petrie M (1992). Are all secondary sexual display structures positively allometric, and, if so, why? *Anim. Behav.* **43;** 173–175. 10.1016/S0003-3472(05)80087-9.

Pfennig KS and Pfennig DW (2009). Character displacement: ecological and reproductive responses to a common evolutionary problem. *Q. Rev. Biol*. **84;** 253 - 276. DOI: 10.1086/605079.

Price T, Kirkpatrick M and Arnold SJ (1988). Directional selection and the evolution of breeding date in birds. *Science*. **240;** 798 – 799. DOI: 10.1126/science.3363360.

Prondvai E and Stein KHW (2014). Medullary bone-like tissue in the mandibular symphysis of a pterosaur suggests non-reproductive significance. *Sci. Rep*. **4;** DOI: 10.1038/srep0625.

Prum RO (1997). Phylogenetic tests of alternative intersexual selection mechanisms: trait macroevolution in a polygynous clade (Aves: Pipridae). *Am. Nat*. **149;** 668 - 692. DOI: 10.1086/286014

Qvarnstrom A, Vallin N and Rudh V (2012). The role of male contest competition over mates in speciation. *Curr. Zool*. **58;** 493 - 509. DOI: 10.1093/czoolo/58.3.493.

R Core Team (2013). R: A language and environment for statistical computing. R Foundation for Statistical Computing, Vienna, Austria. URL http://www.R-project.org/.

Raia P, Passaro F, Carotenuto L, Maiorino P, Piras L, Teresi S, et al. (2015). Cope's rule and the universal scaling law of ornamental complexity. *Am. Nat*. **186;** 165 – 175. DOI: 10.5061/dryad.50dr8.

Rannala B and Yang Z (2007) Inferring speciation times under an episodic molecular clock. *Syst. Biol*. **56;** 453 – 466. DOI: 10.1080/10635150701420643.

Rayfield EJ (2005). Using finite-element analysis to investigate suture morphology: a case study using large carnivorous dinosaurs. *Anat. Rec. A.* **283A**; 349 – 365. DOI: 10.1002/ar.a.20168.

Renne PR et al. (2013). Time Scales of Critical Events Around the Cretaceous-Paleogene Boundary. *Science.* **339;** 684 – 687. DOI: 10.1126/science.1230492.

Roberts EM, Sampson SD, Deino A, Bowring S and Buchwaldt R (2013). The Kaiparowits Formation: a remarkable record of Late Cretaceous terrestrial environments, ecosystems and evolution in Western North America; pp. 85–106 in Titus AL and Loewen MA (eds.), *At the Top of the Grand Staircase: The Late Cretaceous of Southern Utah*. Indiana University Press, Bloomington, Indiana.

Rohlf FJ and Slice D (1990). Extensions of the Procrustes method for the optimal superimposition of landmarks. *Syst. Zool.* **39;** 40 – 59. DOI: 10.2307/2992207.

Ronquist F, Klopfstein S, Vilhelmsen L, Schulmeister S, Murray DL and Rasnitsyn AP (2012). A total-evidence approach to dating with fossils, applied to the early radiation of the Hymenoptera. *Syst. Biol.* **1;** 973 – 99. DOI: 10.1093/sysbio/sys058.

Rowe L and Houle D (1996). The lek paradox and the capture of genetic variance by condition dependent traits. *Proc. R. Soc. Lond. B*. **263;** 1415 – 1421. DOI: 10.1098/rspb.1996.0207.

Rowland JM and Miller KB (2012). Phylogeny and systematics of the giant rhinoceros beetles (Scarabaeidae: Dynastini). *Insecta Mundi*. **263;** 1 – 15.

Ryan MJ, Russell AP, Eberth DA and Currie PJ (2001). The taphonomy of a *Centrosaurus* (Ornithischia: Ceratopsidae) bone bed from the Dinosaur Park Formation (Upper Campanian), Alberta, Canada, with comments on cranial ontogeny. *Palaios.* **16;** 482 – 506. DOI: 10.1669/0883-1351.

Ryan MJ and Russell AP (2005). A new centrosaurine dinosaur from the Oldman Formation of Alberta and its implications for centrosaurine taxonomy and systematics. *Can. J. Earth Sci.* **42;** 1369 – 1387. DOI: 10.1139/e05-029.

Ryan MJ, Chinnery-Allgeier BJ and Eberth DA (eds.). *New Perspectives on Horned Dinosaurs: The Royal Tyrrell Museum Ceratopsian Symposium*. Bloomington and Indianapolis: Indiana University Press; 2010.

Ryan MJ, Eberth DA, Brinkman DB, Currie PJ and Tanke DH (2010). A new *Pachyrhinosaurus*-like ceratopsid from the Upper Dinosaur Park Formation (Late Campanian) of southern Alberta, Canada. In: Michael J. Ryan, Brenda J. Chinnery-Allgeier, and David A. Eberth (eds), *New Perspectives on Horned Dinosaurs: The Royal Tyrrell Museum Ceratopsian Symposium*, Indiana University Press.

Ryan MJ, Evans DC, Currie PJ, Brown CM and Brinkman D (2012). New leptoceratopsids from the Upper Cretaceous of Alberta, Canada. *Cret. Res*. **35;** 69–80. DOI: 10.1016/j.cretres.2011.11.018.

Ryan MJ, Holmes R, Mallon J, Loewen M and Evans DC (2016). A basal ceratopsid (Centrosaurinae: Nasutoceratopsini) from the Oldman Formation (Campanian) of Alberta, Canada. *Can. J. Earth Sci.* **54;** 1–14. DOI: 10.1139/cjes-2016-0110.

Sætre GP Moum T, Bureš S, Král M, Adamjan M and Moreno J (1997). A sexually selected character displacement in flycatchers reinforces premating isolation. *Nature*. **387;** 589 - 592. DOI: 10.1038/42451.

Sampson SD (1995). Two new horned dinosaurs from the Upper Cretaceous Two Medicine Formation of Montana; with a phylogenetic analysis of the Centrosaurinae (Ornithischia: Ceratopsidae). *J. Vert. Paleo*. **15;** 743 – 760. DOI: 10.1080/02724634.1995.10011259.

Sampson SD, Ryan MJ and Tanke DH (1997). Craniofacial ontogeny in centrosaurine dinosaurs (Ornithischia: Ceratopsidae): taxonomic and behavioral implications. *Zool. J. Linn. Soc.* **121;** 293–337. DOI: 10.1006/zjls.1996.0088.

Sampson SD, Loewen MA, Farke AA, Roberts EM, Forster CA, Smith JA and Titus AL (2010). New horned dinosaurs from Utah provide evidence for intracontinental dinosaur endemism. *PLoS ONE*. **5;** DOI: 10.1371/journal.pone.0012292.

Sampson SD and Loewen M (2010). Unraveling a radiation: a review of the diversity, stratigraphic distribution, biogeography and evolution of horned dinosaurs (Ornithischia: Ceratopsidae). In Ryan MJ, Chinnery-Allgeier BJ, and Eberth DA (eds). *New Perspectives on Horned Dinosaurs*. Indiana University Press, Bloomington and Indianapolis.

Sampson SD, Lund EK, Loewen MA, Farke AA and Clayton KE (2013). A remarkable short-horned dinosaur from the Late Cretaceous (late Campanian) of Laramidia. *Proc. R. Soc. B*. **280;** DOI: 10.1098/rspb.2013.1186.

Scanella JB and Horner JR (2010). *Torosaurus* Marsh, 1891, is *Triceratops* Marsh, 1889 (Ceratopsidae: Chasmosaurinae): synonymy through ontogeny. *J. Vert. Paleo.* **30;** 1157 – 1168. DOI: 10.1080/02724634.2010.48632.

Scanella JB and Horner JR (2011). '*Nedoceratops*': an example of a transitional morphology. *PLoS ONE.* **6;** DOI: 10.1371/journal.pone.0028705.

Scanella JB, Fowler DW, Goodwin MB, and Horner JR (2014). Evolutionary trends in *Triceratops* from the Hell Creek Formation, Montana. *PNAS.* **111;** 10245 – 10250. DOI: 10.1073/pnas.1313334111.

Schlager S (2017). Morpho and Rvcg – shape analysis in R. In: Zheng G, Li S, Szekely G (eds). *Statistical Shape and Deformation Analysis.* London, Academic Press.

Schweitzer MH, Wittmeyer JL and Horner JR (2005). Gender-specific reproductive tissue in ratites and *Tyrannosaurus rex*. *Science*. **308;** 1456 – 1460. DOI: 10.1126/science.1112158.

Searcy WA (1982). The evolutionary effects of mate selection. *Annu. Rev. Ecol. Syst*. **13;** 1443 – 1451. DOI: 10.1146/annurev.es.13.110182.000421.

Senter P (2006). Necks for sex: sexual selection as an explanation for sauropod dinosaur neck elongation. *J. Zool.* **271;** 45 – 53. DOI: 10.1111/j.1469-7998.2006.00197.x.

Sereno PC (1986). Phylogeny of the bird-hipped dinosaurs (Order Ornithischia). *Nat. Geo. Res.* **2;** 234 – 256.

Sereno PC, Xijin Z, Brown L and Lin T (2007). New psittacosaurid highlights skull enlargement in horned dinosaurs. *Act. Palaeo. Polon.* **52;** 275 – 284.

Sereno PC (2010). Taxonomy, cranial morphology and relationships of parrot-beaked dinosaurs (Ceratopsia: *Psittacosaurus*). In Ryan MJ, Chinnery-Allgeier BJ and Eberth DA, editors. *New Perspectives on Horned Dinosaurs: The Royal Tyrrell Museum Ceratopsian Symposium*. Bloomington and Indianapolis: Indiana University Press. Pp. 21 – 58.

Sheehan MJ and Bergman TJ (2016). Is there an evolutionary trade-off between quality signalling and social recognition? *Behav. Ecol*. **27;** 2 – 13. DOI: 10.1093/beheco/arv109.

Shine R (1989). Ecological causes for the evolution of sexual dimorphism: a review of the evidence. *Q. Rev. Biol.* **64;** 419 – 461. DOI: 10.1086/416458.

Shuker DM (2009). Sexual selection: endless forms or tangled bank? *Anim. Behav.* **79;** 11 – 17. DOI: 10.1016/j.anbehav.2009.10.031.

Shuvalov VF (2000). The Cretaceous stratigraphy and paleobiologeography of Mongolia. In: Benson MJ, Shishkin MA, Unwin DM and Kurochkin EN *The Age of Dinosaurs in Russia and Mongolia.* Cambridge University Press, Cambridge.

Sievwright H and MacLeod N (2012). Eigensurface analysis, ecology, and modelling of morphological adaptation in the falconiform humerus (Falconiformes: Aves). *Zool. Jour. Linn. Soc*. **165;** 390 – 419. DOI: 10.1111/j.1096-3642.2012.00818.x.

Sorchi G et al. (1998). Plumage dichromatism of birds predicts introduction success in New Zealand. *J. Anim. Ecol.* **67;** 263 – 269. DOI: 10.1046/j.1365-2656.1998.00199.x.

Spassov N (1979). Sexual selection and the evolution of horn-like structures of ceratopsian dinosaurs. *Palaeontol. Stratigr. Lithol*. **11;** 37 – 48.

Stein AC and Uy JAC (2006). Unidirectional introgression of a sexually selected trait across an avian hybrid zone: a role for female choice? *Evolution*. **60;** 1476 – 1485. DOI: 10.1554/05-575.1.

Stubbs TL, Benton MJ, Elsler A and Prieto-Márquez A (2019). Morphological innovation and the evolution of hadrosaurid dinosaurs. *Paleobiology.* **45;** 347 – 362. DOI: 10.1017/pab.2019.9.

Sues HD, and Averianov A (2009). *Turanoceratops tardabilis*—the first ceratopsid dinosaur from Asia. *Naturwissenschaften*. **96**; 645 – 652. DOI: 10.1007/s00114-009-0518-9.

Sullivan RM, Boere AC and Lucas SG (2005). Redescription of the ceratopsid dinosaur *Torosaurus utahensis* (Gilmore, 1946) and a revision of the genus. *J. Paleo.* **79;** 564 – 582. DOI: 10.1666/0022-3360.

Swisher CC, Wang Y, Wang X, Xu X and Wang Y (1999). Cretaceous age for the feathered dinosaurs of Liaoning, China. *Nature.* **400;** 58 – 61. DOI: 10.1038/21872.

Symonds MRE and Blomberg SP (2014). A primer on phylogenetic generalised least squares. In: Garamszegi L. (eds) *Modern Phylogenetic Comparative Methods and Their Application in Evolutionary Biology*. Springer, Berlin, Heidelberg.

Tallman M et al. (2014). Evaluation of a new method of fossil retrodeformation by algorithmic symmetrisation: crania of Papionins (Primates, Cercopithecidae) as a test case. *PLoS ONE*. **9;** DOI: 10.1371/journal.pone.0100833.

Tanke DH and Farke AA (2007). Bone resorption, bone lesions, and extracranial fenestrae in ceratopsid dinosaurs: a preliminary assessment. In Carpenter K (Ed). *Horns and Beaks: Ceratopsian and Ornithopod Dinosaurs.* Indiana University Press, Bloomington and Indianapolis.

Tanke DH and Rothschild BM (2010). Paleopathologies in Albertan ceratopsids and their behavioural significance. In Ryan MJ, Chinnery-Allgeier BJ, and Eberth DA (eds). *New Perspectives on Horned Dinosaurs*. Indiana University Press, Bloomington and Indianapolis.

Taylor MP, Hone DWE, Wedel MJ and Naish D (2011). The long necks of sauropods did not evolve primarily through sexual selection. *J. Zool*. **285;** 1 – 12. DOI: 10.1111/j.1469-7998.2011.00824.x.

Thorne JL, Kishino H and Painter IS (1998). Estimating the rate of evolution of the rate of molecular evolution. *Mol. Biol. Evol.* **15**; 1647 – 1657. DOI: 10.1093/oxfordjournals.molbev.a025892.

Tidière M, LeMaître JF, Pélabon C, Gimenez O and Gaillard JM (2017). Evolutionary allometry reveals a shift in selection pressure on male horn size. *J. Evol. Biol.* **30;** 1826 – 1835. DOI: 10.1111/jeb.13142.

Tobias JA, Montgomerie R and Lyon BE (2012). The evolution of female ornaments and weaponry: social selection, sexual selection and ecological competition. *Phil. Trans. R. Soc. B.* **367;** 2274 – 2293. DOI: 10.1098/rstb.2011.0280.

Tomkins JL, Radwan J, Kotiaho JS and Tregenza T (2004). Genic capture and resolving the lek paradox. *TREE.* **19;** 323 – 328. DOI: 10.1016/j.tree.2004.03.029.

Tomkins JL, LeBas NR, Witton MP, Martill DM and Humphries S (2010). Positive allometry and the prehistory of sexual selection. *Am. Nat*. **176;** 141–148. DOI: 10.1086/653001.

Tonkin T, Midgley NG, Cook SJ and Graham DJ (2016). Ice-cored moraine degradation mapped and quantified using an unmanned aerial vehicle: A case study from a polythermal glacier in Svalbard. *Geomorphology*. **258;** 1 – 10. DOI: 10.1016/j.geomorph.2015.12.019.

Tullberg BS, Ah-King M and Termin H (2002). Phylogenetic reconstruction of parental-care systems in the ancestors of birds. *Phil. Trans. R. Soc. Lond. B.* **357;** 251 – 257. DOI: 10.1098/rstb.2001.0932.

Urbanova P, Hejna P and Jurda M (2015). Testing photogrammetry-based techniques for three-dimensional surface documentation in forensic pathology. *Foren. Sci. Int*. **250**; 77 – 86. DOI: 10.1016/j.forsciint.2015.03.005.

Van Damme T (2015). Computer vision photogrammetry for underwater archaeological site recording in a low-visibility environment. *Int. Archives Photogram. Spatial Info. Sci*. **XL-5/W5**; 231 – 238. DOI: 10.5194/isprsarchives-XL-5-W5-231-2015.

Van Hooydonck B, Herrel A, Meyers JJ and Irschick DJ (2009). What determines dewlap diversity in *Anolis* lizards? An among-island comparison. *J. Evol. Biol.* **22;** 293 - 305. DOI: 10.1111/j.1420-9101.2008.01643.x.

van Oosterhout C et al. (2003). Inbreeding depression and genetic load of sexually selected traits: how the guppy lost its spots. *J. Evol. Biol.* **16;** 273 – 281. DOI: 10.1046/j.1420-9101.2003.00511.x.

Voje KL, Hansen TF, Egset CK, Bolsttad GH and Pélabon C (2013). Allometric constraints and the evolution of allometry. *Evolution.* **68;** 866 – 885. DOI: 10.1111/evo.12312.

Voje KL (2016). Scaling of morphological characters across trait type, sex, and environment: a meta-analysis of static allometries. *Am. Nat*. **187**; 89 – 98. DOI: 10.1086/684159.

von Bertalanffy L and Pirozynski WJ (1952). Ontogenetic and evolutionary allometry. *Evolution.* **6;** 387 – 392. DOI: 10.2307/2405701.

Wade MJ and Shuster SM (2004). Sexual selection: harem size and the variance in male reproductive success. *Am. Nat*. **164;** E83 – E89. DOI: 10.1086/424531.

Waite JN, Schrader WJ, Mellish JAE and Horning M (2011). Three-dimensional photogrammetry as a tool for estimating morphometrics and body mass of stellar sea lions (*Eumetopias jubatus*). *Canadian J. Fisher. Aquat. Sci.* **64;** 296 – 303. DOI: 10.1139/f07-014.

Watanabe A, Fabre AC, Felice RN, Maisano JA, Müller J, Herrel A and Goswami A (2019). Ecomorphological diversification in squamates from conserved pattern of cranial integration. *PNAS.* **116;** 14688 – 14697. DOI: 10.1073/pnas.1820967116.

Watkins GG (1998). Function of a secondary sexual ornament: the crest in the South American iguanian lizard *Microlophus occipitalis* (Peters, Tropiduridae). *Herpetologica.* **54;** 161–169. https://www.jstor.org/stable/3893423.

Watson NL and Simmons LW (2010). Reproductive competition promotes the evolution of female weaponry. *Proc. R. Soc. B*. **277;** 2035 – 2040. DOI: 10.1098/rspb.2009.2335.

Weatherhead PJ and Robertson RJ (1979). Offspring quality and the polygyny threshold: "The sexy son hypothesis." *Am. Nat*. **113;** 201 – 208. https://www.jstor.org/stable/2460199.

Weishampel DB, Dodson P and Osmólska H, editors. *The Dinosauria*. 2nd ed. Berkeley, CA: California University Press; 2004.

West-Eberhard MJ (1979). Sexual selection, social competition and evolution. *Amer. Phil. Soc.* **123**; 222 – 234. https://www.jstor.org/stable/986582.

West-Eberhard MJ (1983). Sexual selection, social competition and speciation. *Q. Rev. Biol.* **58**; 155 – 183. https://www.jstor.org/stable/2828804.

Wick SL and Lehman TM (2013). A new ceratopsian dinosaur from the Javelina Formation (Maastrichtian) of West Texas and implications for chasmosaurine phylogeny. *Naturwissenschaften.* **100**; 667 – 682. DOI: 10.1007/s00114-013-1063-0.

Wiley DF, Amenta N, Alcantara DA, Deboshmita G, Kil YJ, Delson E, Harcourt-Smith W et al. (2005). Evolutionary Morphing. *Proc IEEE.* 431-438. DOI: 10.1109/VISUAL.2005.1532826.

Wilkinson DM and Ruxton GD (2012). Understanding selection for long necks in different taxa. *Biol. Rev.* **87;** 616–630. DOI: 10.1111/j.1469-185X.2011.00212.x.

Wolfe DG, Kirkland JI, Smith D, Poole K, Chinnery-Allgeier BJ and McDonald A (2010). *Zuniceratops christopheri*: The North American ceratopsid sister taxon reconstructed on the basis of new data. In Ryan MJ, Chinnery-Allgeier BJ and Eberth DA, editors. *New Perspectives on Horned Dinosaurs: The Royal Tyrrell Museum Ceratopsian Symposium*. Indiana University Press. 2010. p. 91 – 98.

Xie W, Lewis PO, Fan Y, Kuo L and Chen MH (2011). Improving marginal likelihood estimation for Bayesian phylogenetic model selection. *Syst. Biol.* **60;** 150 – 160. DOI: 10.1093/sysbio/syq085.

Xu X, Makovicky PJ, Wang X, Norell MA and You H (2002). A ceratopsian dinosaur from China and the early evolution of Ceratopsia. *Nature*. **416;** 314 – 317. DOI: 10.1038/416314a.

Xu X, Foster CA, Clark JM and Mo J (2006). A basal ceratopsian with transitional features from the late Jurassic of northwestern China. *Proc. R. Soc. B*. **273;** 2135 – 2140. DOI: 10.1098/rspb.2006.3566.

Xu X, Wang K, Zhao X, Sullivan C and Chen S (2010). A new leptosaurid (Ornithischia: Ceratopsia) from the Upper Cretaceous of Shandong, China and its implications for neoceratopsian evolution. *PLoS ONE*. **5;** e13835. DOI: 10.1371/journal.pone.0013835.

Xu X, Wang K, Zhao X and Li D (2010). First ceratopsid dinosaur from China and its biogeographical implications. *Chi. Sci. Bull.* **55;** 1631 – 1635. DOI: 10.1007/s11434-009-3614-5.

Yang Z and Rannala B (2006). Bayesian estimation of species divergence times under a molecular clock using multiple fossil calibrations with soft bounds. *Mol. Biol. Evol.* **23**; 212 – 226. DOI: 10.1093/molbev/msj024.

Yang Z (2007). PAML 4: Phylogenetic analysis by maximum likelihood. *Mol. Biol. Evol.* **24;** 1586 – 1591. DOI: 10.1093/molbev/msm088.

You HL and Dong Z (2003). A new protoceratopsid (Dinosauria: Neoceratopsia) from the Late Cretaceous of Inner Mongolia, China. *Act. Geol. Sin.* (English edition) **77;** 299 – 303. DOI: 10.1111/j.1755-6724.2003.tb00745.x.

You H and Dodson P (2004). Basal Ceratopsia. In: Weishampel, D.B., Dodson, P. and Osmólska, H. (eds). *The Dinosauria*. California University Press, Berkeley, CA.

You H, Li D, Ji Q, Lamanna M and Dodson P (2005). On a new genus of basal Neoceratopsian dinosaur from the Early Cretaceous of Gansu Province, China. *Act. Geol. Sin.* **79**; 593 – 597.

You H, Tanoue K and Dodson P (2008). New data on cranial anatomy of the ceratopsian dinosaur *Psittacosaurus major*. *Act. Palaeo. Polon.* **53;** 183 – 196. DOI: 10.4202/app.2008.0202.

Zahavi A (1975). Mate selection – a selection for handicap*. J. Theor. Bio*. **53;** 205 – 214. DOI: 10.1016/0022-5193(75)90111-3.

Zahavi A and Zahavi A (1997). *The Handicap Principle.* Oxford: Oxford University Press.

Zelditch ML, Swiderski DL, Sheets HD and Fink WL (2004). *Geometric Morphometrics for Biologists: A Primer.* Elsevier Inc.

Zhang F et al. (2008). A bizarre Jurassic maniraptoran from China with elongate ribbon-like feathers. *Nature*. **455;** 1105 – 1108. DOI: 10.1038/nature07447.

Zhao X, Cheng Z, and Xu X (1999). The earliest ceratopsian from the Tuchengzi Formation of Liaoning, China. *J. Vert. Paleo*. **19;** 681 – 691. DOI: 10.1080/02724634.1999.10011181.

Zhao Q, Barrett PM and Eberth DA (2007). Social behaviour and mass mortality in the basal ceratopsian dinosaur *Psittacosaurus* (Early Cretaceous, People's Republic of China). *Palaeontology.* **50;** 1023 – 1029. DOI: 10.1111/j.1475-4983.2007.00709.x.

Zheng W, Jin X, and Xu X (2015). A psittacosaurid-like basal neoceratopsian from the Upper Cretaceous of central China and its implications for basal ceratopsian evolution. *Sci. Rep*. **5;** 1 – 9. DOI: 10.1038/srep14190.

Appendix

A1: List of characters used for similarity analysis in Chapter 2.

General Skull

1. **Skull, size relative to the body:**
(0) – small, shorter than the length of the upper hindlimb bones
(1) – sub-equal to the length of the femora
(2) – large, at least 150% of the length of the upper limb bones
(Modified from Makovicky and Norell, 2006:1)

2. **Skull, shape of facial skull in dorsal view:**
(0) – elongated and ovoid
(1) – triangular, wide over the jugals
(Makovicky and Norell, 2006:2)

3. **Skull, relative height of snout (premaxilla) to orbital region:**
(0) – low
(1) – deep
(Modified from Makovicky and Norell, 2006:10)

4. **Skull, naris length compared to basal skull length:**
(0) – less than 10% of skull length
(1) – more than 10% but less than 15% of skull length
(2) – more than 18% of skull length
(Modified from Makovicky and Norell, 2006:19)

5. **Skull, preorbital skull length compared to overall skull length (disregarding spikes):**
(0) – more than 41%
(1) – 35 to 40%
(2) – 30 to 34%
(3) – less than 29%
(Modified from Makovicky and Norell, 2006:4)

6. **Palatomaxillary foramen:**
(0) – absent
(1) – present
(Hatcher et al., 1907)

7. **Position of anterior end of choana on palate:**
(0) – anterior to maxillary tooth row
(1) – or even with maxillary tooth row
(Makovicky & Norell, 2006:20)

8. **Skull, suborbital fenestra or pterygopalatine foramen size:**
(0) – large
(1) – diminutive
(Modified from Makovicky and Norell, 2006:45

Rostral

9. **Rostral, presence of the rostral forming beak:**
(0) – absent
(1) – present
(Modified from Makovicky and Norell, 2006:6)

10. **Rostral, shape of body and extent of dorsal and ventral processes:**
(0) – triangular in lateral view, lacks discrete dorsal and ventral processes
(1) – elongated dorsal and ventral processes extending from the rostral body with prominent concavity on the posterior margin invaginated at least 33% or anteroposterior length of the element
(2) – short, broad dorsal and ventral processes
(Dodson et al., 2004:1; Sampson et al., 2010:1; Farke et al., 2011:1)

11. **Rostral, presence of ventral (buccal) process:**
(0) – absent
(1) – present
(Modified from Makovicky and Norell, 2006:7)

12. **Rostral, contact with nasal:**
(0) – present
(1) – absent
(New Character)

13. **Rostral, shape in occlusal view:**
(0) – broad and rounded anteriorly, “U” shaped

(1) – acute, “V”-shaped
(New Character)

Premaxilla

14. Premaxilla, position of ventral border of endonaris compared to infratemporal fenestra:
(0) – significantly above ventral rim of infratemporal fenestra
(1) – about the level of ventral rim of infratemporal fenestra
(2) – significantly below ventral rim of infratemporal fenestra
(Modified from Makovicky & Norell, 2006:16) Ventral border of ectonaris

15. Premaxilla, position of ventral border of nares compared to orbit:
(0) – is positioned well above the ventral extent of the orbit
(1) – extends to just above the ventral extent of the orbit but not below
(2) – extends below the orbit
(Modified from Makovicky & Norell, 2006:15)

16. Premaxilla, position of ventral border of nares compared to alveolar tooth margin:
(0) – extends below the orbit but not to the alveolar margin
(1) – extends to the alveolar margin
(Modified from Makovicky & Norell, 2006:15)

17. Premaxilla, presence of ectonaris:
(0) – absent
(1) – present as slight outline on lateral surface of premaxilla
(2) – present as a discrete invagination
(Modified from Makovicky and Norell, 2006:17; Sampson et al., 2010:4)

18. Premaxilla, ectonaris, shape:
(0) – anteriorly elongate
(1) – tall, hemicircular
(Sampson et al., 2010:4; Farke et al., 2011:2)

19. Premaxilla, osteonarial complex, size:
(0) – small, occupies 50% or less height of snout
(1) – large, occupies entire height of snout
(Modified after Gregory & Mook, 1925; Brown & Schlaikjer, 1940a)

20. Premaxilla, presence of premaxillary septum:
(0) – absent
(1) – present
(Forster, 1990)

21. Premaxillary septum, nasal contribution:
(0) – septum formed by premaxilla only
(1) – septum formed by premaxilla and nasal
(Sampson et al., 2010:5; Farke et al., 2011:3)

22. Premaxilla, narial strut:
(0) – absent
(1) – present, nascent
(2) – present, well-developed
(Farke et al., 2011:4)

23. Premaxilla, narial strut orientation:
(0) – anteriorly inclined
(1) – posteriorly inclined
(Dodson et al., 2004:6; Sampson et al., 2010:7)

24. Premaxilla, septal flange:
(0) – absent
(1) – fin of bone posterior to narial strut present
(Modified from Forster et al., 1993:1)

25. Premaxilla, septal flange length:
(0) – spans entire posterior margin of narial strut
(1) – restricted to ventral portion of narial strut
(Modified from Forster et al., 1993: 1)

26. Premaxilla, septal fossa:
(0) – absent
(1) – present
(Farke et al., 2011:5)

27. Premaxilla, septal recess:
(0) – absent
(1) – present
(Modified from Dodson et al., 2004:9; Farke et al., 2011:7)

28. Premaxilla, accessory strut in septal fossa and septal recess:

(0) – absent
(1) – present
(Sampson et al., 2010:12)

29. Premaxilla, endonarial process:
(0) – absent
(1) – (triangular process) present
(Forster, 1990:21; Sampson et al., 2010:13; Farke et al., 2011:6)

30. Premaxilla, endonarial process shape in lateral view:
(0) – square with straight margins
(1) – triangular with concave margins
(Sampson et al., 2010:14)

31. Premaxilla, endonarial process recess:
(0) – absent
(1) – present
(Forster, 1990: XX; Sampson et al., 2010:15)

32. Premaxilla, ectonarial recess
(0) – absent
(1) – present
(Sampson et al., 2010:16)

33. Premaxilla, endonarial platform:
(0) – present
(1) – absent
(New Character)

34. Premaxilla, ventral palatal region shape:
(0) – flat in ventral view
(1) – vaulted dorsally
(Modified from Makovicky and Norell, 2006:9)

35. Premaxilla, ventral extent compared to level of alveolar margin:
(0) – above or at the level of alveolar margin of maxilla
(1) – expanded ventrally to extend well below alveolar margin of maxilla
(Modified after Makovicky & Norell, 2006:12; Farke et al., 2011:9)

36. Premaxilla, presence of ventral angle:
(0) – absent
(1) – present
(Forster, 1990; Sampson et al., 2010:17; Farke et al., 2011:8)

37. Premaxilla, composition of expanded ventral angle:
(0) – premaxilla and maxilla
(1) – premaxilla
(Modified after Makovicky & Norell, 2006:12; Farke et al., 2011:10)

38. Premaxilla, form of distal end of posterioventral process:
(0) – broad and uniform in width
(1) – broad and expanded, paddle shaped
(2) – thin
(Modified from Forster et al., 1993:7; Farke et al., 2011:12)

39. Premaxilla, form of thin distal end of posterioventral process:
(0) – lancelate
(1) – forked
(Modified from Forster et al., 1993:7; Sampson et al., 2010:18; Farke et al., 2011; 11)

40. Premaxilla, nasal dorsal contact in dorsal view:
(0) – premaxillae inserts between nasals
(1) – nasals insert between premaxillae
(Sampson et al., 2010:20, Farke et al, 2011:13)

41. Premaxilla-nasal dorsal contact, length in dorsal view:
(0) – short
(1) – premaxilla and nasal contact for at least 30% of the length of the nasal
(New Character)

42. Premaxilla, premaxilla-nasal contact in dorsal view:
(0) – premaxilla tapers posteriorly
(1) – premaxilla broadens posteriorly
(New Character)

43. Premaxilla, contribution of premaxilla to posterior margin of external naris
(0) – less than 40%
(1) – more than 45%
(New Character)

44. **Premaxilla, premaxilla-prefrontal contact:**
(0) – absent
(1) – present
(Modified from Makovicky and Norell, 2006:11)

Accessory Antorbital Fenestra

45. **Accessory antorbital fenestra, presence between naris and antorbital fenestra:**
(0) – absent
(1) – present
(Forster 1990; 15; Sampson et al., 2010:21; Farke et al., 2011:14; Farke et al., 2014:143)

46. **Accessory antorbital fenestra size.**
(0) – pronounced, penetration of nasal cavity visible in lateral view
(1) – slight penetration, nasal cavity not visible in lateral view
(Sampson et al., 2010:22; Farke et al., 2011:15)

47. **Accessory antorbital fenestra, nasal contribution to dorsal margin:**
(0) – nasal makes up less than 50%
(1) – nasal makes up more than 60%
(New Character)

Antorbital Fenestra

48. **Antorbital fenestra:**
(0) – present
(1) – nascent or vestigial
(2) – absent
(New Character)

49. **Antorbital fenestra exposure in lateral view:**
(0) – well exposed in lateral view
(1) – fenestra is tucked behind flange of the jugal
(New Character)

50. **External antorbital fenestra/fossa, size:**
(0) – large, 20% or more length of body of maxilla
(1) – greatly reduced, less than 10% length of body of maxilla
(Modified from Granger & Gregory, 1923; Sampson et al., 2010:23; Farke et al., 2011:16; Makovicky and Norell, 2006:23)

Maxilla

51. **Maxilla, shape of oral margin in ventral view:**
(0) – sinuous, laterally concave
(1) – relatively straight, oral margins converge anteriorly
(Modified Makovicky & Norell, 2006:13)

52. **Maxilla, ventral displacement of tooth row relative to ventral surface of premaxilla:**
(0) – absent
(1) – present
(Sampson et al., 2010:24; Farke et al., 2011:17)

53. **Maxilla, tooth row diastema:**
(0) – absent
(1) – present
(Sampson et al., 2010:25)

54. **Maxilla, maxillary cavity opening on the medial surface of the ascending process and penetrating into the interior of the bone:**
(0) – absent
(1) – present
(Sampson et al., 2010:26; Farke et al., 2011:18)

55. **Maxilla, internal maxillary fossa on medial surface dorsal to the palatal process:**
(0) – absent
(1) – present
(New Character)

56. **Maxilla, length of posterior (alveolar) ramus compared to toothrow length:**
(0) – short, 25% or less
(1) – long, 30% or more
(Sereno, 1999)

57. **Maxilla, ectotopterygoid/pterygoid complex exposure on posterior ramus:**
(0) – covers entire dorsal surface and laps onto lateral surface
(1) – reduced to the posterior-most portion
(Farke et al., 2011:19)

58. **Maxilla, relation to vomers:**
(0) – separated by vomers
(1) – contact each other in palatal view; tip of vomer obscured from view
(Modified from Makovicky and Norell, 2006:22)

59. **Maxilla, eminence or tubercle on the rim of the buccal emargination of the maxilla near the junction with the jugal:**
(0) – absent
(1) – present
(Modified from Makovicky and Norell, 2006:24)

Nasal

60. **Nasal, anterior end relative to anterior end of external naris:**
(0) – posterior to
(1) – anterior to
(Modified from Makovicky and Norell, 2006:14)

61. **Nasal, dorsal surface nasal-nasal contact transverse section:**
(0) – concave
(1) – flat
(2) – peaked or convex
(Modified from Farke et al., 2014:137)

62. **Nasal, ornamentation in adult:**
(0) – absent
(1) – present
(Forster, 1990; Sampson et al., 2010:27)

63. **Nasal, ornamentation type in adult:**
(0) – low prominence
(1) – distinct horncore
(2) – pachyostotic boss
(Modified from Forster, 1990: 26,27,28,126; Sampson et al., 2010:28; Farke et al., 2011:20)

64. **Nasal, ornamentation position, measured perpendicular to the toothrow:**
(0) – centered posterior to anterior end of toothrow
(1) – centered anterior to anterior end of of toothrow
(Modified after Forster, 1990; Sampson et al., 2010:29)

65. **Nasal ornamamentation base, cross sectional shape:**
(0) – sub-circular to ovoid
(1) – mediolaterally compressed, width 66% anteroposterior length of base
(2) – elongate width less than 33% anteroposterior length of base
(3) – covers entire nasal
(New Character)

66. **Nasal ornamentation, height compared to the orbit:**
(0) – short, less than or equal to the height of the orbit
(1) – 1.5 to 2 times taller than the orbit
(2) – elongated, more than 3 times taller than the orbit
(New Character)

67. **Nasal, epinasal ossification:**
(0) – absent
(1) – present
(Lehman, 1990; Forster, 1990; Farke et al., 2011:21)

68. **Nasal, dorsoventral thickness at apex of ectonaris:**
(0) – thin, uniform thickness from medial to lateral
(1) – thick, ventral surface of nasal relatively flat
(New Character)

69. **Nasal, vaulting of internal surface:**
(0) – flat
(1) – absent, convex ventrally
(2) – present, ventral surface concave
(New Character)

70. **Nasal, narial spine:**
(0) – absent
(1) – present as a distinct inflection in the posterior or posteriomedial surface of the naris
(Modified from Lehman, 1990; Forster, 1990:22; Sampson et al., 2010:30, Farke et al., 2011:22)

71. **Nasal, contribution to narial spine:**
(0) – forms less than 60 % of narial spine
(1) – forms greater than 70% of narial spine
(New Character)

72. **Nasal, narial spine orientation:**
(0) – nascent process medially directed
(1) – process anteriorly directed
(New Character)

Orbit

73. **Orbital region, facial skeleton, dorsoventral depth:**
(0) – deep, maxilla dorsally expanded, posterior ramus of maxilla entirely visible
(1) – shallow, maxilla dorsoventrally low, posterior ramus of maxilla partially covered by jugal
(Sampson et al., 2010:31)

74. **Orbit, orientation:**
(0) – directed anterolaterally
(1) – directed laterally
(Sampson et al., 2010:32)

75. **Orbit diameter, relative to basal skull length:**
(0) – more than 25%
(1) – less than 20%
(Makovicky & Norell, 2006:3; Sampson et al., 2010:33)

76. **Orbit, contribution of lacrimal to orbital margin:**
(0) – forms 50% or more of the margin
(1) – forms 40% or less of the margin
(Brown and Schlaikjer, 1940a; Sampson et al., 2010:34)

Palpebral

77. **Palpebral, shape and attachment:**
(0) – rod-like, articulates with prefrontal only at its base, ligamentous attachment
(1) – blocky, fully sutured to and fused into prefrontal and frontal around dorsal orbital margin
(Granger & Gregory, 1923; modified from Forster 1990:31; Makovicky and Norell, 2006:25; Sampson et al., 2010:43; Farke et al., 2011:32)

78. **Palpebral, antorbital buttress:**
(0) – absent
(1) – present
(Ostrom and Wellnhofer, 1986; Sampson, 1995:7: Sampson et al., 2010:44; Farke et al., 2011:33)

79. **Palpebral, extent of antorbital buttress:**
(0) – restricted to anterodorsal orbital margin
(1) – present along entire anterior orbit al margin
(Ostrom and Wellnhofer, 1986; Sampson, 1995a: Sampson et al., 2010:45; Farke et al., 2011:34)

Postorbital

80. **Postorbital, overhang projecting into supratemporal fenestra:**
(0) – absent
(1) – present
(Makovicky & Norell, 2006:33)

81. **Postorbital, texture of lateral surface on orbital rim:**
(0)– smooth
(1)– strongly sculptured
(Modified from Farke et al., 2014:134)

82. **Postorbital, supraorbital ornamentation in adult:**
(0) – absent
(1) – low ornamentation
(2) – horncore
(Modified from Forster et al., 1993:5; Makovicky and Norell, 2006:31; Sampson et al., 2010:3; Farke et al., 2011:25 and 28)

83. **Postorbital, form of low supraorbital ornamentation in adult:**
(0) – reduced to low rugosity
(1) – pachyostotic boss
(Modified from Forster et al., 1993:5; Sampson et al., 2010:3; Farke et al., 2011:25 and 28)

84. **Postorbital, type of subadult supraorbital ornamentation:**
(0) – pointed apex, horncore at least as tall as long anteroposteriorly
(1) – rounded apex, horncore longer anteroposteriorly than high
(Modified from Sampson, 1995a:10; Farke et al., 2011:24)

85. **Postorbital ornamentation, size relative to the nasal ornamentation:**
(0) – larger than nasal ornamentation
(1) – smaller than nasal ornamentation
(New Character)

86. **Postorbital, position of supraorbital ornamentation:**
(0) – centered anterodorsal or dorsal to orbit, narrow base with posterior margin of supraorbital horn extending to or only slightly behind posterior margin of orbit
(1) – centered posteriodorsal to orbit, broad base with posterior margin of supraorbital horn extending well behind posterior orbit
(Modified from Lehman, 1996; Sampson et al., 2010:37; Farke et al., 2011:26)

87. **Postorbital, orientation of supraorbital horncore base:**
(0) – dorsally directed

(1) – dorsolaterally directed
(Sampson et al., 2010:38; Farke et al., 2011:27)

88. **Postorbital, curvature of supraorbital horncore of adults in lateral view:**
(0) – posteriorly curved
(1) – anteriorly curved
(2) – straight or too small to have curvature
(Modified from Forster et al., 1993:2; Sampson et al., 2010:40; Farke et al., 2011:29)

89. **Postorbital, curvature of supraorbital horncore of adults in anterior view:**
(0) – medially curved
(1) – laterally curved
(2) – straight or too small to have curvature
(Sampson et al., 2010:41, Farke et al., 2011:30)

90. **Postorbital, cornual sinuses in base of supraorbital ornamentation:**
(0) – absent
(1) – present
(Farke, 2006)

91. **Postorbital, extent of cornual sinuses in base of supraorbital ornamentation:**
(0) – sinus space invades frontal and parietal only
(1) – sinus space enters postorbital
(Modified from Forster 1990: 123; Farke, 2006; Sampson et al., 2010:36; Farke et al., 2011:23)

92. **Postorbital, contribution to laterotemporal fenestra:**
(0) – postorbital participation in margin
(1) – postorbital excluded from margin
(Makovicky & Norell, 2006:34)

93. **Postorbital, separation from laterotemporal fenestra:**
(0) – postorbital excluded from margin slightly by narrow strip of jugal
(1) – jugal–squamosal contact very wide and postorbital situated far from fenestra
(Makovicky & Norell, 2006:34; Sampson et al., 2010:42)

Jugal

94. **Jugal, shape of jugal flange:**
(0) – free jugal flange absent
(1) – broad based, narrows distally (Delta-shaped)
(2) – narrowed base, anterior and posterior margins subparallel (narrow-waisted)
(New Character)

95. **Jugal, thickening of jugal flange along its anterior edge:**
(0) – present
(1) – absent, plate-like flange
(New Character)

96. **Jugal, size and orientation of jugal flange:**
(0) – projects strongly posteriorly, distal end does not extend below maxillary tooth row
(1) – projects more ventrally, distal end extends below maxillary tooth row
(Makovicky 2001:22; Sampson et al., 2010:46; Farke et al., 2011:35)

97. **Jugal, suborbital ramus depth:**
(0) – not as deep as subtemporal ramus
(1) – as deep or deeper than subtemporal ramus
(Modified from Makovicky and Norell, 2006:28)

98. **Jugal infratemporal process:**
(0) – absent
(1) – present
(Modified from Brown and Schlaikjer, 1940a; modified from Forster, 1990:62; Sampson et al., 2010:47; Farke et al., 2011:36)

99. **Jugal infratemporal process:**
(0) – long
(1) – short
(Modified from Brown and Schlaikjer, 1940a; modified from Forster, 1990:62; Sampson et al., 2010:47; Farke et al., 2011:36)

100. **Jugal–lacrimal contact:**
(0) – very limited
(1) – extensive
(Makovicky & Norell, 2006:26; Sampson et al., 2010:48)

101. **Jugal horn orientation:**
(0) – jugal ornamentation lacking
(1) – laterally directed
(2) – ventrolaterally directed
(Makovicky & Norell, 2006:27)

Epijugal

102. **Epijugal**:
(0) – absent
(1) – present
(Makovicky and Norell, 2006:29)

103. **Epijugal, position of epijugal on jugal:**
(0) – covers most of the posterodistal jugal
(1) – restricted to just the distal most tip of the jugal
(Modified from Makovicky and Norell, 2006:30)

104. **Epijugal cross-sectional shape:**
(0) – large blade like triangle with obtuse angle oriented towards quadratojugal
(1) – roughly equilateral in shape
(Sampson et al., 2010:49; Farke et al., 2011:37)

105. **Epijugal length of horn:**
(0) – as long or longer than wide
(1) – substantially shorter than wide
(Modified from Sampson et al., 2010:50)

106. **Epijugal, extent of horn length:**
(0) – as long as wide
(1) – at least 1.5 times longer than wide
(New Character)

Quadratojugal

107. **Quadratojugal shape:**
(0) – mediolaterally compressed
(1) – transversely expanded medial to jugal
(2) – a squat mediolaterally flattened pedestal
(Modified from Makovicky & Norell, 2006:40)

108. **Quadratojugal, shape of contact with jugal:**
(0)– undivided
(1)– bifid around posterior end of jugal
(Modified from Farke et al., 2006:136)

109. **Quadratojugal, contact with squamosal:**
(0) – absent
(1) – present
(Brown and Schlaikjer, 1940a; Sampson et al., 2010:51)

110. **Laterotemporal fenestra, position:**
(0) – extends dorsal to ventral margin of orbit
(1) – positioned entirely below ventral limit of orbit
(Brown and Schlaikjer, 1940a; Forster, 1990)

111. **Laterotemporal fenestra, size:**
(0) – huge, subequal in size to orbit with long axis at least 50% basal skull length
(1) – greatly reduced, much smaller than orbit, no more than 30% skull length,
(Modified after Brown and Schlaikjer, 1940a; Forster, 1990; Makovicky and Norell, 2006:35)

Prefrontal and Frontal

112. **Prefrontal, both prefrontals contact at the midline:**
(0) – absent
(1) – present
(Lambe, 1915; Forster, 1990:30; Sampson, 1995a; Farke et al., 2011:31)

113. **Frontal, contribution to orbital margin:**
(0) – present
(1) – absent
(Brown & Schlaikjer, 1940a; Sampson et al., 2010:53)

114. **Frontal, contribution to supratemporal fenestra:**
(0) – present
(1) – absent
(Lambe, 1915; Sampson et al., 2010:54)

115. **Frontal, supracranial cavity complex:**
(0) – absent
(1) – present, shallow depression
(2) – present, rimmed
(Modified from Forster 1990:3; modified from Makovicky and Norell, 2006:51; modified from Sampson et al., 2010:55; modified from Farke et al., 2011:38)

116. **Frontal fontanelle, shape:**
(0) – present, transversely narrow, slit-like
(1) – present, key-hole shaped, circular or elongate oval

(Modified from Forster 1990:49,50; Forster, 1996a:3; Sampson et al., 2010:56; Farke et al., 2011:39)

Squamosal

117. Squamosal-quadrate contact:
(0) – socket-like cotylus on ventrolateral squamosal for ball-like quadrate head
(1) – elongate groove on medial surface of squamosal to receive lamina of quadrate
(Hatcher et al., 1907; Forster, 1990; Sampson et al., 2010:63; Farke et al., 2011:43)

118. Squamosal, shape of temporal process:
(0) – simple
(1) – deeply bifurcate around temporal process of postorbital
(Modified from Makovicky and Norell, 2006:37)

119. Squamosal, parietosquamosal frill posterior expansion:
(0) – very slight, short shelf subequal to posterior extent of occipital condyle
(1) – intermediate shelf, expands posterior to the occipital condyle
(2) – extensive shelf, squamosal and parietal expanded well beyond the posterior extent of the quadrates forming true frill
(New Character; modified to some extent from Makovicky and Norell, 2006:52)

120. Squamosal, shape of posterior expansion:
(0) – sub-rectangular in outline
(1) – fan-shaped, sub-triangular
(2) – fan-shaped, sub-triangular with an extended posterior ramus
(3) – sickle-shaped, posteriorly narrowed
(Modified from Makovicky and Norell, 2006:36; Sampson et al., 2010:59, Farke et al., 2011:41)

121. Squamosal, posterior otic notch formed by the posterioventral expansion of the squamosal:
(0) – absent
(1) – present
(New Character)

122. Squamosal, length relative to parietal on frill:
(0) – squamosal as long as the parietal and forms part of the posterior margin of the frill
(1) – squamosal shorter than parietal with part of the lateral portion of the frill made up of parietal
(Modified from Sampson et al., 2010:60-61)

123. Squamosal, medial lamina forming the posteriolateral floor of dorsotemporal fossa creating a pocket in the squamosal in dorsal view:
(0) – absent
(1) – present
(Modified from Dodson, 1986; Sampson et al., 2010:60, Farke et al., 2011:42)

124. Squamosal, posterior edge of squamosal is stepped so that lateral portion extends further posteriorly in dorsal view creating a "stepped margin":
(0) – absent
(1) – present
(Modified from Dodson, 1986; Sampson et al., 2010:60)

125. Squamosal, extent of step "stepped margin":
(0) – slight step where posterior expansion of step is less than the dorsoventral thickness of the pocket
(1) – posteriorly expanded to greater than twice the dorsoventral thickness of the pocket
(New Character)

126. Squamosal, thickened, rounded swelling along medial margin:
(0) – absent, lateral surface of squamosal flat to slightly convex
(1) – present, lateral surface of squamosal slightly concave
(Forster, 1990; Farke, 2006; Sampson et al., 2010:64, Farke et al., 2011:44)

127. Squamosals, orientation of temporal bars:
(0) – parallel
(1) – posteriorly divergent
(Modified from Makovicky and Norell, 2006:39)

128. Squamosal, shape of dorsal edge of temporal bar as it meets posterior frill margin:
(0) – curves medially at the posterior end, arcing confluently into posterior frill margin
(1) – frill at acute angle
(Modified from Makovicky and Norell, 2006:53)

129. Squamosals, orientation of posterior edge:
(0) – angled anteromedially
(1) – angled posteromedially, squamosal contributing lateral portion of frill margin
(Modified from Makovicky and Norell, 2006:38)

130. Squamosal, ridge along the posterioventral edge of squamosal:
(0) – absent
(1) – present
(Modified from Farke et al., 2014:141)

131. Squamosal, oblique dorsal ridge or bumps forming ridge along the dorsal surface of the squamosal:

(0) – absent
(1) – present
(2) – pronounced
(Modified from Evans and Ryan, 2015:98)

Parietal

132. Parietal, anterior extent on dorsum of skull relative to occipital condyle:
(0) – anterior end of parietal located well in front of occipital condyle
(1) – anterior end of parietal lies directly over occipital condyle
(Sampson et al., 2010:57; Farke et al., 2011:40)

133. Parietal, shape of skull roof:
(0) – flat or gently convex
(1) – sharp midline crest
(Modified from Farke et al., 2014:138)

134. Parietosquamosal contact, shape in dorsal view:
(0) – lancelet or straight
(1) – curved, medially concave
(Modified from Forster 1990:66; Sampson et al., 2010:57; Farke et al., 2011:45)

135. Parietal, concave median embayment on posterior margin:
(0) – absent
(1) – present
(Makovicky and Norell, 2006:55; Sampson et al., 2010:66; Farke et al., 2011:46)

136. Parietal, shape of concave median embayment on posterior edge of parietal:
(0) – shallow, may include the whole back of the frill
(1) – restricted to center of margin, incipient
(2) – restricted to center of margin, deep notch-like
(Modified from Forster et al., 1993:9; Forster, 1990:83; Sampson et al., 2010:67, Farke et al., 2011:47)

137. Parietal, location of posterior-most point of parietal:
(0) – on midline
(1) – between midline and lateral-most corner
(2) – at lateral-most corner adjacent to squamosal
(Modified from Holmes et al., 2001:18; Sampson et al., 2010:68)

138. Parietosquamosal frill, elongation into frill:
(0) – absent
(1) – present elongation of parietal into frill

139. Parietosquamosal frill, length relative to basal skull length:
(0) – short, 60% or less
(1) – elongate, more than 70%
(Modified from Hatcher et al., 1907; Lehman, 1990; Forster, 1990: XX; Sampson et al., 2010:69)

140. Parietosquamosal frill, location of maximum transverse width true frill:
(0) – anteriorly, in association with proximal third of frill
(1) – widest part in middle, frill round
(2) – lateral edges roughly parallel
(3) – posteriorly
(Modified from Holmes et al., 2001:17; Sampson et al., 2010:70)

141. Parietal, parietal sulci:
(0) – absent
(1) – present or secondarily roofed
(Marsh, 1892; Sampson et al., 2010:71)

142. Parietal, overall shape:
(0) – nearly straight along midline in lateral view and gently arched from side to side
(1) – "saddle-shaped," dorsally concave in lateral view with upturned posterior margin, and arched strongly from side to side
(Sampson et al., 2010:72)

143. Parietal, sharp median crest:
(0) – present as ridge or line
(1) – absent
(Sampson et al., 1997; Sampson et al., 2010:75; Farke et al., 2011:49)

144. Parietal fenestra:
(0) – absent, no fenestra
(1) – present
(Modified from Forster, 1990: XX; Makovicky and Norell, 2006:54; Sampson et al., 2010:73)

145. Parietal, rim on medial margin of dorsotemporal fenestra:
(0) – absent
(1) – present, well-defined but narrow laterally projecting rim defines medial margin of fenestra
(2) – present, well-defined and wide laterally projecting rim defines medial margin of fenestra

(Modified from Forster, 1990; Sampson et al., 2010:74; Farke et al., 2011:48)

146. Parietal, anteroposterior thickness of transverse bar at narrowest point:
(0) – narrow and straplike, less than 10% total parietal length
(1) – broad, 20% or more of total parietal length
(Modified from Forster et al., 1993:3; Sampson et al., 2010:76; Farke et al., 2011:50)

147. Parietal, cross-sectional shape of transverse bar:
(0) – flat
(1) – round
(New Character)

148. Parietal, relative anteroposterior depth of transverse bar:
(0) – subequal medial to lateral
(1) – tapering medially
(Sampson et al., 2010:77)

149. Parietal, cross-sectional shape of median bar:
(0) – subtriangular, tapers laterally
(1) – round to lenticular
(2) – v-shaped without thickening
(Modified from Holmes et al., 2001:24; Sampson et al., 2010:78)

150. Parietal, median bar, transverse width:
(0) – narrow and straplike, transverse width less than 10% total parietal length
(1) – relatively wide, transverse width 15% or more of total parietal length
(Holmes et al., 2001:23; Sampson et al., 2010:79; Farke et al., 2011:51)

151. Parietal fenestra, orientation:
(0) – long axis directed transversely
(1) – long axis directed axially
(2) – axial and transverse axes equal
(Modified from Forster, 1990; Sampson et al., 2010:80)

152. Parietal fenestra size, maximum proximodistal diameter:
(0) – tiny, 35% or less total parietal length
(1) – large, greater than 45% total parietal length
(Modified from Forster et al., 1993:8; Sampson et al., 2010:81)

Epiossifications

153. Marginal dermal ossifications on parietal and squamosal capping marginal undulations:
(0) – absent
(1) – present
(Modified from Forster 1990:91 & 92; Makovicky and Norell, 2006:56; Sampson et al., 2010:84; Farke et al., 2011:53)

154. Parietosquamosal frill, imbrication of undulations:
(0) – absent
(1) – present
(Sampson et al, 1997; Dodson et al., 2004:34; Sampson et al., 2010:83; Farke et al., 2011:52)

Episquamosals

155. Episquamosal, shape:
(0) – crescentic or ellipsoidal, often with constricted base
(1) – triangular/peaked often elongated
(Dodson et al., 2004:45; Sampson et al., 2010 87; Farke et al., 2011:54)

156. Episquamosals, large gaps between epiquamosals:
(0) – large gaps present between episquamosals
(1) – absent, episquamosals nearly touch one another along squamosal margin
(New Character)

157. Episquamosal, size variation:
(0) – all subequal in size
(1) – marked asymmetry in size
(Modified from Sampson et al., 2010:85, 86)

158. Episquamosal, asymmetry:
(0) – only S1 enlarged
(1) – S1 and S2 enlarged
(2) – anterior-most episquamosal is largest
(New Character)

159. Length and height of all episquamosals:
(0) – sub-equilateral delta or crescentic shaped
(1) – all epiquamosals long with high epiquamosal length to height ratio
(Sampson et al., 2010:85)

160. Number of episquamosals on squamosal:
(0) – 4 or less

(1) – five
(2) – six or seven episquamosals
(3) – eight or more episquamosals
(Modified from Farke et al., 2011:55)

Epiparietosquamosals

161. Marginal ossification crossing parietal-squamosal contact (location EPS):
(0) – absent
(1) – present
(Modified from Dodson et al., 2004:43; Sampson et al., 2010:91; Farke et al., 2011:56)

Epiparietals

162. Epiparietal, fusion to adjacent epiparietals at base:
(0) – absent
(1) – present
(Modified from Holmes et al., 2001:29)

163. Epiparietal, number per side not counting midline p0 or eps:
(0) – five or more
(1) – three
(2) – only one
(Modified from Holmes et al., 2001:28; Farke et al., 2011:57)

164. Epiparietal, presence on midline margin (P0 locus):
(0) – absent
(1) – present
(New Character)

165. Epiparietal, shape of P0:
(0) – ellipsoidal or crescentic, with constricted base
(1) – triangular, peaked
(New Character)

166. Epiparietal, epiparietal ep1 coalesced:
(0) – absent
(1) – present
(New character)

167. Epiparietal, shape of general epiparietals:
(0) – ellipsoidal or crescentic, often with constricted base
(1) – triangular, peaked

168. Parietal, nodes or raised bumps on dorsal surface of posterior margin in between epiparietal loci (dorsoparietal processes:
(0) – absent
(1) – present
(New Character)

169. Epiparietal, multiple raised undulations on proximal midline ramus of parietal:
(0) – absent
(1) – present
(New charcter)

Epiparietal Homology Hypothesis C: Clayton and Loewen *(18 characters)*

170. Epiparietal, ep1, presence:
(0) – present
(1) – absent, or vestigial
Note: we interperet the loss of ep1 in *Rubeosaurus, Einiosaurus, Achelosaurus* and *Pachyrhinosaurus canadensis* as evidenced by vestigual ep1s present in some specimens of *Pachyrhinosaurus lacustai* and its presence in *Pachyrhinosaurus perotorum*.
(New Character)

171. Epiparietal, ep1 length:
(0) – short
(1) – elongate, forms spike
(New Character)

172. Epiparietal, ep1 shape:
(0) – flattened
(1) – round or oval cross-section
(New Character)

173. Epiparietal, ep1 orientation relative to plane of frill:
(0) – in the plane of frill
(1) – curled dorsally or anterodorsally
(New Character)

174. Epiparietal, ep1 lateral curvature:
(0) – in plane of frill
(1) – curved laterally or medially

(New Character)

175. Epiparietal, ep1, curved elements:
(0) – curve laterally
(1) – curve medially
(New Character)

176. Epiparietal, ep2, presence:
(0) – absent
(1) – present
(New Character)

177. Epiparietal, shape of ep2:
(0) – flat
(1) – round
(New Character)

178. Epiparietal, ep2 elongation:
(0) – ep2 is similar to other epiparietals
(1) – elongated into either a triangle, hook or spike
(New Character)

179. Epiparietal, elongated ep2:
(0) – hook about 3 times longer than wide
(1) – spike, elongated more than 6 times longer than wide
(New Character)

180. Epiparietal, ep2 elongated epiparietal shape:
(0) – greatly flattened dorsoventrally
(1) – round or oval cross-section
(New Character)

181. Epiparietal, ep2 orientation:
(0) – in plane of the frill
(1) – curled dorsally or anterodorsally
(New Character)

182. Epiparietal, ep2 mediolateral curvature:
(0) – straight
(1) – curled or oriented medially or laterally

183. Epiparietal, ep3, presence:
(0) – absent
(1) – present
(New Character)

184. Epiparietal, elongated ep3:
(0) – flat
(1) – round
(New Character)

185. Epiparietal, ep3 length:
(0) – short, small and crescentic
(1) – elongated into either a triangle, hook or spike
(New Character)

186. Epiparietal, elongated ep3:
(0) – elongated triangular process
(1) – elongated more than 3 times longer than wide
(New Character)

187. Epiparietal, ep4, presence:
(0) – absent
(1) – present
(New Character)

188. Epiparietal, ep4 length:
(0) – short, small and crescentic
(1) – elongated into either a triangle, hook or spike
(New Character)

189. Epiparietal, elongated ep4:
(0) – elongated triangular process
(1) – elongated more than 3 times longer than wide
(New Character)

190. Epiparietal, ep5, presence:
(0) – absent
(1) – present
(New Character)

191. **Epiparietal, ep5 shape:**
(0) – short, retains general shape of unmodified epiparietals
(1) – developed into spike
(New Character)

192. **Epiparietal, shape of the most proximal epiparietal (usually ep7):**
(0) – no ep5, ep6 or ep7
(1) – small and crescentic
(2) – triangular process
(3) – developed into triangular flattened spike

Braincase

193. **Supraoccipital, contribution to foramen magnum:**
(0) – forms dorsal margin of foramen magnum
(1) – eliminated from margin by exoccipital-exoccipital contact on midline
(Brown & Schlaikjer, 1940a; Forster 1990:63; Makovicky and Norell, 2006:65; Farke et al., 2011:69)

194. **Supraoccipital, ventrolateral processes:**
(0) – absent
(1) – present
(Brown & Schlaikjer, 1940a)

195. **Supraoccipital, ventrolateral processes, dorsolateral ridge between midline supraoccipital ridge and top of exoccipital wing:**
(0) – absent
(1) – present

196. **Supraoccipital, ventrolateral processes, dorsolateral ridge orientation:**
(0) – oriented at roughly 45 degrees
(1) – originate at 45 degrees and then extend dorsally parallel to the midline ridge

197. **Supraoccipital, deep fossa between dorsolateral strut and exoccipital:**
(0) – no fossa
(1) – shallow depression
(2) – deep fossa that forms dorsomedially inclined strut that joins dorsolateral strut

198. **Supraoccipital orientation:**
(0) – anteriorly inclined relative to basioccipital
(1) – posteriorly inclined or in same plane as posterior face of basioccipital
(Makovicky & Norell, 2006:66)

199. **Supraoccipital shape:**
(0) – tall, triangular
(1) – or wider than tall, trapezoid
(2) – or square
(Makovicky & Norell, 2006:67)

200. **Supraoccipital, midline vertical ridge:**
(0) – absent
(1) – present
(new character)

201. **Supraoccipital, midline vertical ridge, form:**
(0) – rounded ridge
(1) – ridge forms fin
(new character)

202. **Supraoccipital, shape of posterior surface:**
(0) – flat, convex, or with midline ridge
(1) – midline depression along base of midline ridge
(Modified from Farke et al., 2014:142)

203. **Basioccipital, contribution to occipital condyle:**
(0) – forms more than 2/3 of occipital condyle
(1) – forms less than 1/3 of the occipital condyle
(Brown & Schlaikjer, 1940a)

204. **Basioccipital, participates in foramen magnum:**
(0) – present
(1) – or basioccipital is excluded from foramen magnum
(Makovicky & Norell, 2006:57)

205. **Basioccipital, subcondylar region form:**
(0) – raised ridge ventral to occipital condyle
(1) – flat or rounded
(new character)

206. **Basioccipital, presence of fossa in raised subcondylar region:**
(0) – absent
(1) – fossa is present ventral to occipital condyle

(new character)

207. Basioccipital, subcondylar region, ventral process lateral to midline vertical ridge:
(0) – present between ventral process and basitubera
(1) – absent
(new character)

208. Basioccipital, contribution to basal tubera:
(0) – excluded from basal tubera by basisphenoid and limited to occipital midline
(1) – basioccipital contributes to basal tubera present
(Modified from Makovicky and Norell, 2006:58)

209. Basal tubera, position:
(0) – flat, in plane with basioccipital plate
(1) – everted posterolaterally, forming lip beneath occipital condyle
(Modified from Makovicky and Norell, 2006:60)

210. Basal tubera, fossa on posterior surface:
(0) – absent
(1) – present
(New Character)

211. Basisphenoid, notch between posteroverntral edge of basisphenoid and base of basipterygoid process:
(0) – deep
(1) – shallow and base of basipterygoid process close to basioccipital tubera
(Modified from Makovicky and Norell, 2006:61)

212. Foramen magnum, visible in posterior view:
(0) – visible in posterior view
(1) – dorsally oriented and obscured by occipital condyle
(new character)

213. Olfactory nerve (I), frontal contribution to exit from braincase:
(0) – present, frontal forms roof of olfactory tract
(1) – absent, olfactory tract enclosed entirely by ossification of the laterspenoid.
(Forster, 1990)

214. Exoccipital, exits for cranial nerves in exoccipital:
(0) – three foramina
(1) – two foramina
(Brown & Schlaikjer, 1940a; Forster, 1990; Makovicky and Norell, 2006:62)

215. Exoccipital–quadrate:
(0) – completely separated by ventral flange of squamosal
(1) – or in contact
(Makovicky & Norell, 2006:63)

216. Paroccipital process, dorsoventral distal expansion:
(0) – distal process only slightly expanded
(1) – distal process expanded to at least .8 two times the depth at its narrowest point
(Brown & Schlaikjer, 1940a; Makovicky and Norell, 2006:64)

Pterygoid

217. Pterygoid, contacts maxilla posterior to the tooth row:
(0) – absent
(1) – present
(Makovicky & Norell, 2006:47)

218. Pterygoid, mandibular process:
(0) – long, extending well below maxillary tooth row
(1) – short
(Modified after Makovicky & Norell, 2006:49)

219. Pterygoid, mandibular process makeup:
(0) – jointly formed by pterygoid and ectopterygoid
(1) – formed only by pterygoid
(Modified from Makovicky and Norell, 2006:50)

220. Pterygoid, ventral ridge on mandibular process of pterygoid defining Eustachian canal:
(0) – absent
(1) – present
(Makovicky and Norell, 2006:46)

221. Pterygoid, prominent posterior midline process:
(0) – absent
(1) – present
(Modified from Makovicky and Norell, 2006:48)

Ectopterygoid

222. Ectopterygoid contacts jugal:

(0) – present
(1) – or ectopterygoid reduced and restricted to contact with maxilla
(Brown & Schlaikjer, 1940a; Makovicky & Norell, 2006:44)

223. Ectopterygoid visible in palatal view:
(0) – exposed
(1) – or reduced and concealed in palatal view
(Makovicky & Norell, 2006:43)

Palatine and vomer

224. Secondary palate, relative contribution of maxilla:
(0) – maxilla forms at least 45% of the length of the secondary palate
(1) – maxilla contributes only to the posterior portion, forms 30% or less of secondary palate
(Brown & Schlaikjer, 1940a)

225. Palatine, shape and relationship to maxilla:
(0) – palatine contacts nearly the entire medial surface of the maxilla, restricting size of choanae, anterodorsal process embraces posterior end of vomer
(1) – palatine contacts only the posterior one-third of medial surface of maxilla, contact with vomer lost, choanae enlarged
(Osmólska, 1986)

226. Elongate parasagittal process of the palatine:
(0) – absent
(1) – present
(Makovicky & Norell, 2006:42)

227. Vomer, relationship to maxillae on secondary palate:
(0) – vomers insert between maxillae at the rear of the secondary palate
(1) – vomers meet posterior margin of maxillae on secondary palate, do not insert between maxillae, so that the maxillae contact each other anterior to the choanae in palatal view and obscure the tip of the vomer
(Modified from Makovicky & Norell, 2006:21)

Quadrate

228. Quadrate, shape of the anterior quadrate shaft in lateral view:
(0) – convex
(1) – straight
(Modified from Makovicky and Norell, 2006:41)

Mandible

229. Lower jaw, level of mandibular articulation:
(0) – at or slightly below occlusal surface of tooth row
(1) – depressed well below level of occlusal surface of tooth row
(Ostrom, 1964; Forster, 1990; Sampson et al., 2010:112)

230. External mandibular fenestra:
(0) – present
(1) – absent
(new character)

231. Predentary/dentary anteroposterior ratio:
(0) – less than two thirds of dentary length
(1) – equal to or more than two-thirds of dentary length
(Makovicky & Norell, 2006:70; Sampson et al., 2010:113)

232. Rostral and predentary shape in occlusal view:
(0) – broad and rounded anteriorly, “U” shaped
(1) – acute, “V”-shaped
(new character)

233. Predentary, shape of dorsal surface:
(0) – shallow or flat
(1) – scooplike
(Modified from Makovicky and Norell, 2006:68)

234. Predentary, dentary processes:
(0) – ventral processes much longer than abbreviated dorsal processes
(1) – dorsal and ventral processes elongate and subequal in length
(Sampson et al., 2010:114; Farke et al., 2011:70)

235. Predentary, ventral dentary process shape:
(0) – wedge shaped and mediolaterally broad
(1) – splint shaped
(Modified from Makovicky and Norell, 2006:69)

236. Predentary, occlusal margin:
(0) – mediolaterally thin
(1) – thickened labiolingually
(new character)

237. **Predentary buccal margin:**
(0) – with round beveled edge
(1) – or with grooved, triturating edge
(Makovicky & Norell, 2006:71)

238. **Predentary, orientation of triturating surface:**
(0) – nearly horizontal
(1) – inclined steeply laterally
(2) – inclined medially
(Lehman, 1990; Forster, 1990; Dodson et al., 2004:57; Farke et al., 2011:71)

239. **Predentary, contact of the lateral process with dentary:**
(0) – smooth
(1) – grooved dorsally
(2) – bears large pit
(Modified from Makovicky and Norell, 2006:72)

240. **Dentary, symphyseal area:**
(0) – small excluding splenial
(1) – large, forming strong immobile bond with participation of splenial
(Modified from Makovicky and Norell, 2006:73)

241. **Dentary, presence of diastema at anterior end:**
(0) – absent
(1) – present
(Modified from Makovicky and Norell, 2006:74)

242. **Dentary, presence of ventral flange:**
(0) – absent
(1) – present along ventral edge
(Modified from Makovicky and Norell, 2006:76)

243. **Dentary, lateral ridge confluent with cutting surface of predentary:**
(0) – present
(1) – absent
(Farke et al., 2011:72)

244. **Dentary, prominent medial expansion of the central mandible in the middle of the tooth row formed by wide Meckelian groove separating tooth-bearing part of the jaw from external surface:**
(0) – absent
(1) – present
(Modified from Makovicky and Norell, 2006:77)

245. **Dentary, shape of area lateral to tooth row:**
(0) – smooth
(1) – rugose and sculpted
(Modified from Makovicky and Norell, 2006:78)

246. **Dentary anteroventral fossa below lateral ridge:**
(0) – absent
(1) – present
(new character)

247. **Dentary anteroventral fossa below lateral ridge size:**
(0) – deep
(1) – weakly present
(new character)

248. **Dentary, shape of ventral margin in adults:**
(0) – strongly convexly bowed
(1) – straight
(Brown and Schlaikjer, 1940a; Forster, 1990:73; Makovicky and Norell, 2006:75; Sampson et al., 2010:117)

249. **Dentary, posterior extent of tooth row:**
(0) – terminates anterior to the center of the coronoid process
(1) – terminates even with the coronoid process
(2) – terminates posterior to the coronoid process
(Brown & Schlaikjer, 1940a; Chinnery and Weishampel 1998; modified from Makovicky and Norell, 2006:82; Sampson et al., 2010:118; Farke et al., 2011:73)

250. **Dentary, overall shape of coronoid process:**
(0) – short, with gently convex apex, base of ascending ramus anteroposteriorly expanded
(1) – tall, expanded at apex into anteriorly projecting hook, base of ascending ramus anteroposteriorly restricted
(Lull, 1933; Sampson et al., 2010:119)

251. **Dentary, shape of dorsal end of coronoid process:**
(0) – rounded

(1) – anterior expansion
(Modified from Makovicky and Norell, 2006:81)

252. Dentary, coronoid process notch along posterior edge of dentary:
(0) – absent
(1) – present
(Modified from Farke et al., 2014:145)

253. Dentary, width of coronoid process notch:
(0) – wide
(1) – constricted notch
(Modified from Farke et al., 2014:146)

254. Dentary, separation of body from ascending ramus of coronoid process:
(0) – absent
(1) – present
(Granger & Gregory, 1923; Sampson et al., 2010:120)

255. Splenial, shape:
(0) – nearly as deep as the body of the dentary, does not contact articular, angular exposed in medial view
(1) – shallow, contacts articular, covers angular in medial view
(Brown & Schlaikjer, 1940a, 1940b; Sampson et al., 2010:121)

256. Posterior end of splenial:
(0) – simple or with shallow dent
(1) – or with bifid overlap of angular
(Makovicky & Norell, 2006:80)

257. Coronoid bone, size:
(0) – large and lobate, with expanded dorsal end much deeper than ventral that inserts between the dentary and splenial to contact, contacts the splenial
(1) – small and strap-like with subequal depth throughout, no contact with splenial
(New Character derived from Brown & Schlaikjer, 1940a, 1940b; modified from Makovicky and Norell, 2006:83)

258. Angular, exposure in lateral view:
(0) – extensive
(1) – greatly restricted
(New Character derived from Brown & Schlaikjer, 1940a)

259. Angular, shape of lateral surface:
(0) – or flat or slightly convex
(1) – angular bears a raised emargination along posteroventral margin of mandible, lateral surface distinctly concave
(Modified after Makovicky & Norell, 2006:88)

260. Angular, texture of lateral surface:
(0) – smooth
(1) – strongly sculptured
(Modified from Farke et al., 2014:135)

261. Angular, presence of one or more small lateral tubercles along ventral rib below glenoid articulation:
(0) – absent
(1) – present
(Modified from Makovicky and Norell, 2006:87)

262. Surangular dorsally projecting ridge on lateral margin:
(0) – present
(1) – absent
(Makovicky & Norell, 2006:84)

263. Surangular, lateral surface:
(0) – flat or only weakly convex
(1) – with pronounced laterally convex curvature (in the transverse plane) between the coronoid process and glenoid region
(Modified from Makovicky and Norell, 2006:85)

264. Surangular, lateral process below glenoid:
(0) – absent
(1) – present; surangular knob
(Farke et al., 2014:139)

265. Surangular, presence of tab forming lateral wall to glenoid cotyle:
(0) – absent
(1) – present
(Modified from Makovicky and Norell, 2006:86)

266. Angular–surangular–dentary contact:
(0) – triradiate
(1) – surangular with long ventral process overlapping angular, dentary-surangular and angular-surangular sutures form acute angle on lateral face of mandible
(Makovicky & Norell, 2006:89)

267. **Prearticular-dentary contact:**
(0) – absent
(1) – present
(Brown & Schlaikjer, 1940a, 1940b; Makovicky and Norell, 2006:79; Sampson et al., 2010:122)

268. **Articular, size and contribution to mandibular glenoid:**
(0) – articular forms only the medial 1/3 of the articular surface, extends posteriorly as far as the angular
(1) – articular enlarged, forms half of the articular surface, extends behind angular to form rear of lower jaw
(New Character derived from Brown & Schlaikjer, 1940a)

269. **Articular, mandibular glenoid in dorsal view:**
(0) – narrow and flush with medial margin of surangular flange
(1) – glenoid region medially expanded and forming lingual process
(Modified from Makovicky and Norell, 2006:90)

270. **Glenoid, surface of prearticular and articular below glenoid:**
(0) – smooth
(1) – wide, semicircular ventral process near medial face of glenoid
(Modified from Makovicky and Norell, 2006:91)

271. **Articular, retroarticular process length:**
(0) – long
(1) – short or absent
(Modified from Makovicky and Norell, 2006:92)

Dentition

272. **Tooth, number of roots:**
(0) – one
(1) – two
(Forster 1990:34; Makovicky and Norell, 2006:95; Sampson et al., 2010:123; Farke et al., 2011:74)

273. **Teeth, presence of median primary ridge:**
(0) – absent
(1) – very weak and wide median ridge on at least some maxillary teeth
(2) – all maxillary and dentary teeth with distinct primary ridge
(Modified from Makovicky and Norell, 2006:98)

274. **Teeth, presence of cingulum:**
(0) – absent
(1) – present
(Modified from Makovicky and Norell, 2006:100)

275. **Teeth, relationship of the base of primary ridge and the cingulum:**
(0) – confluent with the cingulum on maxillary teeth
(1) – base of primary ridge set back from cingulum; forms a continuous ridge at the crown base
(Modified from Makovicky and Norell, 2006:99)

276. **Teeth, enamel on lingual and buccal surfaces of teeth:**
(0) – covered with enamel
(1) – enamel restricted to lateral side of maxillary and medial side of dentary teeth
(Modified from Makovicky and Norell, 2006:102)

277. **Tooth crown height in mid tooth row position:**
(0) – subequal to tooth crown width
(1) – taller than wide
(New Character)

278. **Teeth, crown shape in lateral view:**
(0) – radiate or pennate
(1) – ovate
(Modified from Makovicky and Norell, 2006:106)

279. **Cheek teeth, shape of roots:**
(0) – with cylindrical roots
(1) – roots with mesial and distal faces flattened to slightly grooved
(Modified from Makovicky and Norell, 2006:105)

280. **Teeth, cheek teeth spacing:**
(0) – spaced
(1) – closely appressed
(Makovicky & Norell, 2006:96)

281. **Teeth, occlusion:**
(0) – occlude at an oblique angle
(1) – at a vertical angle
(2) – at a vertical angle, but dentary teeth have a horizontal shelf on the labial face
(Makovicky & Norell, 2006:97)

282. **Tooth, number of replacements per alveolus:**

(0) – one or two replacement teeth
(1) – three or more replacement teeth
(Sereno 1999:137; Makovicky and Norell, 2006:101; Farke et al., 2011:76)

283. Tooth magazine, case-like alveolar slots for vertical tooth families formed by spongy bone:
(0) – absent
(1) – present
(Brown & Schlaijker, 1940a)

284. Premaxillary teeth:
(0) – absent
(1) – present
(New Character)

285. Premaxillary teeth:
(0) – three or more teeth in premaxilla
(1) – or two teeth in premaxilla
(2) – or 1 tooth in premaxilla
(Makovicky & Norell, 2006:93)

286. Premaxillary teeth morphology:
(0) – with carinae and in some cases serrations
(1) – premaxillary teeth peglike, crown without carinae
(Makovicky & Norell, 2006:94)

287. Maxillary teeth, number of alveoli in maxilla:
(0) – 11 or less
(1) – more than 12 and less than 14
(2) – more than 15 and less than 18
(3) – more than 20 and less than 29
(4) – more than 30
(New Character)

288. Dentary teeth, number of alveoli in dentary:
(0) – 11 or less
(1) – more than 12 and less than 18
(2) – more than 19 and less than 29
(3) – more than 30
(Modified from Makovicky & Norell, 2006:104; Farke et al., 2011:75)

289. Dentary teeth, shape of tooth crowns:
(0) – continuous, smooth root crown transition
(1) – bulbous expansion at root-crown transition on labial side of tooth, sometimes worn to form notch or shelf
(Modified from Makovicky and Norell, 2006:103)

Axial Skeleton

290. Atlantal intercentrum, shape:
(0) – semicircular
(1) – disc shaped
(Modified from Makovicky and Norell, 2006:107)

291. Atlantal intercentrum, fusion to odontoid:
(0) – absent
(1) – present
(Modified from Makovicky and Norell, 2006:108)

292. Atlantal intercentrum, fusion to atlantal neuropophyses:
(0) – absent
(1) – present
(Modified from Makovicky and Norell, 2006:109)

293. Cervical vertebrae, formation of syncervical:
(0) – absent
(1) – present
(Modified from Forster 1990:122; Sampson et al., 2010:127; Farke et al., 2011:77)

294. Cervical vertebrae, form of syncervical:
(0) – C1-3fused or tightly articulated, atlantal intercentrum present as a ventrally placed, wedge-like bone
(1) – C1-3 firmly fused, atlantal intercentrum (= hypocentrum) forms a complete ring
(Modified from Forster 1990:122; Sampson et al., 2010:127; Farke et al., 2011:77)

295. Axis, neural spine shape and orientation
(0) – blade-like and nearly vertical, overhangs only anterior-most portion of C3
(1) – blade-like morphology lost, spine steeply angled to reach posterior margin of C3
(Brown & Schlaikjer, 1940a; Sereno 1999:141; modified from Makovicky and Norell, 2006:110,111; Sampson et al., 128: Farke et al., 2011:78):

296. Atlantal rib:
(0) – present
(1) – absent
(Brown & Schlaikjer, 1940a; Sampson et al., 2010:129; Farke et al., 2011:79)

297. Cervical centra, presence of ventral keels:
(0)– ventral keels present
(1)– some or all postaxial centra without keels
(Modified from Farke et al 2014:147)

298. Cervical rib shape:
(0) – L-shaped
(1) – y-shaped
(2) – x-shaped accessory dorsal process present
(New Character)

299. Mid-dorsal neural spine height:
(0) – subequal in height to centrum height
(1) – 2 times the centrum height
(2) – three times centrum height
(New Character)

300. Dorsal vertebrae, zygapophyseal articular surfaces shape:
(0) – with flat articulations on zygapophyses
(1) – tongue and grooves articulations on zygapophyses
(Makovicky & Norell, 2006:113)

301. Dorsal vertebrae, shape of centra:
(0) – relatively axially elongate, lengths exceeds width length/height of centra XX or more
(1) – axially shortened, width exceeds length length/height of centra XX or less
(Modified from Sampson et al., 2010:130; Farke et al., 2011:80)

302. Dorsal vertebrae, elongation of tallest neural arches:
(0) – arch shorter than centrum
(1) – present, arch height taller than centrum
(New Character)

303. Dorsal vertebrae, posteriormost dorsals, zygopohyseal facets horizontal, zygopophyses coalesce:
(0) – absent
(1) – present
(New Character)

304. Sacrum, number of vertebrae:
(0) – five
(1) – six
(2) – seven
(3) – eight or more
(Modified from Makovicky and Norell, 2006:114)

305. Sacrum, longitudinal sulcus on ventral surface:
(0) – absent
(1) – present restricted to caudal sacral vertebrae
(2) – deep across nearly all sacral vertebrae
(Modified from Lambe, 1915; Lehman, 1989, 1990; Sampson et al., 2010:131; Farke et al., 2011:81)

306. Sacrum, shape in dorsal view:
(0) – rectangular
(1) – suboval, mid-sacral ribs longest
(Modified from Makovicky and Norell, 2006:115)

307. Sacrum, ventral expansion of 1st sacral rib to attach along entire lateral side of vertebra:
(0) – absent
(1) – present
(New Character derived from Lull, 1933; Lehman, 1990)

308. Anterior caudal neural spines, height:
(0) – short and anteriorly inclined
(1) – tall and erect
(Makovicky & Norell, 2006:116)

309. Mid caudal neural spines, height:
(0) – less than or equal to 2
(1) – 2.1 to 3 times
(2) – 3.1 to 4 times
(3) – more than 4.1 times
(Modified from Farke et al., 2014:140)

310. Distal caudals, tail terminates with:

(0) – series of cylindrical caudals that are devoid of neural spines and chevrons
(1) – neural spines and chevrons persist virtually to the end of tail
(Modified from Makovicky and Norell, 2006:117)

311. Caudal chevrons, shape of distal caudal chevrons:
(0) – lobate expanded shape
(1) – rodlike
(Modified from Makovicky and Norell, 2006:118)

Pectoral Girdle and Limb

312. Scapula, shape in lateral view:
(0) – distinctly curved in lateral view
(1) – relatively straight
(Makovicky & Norell, 2006:120)

313. Scapula, position of blade relative to glenoid:
(0) – at acute angle
(1) – almost perpendicular to glenoid
(Modified from Makovicky and Norell, 2006:121)

314. Scapula, relative contribution to glenoid fossa:
(0) – scapula and coracoid contribute equally
(1) – scapula contributes well over half of the glenoid
(Brown & Schlaikjer, 1940a; Sereno 1999:145; Farke et al., 2011:82)

315. Glenoid fossa, size and shape:
(0) – glenoid relatively short, unexpanded mediolaterally
(1) – glenoid expanded anteroposteriorly and expanded medially
(Chinnery, 2004)

316. Glenoid fossa, position of humeral head:
(0) – positioned in the lateral portion of the glenoid fossa
(1) – positioned medially in the glenoid fossa
(New Character)

317. Scapular ridge or scapular spine:
(0) – absent
(1) – present
(New Character)

318. Scapula, orientation of scapular spine:
(0) – runs obliquely across blade
(1) – runs longitudinally along blade
(Sampson et al., 2010: 133)

319. Scapula, size of acromion process:
(0) – small, restricted to proximal end
(1) – enlarged, extends distal to the glenoid fossa
(Modified from Makovicky and Norell, 2006:123; Maidment and Barrett, 2011:)

320. Coracoid, shape of anterior blade:
(0) – smooth, arcuate anterior portion
(1) – bearing large anterolateral ridge near confluence of anterior and ventral margins
(Modified from Makovicky and Norell, 2006:122)

321. Coracoid, medial opening of coracoid foramen connected to coraco-scapular suture by sulcus:
(0) – absent
(1) – present
(New Character)

322. Coracoid, concave inflection between coraco-scapular suture and anterior margin of coracoid:
(0) – absent
(1) – present
(New Character)

323. Clavicle:
(0) – present
(1) – absent
(Sereno 1999:147; Makovicky & Norell, 2006:119; Farke et al., 2011:84)

324. Humerus, length of deltopectoral crest in adult:
(0) – short, less than 40% total humeral length
(1) – elongate, subequal to or greater than 45% of the total humeral length
(Chinnery, 2001, 2004)

325. Humerus, shape of margin of deltopectoral crest:
(0) – concave
(1) – straight to convex
(Maidment and Barrett, 2011)

326. **Humerus, triceps fossa on posteriolateral deltopectoral crest:**
(0) – shallow with poorly defined margins
(1) – deep with well-defined margins
(Maidment and Barrett, 2011)

327. **Humerus, position of foramen on posteriomedial humerus relative to apex of deltopectoral crest:**
(0) – level with
(1) – proximal to
(Maidment and Barrett, 2011)

328. **Humerus, orientation of deltopectoral crest:**
(0) – projects anteriorly
(1) – projects anterolateraly
(Maidment and Barrett, 2011)

329. **Radius, lateral and medial tuberosities along distal half of shaft:**
(0) – absent
(1) – present
(Modified from Makovicky and Norell, 2006:144)

330. **Ulna, size of olecranon process:**
(0) – moderately tall, occupies 32% of less total length of ulna
(1) – high, occupies at least 40% total length of ulna
(Modified from Adams, 1988; Forster, 1990: 104; Makovicky & Norell, 2006:123; Sampson et al., 2010:134; Farke et al., 2011:83)

331. **Distal carpals:**
(0) – more than two distal carpals
(1) – less than two distal carpals
(Makovicky & Norell, 2006:124)

332. **Manus and pes size:**
(0) – manus much smaller than pes
(1) – closer to pes in size
(Makovicky & Norell, 2006:125)

333. **Manal unguals, shape:**
(0) – mediolaterally compressed, taper to distal tip
(1) – dorsoventrally compressed, blunt or rounded distal tip
(Brown, 1914b; Chinnery & Weishampel, 1998:64; Sampson et al, 2010:136; Farke et al., 2011:85)

334. **Manal penultimate phalanges, shape:**
(0) – length exceeds width
(1) – width exceeds length
(Sampson et al., 2010:137; Farke et al., 2011:86)

335. **Manus, relative lengths in digit three:**
(0) – articulated phalanges exceed MCIII in length
(1) – articulated phalanges shorter than MCIII in length
(New Character)

336. **Manal and pedal phalanges, flexor pits:**
(0) – present
(1) – absent
(New Character)

Pelvic Girdle and Limb

337. **Ilium, lateral eversion of dorsal margin:**
(0) – absent
(1) – present
(Hatcher et al., 1907; Forster 1990: 108 & 109; Chinnery, 2001, 2004; Sampson et al., 2010:138; Farke et al., 2011:87)

338. **Ilium, relative lengths of pubic and ischial peduncles:**
(0) – pubic and ischial peduncles long, extend well below body of ilium approximately the same distance
(1) – ischial peduncle reduced along ventral aspect, pubic peduncle projects further ventrally than ischial peduncle
(Sampson et al., 2010:139; Farke et al., 2011:88)

339. **Pubis, prepubic process:**
(0) – short and unexpanded distally
(1) – elongate, distal end greatly expanded dorsoventrally
(Forster 1990:111; Makovicky and Norell, 2006:128; Sampson et al., 2010:140; Farke et al., 2011:89)

340. **Pubis, position and length of postpubic rod:**
(0) – relatively long but extends past ischial peduncle of ilium, arises ventral to acetabulum and lies along ventral and ventromedial margin of ischium
(1) – very abbreviated, terminates at level of ischial peduncle, arises medial to acetabulum and passes entirely medial to ischium
(Forster, 1990:110; Makovicky and Norell, 2006:127; Sampson et al., 2010:141; Farke et al., 2011:90)

341. **Pubis and ischium, morphology of contributions to acetabulum:**

(0) – pubic acetabular surface faces posteriolaterally, pubis and pubic process of ischium contribute equally to ventral margin of acetabulum

(1) – pubic acetabular surface faces laterally and forms a partial medial wall to the acetabulum, pubic process of ischium elongate and meets pubis close to anterior margin of acetabulum, ventral portion of pubic acetabular surface lies medial to pubic ramus of ischium

(Sampson et al., 2010:142; Farke et al., 2011:91)

342. Pubis, cross-sectional shape of postpubic shaft:

(0) – round

(1) – mediolaterally flattened, bladelike

(Modified from Makovicky and Norell, 2006:126)

343. Ischium, cross-sectional shape of shaft:

(0) – thick and ovoid

(1) – laterally compressed and bladelike, tapered dorsally

(Forster 1990:112; Sampson et al., 2010:143; Farke et al., 2011:92)

344. Ischium, orientation of shaft:

(0) – nearly straight or slightly decurved

(1) – broadly and continuously curved

(Brown & Schlaikjer, 1940a; Forster 1990:113; Makovicky and Norell, 2006:129; Sampson et al., 2010:144; Farke et al., 2011:93)

345. Femur, morphology of greater and lesser trochanters:

(0) – trochanters distinct and located below the level of the femoral head

(1) – trochanters coalesced and level with the femoral head

(Brown & Schlaikjer, 1940a; Dodson et al., 2004:72; Sampson et al., 2010:145; Farke et al., 2011:94)

346. Femur, size of fourth trochanter:

(0) – large and pendant

(1) – small, reduced to low prominence

(Brown & Schlaikjer, 1940a; Sereno 1999:154; Makovicky and Norell, 2006:130; Sampson et al., 2010:146; Farke et al., 2011:95)

347. Femur-tibia proportion:

(0) – tibia longer than, or equal to femur length

(1) – femur longer than tibia

(Brown & Schlaikjer, 1940a; Forster 1990:103; Makovicky and Norell, 2006: 131; Sampson et al., 2010:147; Farke et al., 2011:96)

348. Pes, metatarsal proportions:

(0) – length of MT I 80% the length of MT II

(1) – MT I reduced less than 70% the length of MT II

(Modified from Sampson et al., 2010:148; Farke et al., 2011:97)

349. Pes, shape:

(0) – gracile with long, constricted metatarsus, elongate phalanges

(1) – short and uncompressed, all phalanges wider than long

(Modified from Makovicky and Norell, 2006:132)

350. Pedal unguals, shape:

(0) – pointed

(1) – rounded, hooflike

(Modified from Makovicky and Norell, 2006:133)

A2: Landmark definitions for geometric morphometric analysis (Chapters 3 and 4). Landmarks used for both analyses, except those in bold which were used only for all-taxa analysis (Chapter 4).

Landmark	Description
1	Distal tip of rostrum
2	Upper junction of rostrum and maxilla in midline
3	Junction of maxilla and nasal on midline
4	Tip of nasal horn
5	Junction of nasal and postorbitals on midline
6	Midline anterior tip of parietal
7	Rearmost point of parietal on midline
8	Junction of parietal and squamosal at outermost edge of frill
9	Lower angle of squamosal on frill margin
10	Innermost contact point of squamosal and quadrate

11	Innermost contact point of quadrate and jugal
12	Tip of jugal
13	Contact of maxilla and jugal at lower edge of zygomatic ridge
14	Junction of maxilla, jugal, and lachrymal
15	Rearmost junction of premaxilla and maxilla
16	Junction of maxilla and premaxilla at lower margin of skull
17	Rearmost point of maxilla on tooth row
18	Junction of premaxilla and rostrum on lower margin of skull
19	Junction of premaxilla and nasal on rear margin of nares at narial process
20	Midpoint of line between points s18 and s17 on margin of narial fossa
21	Midpoint of line between points s19 and s2 on margin of narial fossa
22	Junction of jugal and lachrymal on orbit margin
23	Junction of lachrymal and postorbital on orbit margin
24	Upper posterior margin of orbit
25	Junction of jugal and postorbital on orbit margin
26	Junction of jugal, squamosal and postorbital
27	Junction of squamosal and postorbital on margin of supratemporal fenestra
28	Anterior inner point of parietal fenestra
29	Outermost point of supratemporal fossa
30	Posterior inner margin of parietal fenestra
31	Posterior outer margin of parietal fenestra
32	Anterior outer margin of parietal fenestra
33	**Tip of postorbital horn**
Semilandmark curves	
33-40	Landmarks 1-2 along rostral midline
41-48	Landmarks 2-3 along premaxilla midline
49-65	Landmarks 3-4 along nasal midline
66-82	Landmarks 4-5 along nasal midline
83-90	Landmarks 5-6 along postorbital midline
91-107	Landmarks 6-7 along parietal midline
108-142	Landmarks 7-8 along rear margin of parietal
143-159	Landmarks 8-6 along basal margin of parietal and supratemporal fossa
160-176	Landmarks 8-9 along exterior margin of squamosal to tip of squamosal angle
177-193	Landmarks 9-10 along margin of squamosal to junction of jugal and squamosal
194-201	Landmarks 10-11 around jugal margin of infratemporal fenestra
202-209	Landmarks 11-12 along caudal margin of jugal
210-226	Landmarks 12-13 along rostral margin of jugal
227-234	Landmarks 13-14 along jugal/maxilla suture
235-242	Landmarks 14-15 along lachrymal/maxilla suture
243-250	Landmarks 15-16 along premaxilla/maxilla suture
251-258	Landmarks 16-17 along basal margin of maxilla
259-266	Landmarks 17-13 along caudal margin of maxilla
267-274	Landmarks 16-18 along ventral margin of premaxilla
275-282	Landmarks 18-2 along caudal margin of rostral
283-290	Landmarks 18-1 along ventral margin of rostral

291-298	Landmarks 15-19 along premaxilla/nasal suture
299-306	Landmarks 19-20 along caudal-basal margin of naris
307-314	Landmarks 19-21 along dorsal margin of naris
315-322	Landmarks 21-3 along maxilla/nasal suture
323-330	Landmarks 20-21 along rostral margin of naris
331-338	Landmarks 14-22 along lachrymal/jugal suture
339-346	Landmarks 22-23 along rostral orbit margin
347-363	Landmarks 23-24 along dorsal margin of orbit
364-371	Landmarks 24-25 along caudal margin of orbit
372-379	Landmarks 25-22 along ventral margin of orbit
380-396	Landmarks 5-15 along nasal/postorbital suture
397-413	Landmarks 25-26 along postorbital/jugal suture
414-421	Landmarks 26-10 along jugal/squamosal suture
422-438	Landmarks 26-27 along postorbital/squamosal suture
439-446	Landmarks 27-6 along caudal margin of postorbital
447-454	Landmarks 27-28 along caudal edge of squamosal at margin with supratemporal fossa
455-471	Landmarks 29-30 along interior margin of parietal fenestra
472-488	Landmarks 30-31 along caudal margin of parietal fenestra
489-505	Landmarks 31-32 along exterior margin of parietal fenestra
506-522	Landmarks 32-29 along rostral margin of parietal fenestra
523-540	Landmarks 5-33 tracing curve of postorbital horn
541-557	Landmarks 6-33 tracing curve of postorbital horn
558-574	Landmarks 23-33 tracing curve of postorbital horn
575-591	Landmarks 24-33 tracing curve of postorbital horn
Surface semilandmarks	
Jugal	524-563,793,794
Maxilla	589-622
Postorbital	523,650-694,795-821
Premaxilla	623-649
Nasal	695-721
Squamosal	564-588
Parietal	722-792

A3: Module hypotheses guide for maximum likelihood (EMMLi) analyses performed in Chapters 3 and 4. Hypotheses in bold were tested in both analyses. Hypotheses 21 – 24 were only tested in the all-taxa analysis (Chapter 4).

Hypothesis	Number of modules	Description
1	2	Parietal-squamosal frill is separate module to rest of skull
2	3	Hypothesis 1 with jugal as separate module
3	2	Jugals separate module, rest of skull integrated
4	2	Nasals separate module, rest of skull integrated
5	3	Hypothesis 1 with nasal as separate module
6	4	Hypothesis 1 with jugal and nasal as separate modules
7	3	Jugal and nasal separate modules, rest of skull integrated

8	8	All bones individual modules
9	2	Hypothesis 1 with postorbitals incorporated into frill module
10	3	Hypothesis 9 with nasal as separate module
11	2	Hypothesis 1 with jugal incorporated into frill module
12	2	Hypothesis 11 with nasal incorporate into frill/jugal module
13	2	Hypothesis 1 with nasal incorporated into frill
14	2	Hypothesis 3 with nasal and jugal incorporated into single module
15	7	Hypothesis 8 with nasal and premax incorporated into single module
16	7	Hypothesis 8 with rostrum and premax incorporated into single module
17	6	Hypothesis 8 with nasal, rostrum and premax incorporated into separate module
18	7	Hypothesis 8 with parietal and squamosal incorporated into single module
19	7	Hypothesis 8 with nasal and postorbital incorporated into single module
20	7	Hypothesis 8 with squamosal and jugal incorporated into single module
21	10	Hypothesis 8 with separate nasal and postorbital horn
22	3	Integrated skull, separate nasal and postorbital horn
23	4	Hypothesis 22 with frill as separate module
24	7	Jugal, frill, maxilla, premaxilla/rostral, postorbital/nasal, nasal horn, postorbital horn as separate modules

A4: List of specimens used in geometric morphometric analyses. Specimens marked with an asterisk (*) were used as 'representative specimens' for phylogenetic analyses in Chapter 4.

specimen	subfamily	species
Achelousaurus_horneri_MOR_485*	Centrosaurinae	*Achelousaurus horneri*
Anchiceratops_ornatus_CMN_8535*	Chasmosaurinae	*Anchiceratops ornatus*
Anchiceratops_ornatus_RTMP_1983.001.0001	Chasmosaurinae	*Anchiceratops ornatus*
Arrhinoceratops_brachyops_ROM_796*	Chasmosaurinae	*Arrhinoceratops brachyops*
Centrosaurus_apertus_AMNH_5239*	Centrosaurinae	*Centrosaurus apertus*
Centrosaurus_apertus_AMNH_5351	Centrosaurinae	*Centrosaurus apertus*
Centrosaurus_apertus_CMN_348	Centrosaurinae	*Centrosaurus apertus*
Centrosaurus_apertus_CMN_8790	Centrosaurinae	*Centrosaurus apertus*
Centrosaurus_apertus_CMN_8795	Centrosaurinae	*Centrosaurus apertus*
Centrosaurus_apertus_NMNH_8897	Centrosaurinae	*Centrosaurus apertus*
Centrosaurus_apertus_ROM_767	Centrosaurinae	*Centrosaurus apertus*
Centrosaurus_apertus_RTMP_1992.082.0001	Centrosaurinae	*Centrosaurus apertus*
Centrosaurus_apertus_RTMP_1997.085.0001	Centrosaurinae	*Centrosaurus apertus*
Centrosaurus_apertus_UALVP_11735	Centrosaurinae	*Centrosaurus apertus*
Centrosaurus_apertus_UALVP_16248	Centrosaurinae	*Centrosaurus apertus*
Centrosaurus_apertus_YPM_2015	Centrosaurinae	*Centrosaurus apertus*
Chasmosaurus_belli_AMNH_5402	Chasmosaurinae	*Chasmosaurus belli*
Chasmosaurus_belli_CMN_2245	Chasmosaurinae	*Chasmosaurus belli*
Chasmosaurus_belli_ROM_839*	Chasmosaurinae	*Chasmosaurus belli*
Chasmosaurus_belli_ROM_843	Chasmosaurinae	*Chasmosaurus belli*
Chasmosaurus_belli_UALVP_52613	Chasmosaurinae	*Chasmosaurus belli*
Chasmosaurus_belli_YPM_2016	Chasmosaurinae	*Chasmosaurus belli*
Chasmosaurus_russelli_CMN_2280*	Chasmosaurinae	*Chasmosaurus russelli*

Chasmosaurus_russelli_CMN_8800	Chasmosaurinae	*Chasmosaurus russelli*
Diabloceratops_eatoni_CMNH_81377*	Centrosaurinae	*Diabloceratops eatoni*
Kosmoceratops_richardsoni_UMNH_17000*	Chasmosaurinae	*Kosmoceratops richardsoni*
Leptoceratops_gracilis_CMN_8887*	Leptoceratopsidae	*Leptoceratops gracilis*
Leptoceratops_gracilis_CMN_8889	Leptoceratopsidae	*Leptoceratops gracilis*
Nasutoceratops_titusi_UMNH_16800*	Centrosaurinae	*Nasutoceratops titusi*
Nedoceratops_hatcheri_NMNH_2412*	Chasmosaurinae	*Nedoceratops hatcheri*
Pachyrhinosaurus_lakustai_TMP_1989.055.1234*	Centrosaurinae	*Pachyrhinosaurus lakustai*
Pachyrhinosaurus_lakustai_TMP_2000.002.0002	Centrosaurinae	*Pachyrhinosaurus lakustai*
Protoceratops_andrewsi_AMNH_6408	Protoceratopsidae	*Protoceratops andrewsi*
Protoceratops_andrewsi_AMNH_6409	Protoceratopsidae	*Protoceratops andrewsi*
Protoceratops_andrewsi_AMNH_6413	Protoceratopsidae	*Protoceratops andrewsi*
Protoceratops_andrewsi_AMNH_6414	Protoceratopsidae	*Protoceratops andrewsi*
Protoceratops_andrewsi_AMNH_6419	Protoceratopsidae	*Protoceratops andrewsi*
Protoceratops_andrewsi_AMNH_6425	Protoceratopsidae	*Protoceratops andrewsi*
Protoceratops_andrewsi_AMNH_6429	Protoceratopsidae	*Protoceratops andrewsi*
Protoceratops_andrewsi_AMNH_6431	Protoceratopsidae	*Protoceratops andrewsi*
Protoceratops_andrewsi_AMNH_6433	Protoceratopsidae	*Protoceratops andrewsi*
Protoceratops_andrewsi_AMNH_6434	Protoceratopsidae	*Protoceratops andrewsi*
Protoceratops_andrewsi_AMNH_6439	Protoceratopsidae	*Protoceratops andrewsi*
Protoceratops_andrewsi_AMNH_6466	Protoceratopsidae	*Protoceratops andrewsi*
Protoceratops_andrewsi_AMNH_6467	Protoceratopsidae	*Protoceratops andrewsi*
Protoceratops_andrewsi_CMNH_9185	Protoceratopsidae	*Protoceratops andrewsi*
Protoceratops_andrewsi_HM_1	Protoceratopsidae	*Protoceratops andrewsi*
Protoceratops_andrewsi_MAS_100.503	Protoceratopsidae	*Protoceratops andrewsi*
Protoceratops_andrewsi_MAS_100.517	Protoceratopsidae	*Protoceratops andrewsi*
Protoceratops_andrewsi_MAS_100.519	Protoceratopsidae	*Protoceratops andrewsi*
Protoceratops_andrewsi_MAS_100.523	Protoceratopsidae	*Protoceratops andrewsi*
Protoceratops_andrewsi_MAS_100.524	Protoceratopsidae	*Protoceratops andrewsi*
Protoceratops_andrewsi_MAS_100.526.C	Protoceratopsidae	*Protoceratops andrewsi*
Protoceratops_andrewsi_MAS_100.530.B	Protoceratopsidae	*Protoceratops andrewsi*
Protoceratops_andrewsi_MAS_100.530.D	Protoceratopsidae	*Protoceratops andrewsi*
Protoceratops_andrewsi_MAS_100.530.G	Protoceratopsidae	*Protoceratops andrewsi*
Protoceratops_andrewsi_MAS_100.530.H	Protoceratopsidae	*Protoceratops andrewsi*
Protoceratops_andrewsi_MAS_100.530.K	Protoceratopsidae	*Protoceratops andrewsi*
Protoceratops_andrewsi_MAS_100.531*	Protoceratopsidae	*Protoceratops andrewsi*
Protoceratops_andrewsi_MAS_100.534	Protoceratopsidae	*Protoceratops andrewsi*
Protoceratops_andrewsi_MAS_100.x	Protoceratopsidae	*Protoceratops andrewsi*
Protoceratops_andrewsi_NHM_5134	Protoceratopsidae	*Protoceratops andrewsi*
Protoceratops_andrewsi_QMUL_1	Protoceratopsidae	*Protoceratops andrewsi*
Protoceratops_hellenikorhinus_IMM_95*	Protoceratopsidae	*Protoceratops hellenikorhinus*
Psittacosaurus_lujiatunensis_QMUL_3*	Psittacosauridae	*Psittacosaurus lujiatunensis*

Psittacosaurus_mongolienesis_AMNH_6254*	Psittacosauridae	*Psittacosaurus mongoliensis*
Psittacosaurus_neimongoliensis_IVPP_120888*	Psittacosauridae	*Psittacosaurus neimongoliensis*
Psittacosaurus_sinensis_BMNH_BPV149*	Psittacosauridae	*Psittacosaurus sinensis*
Regaliceratops_peterhewsi_TMP_2005.055.0001*	Chasmosaurinae	*Regaliceratops peterhewsi*
Spiclypeus_shipporum_CMN_57081*	Chasmosaurinae	*Spiclypeus shipporum*
Styracosaurus_albertensis_CMN_344*	Centrosaurinae	*Styracosaurus albertensis*
Styracosaurus_albertensis_TMP_1986.126.0001	Centrosaurinae	*Styracosaurus albertensis*
Torosaurus_latus_ANSP_15192	Chasmosaurinae	*Torosaurus latus*
Torosaurus_latus_YPM_1830*	Chasmosaurinae	*Torosaurus latus*
Triceratops_horridus_AMNH_05116	Chasmosaurinae	*Triceratops horridus*
Triceratops_horridus_AMNH_30609	Chasmosaurinae	*Triceratops horridus*
Triceratops_horridus_MNHN_1912.20	Chasmosaurinae	*Triceratops horridus*
Triceratops_horridus_NMNH_1201	Chasmosaurinae	*Triceratops horridus*
Triceratops_horridus_NMNH_2580*	Chasmosaurinae	*Triceratops horridus*
Triceratops_horridus_ROM_55380	Chasmosaurinae	*Triceratops horridus*
Triceratops_horridus_YPM_2014	Chasmosaurinae	*Triceratops horridus*
Triceratops_prorsus_BTT_1958G3.1	Chasmosaurinae	*Triceratops prorsus*
Triceratops_prorsus_CMNH_1219	Chasmosaurinae	*Triceratops prorsus*
Triceratops_prorsus_YPM_1822*	Chasmosaurinae	*Triceratops prorsus*
Utahceratops_gettyi_UMNH_16784*	Chasmosaurinae	*Utahceratops gettyi*
Vagaceratops_irvinensis_CMN_41357*	Chasmosaurinae	Vagaceratops irvinensis
Zuniceratops_christopheri_CMNH_81376*	Ceratopsoidae	Zuniceratops christopheri